NASA CR-152311

(NASA-CR-152311) SYNTHESIS OF ROTOR TEST DATA FOR REAL-TIME SIMULATION (Boeing Vertol Co., Philadelphia, Pa.) 232 p HC A11/MF A01 CSCL 01C
N80-18029
Unclas
G3/05 13293

SYNTHESIS OF ROTOR TEST DATA FOR REAL-TIME SIMULATION

M. A. McVeigh

March 1979

Prepared Under Contract NAS 2-9015

for

National Aeronautics and Space Administration
Ames Research Center

by

BOEING VERTOL COMPANY
A DIVISION OF THE BOEING COMPANY
PHILADELPHIA, PENNSYLVANIA

REV LTR

BOEING VERTOL COMPANY

A DIVISION OF THE BOEING COMPANY

P.O. BOX 16858
PHILADELPHIA, PENNSYLVANIA 19142

CODE IDENT. NO. 77272

NUMBER D210-11505-1

TITLE Synthesis of Rotor Test Data for Real-Time Simulation

ORIGINAL RELEASE DATE ________. FOR THE RELEASE DATE OF SUBSEQUENT REVISIONS, SEE THE REVISION SHEET. FOR LIMITATIONS IMPOSED ON THE DISTRIBUTION AND USE OF INFORMATION CONTAINED IN THIS DOCUMENT, SEE THE LIMITATIONS SHEET.

MODEL ________ CONTRACT NAS2-9015

ISSUE NO. ________ ISSUED TO: ________

PREPARED BY	M.A. McVeigh M.A. McVeigh	DATE	4/17/79
APPROVED BY	H. Rosenstein	DATE	4/17/79
APPROVED BY	H.R. Alexander	DATE	4/17/79
APPROVED BY		DATE	

LIMITATIONS

PRECEDING PAGE BLANK NOT FILMED

This document is controlled by 7040

All revisions to this document shall be approved by the above noted organization prior to release.

THE **BOEING** COMPANY

NUMBER D210-11505-1
REV LTR

ACTIVE SHEET RECORD

SHEET NUMBER	REV LTR	ADDED SHEETS: SHEET NUMBER	REV LTR	ADDED SHEETS: SHEET NUMBER	REV LTR	SHEET NUMBER	REV LTR	ADDED SHEETS: SHEET NUMBER	REV LTR	ADDED SHEETS: SHEET NUMBER	REV LTR
I						20					
						21					
III						22					
IV						23					
V						23					
VI						25					
VII						26					
VIII						27					
IX						28					
X						29					
XI						30					
XII						31					
XIII						32					
XIV						33					
XV						34					
XVI						35					
XVII						36					
XVIII						37					
XIX						38					
XX						39					
XXI						40					
.						41					
						42					
						43					
						44					
1						45					
2						46					
3						47					
4						48					
5						49					
6						50					
7						51					
8						52					
9						53					
10						54					
11						55					
12						56					
13						57					
14						58					
15						59					
16						60					
17						61					
18						62					
19						63					

FORM 46283 (7/67)

THE **BOEING** COMPANY

NUMBER D210-11505-1
REV LTR

ACTIVE SHEET RECORD

SHEET NUMBER	REV LTR	ADDED SHEETS				SHEET NUMBER	REV LTR	ADDED SHEETS			
		SHEET NUMBER	REV LTR	SHEET NUMBER	REV LTR			SHEET NUMBER	REV LTR	SHEET NUMBER	REV LTR
64						109					
65						110					
66						111					
67						112					
68						113					
69						114					
70						115					
71						116					
72						117					
73						118					
74						119					
75						120					
76						121					
77						122					
78						123					
79						124					
80						125					
81						126					
82						127					
83						128					
84						129					
85						130					
86						131					
87						132					
88						133					
89						134					
90						135					
91						136					
92						137					
93						138					
94						139					
95						140					
96						141					
97						142					
98						143					
99						144					
100						145					
101						146					
102						147					
103						148					
104						149					
105						150					
106						151					
107						152					
108											

FORM 46283 (7/67)

ACTIVE SHEET RECORD

SHEET NUMBER	REV LTR	ADDED SHEETS				SHEET NUMBER	REV LTR	ADDED SHEETS			
		SHEET NUMBER	REV LTR	SHEET NUMBER	REV LTR			SHEET NUMBER	REV LTR	SHEET NUMBER	REV LTR
153						B-19					
154						B-20					
155						B-21					
156						B-22					
157						B-23					
158						B-24					
159						B-25					
160						B-26					
161											
162						C-1					
163						C-2					
164						C-3					
165						C-4					
166						C-5					
167						C-6					
168						C-7					
169						C-8					
170						C-9					
171											
A-1											
A-2											
A-3											
A-4											
A-5											
B-1											
B-2											
B-3											
B-4											
B-5											
B-6											
B-7											
B-8											
B-9											
B-10											
B-11											
B-12											
B-13											
B-14											
B-15											
B-16											
B-17											
B-18											

FORM 46283 (7/67)

REVISIONS

LTR	DESCRIPTION	DATE	APPROVAL

FORM 46282 (3/67)

ABSTRACT

A mathematical model of a hingeless tilting rotor is presented. The model was obtained by a systematic curve-fit procedure applied to an extensive set of model-scale wind tunnel data. The math model equations were used in a real-time flight simulation model of a hingeless tilt rotor XV-15 to assess changes in flying qualities compared to those obtained using a previous rotor model. Extensive plots of the rotor derivatives are given. Discussions of attempts to apply multivariable linear regression techniques to the data and the use of an analytical rotor representation are included.

FOREWORD

This report was prepared by the Boeing Vertol Company of Philadelphia, Pennsylvania for the National Aeronautics and Space Administration, Ames Research Center under NASA Contract NAS2-9015.

Mr. T. Galloway of Ames Research Center was technical monitor for this work. Mr. M. A. McVeigh was the project engineer and the Boeing program manager was Mr. H. R. Alexander.

TABLE OF CONTENTS

LIST OF FIGURES

LIST OF TABLES

LIST OF SYMBOLS

A	Rotor disc area	m^2 (ft^2)
A_1	Lateral cyclic pitch	degrees
B_1	Longitudinal cyclic pitch	degrees
C_T	Rotor thrust coefficient, $T/\rho A V_T^2$	-
C_P	Rotor power coefficient, $HPX550/\rho A F_T^3$	-
C_{NF}	Rotor normal force coefficient, $NF/\rho A V_T^2$	-
C_{SF}	Rotor sideforce coefficient, $SF/\rho A V_T^2$	-
C_{PM}	Rotor pitching moment coefficient, $PM/\rho A V_T^2 R$	-
C_{YM}	Rotor yawing moment coefficient, $YM/\rho A V_T^2 R$	-
C_{BM}	Chordwise bending moment	Nm (in.lb)
HP	Rotor shaft horsepower	W (HP)
I_N	Nacelle angle	degrees
NF	Rotor normal force	N (lb)
PM	Rotor pitching moment	N.m (ft.lb)
R	Rotor radius	m (ft)
r	Blade radial station	m (ft)
SF	Rotor sideforce	N (lb)
T	Rotor thrust	N (lb)
V	Flight speed	m/s (ft/sec)
V_T	Tip speed	m/s (ft/sec)
YM	Rotor yawing moment	N.m (ft.lb)
a_i	Coefficients in a power series	-
α	Angle of attack	degrees

LIST OF SYMBOLS (CONTINUED)

β	Sideslip angle	degrees
δ_F	Wing flap setting	degrees
θ	Aircraft pitch attitude	degrees
$\theta_{.75}$	Blade angle at 75% radius	degrees
μ	Rotor tip speed ratio, V/V_T	-
ψ	Rotor shaft sideslip angle	degrees
Ω	Rotor rotational speed	rad/sec

SUMMARY

This report presents the results of a study whose principal objective was the development of a mathematical model of a hingeless rotor for a tilt-rotor aircraft by synthesizing a set of wind tunnel data obtained on a model of the rotor. A secondary objective was to incorporate this rotor math model into a real-time flight simulation model of a hingeless rotor XV-15 tilt rotor aircraft and determine the effects on the aircraft trim and stability as compared to a former model developed under a previous contract.

The wind tunnel data used in the synthesis was obtained on a 1/4.622 scale model of the Boeing Model 222 tilt rotor aircraft tested under an earlier phase of the contract. The test generated sufficient data to define the rotor behavior over the range of flight speeds anticipated for the modified XV-15 aircraft.
The study was aimed at developing a set of equations that (1) would represent the rotor behavior as determined by the wind tunnel test data, (2) could be evaluated rapidly by a computer so that the computation cycle time requirements of real-time piloted simulation would be met.

Two approaches to developing the math model equations were tried before the final method was selected. The first approach was to apply the techniques of statistical linear regression to the wind tunnel model rotor data. The second approach was to develop a simplified analytical model for the hingeless rotor, correlate the predictions of the analytical model with the measured data and then use the correlation functions with the analysis to yield corrected values. These approaches are presented as appendices.

The actual method adopted was to apply a systematic curve-fitting procedure. The resulting equations together with an extensive set of graphs of the rotor derivatives as obtained from the test data are presented. Numerous plots of the math model results against the corresponding wind tunnel data are provided. These show that the math model equations reproduce the test data very well.

The equations for the rotor were programmed into a previously developed flight simulation math model of the hingeless rotor XV-15 and the effect on aircraft trim and stability observed. It was found that trim is about the same as that calculated with the former rotor math model. The aircraft control derivatives are sufficiently different, however, that control phasing and rescheduling are required in order to maximize control efficiency.

1.0 INTRODUCTION

In many applications of rotor technology, there arises a need to be able to compute rotor forces and moments rapidly and accurately. One such application is real-time flight simulation where the rotor effects must be updated at intervals of less than 60 milliseconds. Existing finite element programs or even modal programs which solve the blade dynamic equations cannot satisfy the requirement for fast computation. In addition, the accuracy of the answers is limited by the sophistication of the analytical model, greater accuracy demands more detailed modeling which increases computation time.

Data Bank

One solution that has been used extensively in the past is to construct a bank of experimental or, less desirably, analytically derived data. Values of rotor hub forces and moments are then obtained by a rapid search and interpolation procedure at specified values of the rotor flight parameters. While this approach may be faster than a purely analytical computation, the range of flight parameters over which the interpolation must take place (airspeed, collective, shaft angle of attack, tip speed, cyclic control) and the need, in some cases, for quadratic rather than linear interpolation, place large demands on data storage and retrieval.

Functional Representation

A more promising approach is to synthesize the data obtained from test or analysis into a set of equations for each variable. For example, it may be possible to develop an equation for rotor normal force involving basic parameters such as μ, $\theta_{.75}$, α, A_1, B_1. The resulting equations may be lengthy and complex, involving products and trigonometric functions of the basic variables, nevertheless, they can provide a very rapid means of calculating the forces or moments. The data synthesis approach may also yield benefits beyond the rapid reproduction of the data, in that functional relationships of a general character may be recognized and may be useful in understanding the physical behavior of the rotor. A further advantage of having a set of equations to represent the rotor forces and moments is that the equations may be used to estimate the behavior of a similar but untested rotor, and provide guidance in the preparation of a cost-effective wind tunnel test plan. In fact, once the general form of the equations is established, the wind tunnel testing could be regarded as a calibration activity.

Previous Work

The functional synthesis approach was adopted during a recent study (Reference 1) which involved development of a mathematical model of the XV-15 aircraft with a hingeless rotor for piloted simulation. In this study, wind tunnel data on a full-scale hingeless rotor obtained under a previous phase of this contract (Reference 2) was reduced to a relatively simple set of equations. Gaps in the wind tunnel data resulting from pressure of time and limitations on the tunnel speed were filled by calculation.

Satisfactory experience with this functional model of the rotor led to the conclusion that it would be worthwhile proceeding to a more definitive and complete model based on the extensive data, reported in Reference 3, that was acquired by testing a 1/4.622 scale model of the same rotor. The development of this new functional representation and the definition of a broad general procedure for performing functional synthesis of rotor test data is the subject of the present report.

Present Studies

Three approaches were explored. The first was an attempt to apply multivariable linear regression techniques to the data. This was motivated by the need to process the large amount of data available in the shortest time. The attempt met with limited success and is described in Appendix A. One of the difficulties encountered using the regression method was in making the correct choice of regression variables. From the previous work it was known that functions like $\mu\cos\alpha$, $\mu^2 C_T\sin\alpha$, etc. would be required. There are, of course, many possible combinations of functions of the basic variables that will yield a satisfactory correlation, and a large factor in the success of the regression technique is making the correct choice of functions. It was, therefore, concluded that theoretical guidance was required. A simplified theoretical analysis was then written to identify these functions. Later, the analysis was tried in a predictor-corrector technique wherein the theoretical predictions were to be correlated with the test data and a correlation function generated. This approach was not pursued when it became evident that the analysis did not correctly predict trends with advance ratio. Results of the analysis and the approach are included as Appendix B.

The approach finally adopted was to develop curve fit equations for the derivatives $\partial C_{NF}/\partial\alpha$, $\partial C_{NF}/\partial A_1$, etc. These were then used to reduce the data to a reference set of values of C_P, C_{NF}, C_{SF}, etc., that were dependent on thrust coefficient, advance ratio and angle of attack only. This dependence was then curve fitted. A full description of the approach to together with extensive correlations with test data is presented in Section 3.

2.0 DATA BASE

The data which forms the basis for the study reported herein was obtained during extensive tests of a 1/4.622 Froude-scale model of the Boeing Model 222 tilt rotor aircraft. The testing and results are reported fully in the four volumes composing Reference 3. A brief description of the test and the nature and extent of the data is provided in this section.

Figure 2.1 shows the tilt rotor model installed in the Boeing Vertol wind tunnel. The test was designed to provide force and moment data on both the airframe and rotor over the expected normal range of flight speeds and attitudes. Data was obtained at seventeen points in the flight spectrum as shown by Figure 2.2. At each of these points, variations were made in fuselage angle of attack, yaw angle, collective pitch, cyclic pitch, wing flap setting and rotor rpm.

The extend of the data is indicated by Table I, which presents a summary of the configurations tested. The selection of test points was made in such a way that a comprehensive set of data was obtained for all potential flight conditions from hover through transition to cruise flight at simulated speeds up to 300 knots. Rotor force and moment data on each rotor was obtained from nacelle-mounted balances. The blades were strain gauged to provide flap and chordwise bending moment information.

Data Inspection

Before beginning a synthesis of the data, the plotted results contained in the four volumes of Reference 3 were inspected in order to identify possible bad data points attributable to such effects as zero shifts. This process resulted in a decision to utilize the data measured on the left-hand rotor only since the right-hand rotor data was questionable in some areas due to strain gauge failures. The acceptable portions of the data on the right rotor were used, however, to cross check the behavior of the left-hand rotor.

Data points that were called into question were inspected further using the microfiched records of the balance force data. As a result of this, the data points were either retained or discarded. The good data points were then punched out on cards and read into a computer program for formating and analysis during the next processing step.

3.0 REDUCTION METHOD AND COMPARISON WITH TEST DATA

Rotor forces and moments (referred to axes fixed in the rotor) depend on seven independent parameters - collective pitch ($\theta_{.75}$), lateral cyclic (A_1), longitudinal cyclic (B_1), shaft angle of attack (α), rotor sideslip angle (ψ), rotor rpm and airspeed. For data reduction purposes it was assumed that any of the force or moment coefficients could be represented by an equation of the form

$$C_F = C_{FR} + \frac{\partial CF}{\partial A_1}(A_1 - A_{1\ ref}) + \frac{\partial CF}{\partial B_1}(B_1 - B_{1\ ref}) + \frac{\partial CF}{\partial \alpha}(\alpha - \alpha_{ref})$$

$$+ \partial C_F/\partial\psi\ \psi + \partial C_F/\partial RPM\ (RPM - RPM_{ref}) \qquad (1)$$

In this equation, C_{FR} is the value of the coefficient at reference values of cyclic, angle of attack and rpm. The reference values are the nominal values at which the rotor was first trimmed to minimum blade loads and then collective pitch varied. Thus the coefficient C_{F_R} may be written

$$C_{F_R} = f(\theta_{75},\ \mu\cos\alpha_{ref},\ A_{1\ ref},\ B_{1\ ref},\ RPM_{ref}) \qquad (2)$$

The variation of these nominal values with the effective rotor advance ratio, $\mu\cos\alpha$, are presented in Figures 3.1 and 3.2. Deviations from these reference conditions are then accounted for by the derivative terms.

In order to establish the derivatives $\partial C_F/\partial A_1$, etc, a run-by-run, data point-by data point inspection of the plots of Reference 3 was conducted. It was found that quite often shifts occurred in one or more of the parameters that were to be held constant. For example, Run 41 was a run in which lateral cyclic was varied with the rotor at 80° angle of attack and 80 knots airspeed. For the first six data points, the longitudinal cyclic (B_1) was held fixed at 5.0 degrees. However for data points 7 through 11, the value of B_1 jumped by 0.3 degrees. By carefully noting such shifts and by using only those data points that met the criteria for a derivative, it was found that a reasonably consistent set of derivatives could be obtained. The values of the derivatives were plotted against $\mu\cos\alpha$ and curves hand-faired through the points. These curves were then fitted by a polynomial in $\mu\cos\alpha$ of the form

$$\frac{\partial CF}{\partial X} = \sum a_i(\mu\cos\alpha)^i \qquad (3)$$

where X represents A_1, B_1, α, ψ and rpm. The values of these coefficients are listed in Tables II through IX. The variation of the derivatives with $\mu\cos\alpha$ are presented in Figures 3.3 through 3.38.

3.1 Determination of the Values of the Coefficients, C_{FR}

The equations for the derivatives, together with the reference values of cyclic, angle of attack and rpm obtained from Figures 3.1 and 3.2 were then used in Equation (1) to compute values for C_{FR} for those runs in which collective alone was varied. The expectation was that the C_{FR} could be a linear function of $\theta_{.75}$ or C_{TR}. Figures 3.39 through 3.44 present the results of this procedure and it can be seen that the expectation of linearity is confirmed.

The next step in the reduction process was to obtain a set of equations that would reproduce the behavior of C_{FR} vs C_{TR} at the different flight conditions, i.e. since

$$C_{FR} = C_{F0} + \frac{\partial C_{FR}}{\partial C_{TR}} C_{TR} \tag{4}$$

the dependence of C_{F0} and $\partial C_{FR}/\partial C_{TR}$ on μ must be established.

The values of C_{F0} and $\partial C_{FR}/\partial C_{TR}$ were plotted against $\mu\sin\alpha$ since previous work indicated that the dependence would be of the form

$$C_{F0} = f\ (\mu\sin\alpha, \mu)$$

$$\frac{\partial C_{FR}}{\partial C_{TR}} = f\ (\mu\sin\alpha, \mu)$$

Figure 3.45 shows the result of this for the case of pitching moment at zero thrust, C_{PM0}. It can be seen that there is insufficient data at fixed μ and different values of α to be able to establish the form of the functions. Various combinations of $\mu\sin\alpha$, $\mu\cos\alpha$ were tried in an attempt to obtain smooth variations of the C_{F0} and $\partial C_{FR}/\partial C_{TR}$ that would include all the data points. None was successful. The most satisfactory approach was to plot the data against μ, fair a line through those points that lay closest to the nominal shaft angle of attack schedule (Figure 3.1), and then fit an equation to the line. A typical result is shown in Figure 3.46. This process was repeated for all the rotor force and moment components.

3.2 Math Model Equations

The final equations for the rotor forces and moments are lengthy since they are combinations of polynomials in μ and $\mu\cos\alpha$ whose coefficients change depending on which portion of the range of μ or $\mu\cos\alpha$ the rotor is operating in. For this reason, the entire set of equations will not be presented here. The equations are given in the form of a small computer subroutine in Appendix C.

The general equation used to calculate the forces and moments is Equation (1) viz

$$C_F = C_{FR} + \frac{\partial CF}{\partial A_1}(A_1 - A_{1\ ref}) + \frac{\partial CF}{\partial B_1}(B_1 - B_{1\ ref}) + \frac{\partial CF}{\partial \alpha}(\alpha - \alpha_{ref})$$

$$+ \partial C_F/\partial\psi\ \psi + \partial C_F/\partial RPM\ (RPM - RPM_{ref})$$

where

$$C_{TR} = \frac{\partial C_{TR}}{\partial \theta_{.75}}(\theta_{.75} - \theta_0) \quad (5)$$

$$C_{PR} = C_{P_0} + \frac{\partial C_{PR}}{\partial C_{TR}} C_{T_R} \quad (6)$$

$$C_{NF_R} = C_{NF_0} + \frac{\partial C_{NFR}}{\partial C_{TR}} C_{TR} \quad (7)$$

$$C_{SF_R} = C_{SF_0} + \frac{\partial C_{SFR}}{\partial C_{TR}} \quad (8)$$

$$C_{PM_R} = C_{PM_0} + \frac{\partial C_{PMR}}{\partial C_{TR}} C_{TR} \quad (9)$$

$$C_{YM_R} = C_{YM_0} + \frac{\partial C_{YMR}}{\partial C_{TR}} C_{TR} \quad (10)$$

in which the quantities $\partial C_{TR}/\partial\theta_{.75}, \theta_0, C_{P0}, \partial C_{PR}/\partial C_{TR}$, etc, are obtained from piecewise curve fit equations with μ or $\mu\cos\alpha$ as argument. The derivatives, $\partial C_T/\partial A_1$, $\partial C_{NF}/\partial B_1$, $\partial C_{PM}/\partial\alpha$, etc., are obtained from

$$\frac{\partial CF}{\partial X} = \sum a_i (\mu\cos\alpha)^i \quad (11)$$

where the a_i are listed in Tables II through IX, and are furnished by the array X(I,J,K) in the subroutine.

The equations that define the reference quantities α_{ref}, A_{1ref}, B_{1ref} and RPM_{ref}, presented in Figures 3-1 and 3-2, are:

$$\alpha_{ref} = 89.72 - 322.8Z + 770.41Z^2 - 1446.34Z^3 + 1449.9Z^4 - 545.115Z^5 \qquad (12)$$

where

$$Z = \mu\cos\alpha$$

$$A_{1ref} = B_{1ref} = 5.0° \qquad (13)$$

and the reference rpm is a function of nacelle angle, i_N,

$$RPM_{ref} = 1185 \qquad i_N > 45°$$

$$= 1185 - 7.89(45 - i_N) \qquad i_N < 45°$$

The calculation procedure is illustrated by the following example.

If $0 < \mu\cos\alpha < .015$,

$$\frac{\partial C_{TR}}{\partial \theta_{.75}} = (11.933Z + 0.882)/1000$$

$$\theta_0 = -1.5 + 106.667Z$$

and equation (5) yields the reference thrust coefficient C_{TR}. Equation (11) is now used to calculate the derivatives and equations (12), (13) and (14) used to compute the reference quantities. The total thrust coefficient C_T is then calculated for the given values of cyclic, angle of attack, yaw angle, and rpm.

For the same range of $\mu\cos\alpha$ the power coefficient at zero thrust, C_{P0} is

$$C_{P0} = (.035 - 9.667Z)/1000$$

and

$$\frac{\partial C_{PR}}{\partial C_{TR}} = .094 - .267Z$$

The total power coefficient is then obtained in the same way as thrust.

If $0<\mu<.51$ the equation for normal force coefficient at zero thrust, C_{NF0}, is

$$1000 \times C_{NF_0} = -1.45 + 1.1164\mu + 46.159\mu^2 + 46.153\mu^3 -4118.75\mu^4 + 27714.8\mu^5 -74786\mu^6 + 89304\mu^7 -39318\mu^8$$

and the gradient with thrust coefficient is given by

$$\frac{dC_{NFR}}{dC_{TR}} = -.0087 + 2.122\mu -10.95\mu^2 -34.52\mu^3 + 420\mu^4 -1043\mu^5 + 520.8\mu^6 + 1029\mu^7 -966\mu^8$$

Using these quantities in equation (7) the reference normal force coefficient is calculated and finally the total normal force obtained from equation (1). The same procedures are used to calculate sideforce, pitching moment and yawing moment.

3.3 Comparison with the Test Data

The equations described in 3.2 were used to generate estimated values for the left rotor forces and moments at all the conditions investigated during the entire wind tunnel test. An extensive series of plots of the estimated and actual forces and moments were then made.

3.3.1 Collective Sweeps

The first test of the ability of the equations to reproduce the test data is to see how well the forces obtained during collective sweeps are estimated, since this is the data which was the most difficult to collapse. Figures 3.47 through 3.52 present comparisons of estimated and test values of C_T, C_P, C_{NF}, C_{SF}, C_{PM} and C_{YM}, respectively. Thrust is estimated to within 10% of the measured thrust at the same value of collective pitch. The estimated variation of power coefficient with thrust coefficient is also satisfactory at all the test conditions with the exception of hover at high values of C_T(.013) where the estimate is about 9% too low. Normal force estimates are also acceptable bearing in mind that, unlike power and thrust, normal force is very sensitive to cyclic and the accuracy achieved depends on how well the values of

the cyclic derivatives are fitted. Similar remarks apply to the comparisons of estimated and actual values for sideforce, pitching moment and yawing moment.

3.3.2 Detailed Comparisons at Points in the Transition Corridor

Figures 3.53 through 3.135 present a detailed comparison of the estimates obtained from the math model equations with the test values at three points in a typical tilt rotor transition corridor:

1. Hover
2. 45 knots and 90 degrees nacelle angle
3. 180 knots and 15 degrees nacelle angle

The comparisons are presented in the form of copies of the original wind tunnel data plots with the estimated values superimposed.

In hover, Figures 3.53 to 3.70, the rotor response to lateral and longitudinal cyclic is estimated very well considering the degree of scatter that exists in the measured data. The behavior with collective is reproduced nearly exactly.

For the early transition test condition of 45 knots and 90 degrees nacelle angle, Figures 3.71 to 3.106, the estimated variation of the forces and moments with lateral cyclic, A_1, is generally in good agreement while the response to longitudinal cyclic, B_1, is in very good agreement with the exception that the estimated yawing moment is displaced from the measured values. The correct slope of yawing moment with B_1 is predicted correctly, however. The dependence of the forces and moments on θ_{75} is estimated well, again with the observation that yawing moment is displaced. For those runs where shaft angle was varied, Figures 3.89 through 3.94, it can be seen that the math model shows a weak dependence on shaft angle, α. This is attributed to the use of the parameter $\mu\cos\alpha$ in the equations since $\mu\cos\alpha$ changes rapidly near α = 90 degrees. Comparison of the estimated and test behavior of the data during yaw angle sweeps shows that the effect of yaw angle is not correctly estimated for normal force and pitching moment. This defect is probably due to the derivative curve fit in this region. The effect of rpm changes is reproduced well.

Figures 3.107 through 3.135 present the comparisons for a high speed end of transition condition, 180 knots and 15 degrees nacelle angle. Response to longitudinal cyclic is estimated extremely well for thrust, normal force, sideforce, pitching moment and yawing moment. The response of power coefficient

to B_1 is too exaggerated, however. The angle of attack sensitivities are reproduced very well and predicted yaw angle effects are also satisfactory. The effect of rpm variations are less satisfactory for this condition.

From the comparisons presented here it is concluded that the curve fit equations reproduce the test data sufficiently accurately for simulation purposes. The incorporation of the equations into the simulation math model of Reference 1 and the results are discussed in the following section.

4.0 EFFECT ON AIRCRAFT TRIM AND STABILITY

The math model equations for the rotor described in Section 3.0 were incorporated in the simulation model of the hingeless rotor XV-15 aircraft. This simulation model is detailed in Reference 1. The new equations, in the form of the subroutine given in Appendix C, replace the set of equations described in that Reference. An exception is that the pitch and yaw rate derivatives were retained since the test data on which the new equations are based does not contain rate effects.

The new rotor equations yield the forces and moments in a set of axes fixed in the rotor rather than the wind axes system used in the former equations. Some existing transformations from wind to body axes were therefore eliminated and others added.

4.1 Comparison with the Former Rotor Model

The simulation math model incorporating the new rotor equations was used to assess the effect of the updated rotor representation on the trim and stability of the XV-15/hingeless rotor aircraft and to ascertain whether control schedule changes would be required. Tables X through XIV present comparisons of aircraft trim attitude and control settings required and derivatives at selected points in the transition corridor.

From Table X it can be seen that the introduction of the updated rotor representation does not substantially change the values of trim pitch attitude (θ), stick position (δ_B) or throttle setting (δ_{TH}). The values of lateral (A_1) and longitudinal (B_1) cyclic (referred to the classical wind axes) are changed, however. With the new rotor math model, approximately twice as much lateral cyclic is required and about half as much longitudinal cyclic. The total cyclic, $\sqrt{A_1{}^2+B_1{}^2}$, is about the same with both rotor representations. The different cyclic requirements reflect the different sensitivities to cyclic and angle of attack given by the two models. Since the new rotor representation has been shown to be in very good agreement with the test data, a re-phasing of the cyclic inputs to maximize control force and moment is indicated.

Tables XI through XIV present preliminary comparisons of the aircraft derivatives obtained using the present and former rotor models. Because of the altered cyclic sensitivities some of the control derivatives are changed and the control system gains and schedules require reworking to provide acceptable flying qualities. The controls-fixed derivatives L_p, M_q, N_r, X_u, Y_v, Z_w, for the 60 knot, $i_N = 75°$ condition

are comparable with the two models. The off-diagonal derivative, Y_p, side force due to roll rate, is changed in sign compared to the present model. The reason for this has not yet been established. For the 140 Kt, $i_N = 60°$ case (Tables XI and XII), the principal derivatives L_p and Z_w differ from the former model. The source of these differences is yet to be uncovered but a preliminary examination indicates that the new model exhibits a higher sensitivity of thrust to combinations of angle of attack and effective rpm changes such as occur during rolling, than did the former model.

5.0. CONCLUSIONS AND RECOMMENDATIONS

The objective of the study was to develop a functional representation of a hingeless rotor based on extensive wind tunnel data and to incorporate this representation into a real-time simulation math model of a hingeless rotor XV-15. Changes in flying qualities caused by the new rotor representation were to be determined and noted.

Conclusions

1. A mathematical representation of the rotor data was developed through a systematic curve-fitting approach. The results show that the curve-fit equations reproduce the wind tunnel data very well.

2. The rotor equations were incorporated into the simulation model. Preliminary evaluation of trim and derivative data show that cyclic rephasing is required in order to optimize the aircraft response to control. Stick-fixed behavior of the aircraft is generally comparable to that obtained using the former rotor representation.

3. Extensive plots of the rotor derivatives as functions of the effective advance ratio have been presented. These are of considerable value in themselves since they may be used to assess rotor behavior for similar configurations.

4. A curve-fit representation of the rotor, although lengthy, satisfies the computational speed requirements of real-time simulation just as well as the equations in a functional representation. This is because the functional representation, although simpler in form, involves computer evaluations of transcendental functions, e.g., $\mathrm{Tan}^{-1}x$, $\sin\alpha$ etc. which require as much time as the evaluation of polynomials in the curve-fit approach.

5. An attempt was made to automate the process of data synthesis using multivariable linear regression. In principle, if a sufficiently large number of candidate correlates are available to the regression algorithm then a successful synthesis should result. However, the likely correlates must be supplied to the computer and the selection of the correct correlates requires a considerable amount of skill, if not luck. The final equations produced by the regression, while they may fit the particular set of data used, are not necessarily of a general enough nature that they can be extended to other rotor configurations by simply altering constants in the equations.

Recommendations

1. Probably the best overall approach to the problem of providing a fast, but general, algorithm for rotor representation in real-time simulation is to develop a simplified analysis whose predictions can be calibrated against wind tunnel data. These analytical predictions would then be operated on by the calibration functions to produce estimates of the rotor forces and moments. A step in this direction was made in this study but more work is required.

2. A further recommendation is that during the preparation of wind tunnel test run schedules, every effort should be made to select the runs so that the natural parameters of the rotor are systematically varied over a broad enough range that the data synthesis process is facilitated. For example, when testing at different rotor shaft angles at fixed airspeed, such as is required for transition corridor definition, it is desirable to do this at a series of fixed values of rotor rpm even though the aircraft will not necessarily operate at some of the rpm values. This will, however, ensure that data exists over a wide enough range of values of μ, $\mu\sin\alpha$, $\mu\cos\alpha$ that curves may be confidently drawn through points of constant $\mu\sin\alpha$, for example, and equations fitted to them.

3. The final recommendation arises from the difficulties experienced in extracting rotor derivatives from the test data. The wind tunnel run schedule was purposely designed to acquire rotor derivative data directly, by making runs in which one control at a time was varied while the others were fixed.

   Unfortunately, during many of the runs, shifts in cyclic, collective pitch or shaft angle occurred. This made the job of extracting rotor derivatives very laborious since each point had to be inspected to make sure that the fixed controls had actually remained fixed during the run. It is therefore recommended that in future tests of this nature every effort should be made to ensure that the control settings remain at the desired levels. This may require the use of more complex and more accurate rotor control systems than the simple position-feedback system used in this test.

6.0 REFERENCES

1. McVeigh, M.A.: "Preliminary Simulation of an Advanced Hingeless Rotor XV-15 Tilt Rotor Aircraft", NASA CR151950, December 1976

2. Magee, J.P. and Alexander, H.R.: "Wind Tunnel Tests of a Full Scale Hingeless Prop/Rotor Designed for the Boeing Model 222 Tilt Rotor Aircraft", NASA CR114644, September 1973

3. Magee, J.P. and Alexander, H.R.: "Wind Tunnel Tests of a 1/4.622 Froude-Scale Hingeless Rotor Tilt Rotor Model", In four volumes, NASA CR-151936 through 151939, September 1976

4. Dommasch, D.O.: "Force and Moment Coefficients for the Elastic "Rigid" Rotor" DODCO Inc., DODCO TR#231 October 1967

5. Bramwell, A.R.S.: "Helicopter Dynamics", Wiley, New York

CONDITION	PARAMETER VARIED	FIGURES	V	α_{FUSE}	i_N	RPM	TEST VARIABLES HELD CONSTANT									DATA SET
							θ_{75_L}	A_{1_L}	B_{1_L}	δ_{F_L}	θ_{75_R}	A_{1_R}	B_{1_R}	δ_{F_R}	β	
HOVER $I_N = 90°$	$\theta_{.75}$	1-18	0	0	90	1185		-.6	.4	70.0		-.6	-.7	70	0	1
	$\theta_{.75}$	1-18	0	0	90	1110		-.6	.4	70.0		-.6	-.7	70	0	
	LONG. CYC.	19-36	0	0	90	1110	10.0	-.5		70.0	10.0	.1		70	0	
	LAT. CYC.	37-54	0	0	90	1110	10.0		.2	70.0	10.0		-.2	70	0	
TRANSITION $I_N = 90°$ $V_{FS} = 45$ KTS	α	1-24	43		90	1185	7.8	-.4	4.7	73.6	9.0	.09	4.9	70	0	2
	YAW ANGLE	25-48	44	0	90	1183	8.0	-.4	5.0	64.0	9.3	.55	5.0	71		
	LONG. CYC.	49-72	44	-10.0	90	1183	8.0	-.4		73.0	9.0	1.1		70	0	
	LAT. CYC.	73-96	44	-10.0	90	1183	8.0		5.0	71.0	9.3		5.0	71	0	
	$\theta_{.75}$	97-120	44	-9.9	90	1183		.4	4.7	69.0		.43	4.7	71	0	
	δ_{FLAP}	121-144	45	-9.9	90	1185	8.0	-.2	4.8		9.3	.5	4.8	69	.8	
	RPM	145-168	44	-9.9	90		8.1	-.25	4.8	69.0	9.4	.5	4.8	69	.8	
TRANSITION $I_N = 90°$ $V_{FS} = 100$ KTS	α	1-24	100		90	1183	12.0	4.1	6.2	70.0	11.3	5.2	6.8	70	0	3
	YAW ANGLE	25-48	100	-15.0	90	1183	12.1	4.1	6.2	70.0	11.3	5.4	6.8	70		
	LONG. CYC.	49-72	100	-15.0	90	1185	11.8	4.1		70.0	10.9	5.3		70	0	
	LAT. CYC.	73-96	100	-15.0	90	1183	12.2		6.2	70.0	11.4		6.8	70	0	
	$\theta_{.75}$	97-120	100	-15.0	90	1185		4.5	6.5	70.0		5.1	6.5	70	0	
	δ_{FLAP}	121-144	100	-15.0	90	1183	12.0	4.0	6.4		11.2	5.1	6.6	70	0	
	RPM	145-168	100	-15.0	91		12.0	4.0	6.4	70.0	11.2	5.1	6.6	70	0	
TRANSITION $I_N = 70°$ $V_{FS} = 45$ KTS	α	1-24	45		70	1185	8.9	-.75	5.0	61.0	10.0	.7	4.9	61	.4	4
	YAW ANGLE	25-48	45	12.0	70	1183	8.9	-.75	5.0	61.0	10.0	.15	5.0	61		
	LONG. CYC.	49-72	43	12.0	70	1185	8.4	-.8		61.0	9.7	.7		61	.4	
	LAT. CYC.	73-96	44	11.9	70	1185	9.2		5.0	61.0	9.9		5.0	61	.5	
	$\theta_{.75}$	97-120	44	11.9	70	1183		-.5	5.0	61.0		-.45	5.0	61	.1	
	δ_{FLAP}	121-144	44	11.9	70	1185	8.9	-.7	5.0		10.0	.85	5.0		.1	
	RPM	145-168	44	11.9	70		8.9	-.7	5.0	30.0	10.0	.85	5.0	30	.1	

TABLE I. CONFIGURATIONS TESTED

							TEST VARIABLES HELD CONSTANT									
CONDITION	PARAMETER VARIED	FIGURES	V	α_{FUSE}	I_N	RPM	θ_{75_L}	A_{1_L}	B_{1_L}	δ_{F_L}	θ_{75_R}	A_{1_R}	B_{1_R}	δ_{F_r}	β	DATA SET
TRANSITION I_N = 70° V_{FS} = 100 KTS	α	1-24	99		70	1185	13.6	3.6	5.2	61	12.5	3.9	4.6	61.0	.1	5
	YAW ANGLE	25-48	99	-5.0	70	1184	13.4	3.7	5.4	61	12.3	4.0	5.4	61.0		
	LONG. CYC.	49-72	100	-6.0	70	1185	13.3	4.3		61	12.6	4.3		61.0	0	
	LAT. CYC.	73-96	100	-6.0	70	1185	13.3		5.6	61	12.2		5.4	61.0	0	
	$\theta_{.75}$	97-120	100	-6.0	70	1185		4.2	5.5	61		4.6	5.0	61.0	0	
	δ_{FLAP}	121-144	100	-6.0	70	1183	13.5	4.2	5.3		12.2	4.5	5.2		0	
	RPM	145-168	100	-6.0	70		13.5	4.2	5.3	61	12.2	4.5	5.2	61.0	0	
TRANSITION I_N = 70° V_{FS} = 140 KTS	α	1-18	140		70	1185	18.2	6.0	5.9	60	17.3	7.2	6.6	60.0	-.5	6
	YAW ANGLE	19-36	140	-11.0	70	1183	18.2	6.0	5.9	60	17.2	7.2	6.6	60.0		
	LONG. CYC.	37-54	140	-10.9	70	1183	17.9	5.7		60	17.7	7.1		60.0	-.5	
	LAT. CYC.	55-72	140	-10.9	70	1185	18.3		5.9	60	17.5		6.9	60.0	-.5	
	$\theta_{.75}$	73-90	140	-10.9	70	1183		5.7	5.7	60		7.0	5.5	60.0	-.5	
	δ_{FLAP}	91-108	140	-10.9	70	1183	18.0	5.8	6.1		17.3	7.0	6.4		-.5	
	RPM	109-126	140	-10.9	70		18.0	5.8	6.1	61	17.3	7.0	6.4	61.0	-.5	
TRANSITION I_N = 50° V_{FS} = 100 KTS	α	1-24	100		50	1185	15.9	3.0	4.3	42	14.6	3.5	4.0	42.0	0	7
	YAW ANGLE	25-48	100	-9.5	50	1184	16.3	3.5	4.2	41	15.0	4.1	4.1	42.0		
	LONG. CYC.	49-72	100	-9.5	50	1185	16.0	3.0		41	15.0	4.0		42.0	-.6	
	LAT. CYC.	73-96	100	-9.5	50	1183	16.0		4.3	41	15.0		4.2	42.0	-.6	
	$\theta_{.75}$	97-120	100	-9.5	50	1183		3.2	4.1	41		4.0	3.8	42.0	-.6	
	δ_{FLAP}	121-144	100	-9.5	50	1185	16.2	3.2	4.1		14.9	4.8	4.6		-.6	
	RPM	145-168	100	-9.5	50		16.2	3.2	4.0	42	14.9	4.0	4.0	42.0	-.6	
TRANSITION I_N = 50° V_{FS} = 140 KTS	α	1-18	140		50	1185	22.5	5.0	4.75	42	20.6	5.9	4.5	42.0	-.6	8
	YAW ANGLE	19-36	140	-8.0	50	1185	22.5	5.0	4.75	42	20.6	5.9	4.5	42.0		
	LONG. CYC.	37-54	140	-8.0	50	1185	22.5	5.0		42	20.5	5.7		42.0	-.5	
	LAT. CYC.	55-72	140	-8.0	50	1185	22.5		4.5	42	20.6		4.5	42.0	-.5	
	$\theta_{.75}$	73-90	140	-8.0	50	1185		5.2	4.4	42		5.6	4.0	42.0	-.5	
	δ_{FLAP}	91-108	140	-8.0	50	1185	22.2	5.5	4.3		20.7	5.7	4.6		-.5	
	RPM	109-126	140	-8.0	50		22.6	5.4	4.6	42	20.9	5.8	4.7	42.0	-.5	

TABLE I. CONFIGURATIONS TESTED (Continued)

					TEST VARIABLES HELD CONSTANT										
CONDITION	PARAMETER VARIED	FIGURES	V	α_{FUSE}	i_W	RPM	$\theta_{.75_L}$	A_{1_L}	B_{1_L}	δ_{F_L}	$\theta_{.75_R}$	A_{1_R}	B_{1_R}	δ_{F_r}	β	DATA SET
TRANSITION	α	1-24	100		26	1063	20.0	2.8	3.4	30.0	18.2	3.7	3.8	30.0	0	9
i_W = 30°	YAW ANGLE	25-48	100	3.5	28	1063	20.6	2.8	3.4	30.0	18.2	3.7	3.6	30.0		
V_{FS} = 100 KTS	LONG. CYC.	49-72	100	3.5	29	1063	20.7	2.8		30.0	18.0	3.6		30.0	0	
	LAT. CYC.	73-96	100	3.5	29	1063	20.8		3.6	30.0	18.1		3.6	30.0	0	
	$\theta_{.75}$	97-120	100	3.5	29	1063		3.1	3.4	30.0		3.7	3.5	30.0	0	
	δ_{FLAP}	121-144	100	3.5	30	1063	20.7	3.1	3.5		18.1	3.8	3.5		0	
	RPM	145-168	100	3.5	30		20.7	3.1	3.5	30.0	18.1	3.8	3.5	30.0	0	
TRANSITION	α	1-24	140		30	1065	28.8	4.5	4.0	33.0	26.9	5.1	4.3	32.0	0	10
i_W = 30°	YAW ANGLE	25-48	140	-3.0	30	1065	29.0	4.5	3.9	33.0	27.1	5.0	4.4	32.0		
V_{FS} = 140 KTS	LONG. CYC.	49-72	140	-3.0	30	1064	29.0	4.4		33.0	26.0	5.0		32.0	0	
	LAT. CYC.	73-96	140	-3.0	30	1064	29.0		3.9	33.0	27.0		4.4	32.0	0	
	$\theta_{.75}$	97-120	140	-3.0	30	1065		4.4	3.7	33.0		5.0	4.3	32.0	0	
	δ_{FLAP}	121-144	140	-3.0	30	1063	29.1	4.4	3.9		27.0	5.1	4.3		0	
	RPM	145-168	140	-3.0	30		29.1	4.4	3.9	31.0	27.0	5.1	4.3	31.0	0	
TRANSITION	α	1-24	180		30	1065	32.1	6.0	5.0	30.0	32.3	6.0	5.3	30.0	0	11
i_W = 30°	YAW ANGLE	25-48	180	-5.9	30	1065	32.1	5.9	5.0	30.0	32.2	6.0	5.3	30.0		
V_{FS} = 180 KTS	LONG. CYC.	49-72	180	-5.9	30	1065	32.0	6.2		30.0	32.0	6.0		30.0	0	
	LAT. CYC.	73-96	180	-5.9	30	1063	32.3		4.8	30.0	32.2		5.3	30.0	0	
	$\theta_{.75}$	97-120	180	-5.9	30	1065		6.3	5.0	30.0		6.2	5.5	30.0	0	
	δ_{FLAP}	121-144	180	-5.9	30	1063	31.9	6.3	5.0		32.3	6.4	5.5		.1	
	RPM	145-168	180	-5.9	30		31.9	6.3	5.0	30.0	32.3	6.4	5.6	30.0	.1	
TRANSITION	α	1-24	180		15	945	37.5	4.2	3.5	19.5	38.0	4.0	4.1	19.7	0	12
i_W = 15°	YAW ANGLE	25-48	180	-1.99	15	946	37.5		3.4	19.5	37.6	4.5	3.8	19.7		
V_{FS} = 180 KTS	LONG. CYC.	49-72	180	-1.99	15	945	37.5			19.5	37.7	4.0		19.7	.5	
	LAT. CYC.	73-96	180	-1.99	15	942	37.7		3.5	19.5	38.0		4.0	19.7	.5	
	$\theta_{.75}$	97-120	180	-1.99	15	945			3.5	19.5		4.0	4.0	19.7	.5	
	δ_{FLAP}	121-144	180	-1.99	15	945	37.4		3.3		37.6	4.3	4.0		.5	
	RPM	145-168	180	-1.99	15		37.5		3.3	20.7	37.6	4.1	4.0	20.0	.5	

TABLE I. CONFIGURATIONS TESTED (Continued)

CONDITION	PARAMETER VARIED	FIGURES	V	α_{FUSE}	I_H	RPM	θ_{75_L}	A_{1_L}	B_{1_L}	δ_{F_L}	θ_{75_R}	A_{1_R}	B_{1_R}	δ_{F_r}	β	DATA SET
							TEST VARIABLES HELD CONSTANT									
CRUISE	α	1-24	140		-1.4	830	33.8	-.18	-.7	0	34.6	0	0	0	0	13 →
I_H = -1°	α		140		-1.4	830	33.8	-.18	-.7	10.0	34.6	0	0	10.0	0	
V_{FS} = 140 KTS	α		140		-1.4	830	33.8	-.18	-.7	20.0	34.6	0	0	20.0	0	
	YAW ANGLE	25-48	139	0	-1.5	829	34.1	-.2	-.5	0	34.8	-.1	.1	0		
	LONG. CYC.	49-72	137	0	-1.3	829	33.7	-.2		0	34.1	-.1		0	0	
	LAT. CYC.	73-96	139	0	-1.4	829	33.9		-.4	0	35.2		0	0	0	
	α	97,98,100,101	139		-1.4	830	33.8	-.18	-.7	-6.8	34.6	0	0	-.1	0	
	α	97-102	137		-1.1	830	33.7			0	34.3			0	0	
CRUISE	α	1-24	180		-1.4	830	41.4	-.3	-1.0	-.1	42.2	-.3	-.2	0	.3	14 →
I_H = -1°	α		180		-1.4	829	41.4	-.3	-1.0	9.8	42.3	-.4	-.1	9.6	.3	
V_{FS} = 180 KTS	α		180		-1.4	830	41.4	-.3	-1.0	19.9	42.3	-.4	-.1	19.9	.3	
	YAW ANGLE	25-48	180	0	-1.4	830	41.4	-.3	-1.0	.2	42.3	-.5	-.2	0		
	LONG. CYC.	49-72	180	0	-1.4	830	41.5	-.5		.2	42.5	-.6		0	.2	
	LAT. CYC.	73-97	180	0	-1.4	830	41.9		-1.0	.1	42.6		-.7	0	.2	
	α	88,89,91,92	180		-1.4	830	41.4	-.3	-1.0	-.1	42.2	-.3	-.2	0	.3	
	α	88-93	180		-1.4	828	41.5			.2	42.5			.1	.2	
CRUISE	α	1-24	220		-1.5	830	47.1	.1	-.8	.2	48.1	-.3	-.1	.5	.2	15 →
I_H = -1.5°	α		220		-1.5	830	47.1	.1	-.8	4.0	48.1	-.3	-.1	5.0	.2	
V_{FS} = 220 KTS	α		220		-1.5	830	47.1	.1	-.8	9.7	48.1	-.3	-.1	9.7	.2	
	YAW ANGLE	25-48	220	0	-1.5	829	47.1	.1	-.8	0	48.1	-.3	-.1	0		
	LONG. CYC.	49-72	219	0	-1.4	829	46.9	.1		0	47.5	-.3		0	0	
	LAT. CYC.	73-96	219	0	-1.4	828	47.0		-.6	0	48.1		-.1	0	0	
	α	97,98,100,101	220		-1.5	830	47.1	.1	-.3	.2	48.1	-.3	-.1	.5	.2	
	α	97-102	219		-1.4	826	47.3			.7	48.1			.2	.1	

TABLE I. CONFIGURATIONS TESTED (Continued)

CONDITION	PARAMETER VARIED	FIGURES	V	α_{FUSE}	I_N	RPM	θ_{75_L}	A_{1_L}	B_{1_L}	δ_{F_L}	θ_{75_R}	A_{1_R}	B_{1_R}	δ_{F_r}	β	DATA SET
							TEST VARIABLES HELD CONSTANT									
CRUISE	α	1-24	259		-1.4	827	52.1	.2	-.1	.5	53.2	0	-.3	.3	.1	16
I_N = -1°	α		259		-1.4	827	52.1	.2	-.1	4.9	53.2	0	-.3	5.2	.1	
V_{FS} = 260 KTS	YAW ANGLE	25-48	259	0	-1.5	828	51.9	-.5	-.9	-.1	53.2	0	-.3	-.1		
	LONG. CYC.	49-72	259	0	-1.5	829	51.7	.3		-.4	53.3	0		-.1	.1	
	LAT. CYC.	73-96	259	0	-1.5	831	51.6		-1.0	-.1	53.2		-.4	-.1	.1	
	α	97,98,100,101	259		-1.4	827	52.1	.2	-.1	.5	53.2	0	-.4	-.1	.1	
	α	97-102	259		-1.3	830	51.8			-.1	53.4			-.1	.1	
CRUISE	α	1-24	299		-1.5	827	56.2	.3	-.75	-1.5	57.9	.35	-.27	-.1	.1	17
I_N = -1°	YAW ANGLE	25-48	299	0	-1.4	827	56.4	0	-.8	-1.5	57.9	.35	-.27	-.1		
V_{FS} = 300 KTS	LONG. CYC.	49-63	299	0	-1.4	825	56.3	.2		-1.5	57.9	.35		-.1	0	
	LAT. CYC.	64-87	299	0	-1.4	825	56.0		-.8	-1.5	57.7		-.27	-.1	0	
	α	88,89,91,92	299		-1.5	827	56.2	.3	-.75	-.15	57.9	.35	-.27	-.1	.1	
	α	88-93	299		-1.5	827	56.0			-.15	57.7			-.1	.1	

TABLE I. CONFIGURATIONS TESTED (Concluded)

Table II. Coefficients for Thrust Coefficient Derivatives

	a_1	a_2	a_3	a_4	a_5	a_6	a_7	a_8
$\partial C_T/\partial A_1$	-0.4606E 00	-0.4788E 01	-0.2745E 03	0.1200E 04	-0.1752E 04	0.9966E 03	-0.1652E 03	0.0000E 00
$\partial C_T/\partial B_1$	-0.1416E 00	-0.5737E 02	0.2480E 03	-0.4604E 03	0.3999E 03	-0.1319E 03	0.0000E 00	0.0000E 00
$\partial C_T/\partial \alpha$	-0.7110E-01	0.1453E 03	-0.1733E 04	0.8800E 04	-0.2198E 05	0.2850E 05	-0.1849E 05	0.4753E 04
$\partial C_T/\partial \psi$	0.0000E 00	0.0000E 00	0.0000E 00	0.0000E 00	0.0000E 00	0.0000E 00	0.0000E 00	0.0000E 00
$\partial C_T/\partial_{RPM}$	0.0000E 00	0.9400E 00	0.0000E 00	0.0000E 00	0.0000E 00	0.0000E 00	0.0000E 00	0.0000E 00

Table III. Coefficients for Power Coefficient Derivatives

	a_1	a_2	a_3	a_4	a_5	a_6	a_7	a_8
$\partial C_p/\partial A_1$	-0.3530E-01	0.1495E 01	-0.2166E 02	0.2054E 02	0.0000E 00	0.0000E 00	0.0000E 00	0.0000E 00
$\partial C_p/\partial B_1$	0.2670E-01	-0.2693E 01	0.6550E 00	-0.1486E 02	0.1711E 02	0.0000E 00	0.0000E 00	0.0000E 00
$\partial C_p/\partial \alpha$	0.1100E-01	0.1651E 01	0.6509E 01	0.3814E 02	-0.2203E 03	0.2877E 03	-0.1156E 03	0.0000E 00
$\partial C_p/\partial \psi$	0.0000E 00	0.0000E 00	0.0000E 00	0.0000E 00	0.0000E 00	0.0000E 00	0.0000E 00	0.0000E 00
$\partial C_p/\partial_{RPM}$	-0.9700E-0[illegible]	-0.7640E-02	0.8940E 00	0.0000E 00	0.0000E 00	0.0000E 00	0.0000E 00	0.0000E 00

Table IV. Coefficients for Normal Force Derivatives

	a_1	a_2	a_3	a_4	a_5	a_6	a_7	a_8
$\partial C_{NF}/\partial A_1$	-0.1371E 01	0.1690E 02	-0.2104E 03	0.5176E 03	-0.5038E 03	0.1773E 03	0.0000E 00	0.0000E 00
$\partial C_{NF}/\partial B_1$	-0.1422E 01	0.5147E 01	-0.2742E 02	0.0000E 00	0.0000E 00	0.0000E 00	0.0000E 00	0.0000E 00
$\partial C_{NF}/\partial \alpha$	0.2853E 00	-0.7502E 01	0.3427E 02	0.0000E 00	0.0000E 00	0.0000E 00	0.0000E 00	0.0000E 00
$\partial C_{NF}/\partial \psi$	0.2030E-01	0.2633E 01	-0.2825E 02	0.4968E 02	-0.1105E 02	0.0000E 00	0.0000E 00	0.0000E 00
$\partial C_{NF}/\partial_{RPM}$	0.1600E-03	0.2342E-01	-0.1129E 01	0.1712E 01	-0.7423E 00	0.0000E 00	0.0000E 00	0.0000E 00

Table V. Coefficients for Sideforce Derivatives.

	a_1	a_2	a_3	a_4	a_5	a_6	a_7	a_8
$\partial C_{SF}/\partial A_1$	0.7213E 00	0.1084E 02	-0.1761E 03	0.6883E 03	-0.8232E 03	0.3206E 03	0.0000E 00	0.0000E 00
$\partial C_{SF}/\partial B_1$	-0.1232E 01	0.1765E 01	-0.4897E 02	0.6304E 02	-0.2846E 02	0.0000E 00	0.0000E 00	0.0000E 00
$\partial C_{SF}/\partial \alpha$	-0.1170E-01	-0.5595E 01	0.7841E 02	-0.1572E 03	0.7496E 02	0.0000E 00	0.0000E 00	0.0000E 00
$\partial C_{SF}/\partial \psi$	0.1416E 00	-0.5063E 01	0.3599E 02	-0.1030E 02	0.0000E 00	0.0000E 00	0.0000E 00	0.0000E 00
$\partial C_{SF}/\partial_{RPM}$	0.5500E-03	-0.1219E-01	-0.5270E 01	0.4619E 02	-0.1262E 03	0.1411E 03	-0.5569E 02	0.0000E 00

Table VI. Coefficients for Pitching Moment Derivatives

	a_1	a_2	a_3	a_4	a_5	a_6	a_7	a_8
$\partial C_{PM}/\partial A_1$	-0.9261E 00	-0.1969E 02	0.1161E 03	-0.1508E 03	0.6084E 02	0.0000E 00	0.0000E 00	0.0000E 00
$\partial C_{PM}/\partial B_1$	-0.3212E 01	-0.5118E 01	-0.1174E 02	0.4390E 02	-0.2674E 02	0.0000E 00	0.0000E 00	0.0000E 00
$\partial C_{PM}/\partial \alpha$	0.3494E 00	0.4544E 01	-0.7210E 01	0.0000E 00	0.0000E 00	0.0000E 00	0.0000E 00	0.0000E 00
$\partial C_{PM}/\partial \psi$	0.5250E-01	-0.2972E 01	0.2979E 02	-0.3286E 02	0.1048E 02	0.0000E 00	0.0000E 00	0.0000E 00
$\partial C_{PM}/\partial_{RPM}$	-0.1000E-03	-0.9926E-01	0.1248E 00	-0.5549E-01	0.0000E 00	0.0000E 00	0.0000E 00	0.0000E 00

Table VII. Coefficients for Yawing Moment Derivatives

	a_1	a_2	a_3	a_4	a_5	a_6	a_7	a_8
$\partial C_{YM}/\partial A_1$	0.3008E 01	-0.7260E 00	0.6013E 02	-0.1995E 03	0.2035E 03	-0.7061E 02	0.0000E 00	0.0000E 00
$\partial C_{YM}/\partial B_1$	-0.9117E 00	-0.1735E 02	0.1066E 03	-0.1226E 03	0.4007E 02	0.0000E 00	0.0000E 00	0.0000E 00
$\partial C_{YM}/\partial \alpha$	0.5790E-01	0.8252E 01	-0.5661E 02	0.6781E 02	-0.2567E 02	0.0000E 00	0.0000E 00	0.0000E 00
$\partial C_{YM}/\partial \psi$	0.1063E 00	0.5334E 01	-0.1209E 02	0.2367E 01	0.0000E 00	0.0000E 00	0.0000E 00	0.0000E 00
$\partial C_{YM}/\partial_{RPM}$	0.5283E-03	0.1724E 00	-0.7342E 00	0.1638E 01	-0.1733E 01	0.6788E 00	0.0000E 00	0.0000E 00

Table VIII. Coefficients for Chord Bending Moment Derivative

	a_1	a_2	a_3	a_4	a_5	a_6	a_7	a_8
$\partial C_{BM}/\partial A_1$	0.2165E 02	0.8097E 02	-0.1026E 02	-0.3775E 03	0.3345E 03	0.0000E 00	0.0000E 00	0.0000E 00
$\partial C_{BM}/\partial B_1$	0.2294E 02	0.4346E 02	0.2671E 03	-0.2580E 03	0.0000E 00	0.0000E 00	0.0000E 00	0.0000E 00
$\partial C_{BM}/\partial \alpha$	0.2166E 01	0.4014E 02	0.0000E 00	0.0000E 00	0.0000E 00	0.0000E 00	0.0000E 00	0.0000E 00
$\partial C_{BM}/\partial \psi$	0.3600E-01	0.4836E 02	-0.9337E 02	0.3934E 03	-0.6282E 03	0.2932E 03	0.0000E 00	0.0000E 00
$\partial C_{BM}/\partial_{RPM}$	0.0000E 00	0.0000E 00	0.0000E 00	0.0000E 00	0.0000E 00	0.0000E 00	0.0000E 00	0.0000E 00

Table IX. Coefficients for Flap Bending Moment Derivative

	a_1	a_2	a_3	a_4	a_5	a_6	a_7	a_8
$\partial F_{BM}/\partial A_1$	0.6724E 01	0.4796E 01	-0.1416E 03	0.4634E 03	-0.3272E 03	0.0000E 00	0.0000E 00	0.0000E 00
$\partial F_{BM}/\partial B_1$	0.3365E 01	0.1043E 03	-0.8547E 03	0.2364E 04	-0.2458E 04	0.9075E 03	0.0000E 00	0.0000E 00
$\partial F_{BM}/\partial \alpha$	0.1292E 01	0.3948E 02	-0.3031E 03	0.8403E 03	-0.9768E 03	0.4470E 03	0.0000E 00	0.0000E 00
$\partial F_{BM}/\partial \psi$	-0.3010E-01	0.6626E 01	-0.2384E 02	0.8028E 02	-0.3817E 02	0.0000E 00	0.0000E 00	0.0000E 00
$\partial F_{BM}/\partial_{RPM}$	0.0000E 00	0.0000E 00	0.0000E 00	0.0000E 00	0.0000E 00	0.0000E 00	0.0000E 00	0.0000E 00

V_{KT}	i_N	δ_F	θ	δ_B	δ_{TH}	A_1	B_1	$\theta_{.75}$	
0	90.	40.	1.16	-.07	5.87	-.06	.11	10.2	FORMER ROTOR MODEL
			1.04	0	5.36	-.01	0	9.7	PRESENT ROTOR MODEL
60.	75.	40.	8.08	.69	3.5	-1.46	2.71	8.26	
			7.23	.24	3.3	-3.23	1.94	7.42	
140.	60.	0.	-.44	-1.56	5.5	-3.13	5.42	18.49	
			.27	-1.41	5.04	-5.26	2.99	15.06	
140.	30.	0.	5.14	-.09	3.85	-1.90	4.00	24.8	
			3.39	-.92	3.60	-3.05	1.73	24.4	
200.	0.	0.	3.08	-.09	2.67	-.71	2.30	41.7	
			3.3	.5	2.70	-1.87	1.67	44.1	

TABLE X. COMPARISON OF AIRCRAFT TRIM CONDITIONS AS COMPUTED WITH THE PRESENT AND FORMER ROTOR MODELS

XV-15 STABILITY AND CONTROL DERIVATIVES

G.W. = 13564.15 LBS VEL. = 140.00 KTS ALT. = .00 FT
C.G. = .16 IN R/C = -.01 FPM TEMP = 59.00 DEG

	L/IXX	M/IYY	N/IZZ	X/M	Y/M	Z/M
DELA	.0000	1.4122	.0000	-.3917	.0000	.9664
DELS	.4370	.0029	.1331	-.0103	-.3151	.3319
DELR	-.0778	.0588	.2436	-.0632	-.6960	-.0191
THEOM	-.0000	-.0001	.0000	-.0006	-.0000	.0013
P	-1.9009	.0013	-.5984	-.0344	.7793	.0556
Q	-.0000	-5.0223	.0046	.4346	-.0000	-2.3391
R	-.4260	-.0243	-.7252	.0126	2.0453	-.0150
U	-.0000	.0135	-.0000	-.1413	.0000	-.0767
V	-.0115	.0043	.0083	-.0026	-.2198	.0118
W	-.0000	-.0051	.0000	.0724	-.0000	-.6668
INACL	-.0000	-.0001	.0000	-.0006	.0000	.0013

TABLE XI. DERIVATIVES AT 140 KT, $i_N = 60°$, $\delta_F = 0°$, - FORMER ROTOR MODEL.

XV-15 STABILITY AND CONTROL DERIVATIVES

G.W. = 13564.15 LBS VEL. = 140.00 KTS ALT. = .00 FT
C.G. = .16 IN R/C = -.07 FPM TEMP = 59.00 DEG

	L/IXX	M/IYY	N/IZZ	X/M	Y/M	Z/M
DFI A	-.0000	1.5118	-.0000	.1760	-.0000	.2172
DFI S	.2397	.0095	.0366	.0058	-.7757	.2805
DFI R	-.5170	.0019	.0701	-.0188	-2.3158	.0050
THERM	-.0000	.0000	-.0000	-.0005	-.0000	.0011
P	-3.1941	-.0021	-.8557	-.0458	1.5398	.1152
Q	-.0000	-5.3254	.0045	.2313	-.0000	-2.1627
R	-.7579	-.1445	-.7474	-.0182	3.1010	.0626
U	-.0000	.0252	-.0000	-.0564	-.0000	-.2231
V	-.0081	.0050	.0056	-.0005	-.1762	.0083
W	-.0000	-.0168	.0000	-.0367	-.0000	-.3834
INACL	-.0000	.0000	-.0000	-.0005	-.0000	.0011

TABLE XII. DERIVATIVES AT 140 KT, $i_N = 60°$, $\delta_F = 0°$ - PRESENT ROTOR MODEL.

XV-15 STABILITY AND CONTROL DERIVATIVES

G.W. = 13564.15 LBS VEL. = 60.00 KTS ALT. = .00 FT
C.G. = .01 IN R/C = -.01 FPM TEMP = 59.00 DEG

	L/IXX	M/IYY	N/IZZ	X/M	Y/M	Z/M
DELA	.0000	.7450	-.0000	-.4612	.0000	.1432
DELS	.3633	-.0042	.0541	.0079	-.1679	.1530
DELR	-.0777	.0014	.0945	-.0163	-.2686	-.0139
THEOM	.0000	.0001	-.0000	.0005	.0000	-.0028
P	-1.5362	.0086	-.3045	.0349	-.3427	-.1881
Q	-.0000	-3.0395	.0043	.2876	-.0000	-1.2513
R	-.1652	-.0147	-.1385	.0187	.0609	-.1117
U	-.0000	.0230	-.0000	-.0565	-.0000	-.1075
V	-.0107	.0040	-.0021	-.0100	-.0686	.0423
W	-.0000	.0100	-.0000	.1207	.0000	-.5685
INACL	-.0000	.0001	-.0000	.0006	.0000	-.0032

TABLE XIII. DERIVATIVES AT 60 KT, $i_N = 75°$, $\delta_F = 40°$ - FORMER ROTOR MODEL.

XV-15 STABILITY AND CONTROL DERIVATIVES

G.W. = 13564.15 LBS VEL. = 60.00 KTS ALT. = .00 FT
C.G. = .01 IN R/C = -.00 FPM TEMP = 59.00 DEG

	L/IXX	M/IYY	N/IZZ	X/M	Y/M	Z/M
DELA	-.0000	.8951	.0000	-.5418	-.0000	-.3302
DELS	.3018	-.0008	.0404	.0193	-.4890	.0711
DELR	-.2382	.0009	.0922	-.0166	-1.0588	-.0088
THEOM	.0000	.0000	-.0000	.0004	.0000	-.0020
P	-1.7181	.0022	-.2632	-.0105	.4723	-.0302
Q	.0000	-3.0008	.0043	.2445	.0000	-1.3504
R	-.2065	-.0159	-.1261	.0106	.1634	-.0797
U	.0000	.0116	-.0000	-.0473	.0000	-.0623
V	-.0045	.0050	-.0004	-.0004	-.0542	.0035
W	-.0000	.0105	.0003	.0955	-.0000	-.6283
INACL	.0000	.0000	-.0000	.0004	.0000	-.0020

TABLE XIV. DERIVATIVES AT 60 KT, i_N = 75°, δ_P = 40°- PRESENT ROTOR MODEL.

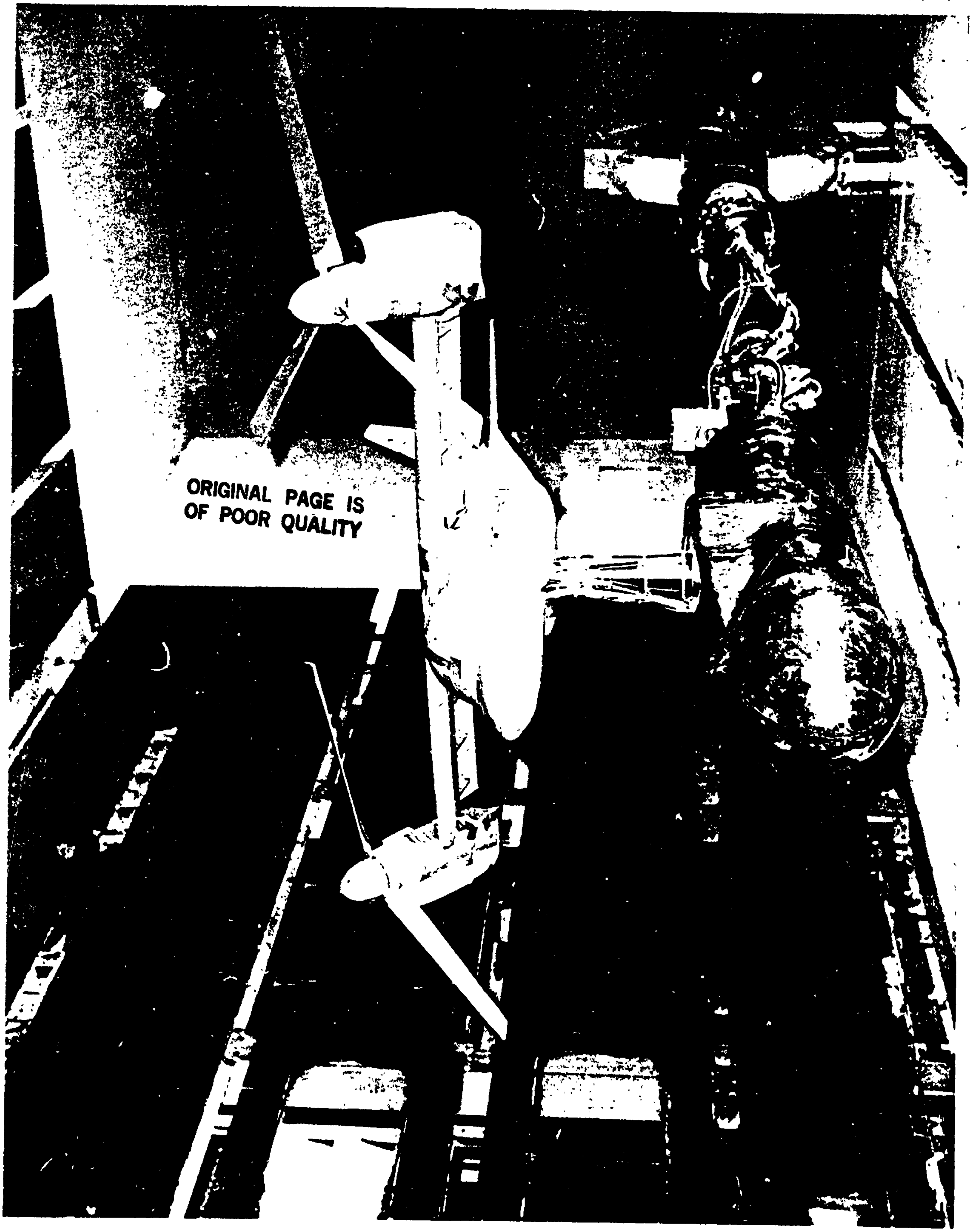

Figure 2.1. 1/4.622 Scale Model Installed in the Wind Tunnel Test Section

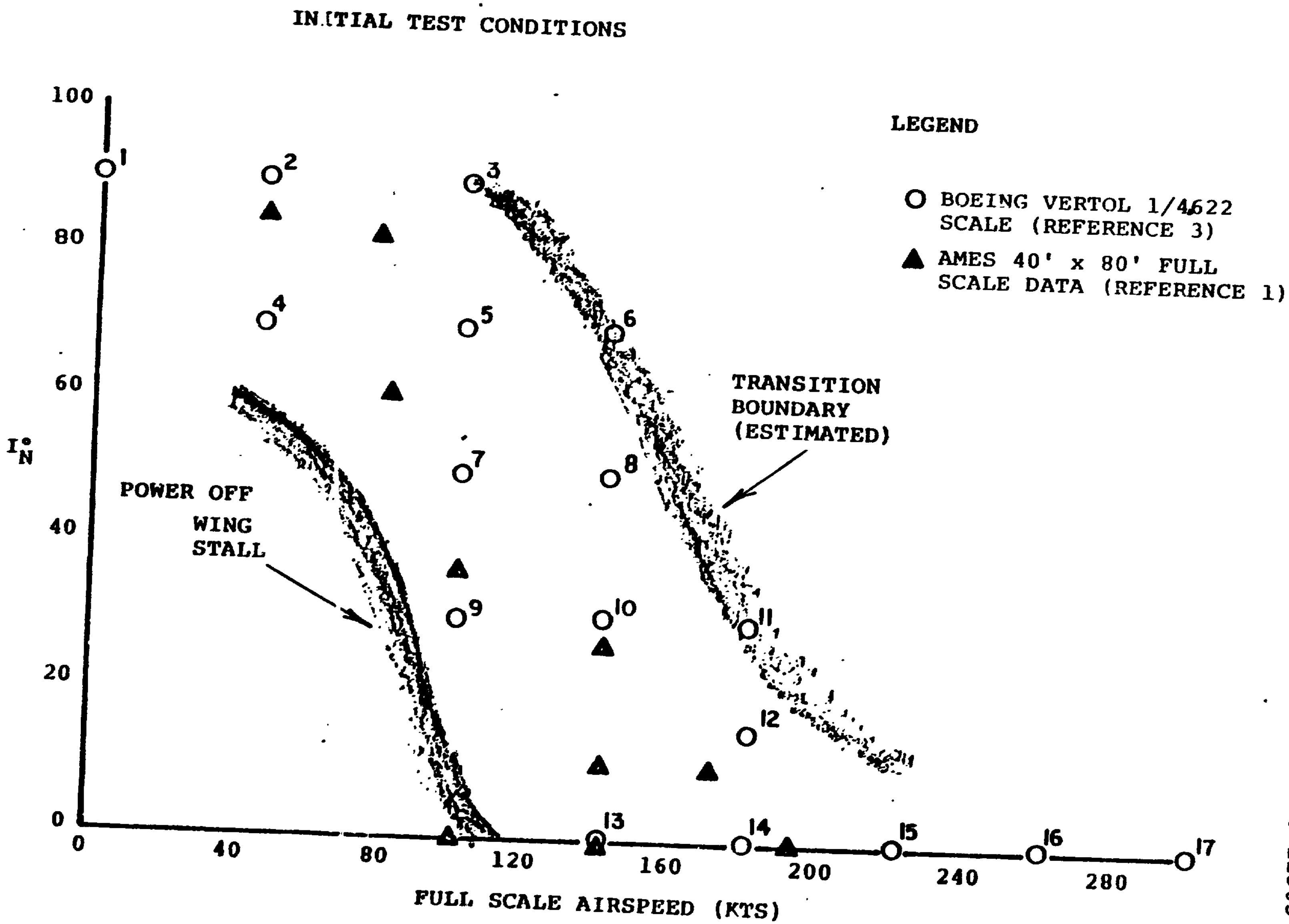

Figure 2.2. Scope of Test of Reference 3

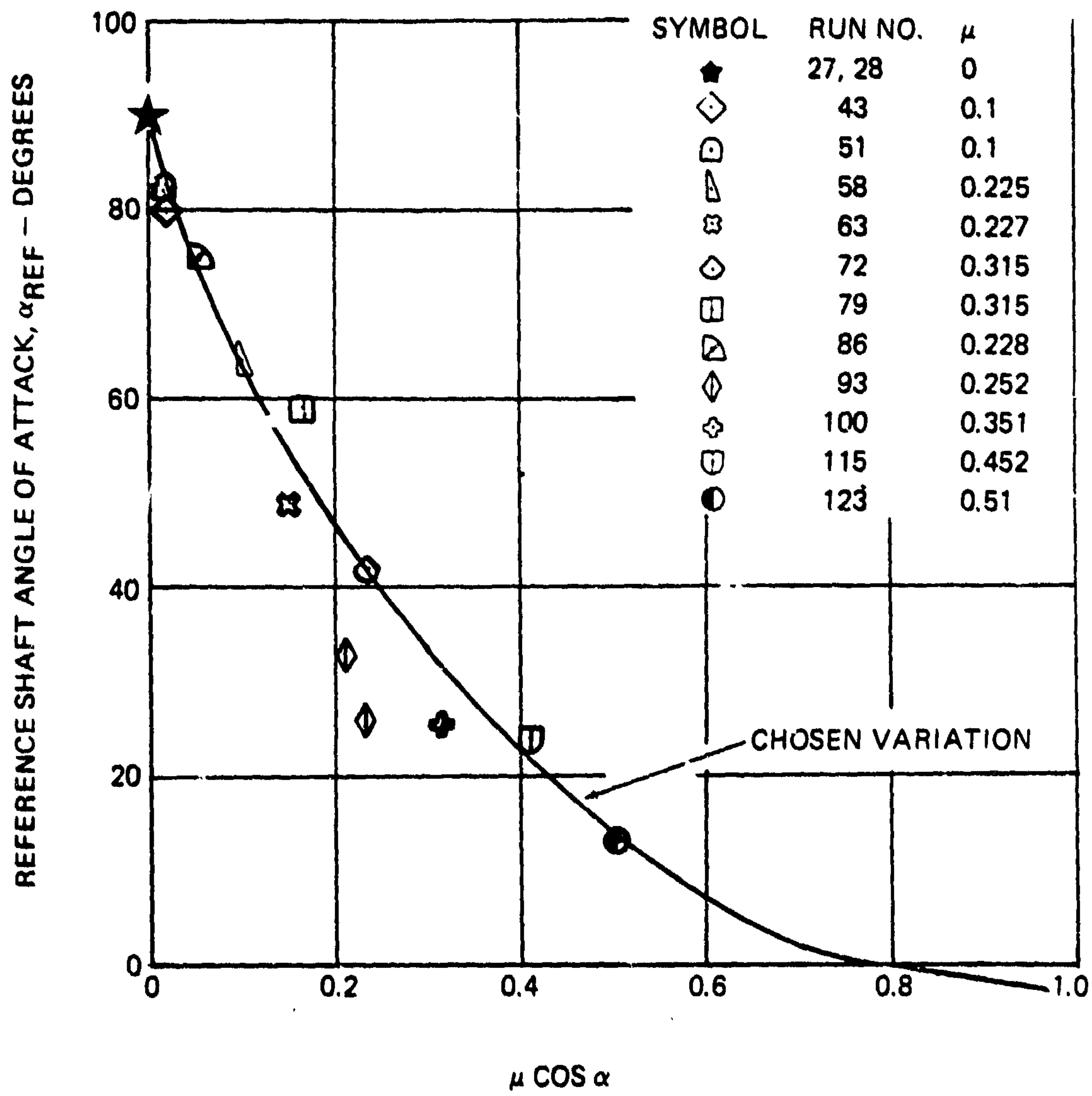

Figure 3.1. Variation of Reference Angle of Attack With μ Cos α

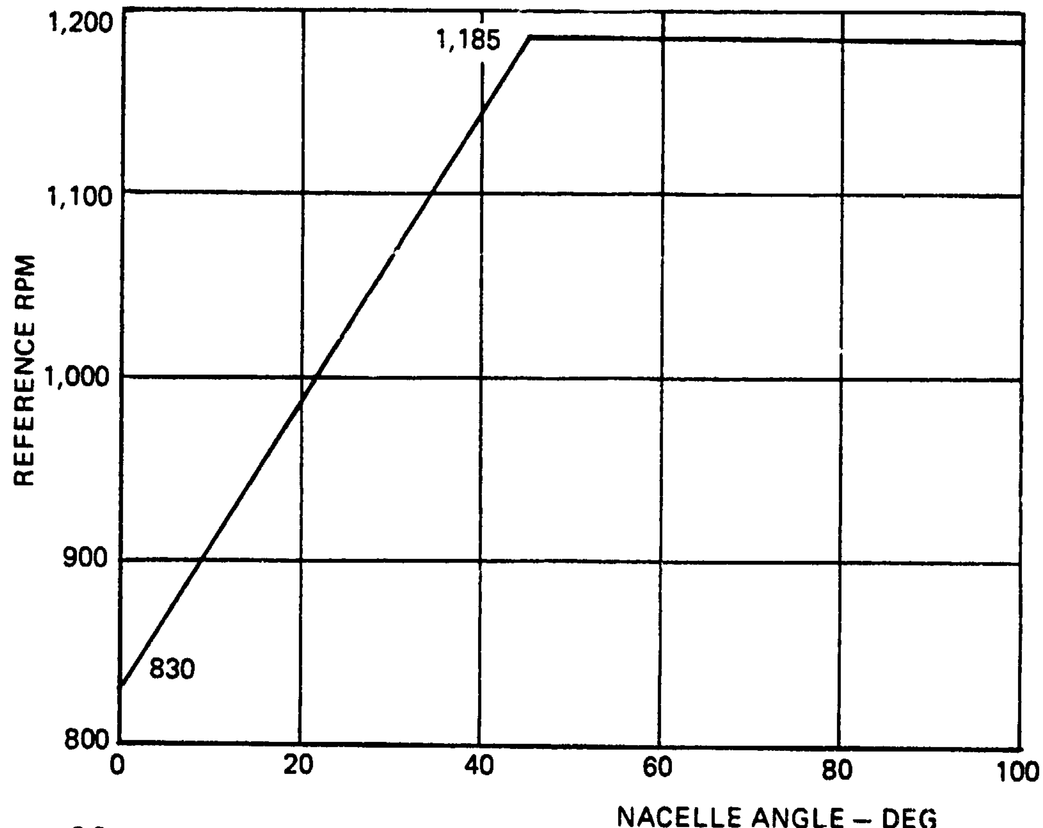

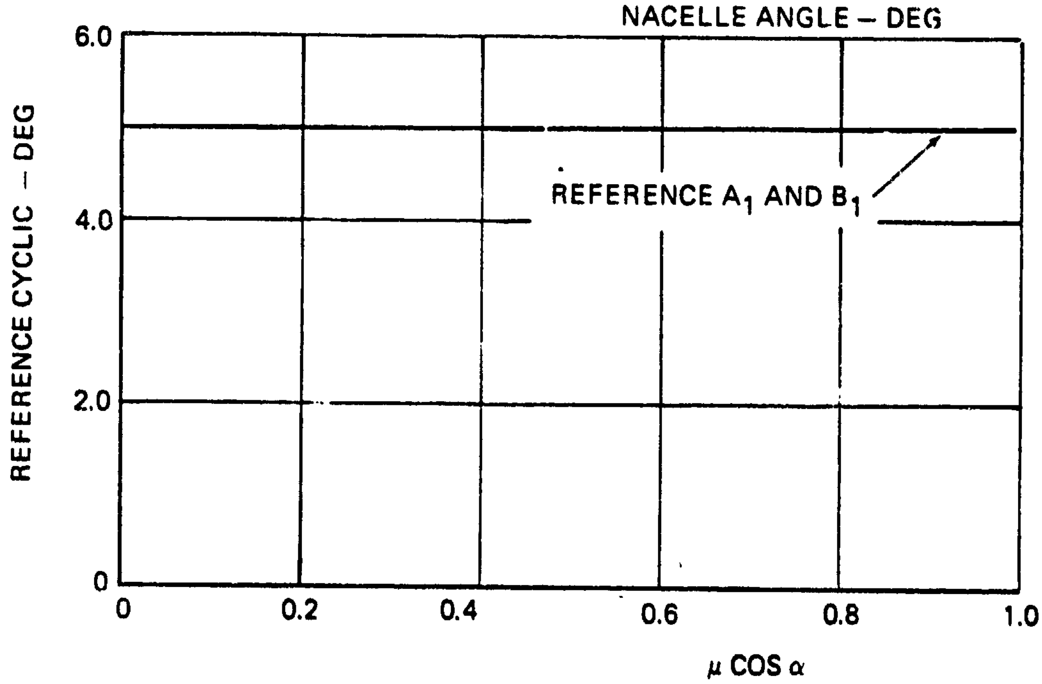

Figure 3.2. Definition of Reference Values of Cyclic and RPM

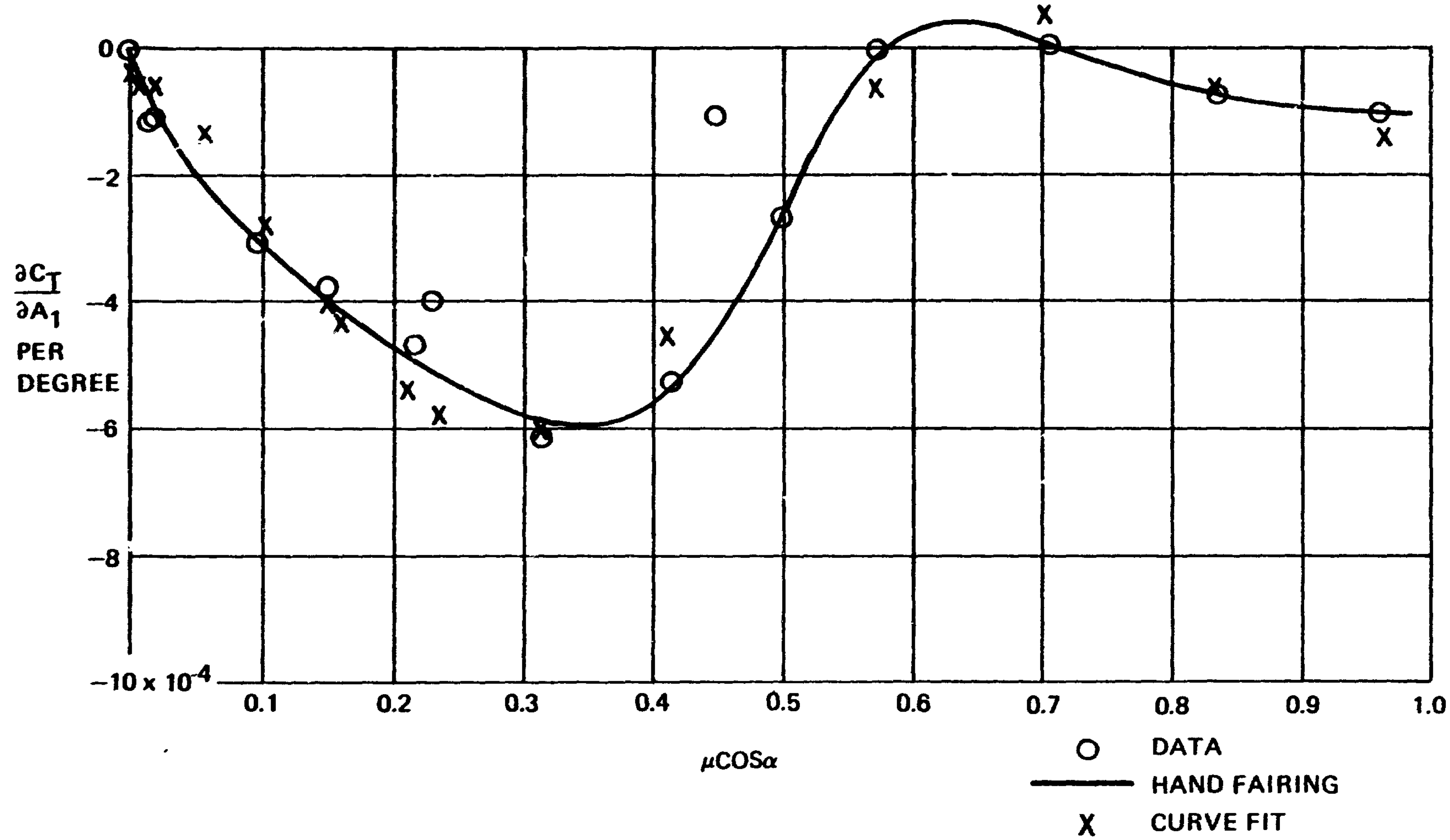

Figure 3-3. Variation of $\frac{\partial C_T}{\partial A_1}$ with $\mu\cos\alpha$.

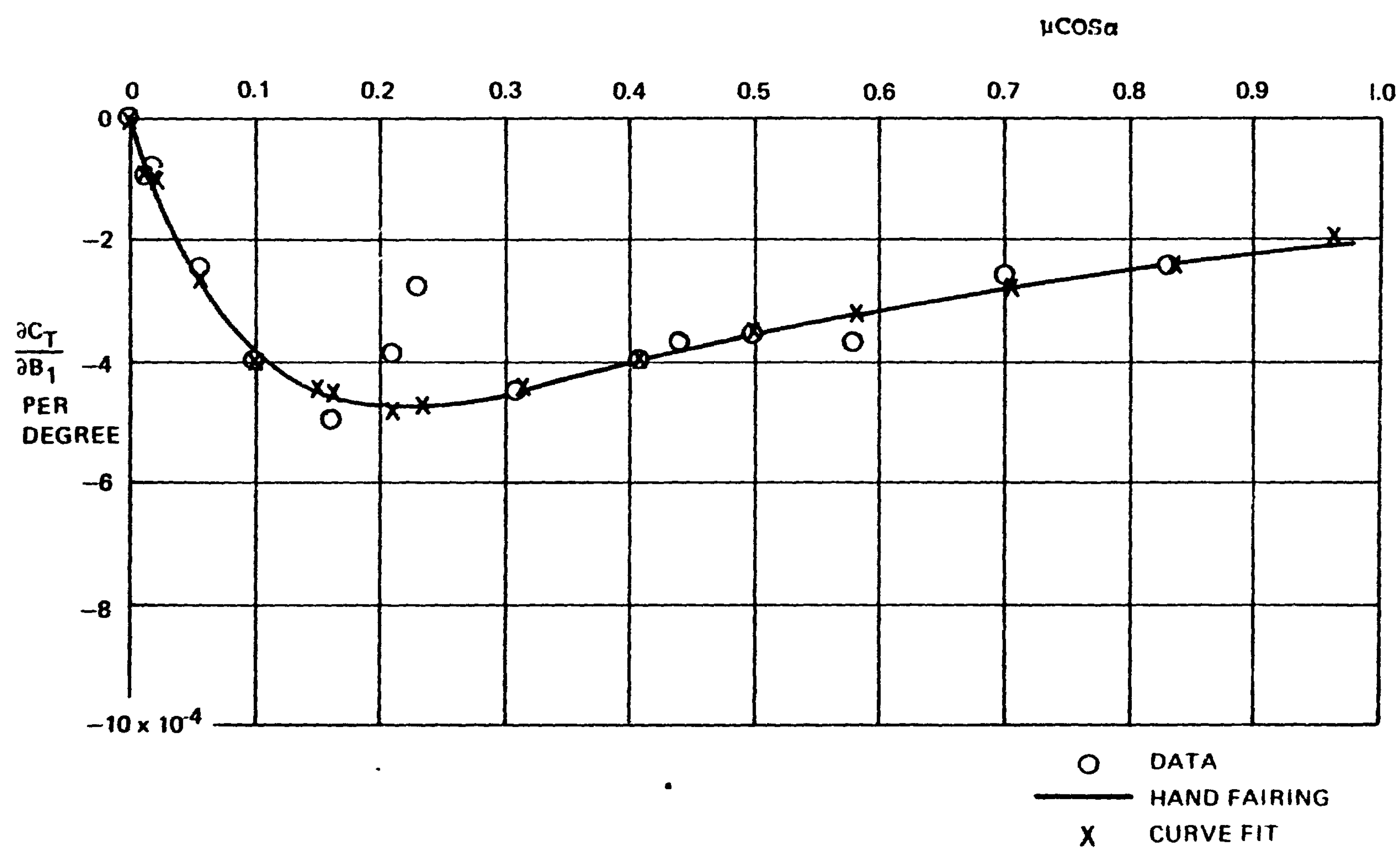

Figure 3-4. Variation of $\frac{\partial C_T}{\partial B_1}$ with μCOSα.

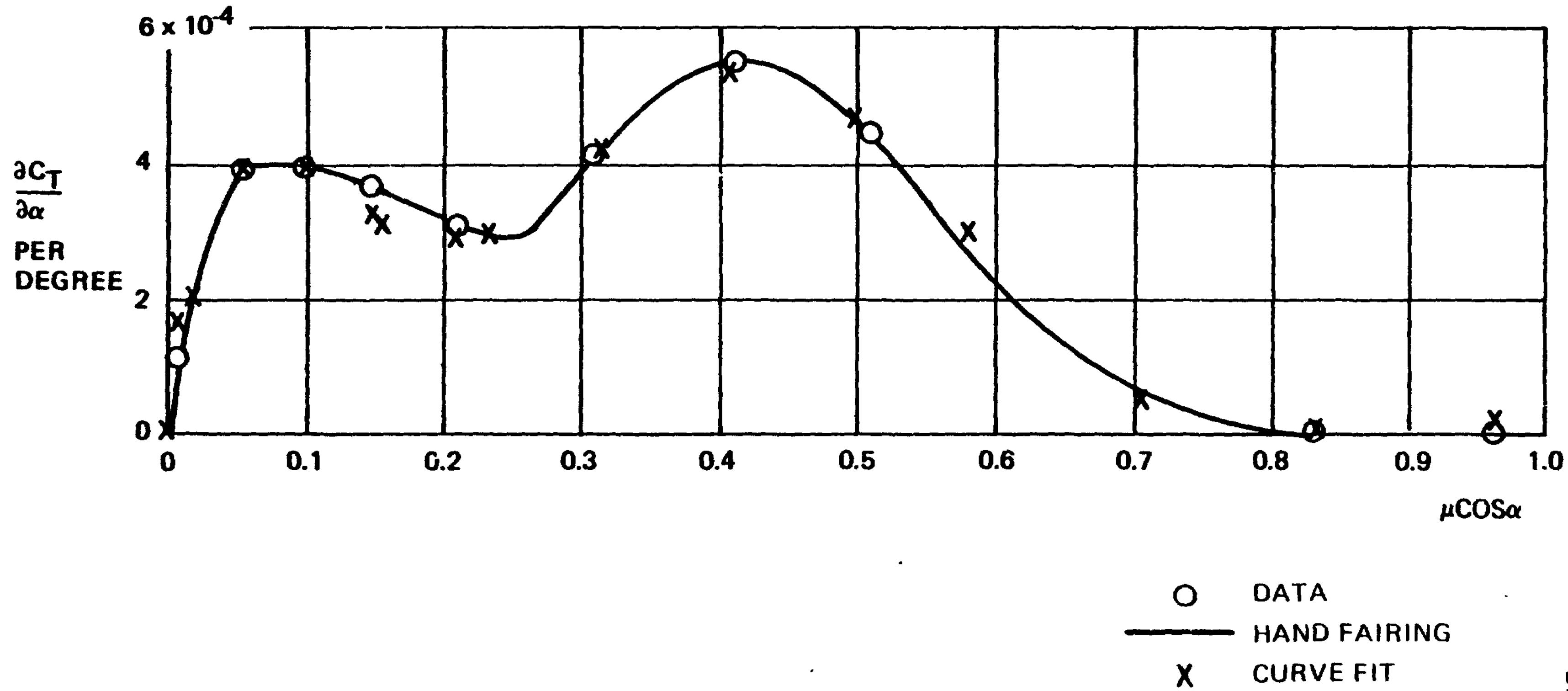

Figure 3-5. Variation of $\frac{\partial C_T}{\partial \alpha}$ with $\mu\cos\alpha$.

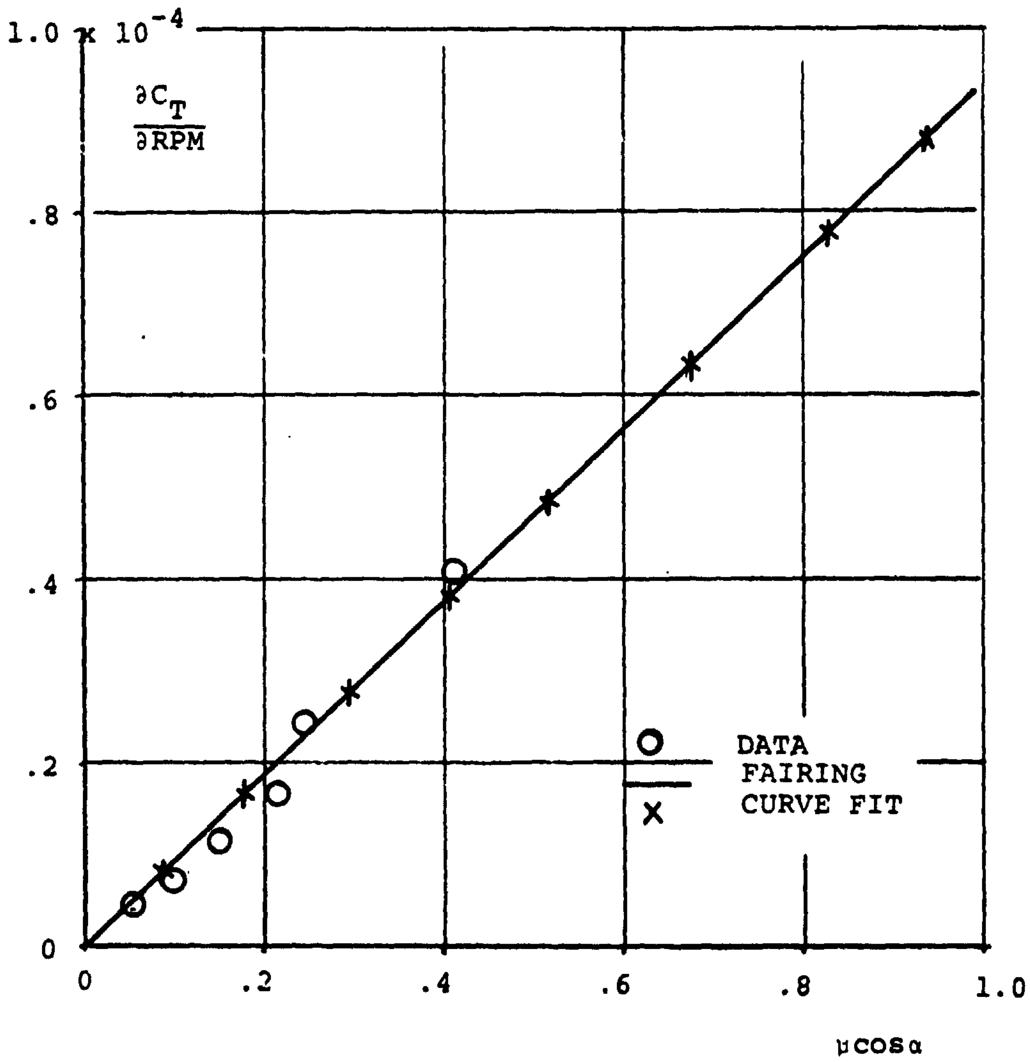

Figure 3.6. Variation of $\partial C_T/\partial RPM$ with $\mu\cos\alpha$.

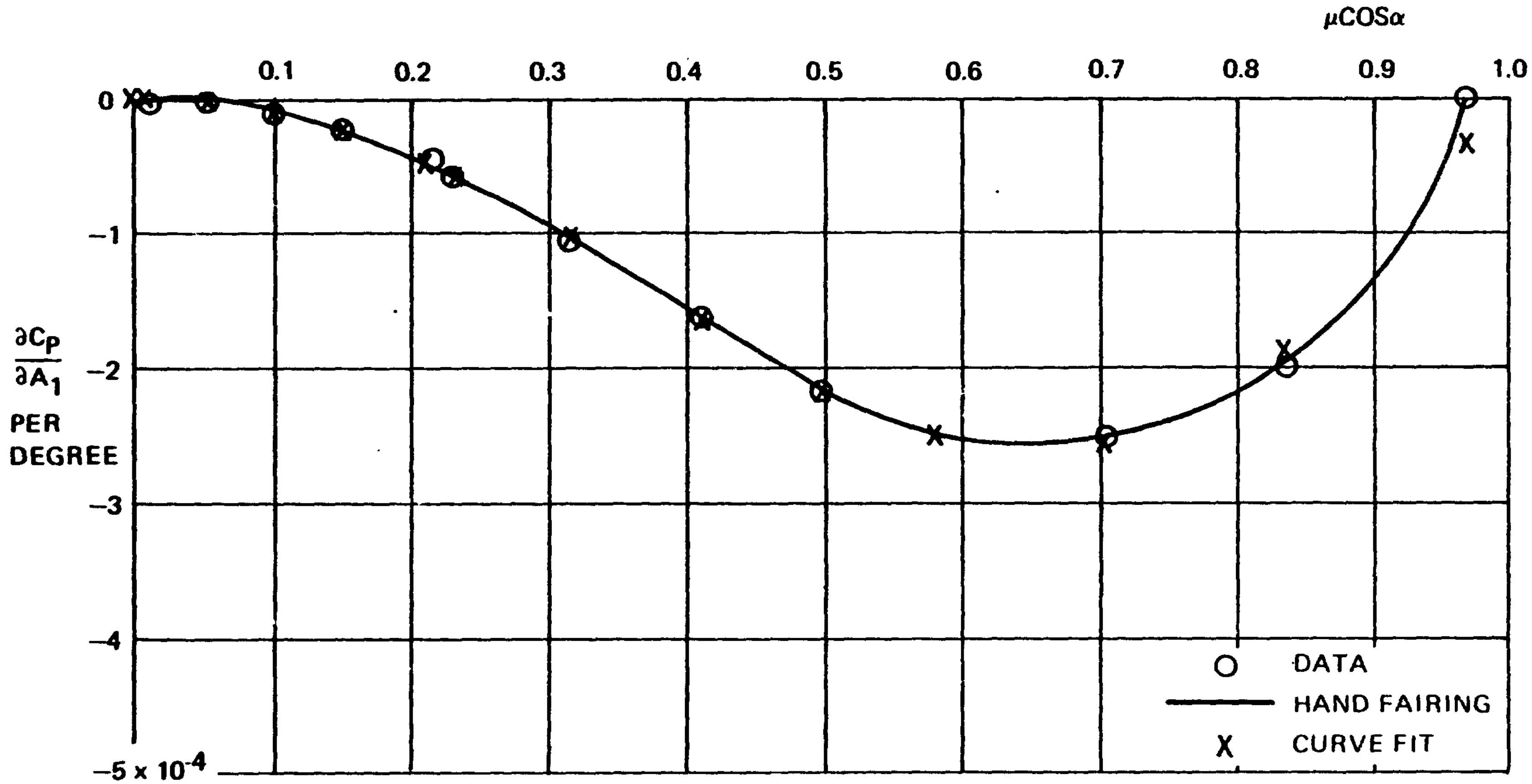

Figure 3-7. Variation of $\frac{\partial C_p}{\partial A_1}$ with $\mu\cos\alpha$.

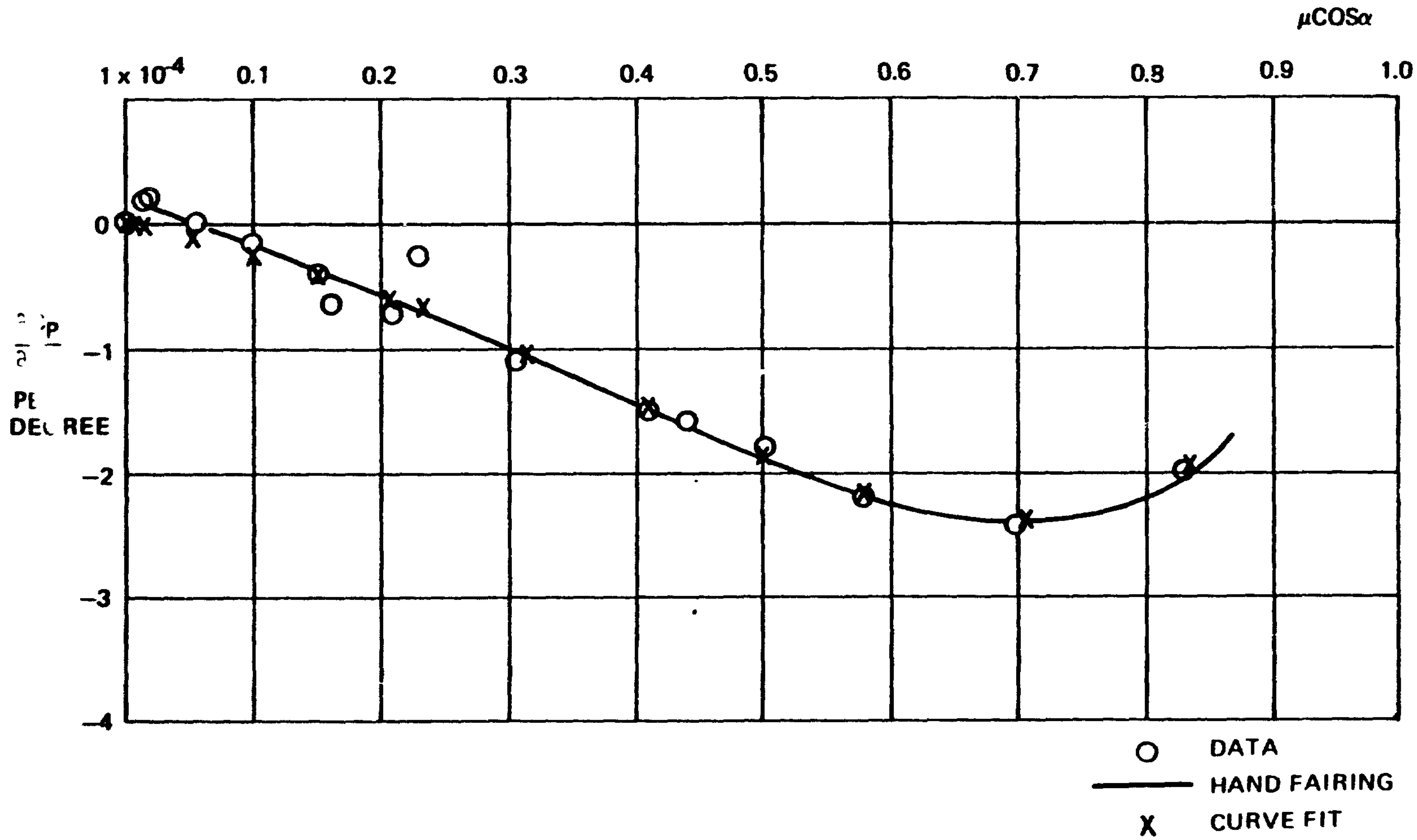

Figure 3-8. Variation of $\frac{\partial C_P}{\partial B_1}$ with μcosα.

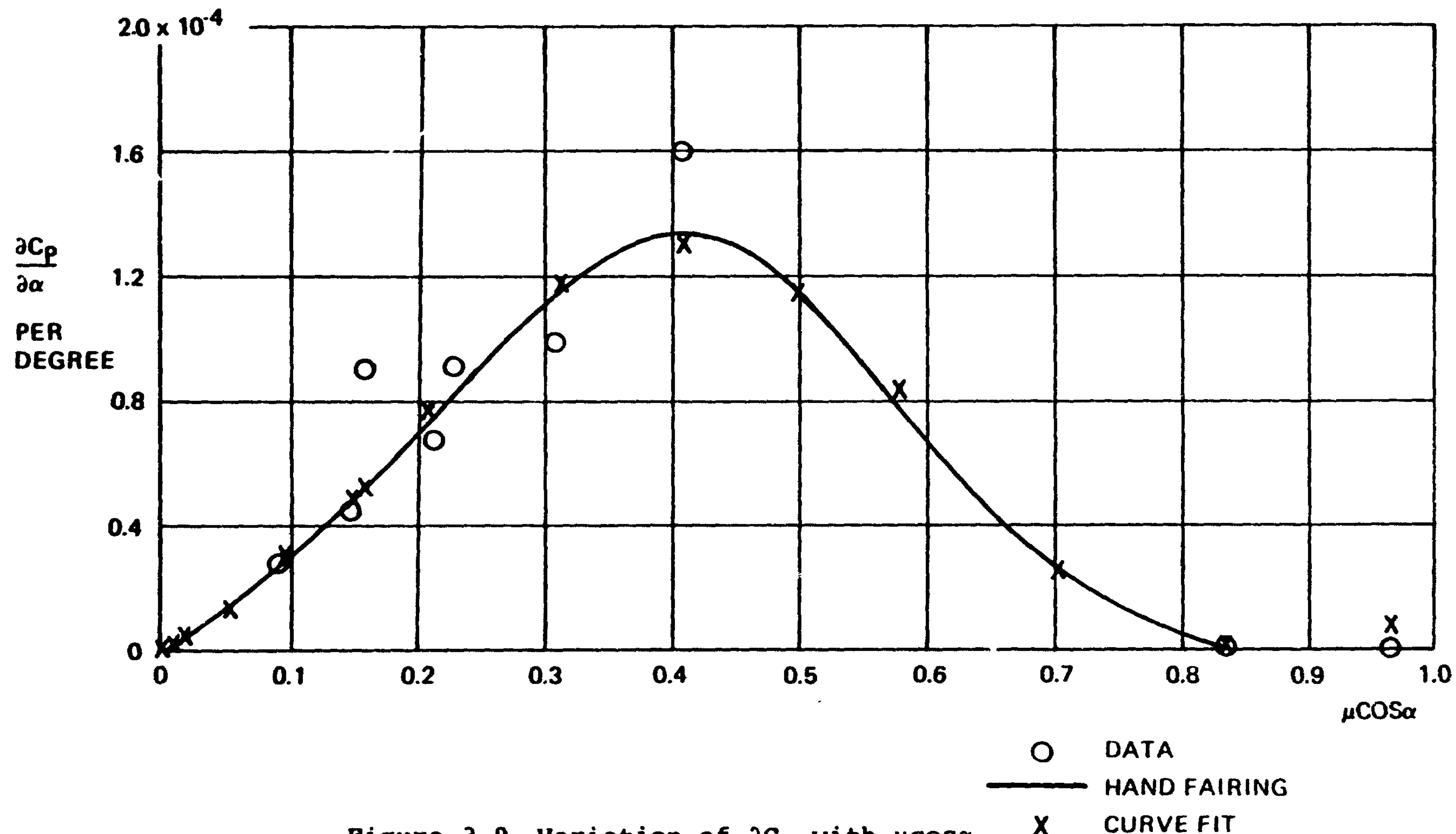

Figure 3-9. Variation of $\frac{\partial C_p}{\partial \alpha}$ with $\mu\cos\alpha$.

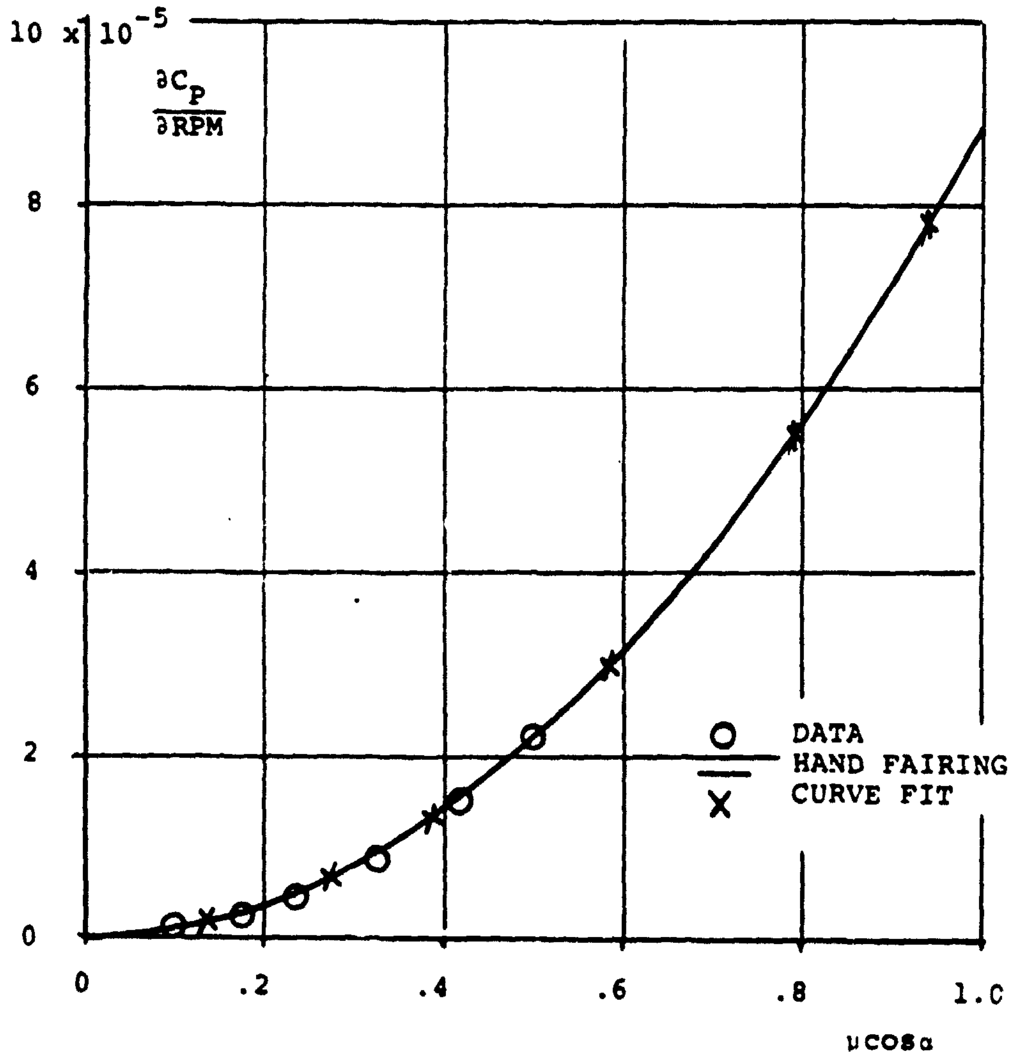

Figure 3.10. Variation of $\partial C_P/\partial RPM$ with $\mu\cos\alpha$.

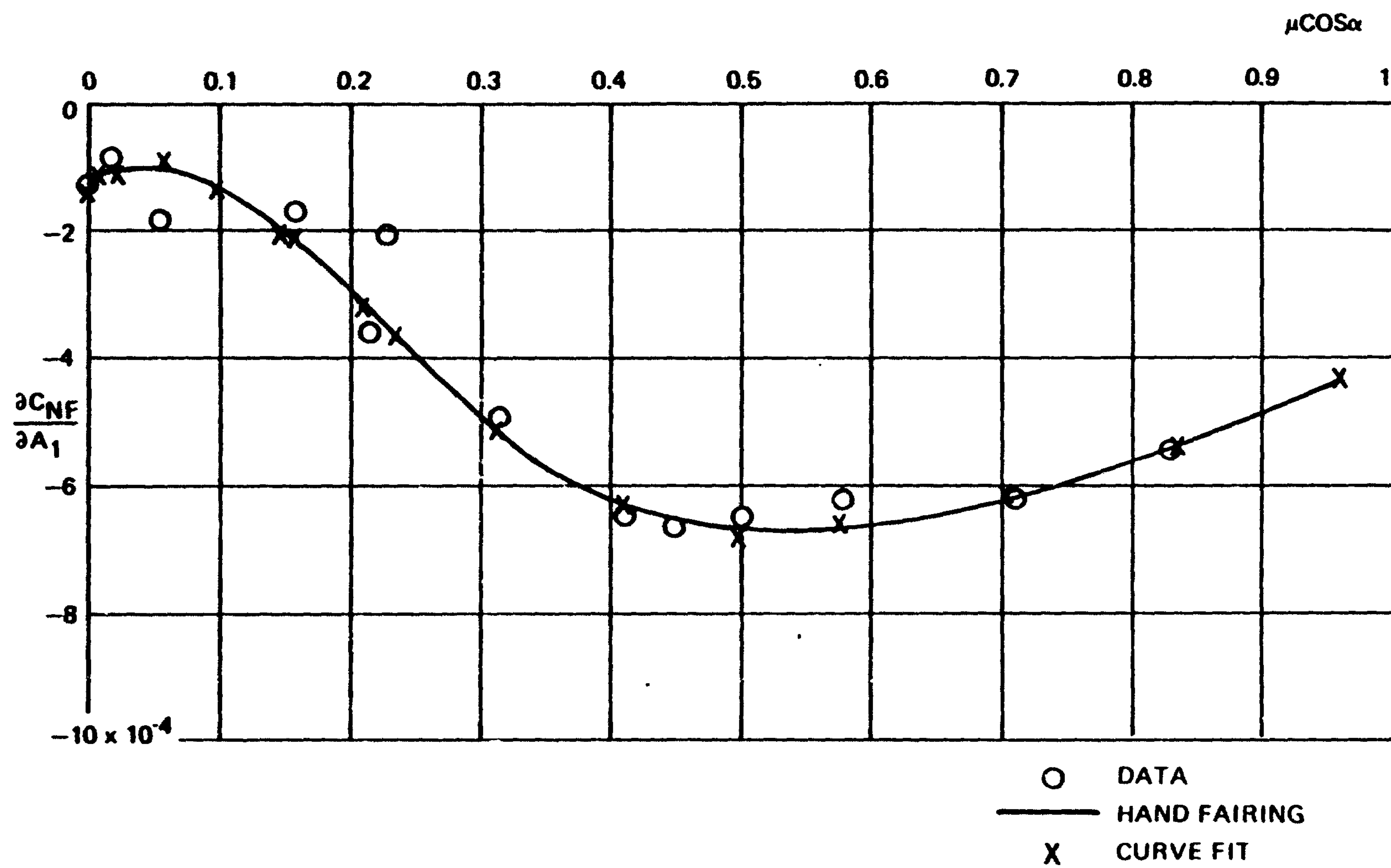

Figure 3-11. Variation of $\frac{\partial C_{NF}}{\partial A_1}$ with $\mu\cos\alpha$.

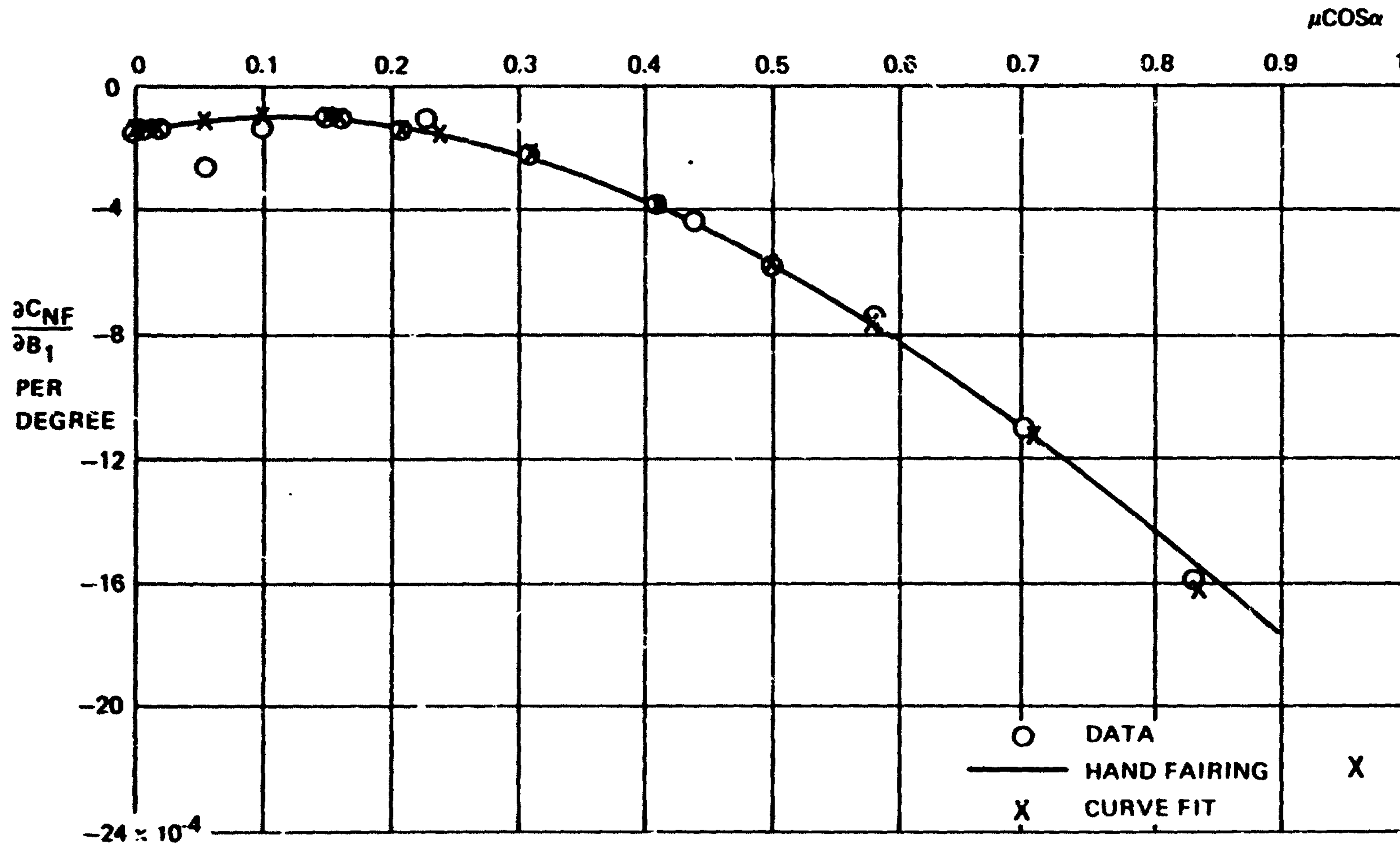

Figure 3-12. Variation of $\frac{\partial C_{NF}}{\partial B_1}$ with μcosα.

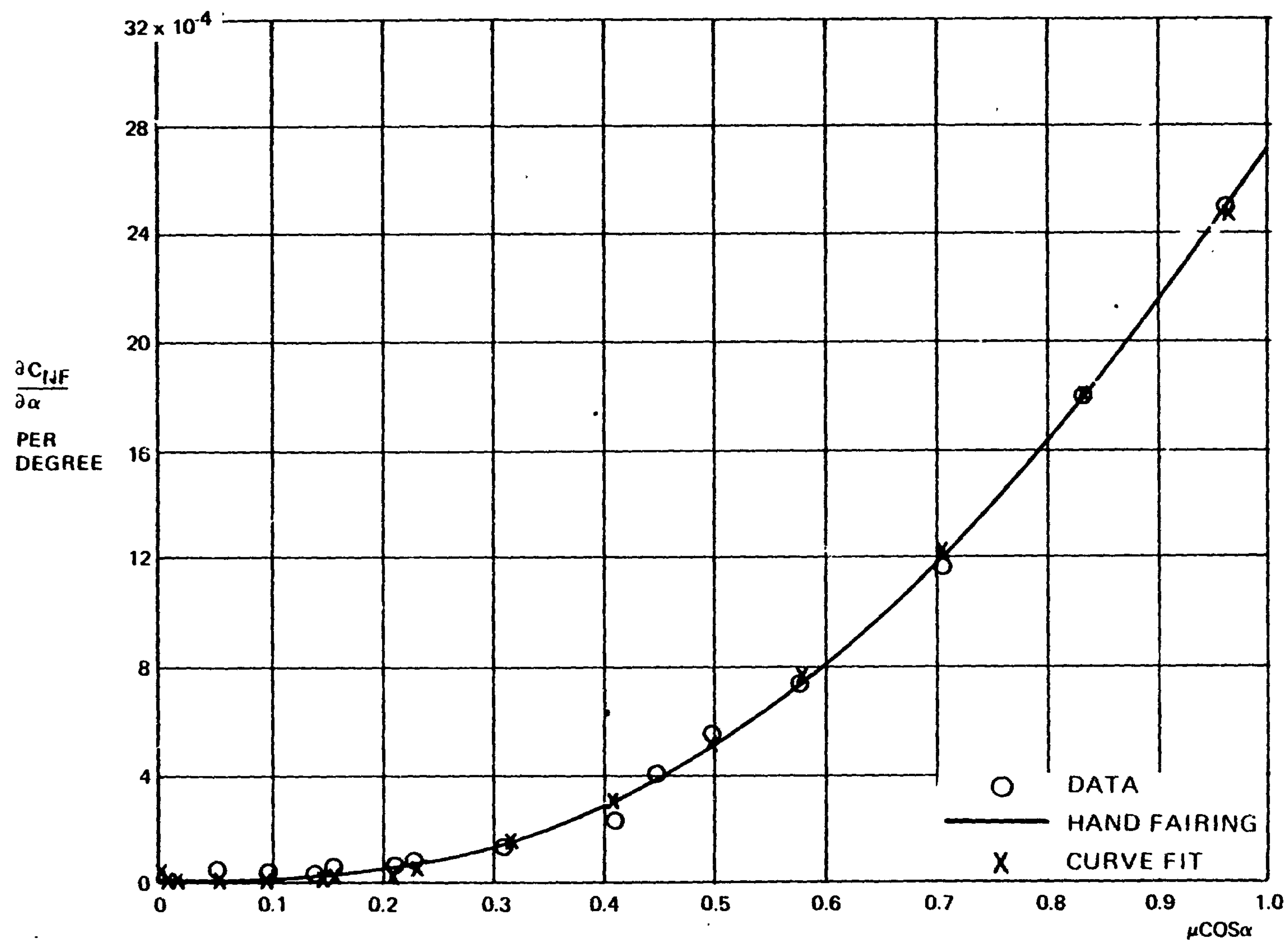

Figure 3-13. Variation of $\frac{\partial C_{NF}}{\partial \alpha}$ with $\mu\cos\alpha$.

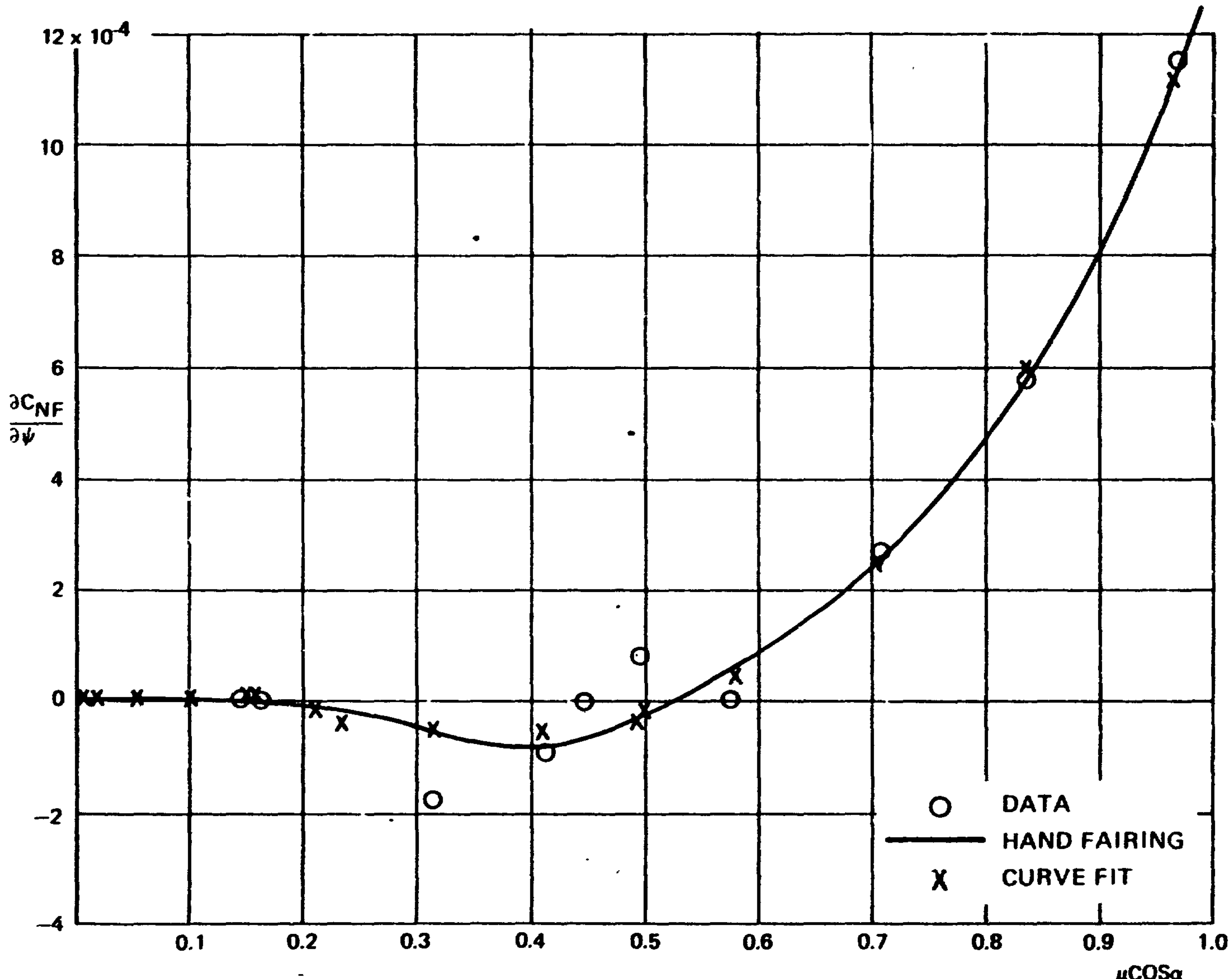

Figure 3-14. Variation of $\frac{\partial C_{NF}}{\partial \psi}$ with $\mu \cos\alpha$.

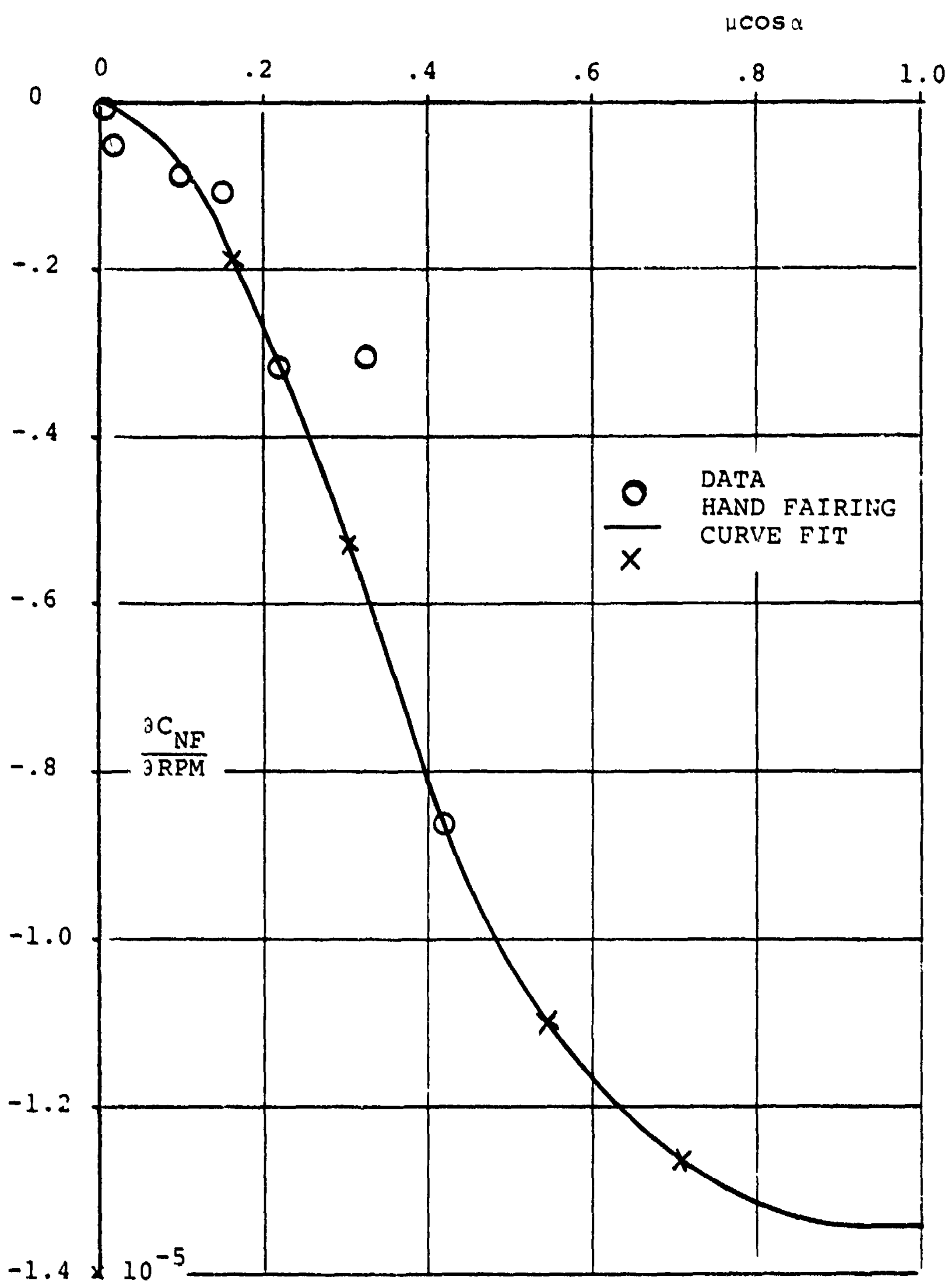

Figure 3.15. Variation of $\partial C_{NF}/\partial RPM$ with $\mu\cos\alpha$.

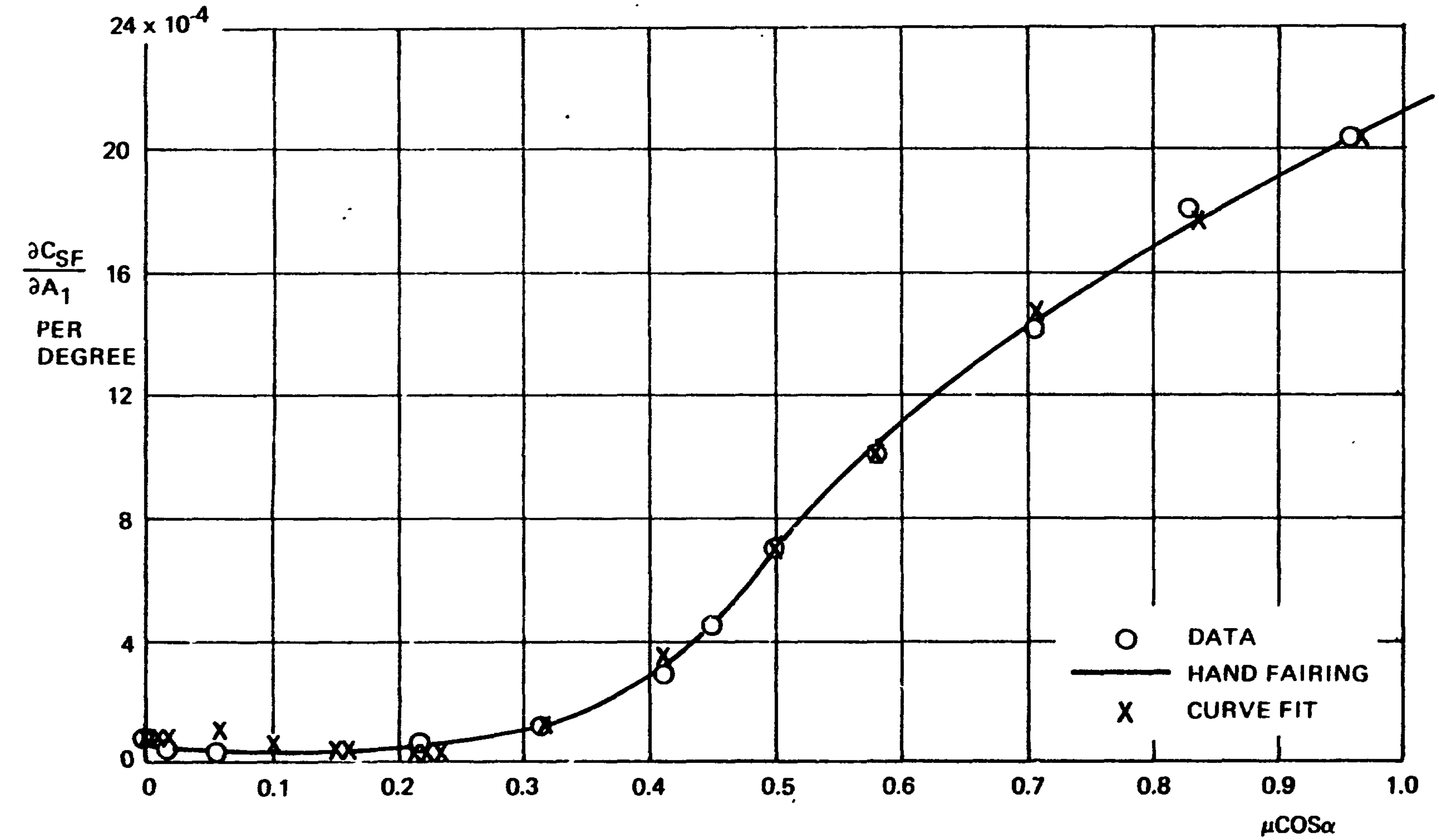

Figure 3-16. Variation of $\frac{\partial C_{SF}}{\partial A_1}$ with $\mu\cos\alpha$.

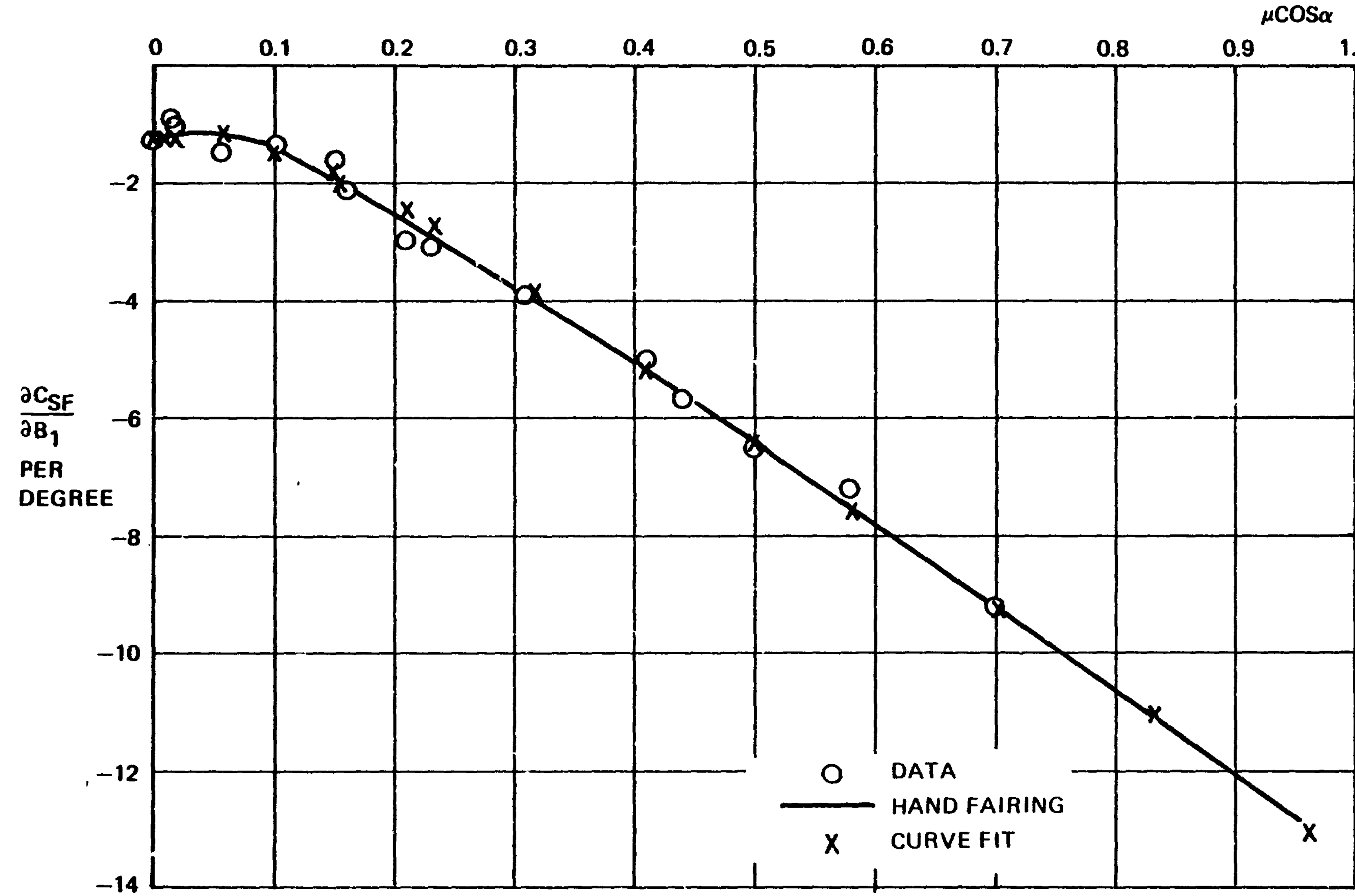

Figure 3-17. Variation of $\frac{\partial C_{SF}}{\partial B_1}$ with $\mu \cos\alpha$.

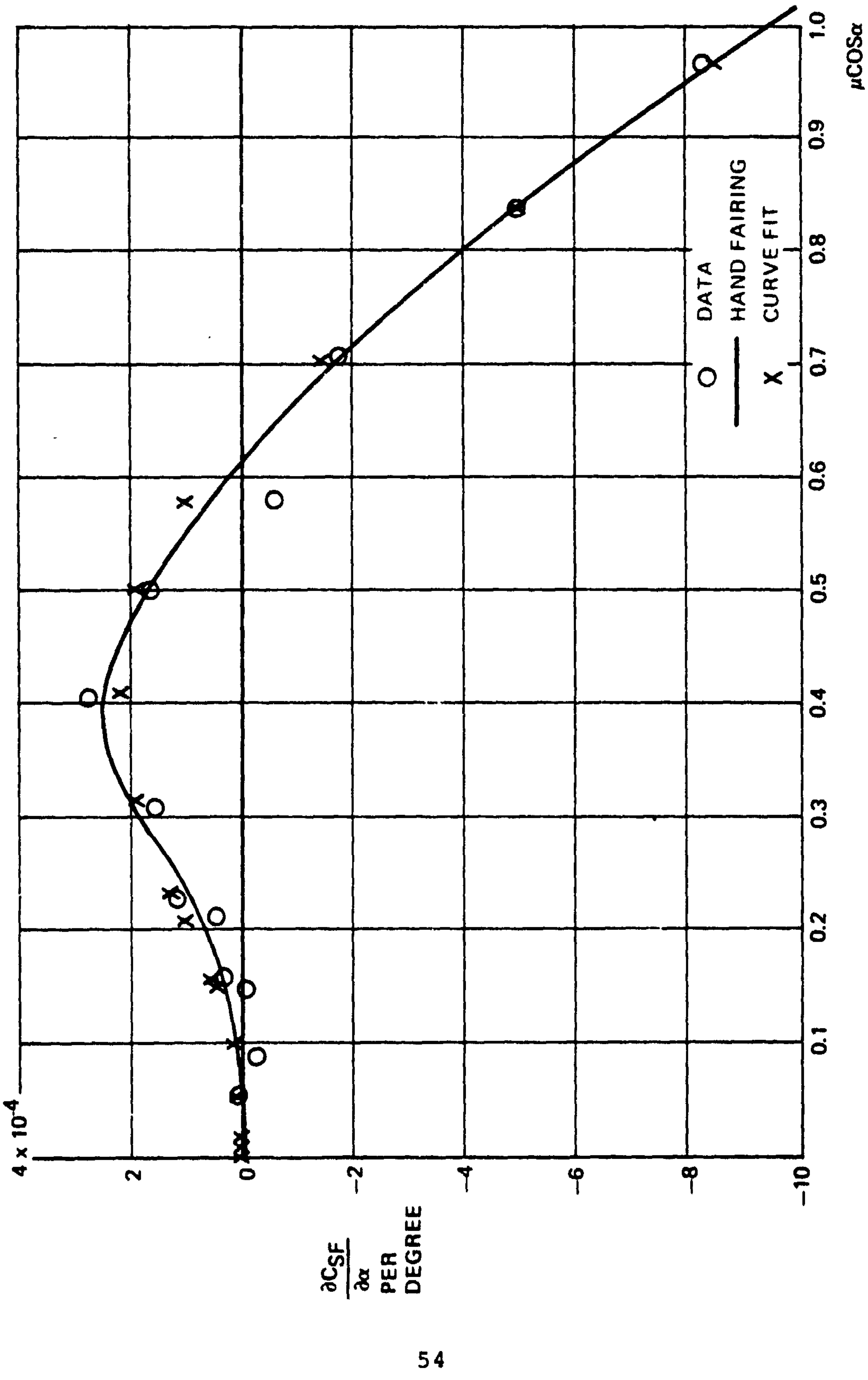

Figure 3-18. Variation of $\frac{\partial C_{SF}}{\partial \alpha}$ with $\mu \cos\alpha$.

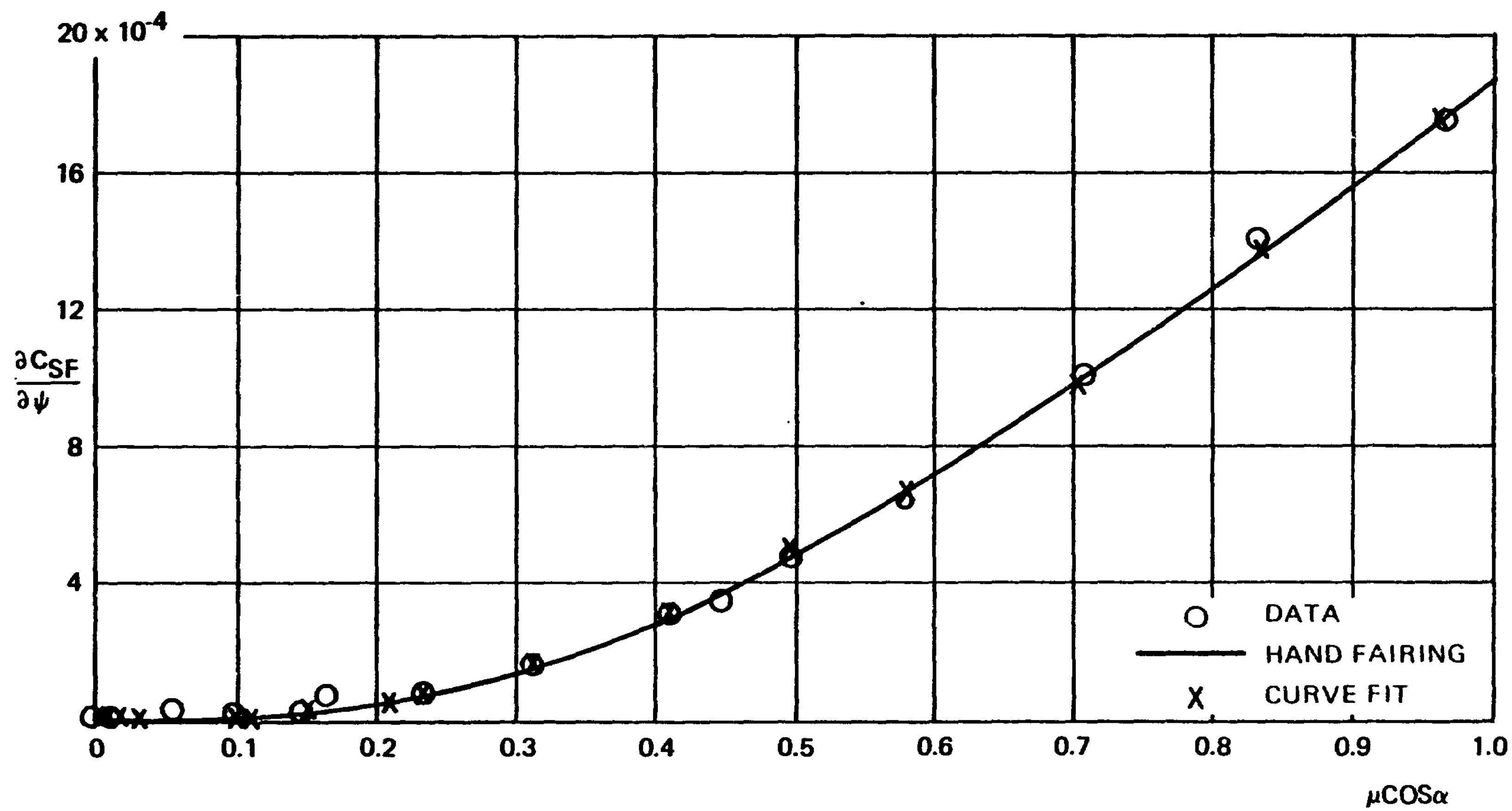

Figure 3-19. Variation of $\frac{\partial C_{SF}}{\partial \psi}$ with $\mu\cos\alpha$.

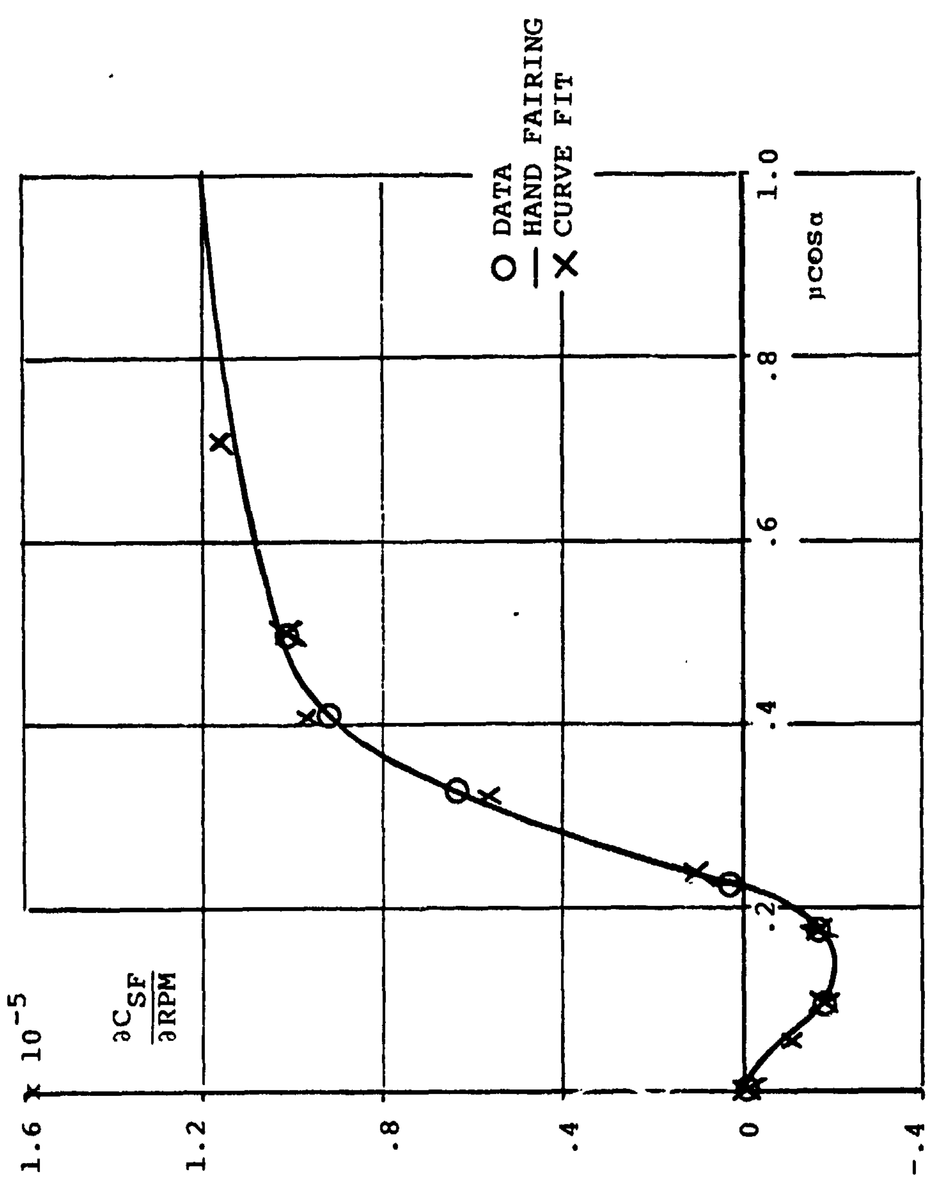

Figure 3.20. Variation of $\partial C_{SP}/\partial RPM$ with $\mu\cos\alpha$.

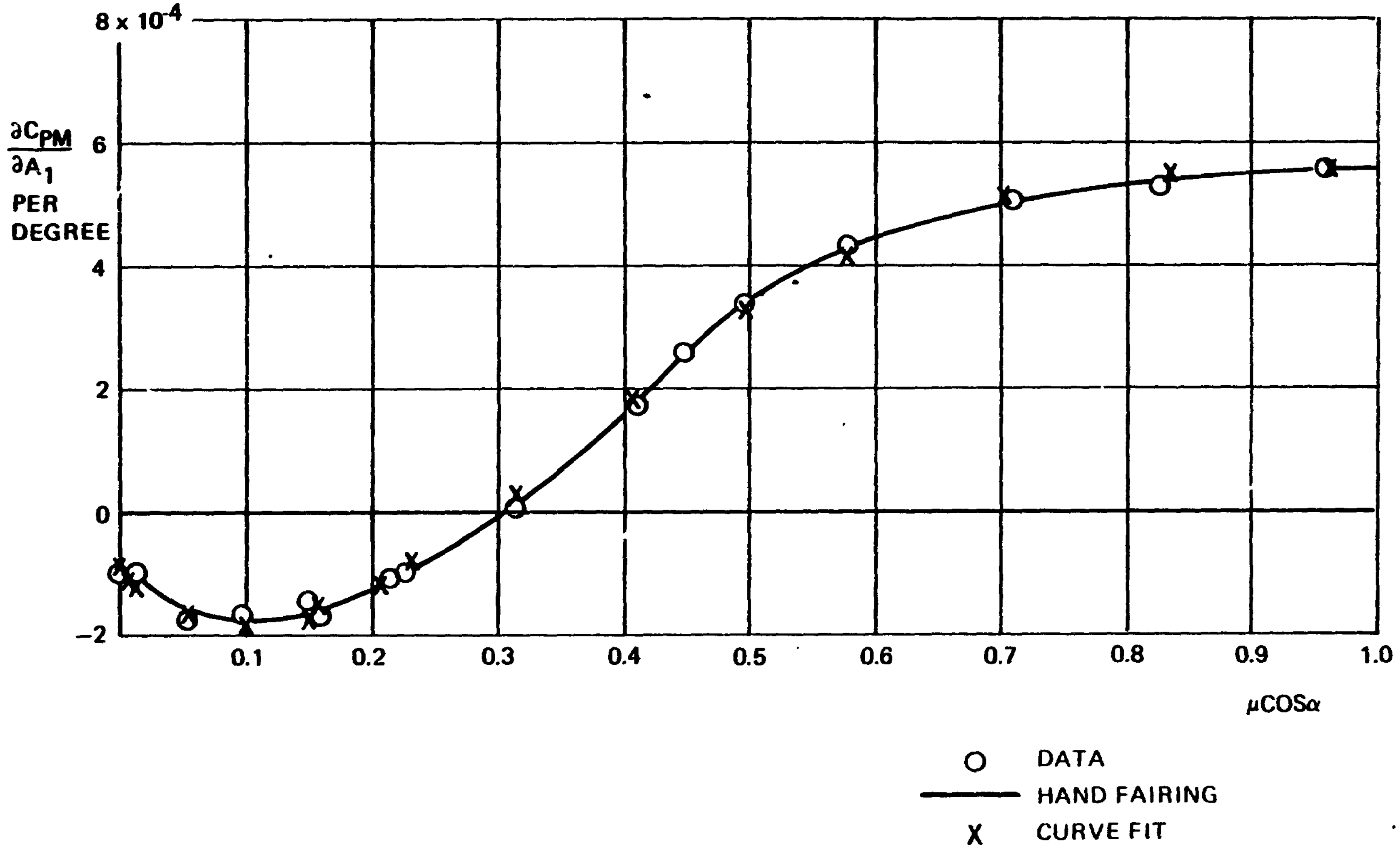

Figure 3-21. Variation of $\frac{\partial C_{PM}}{\partial A_1}$ with $\mu\cos\alpha$.

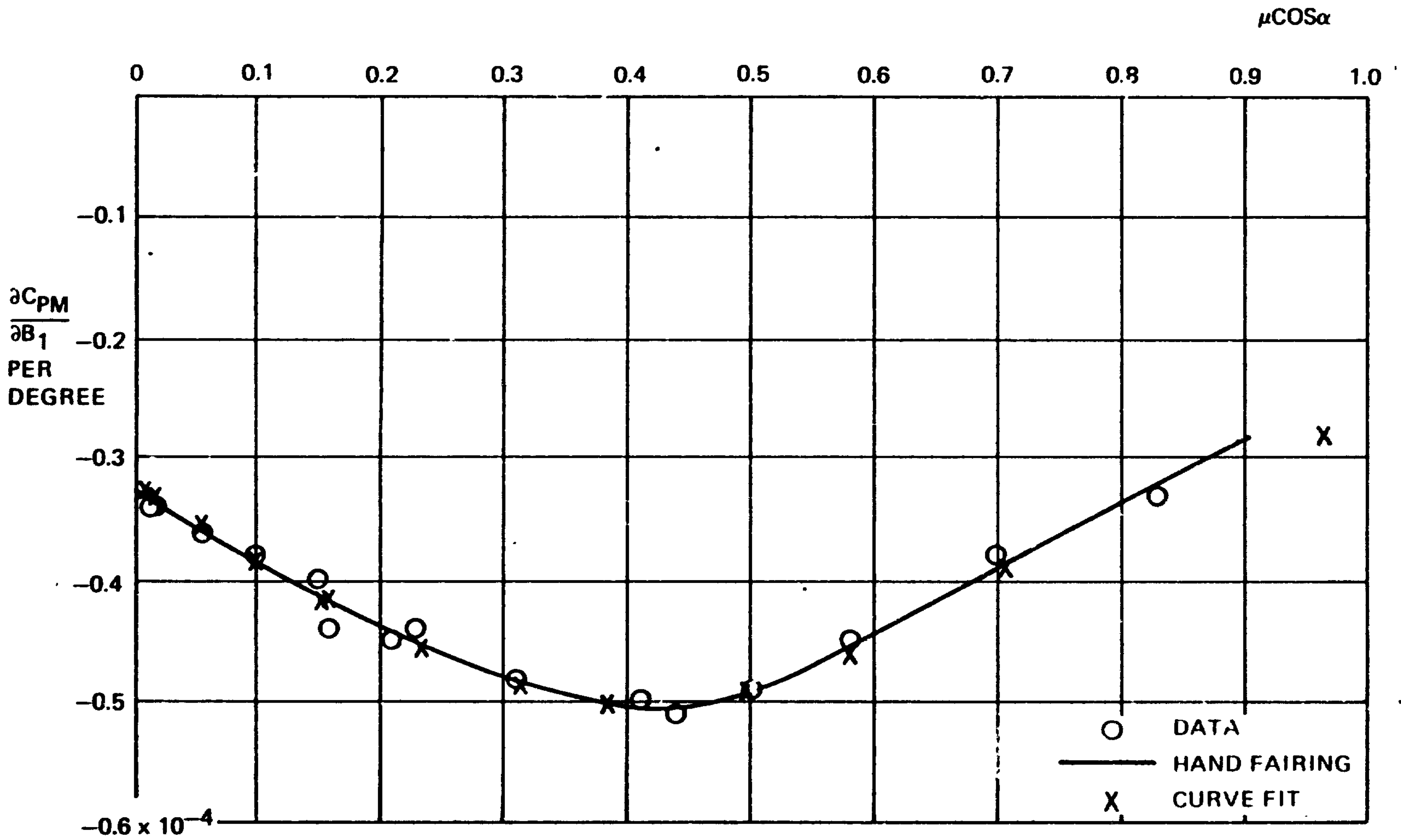

Figure 3-22. Variation of $\frac{\partial C_{PM}}{\partial B_1}$ with $\mu\cos\alpha$.

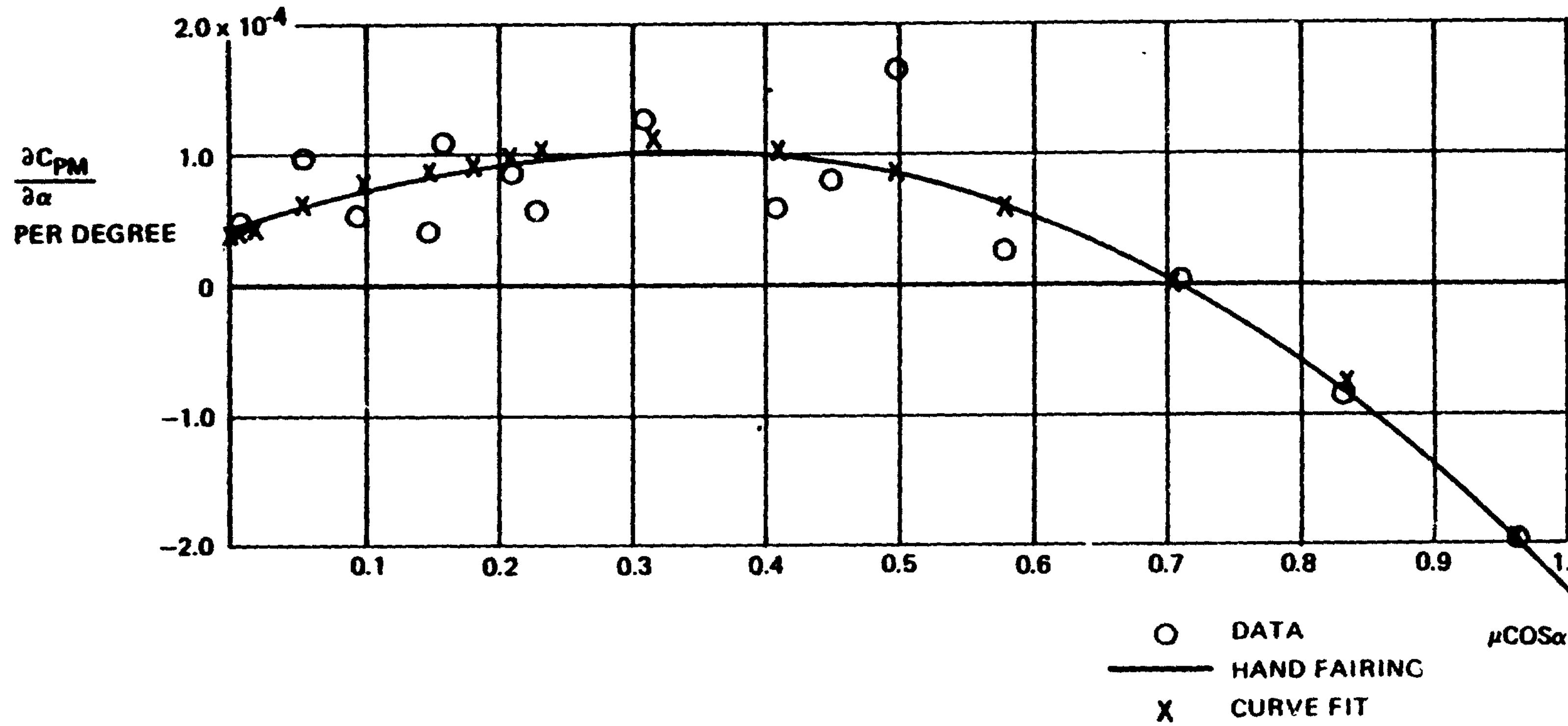

Figure 3-23. Variation of $\frac{\partial C_{PM}}{\partial \alpha}$ with $\mu\cos\alpha$.

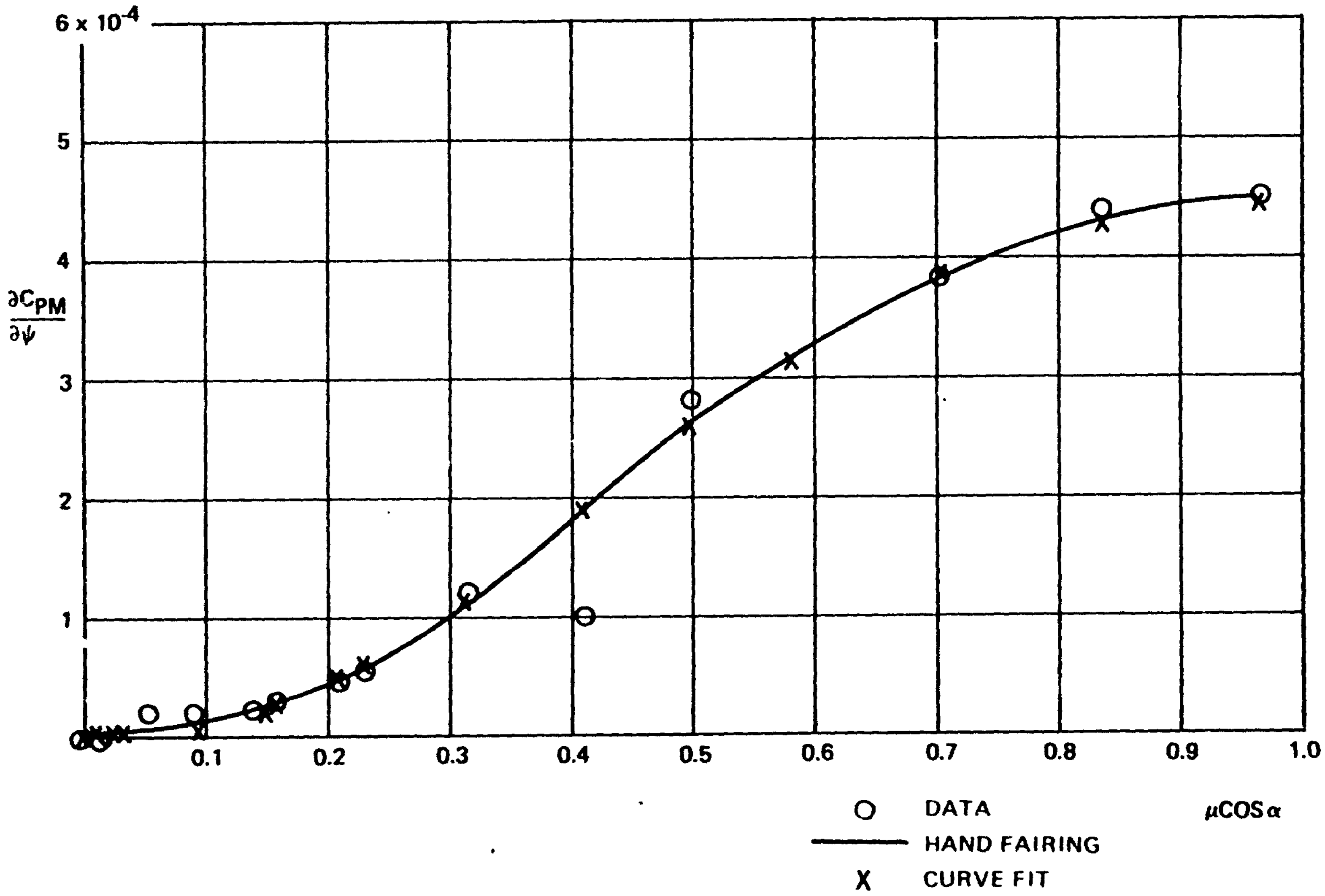

Figure 3-24. Variation of $\frac{\partial C_{PM}}{\partial \psi}$ with $\mu \cos\alpha$.

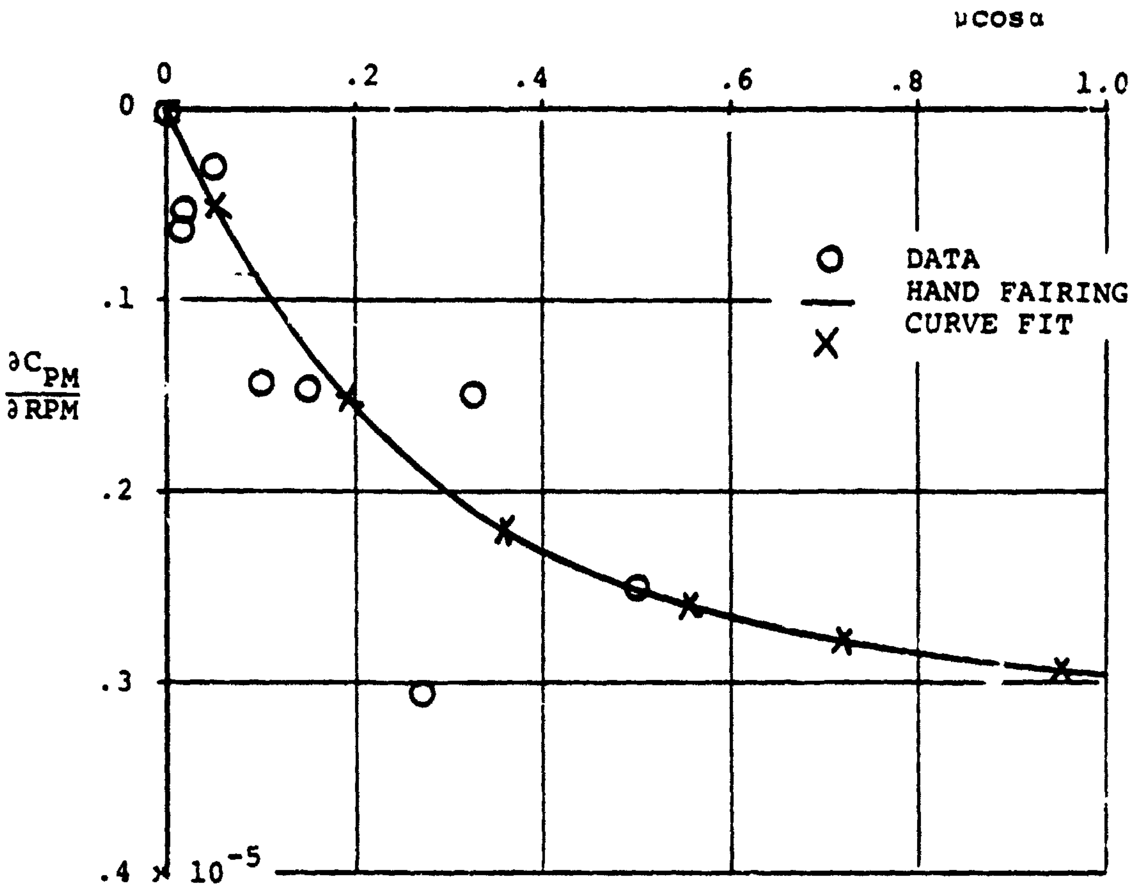

Figure 3.25. Variation of $\partial C_{PM}/\partial RPM$ with $\mu\cos\alpha$.

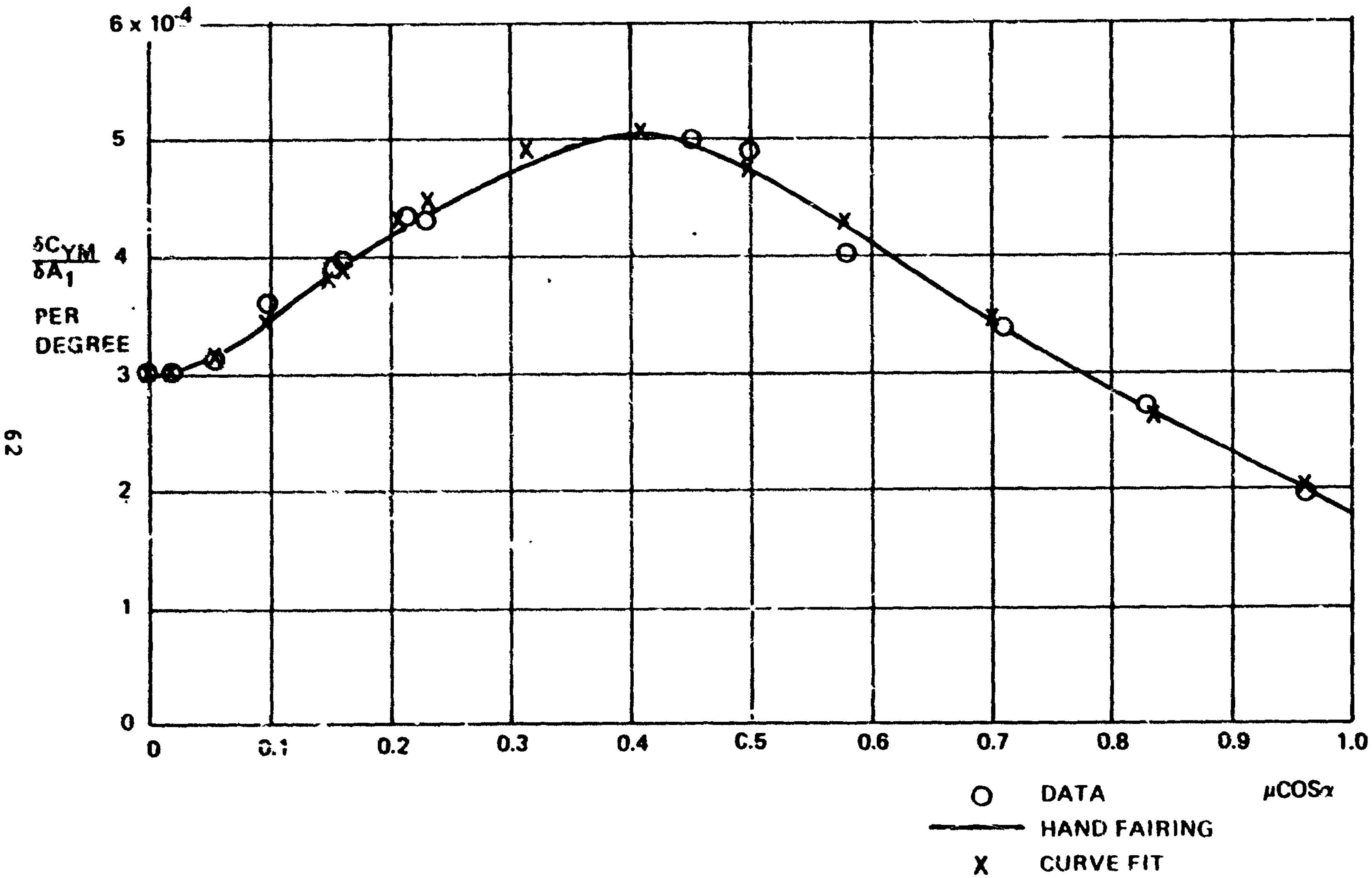

Figure 3-26. Variation of $\frac{\partial C_{YM}}{\partial A_1}$ with μcosα.

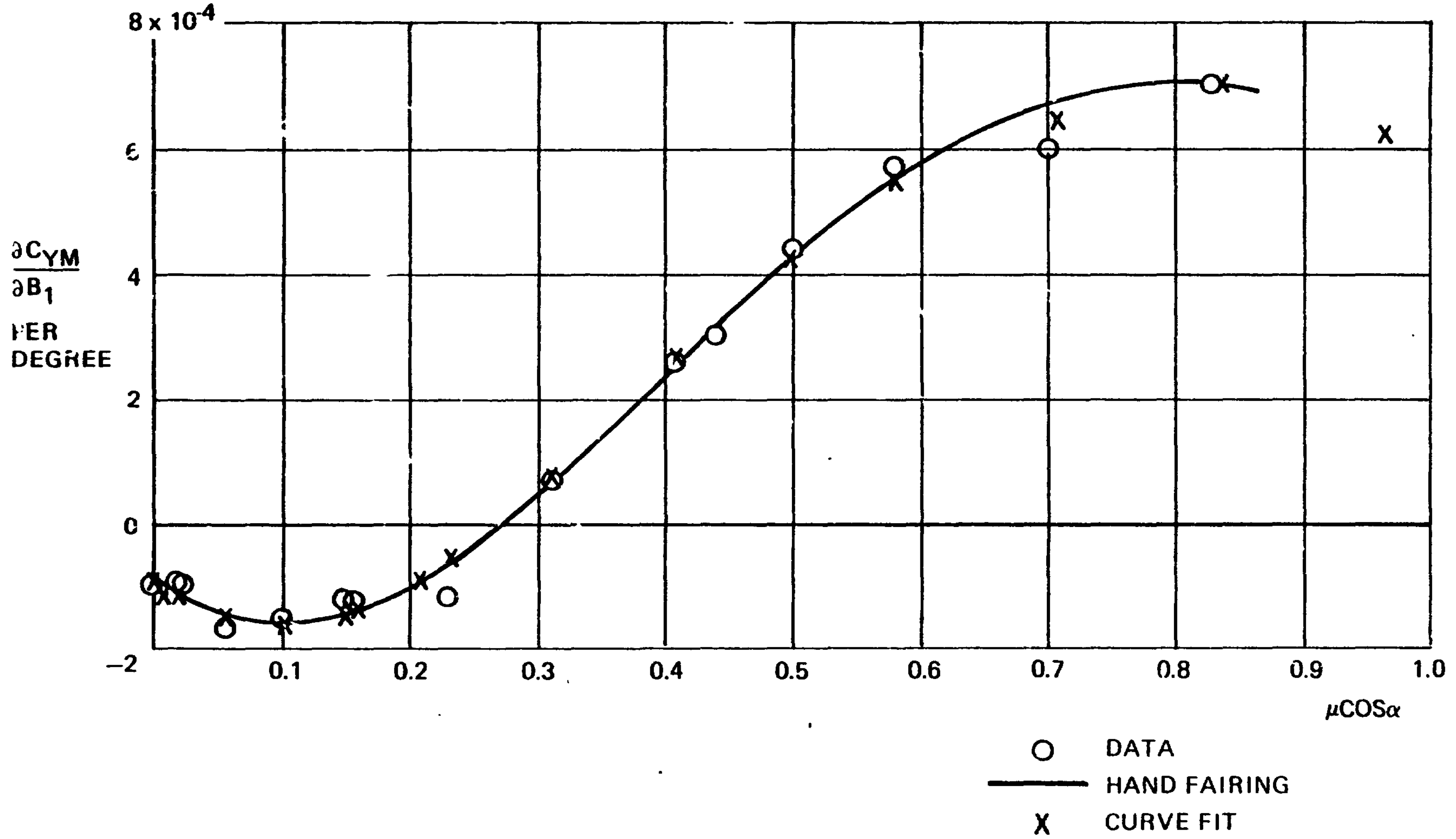

Figure 3-27. Variation of $\frac{\partial C_{YM}}{\partial B_1}$ with μcosα.

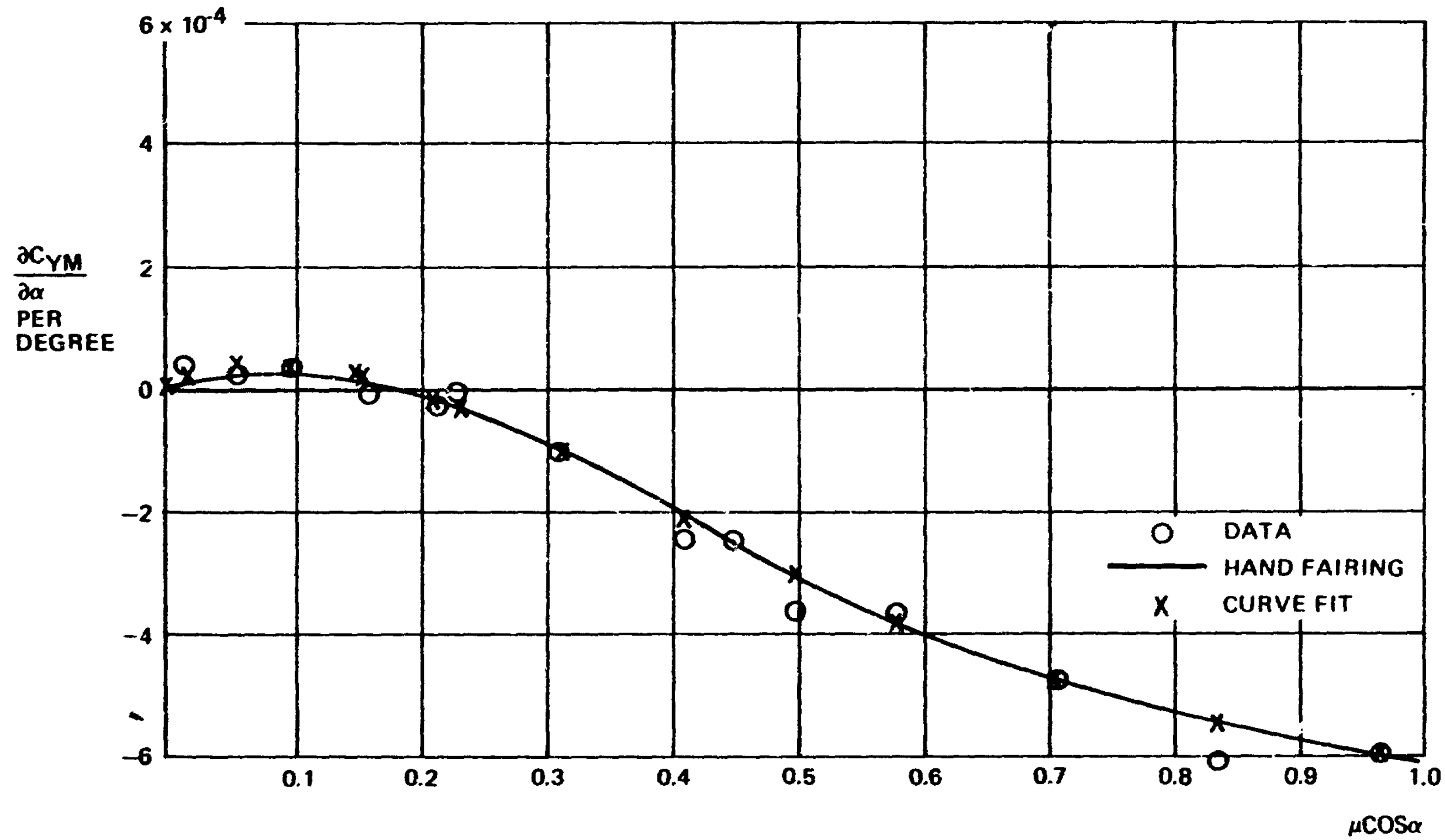

Figure 3-28. Variation of $\frac{\partial C_{YM}}{\partial \alpha}$ with $\mu\cos\alpha$.

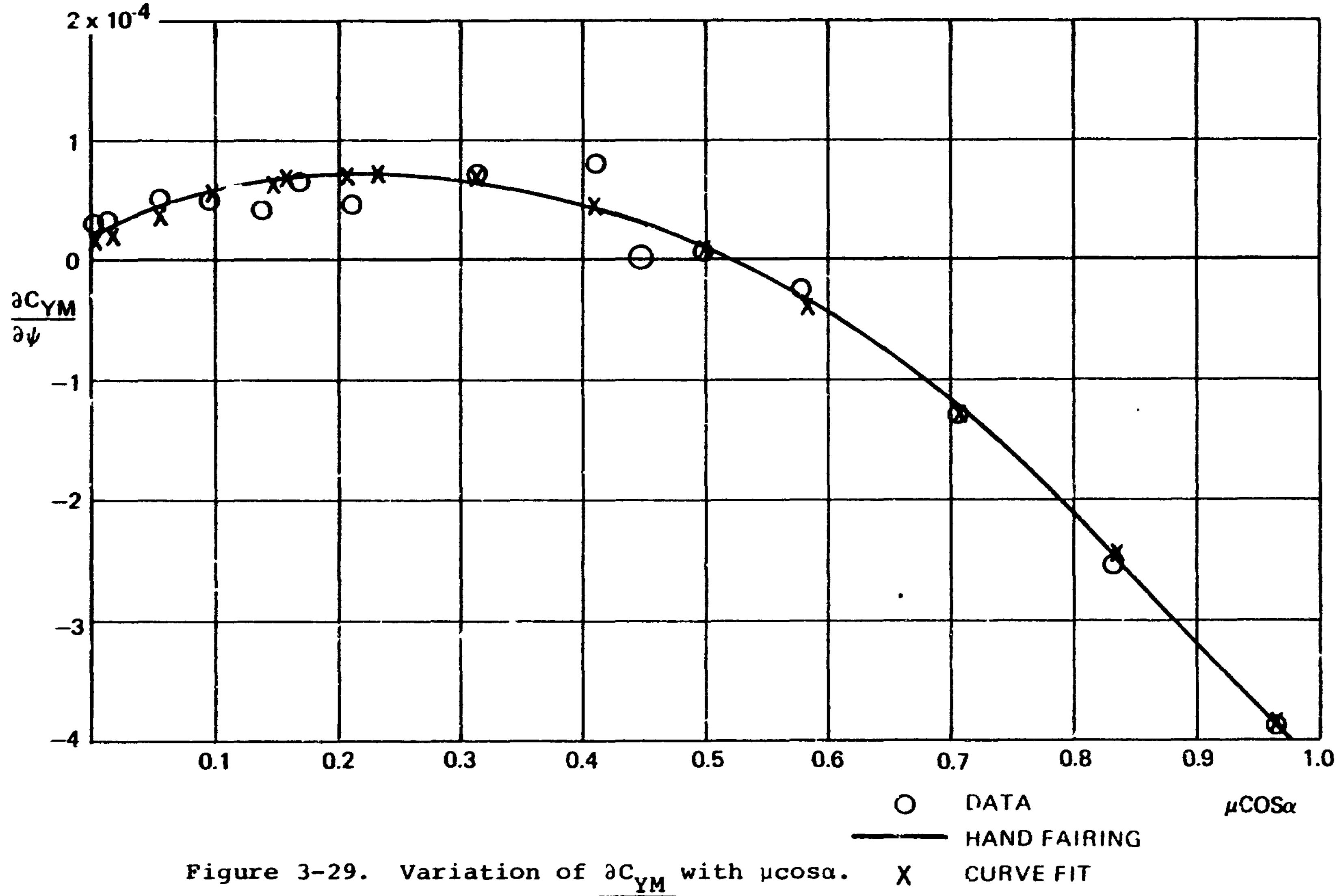

Figure 3-29. Variation of $\frac{\partial C_{YM}}{\partial \psi}$ with μcosα.

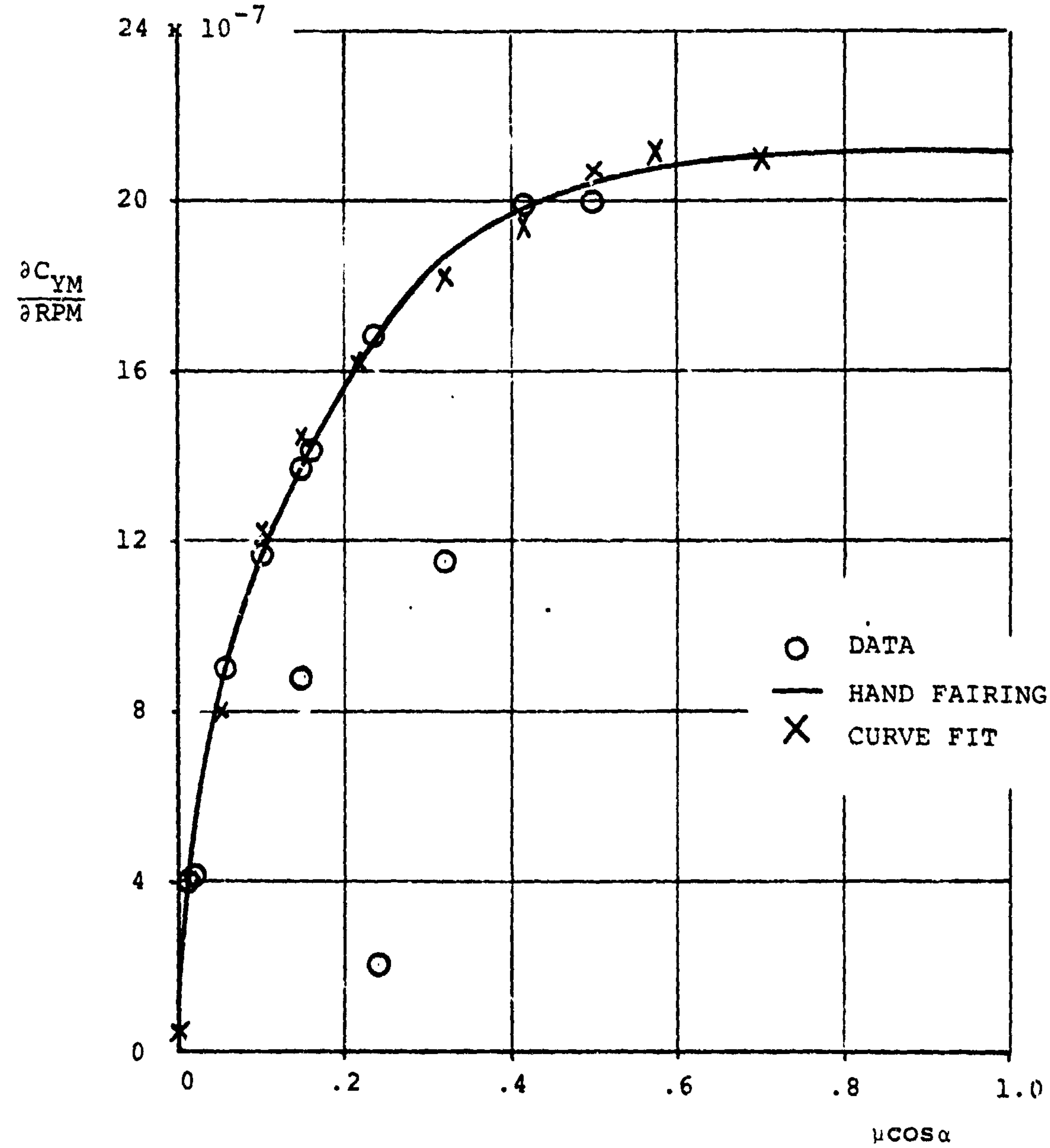

Figure 3.30. Varation of $\partial C_{YM}/\partial RPM$ with $\mu\cos\alpha$.

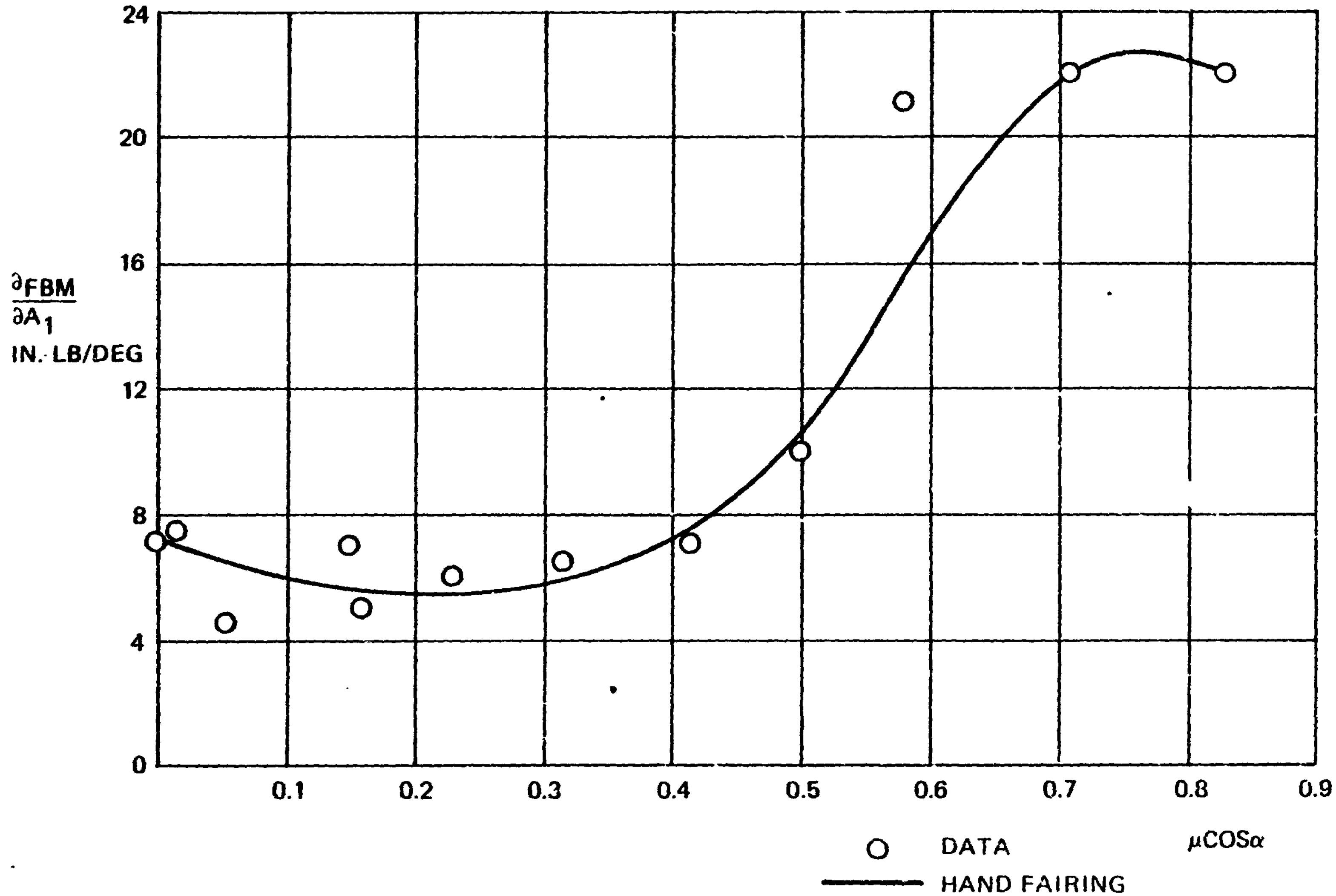

Figure 3-31. Variation of $\frac{\partial FBM}{\partial A_1}$ with $\mu\cos\alpha$.

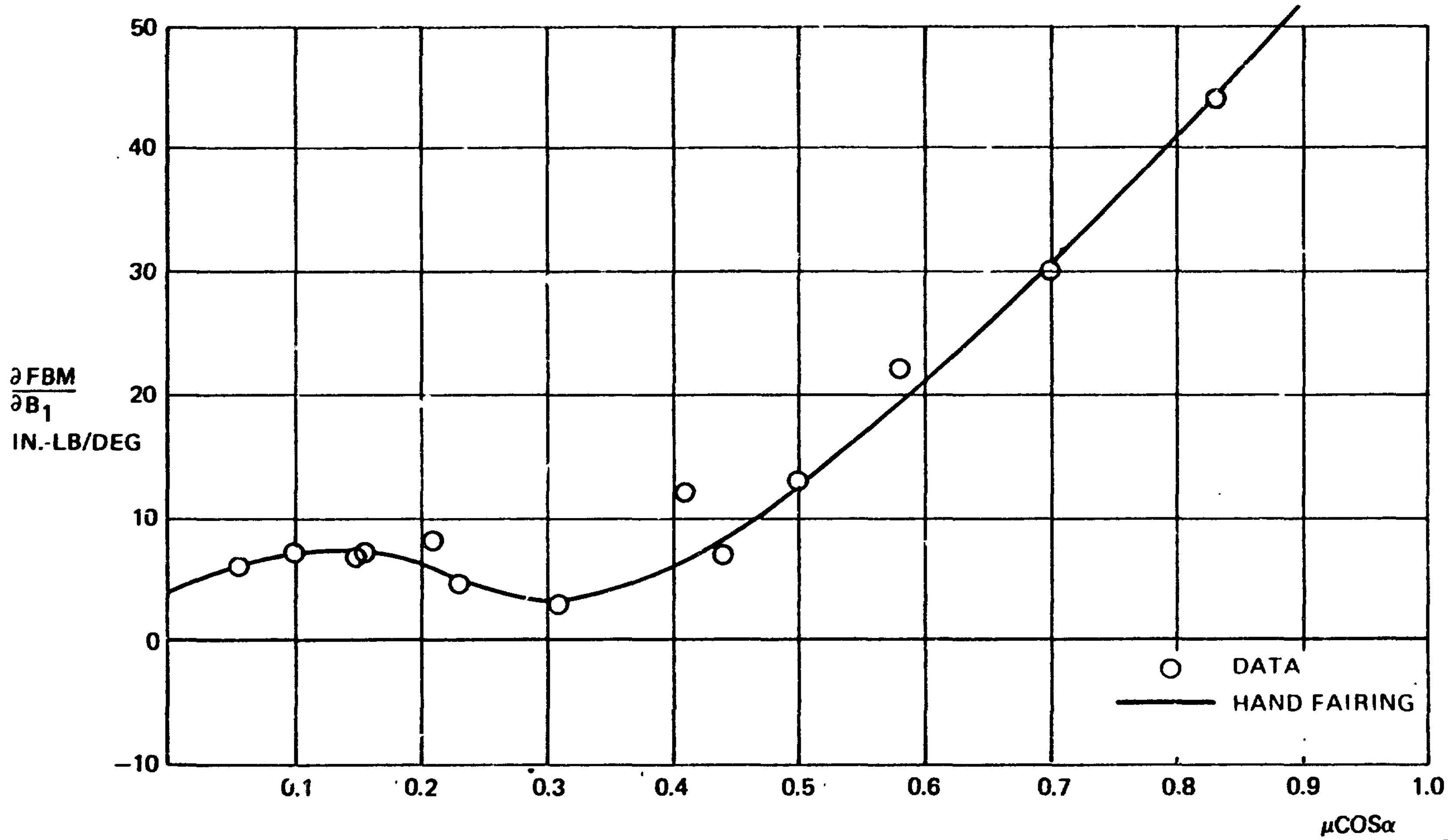

Figure 3-32. Variation of $\frac{\partial FBM}{\partial B_1}$ with $\mu \cos\alpha$.

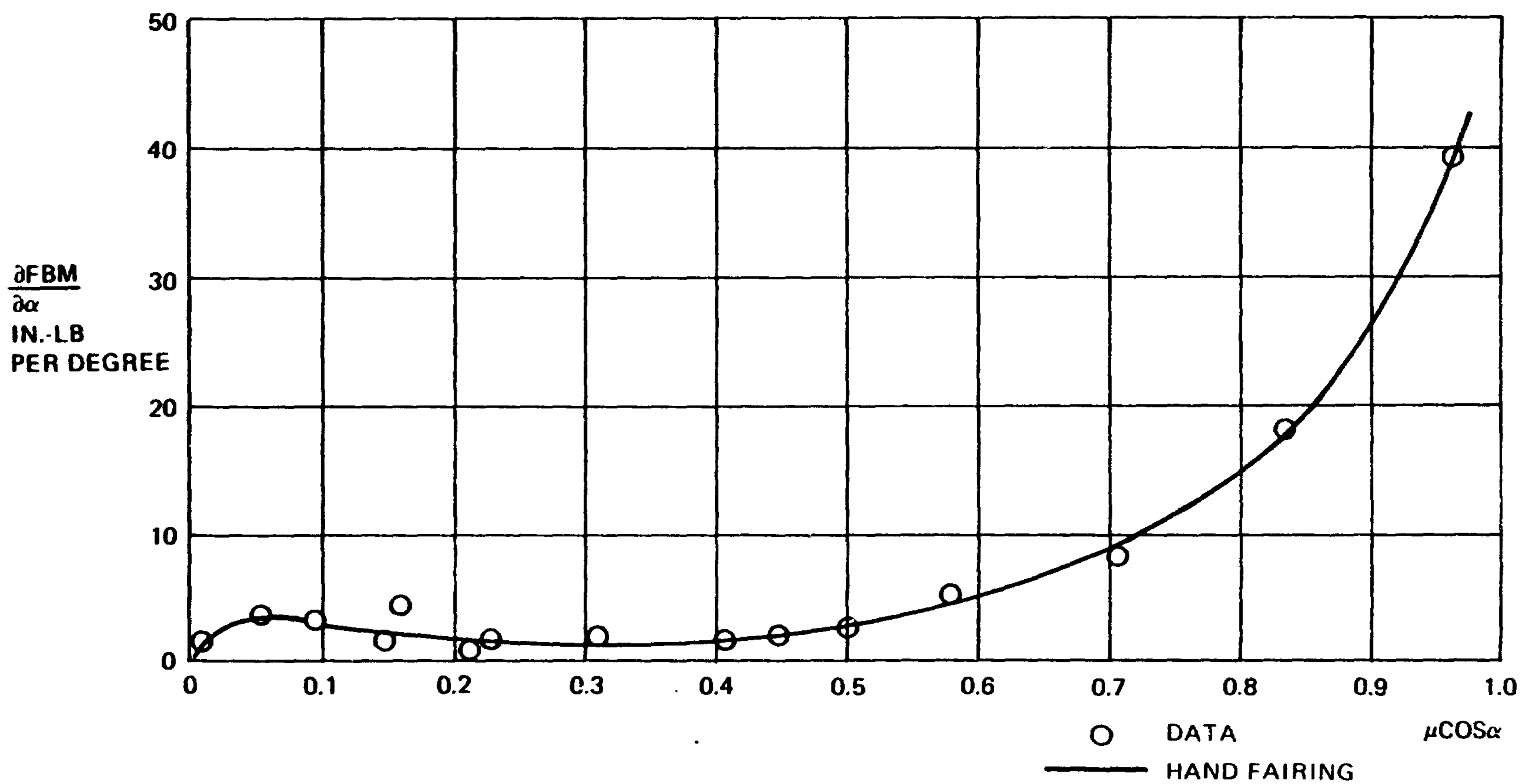

Figure 3-33. Variation of $\frac{\partial FBM}{\partial \alpha}$ with $\mu\cos\alpha$.

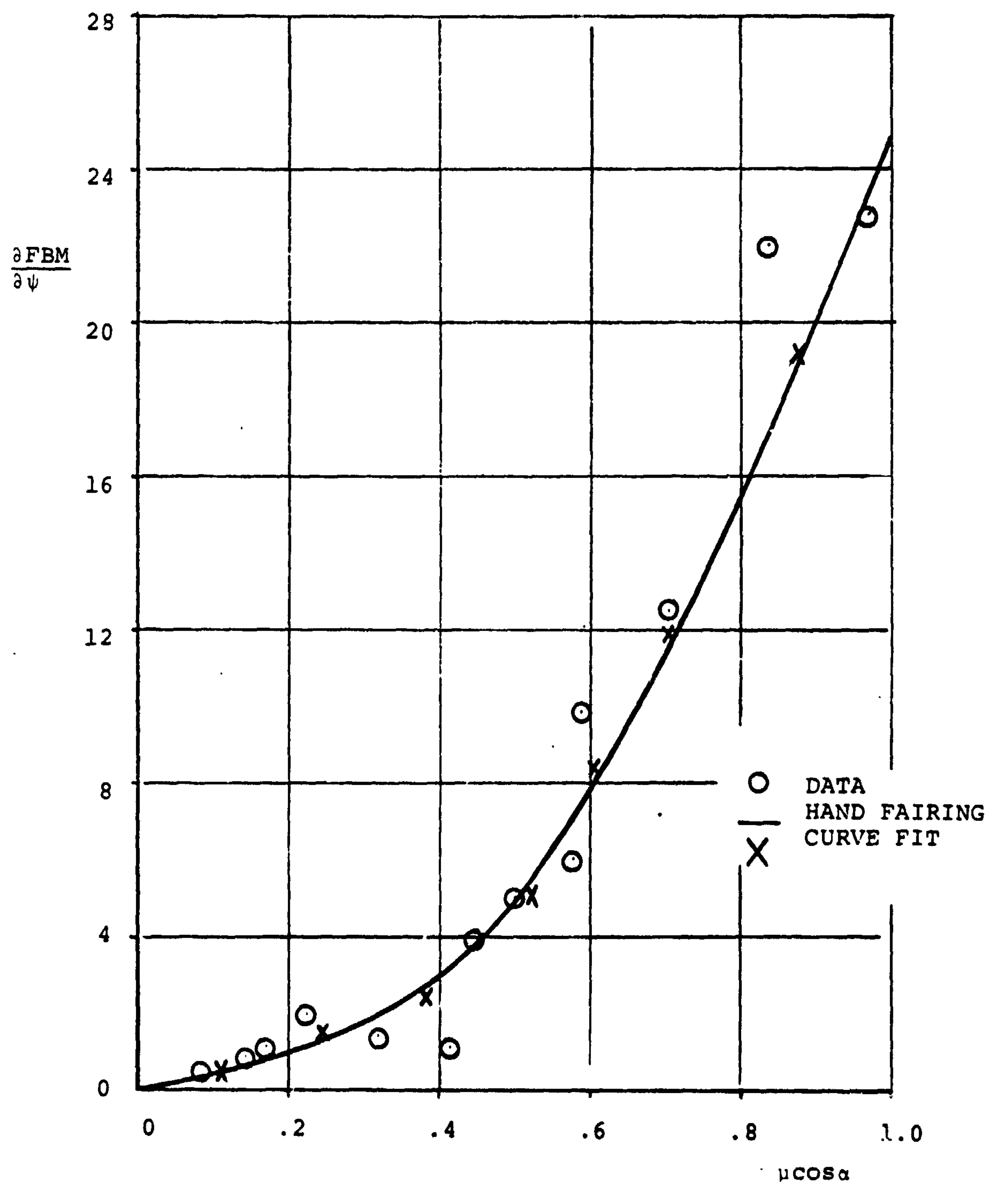

Figure 3.34. Variation of ∂FBM/∂ψ with μcosα.

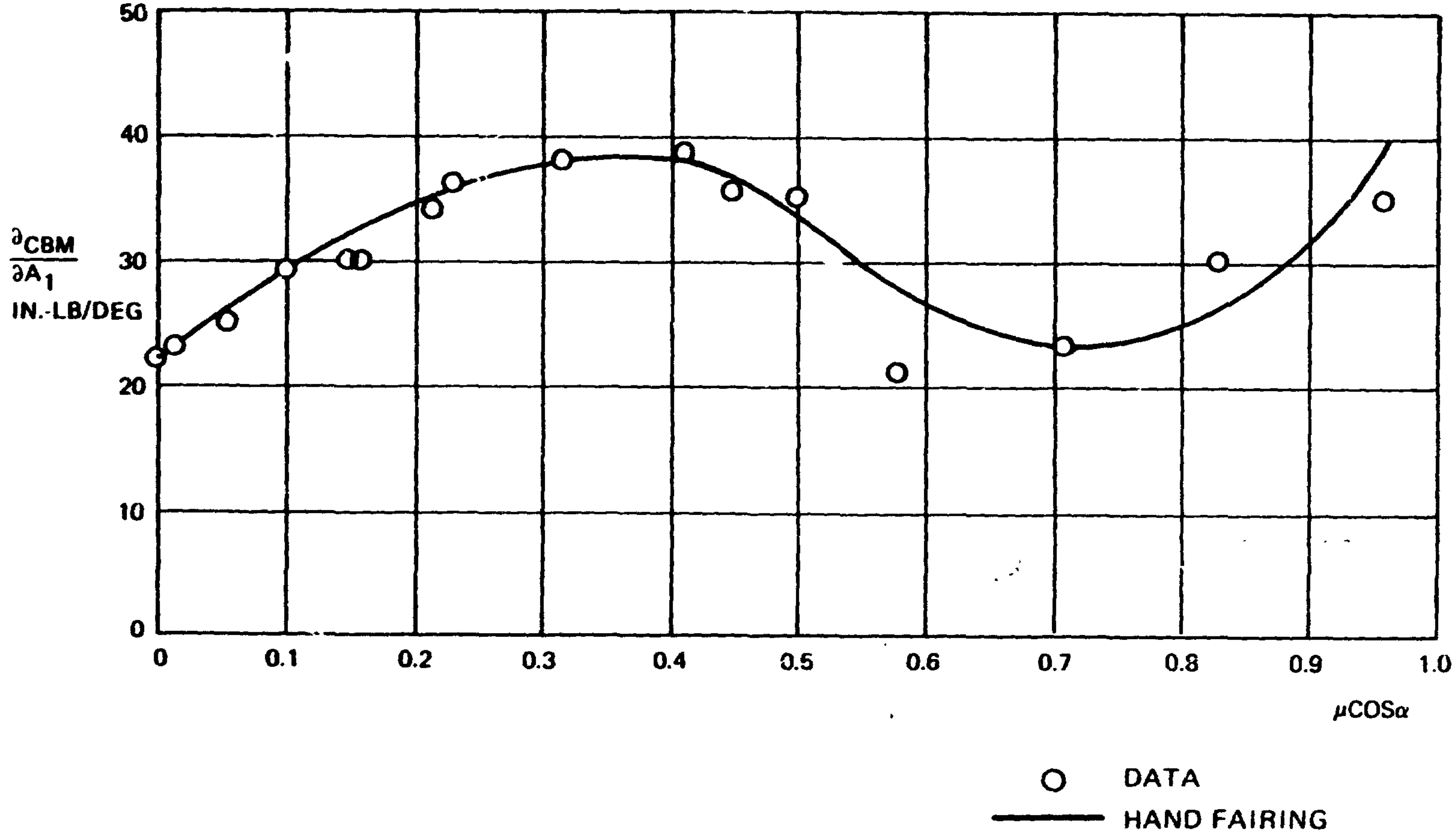

Figure 3-35. Variation of $\frac{\partial CBM}{\partial A_1}$ with $\mu \cos\alpha$.

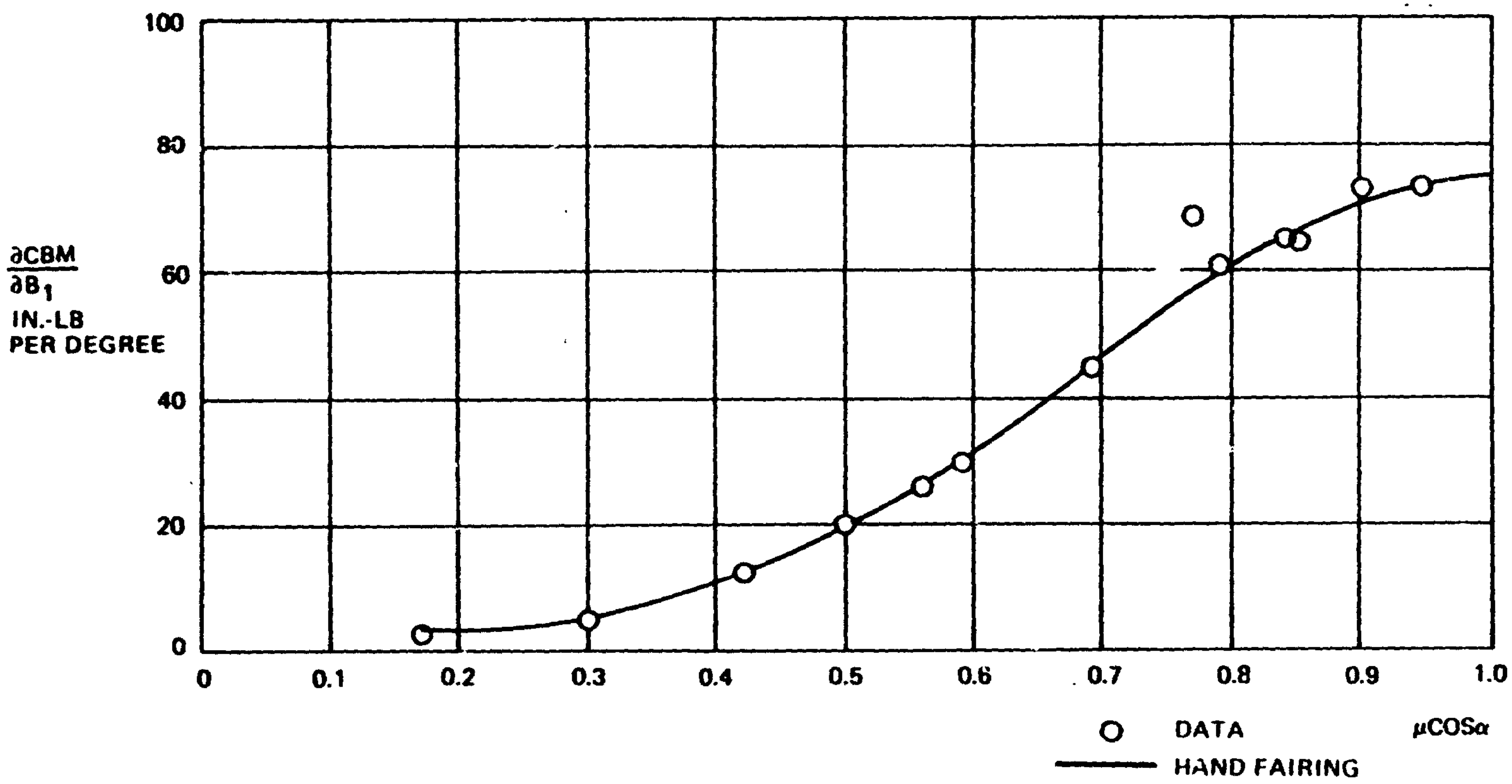

Figure 3-36. Variation of $\frac{\partial CBM}{\partial B_1}$ with $\mu\cos\alpha$.

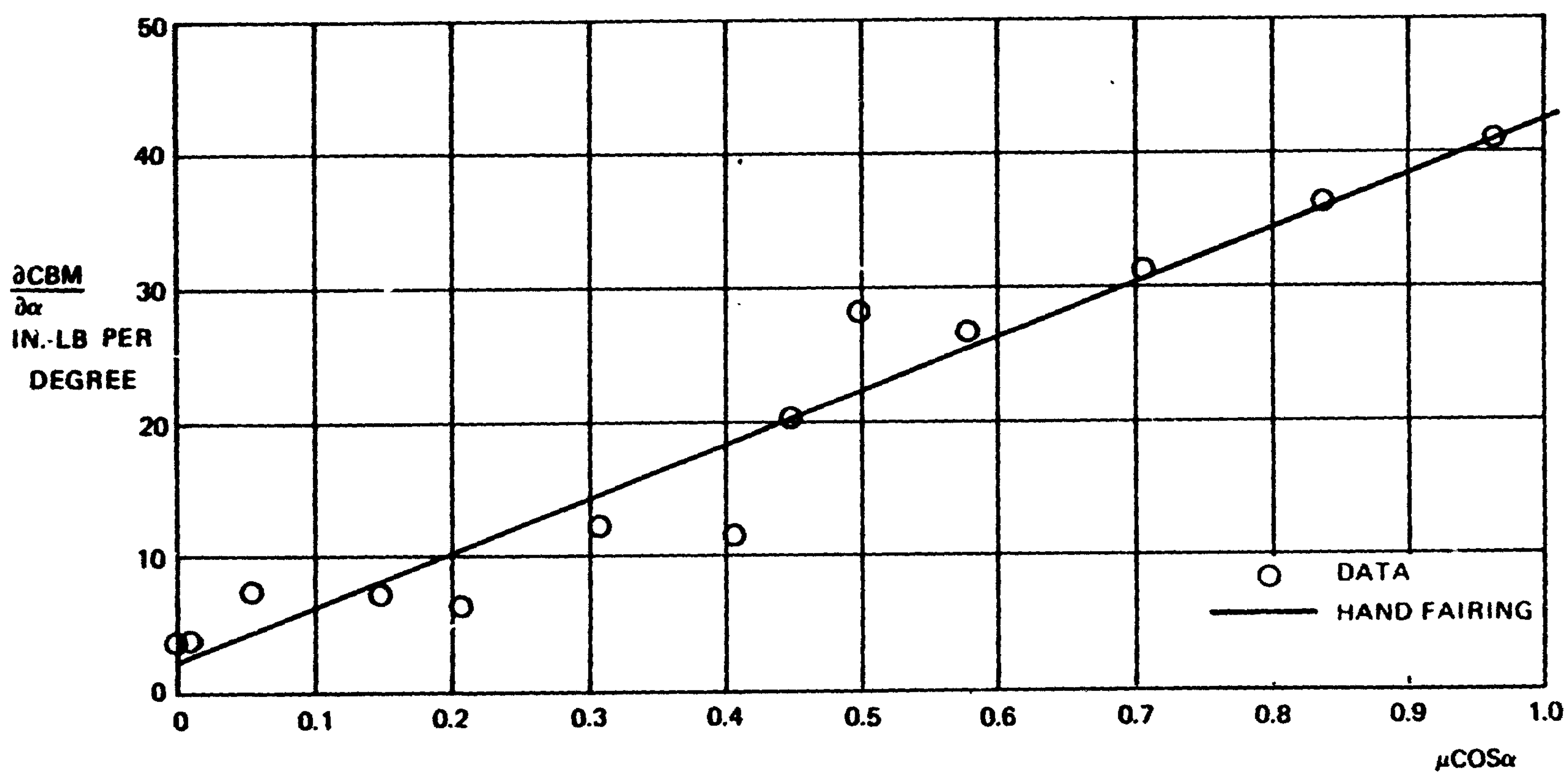

Figure 3-37. Variation of $\frac{\partial CBM}{\partial \alpha}$ with $\mu\cos\alpha$.

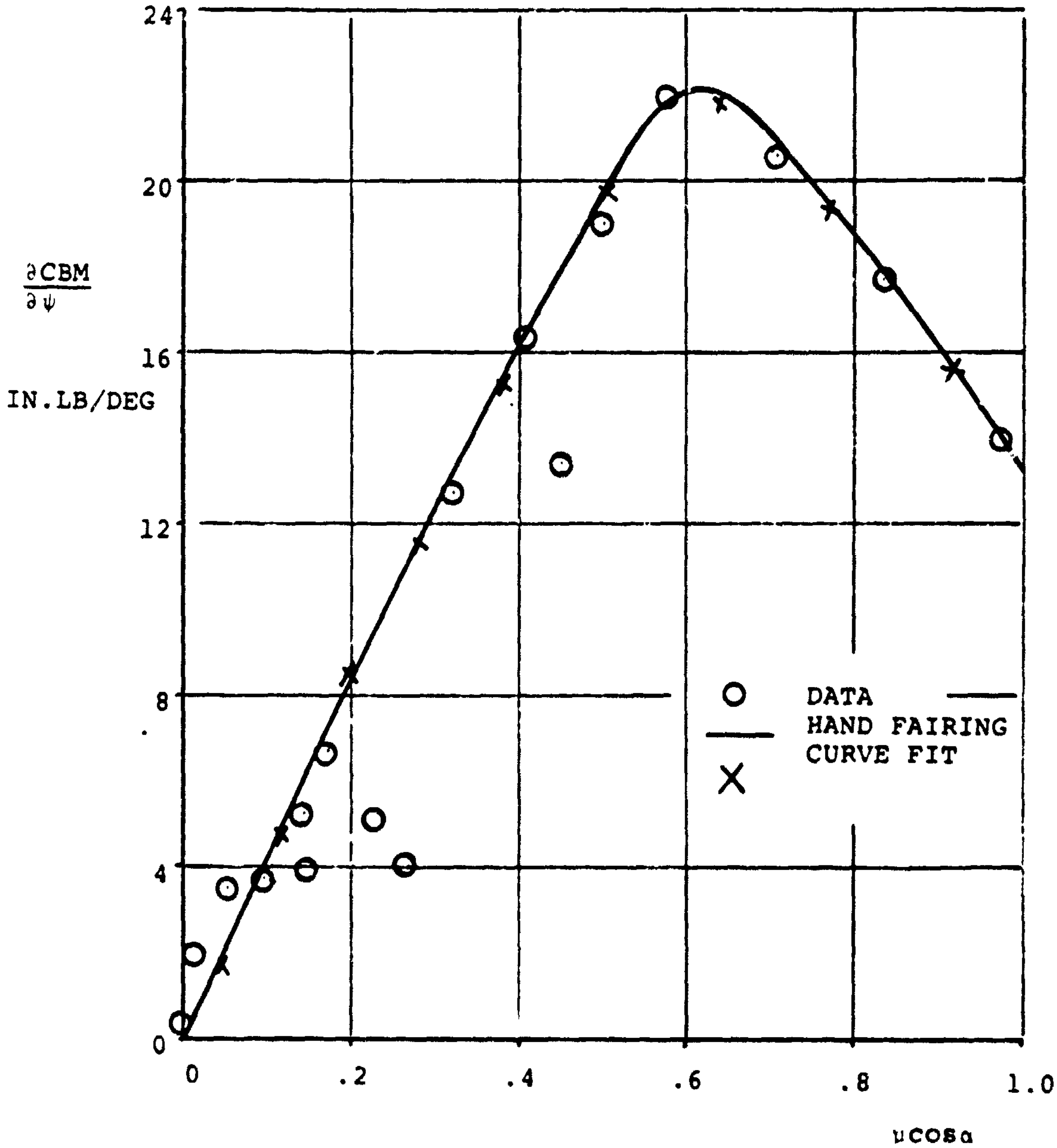

Figure 3.38. Variation of ∂CBM/∂ψ with μcosα.

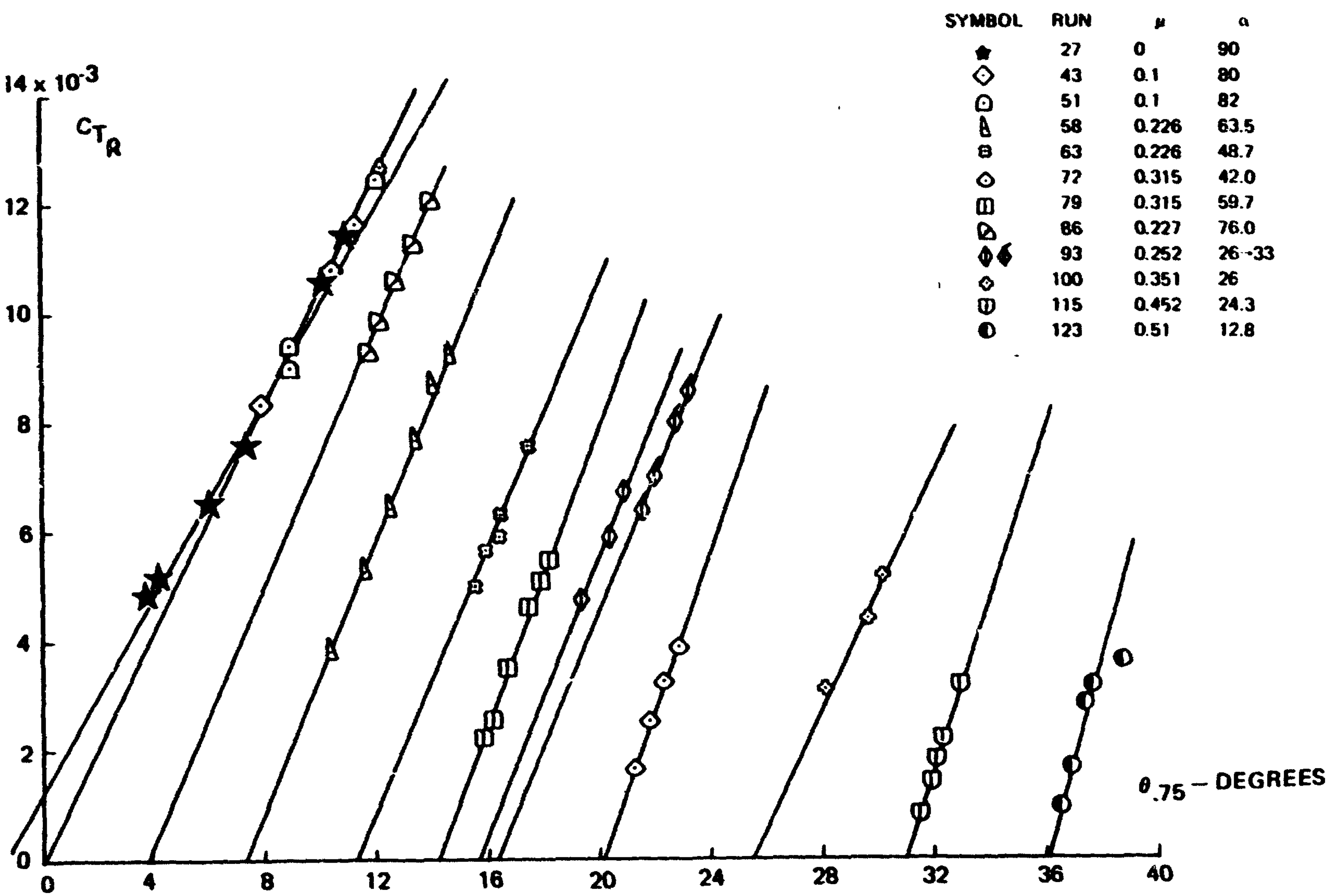

Figure 3.39. Variation of Corrected Thrust Coefficient With Collective Pitch

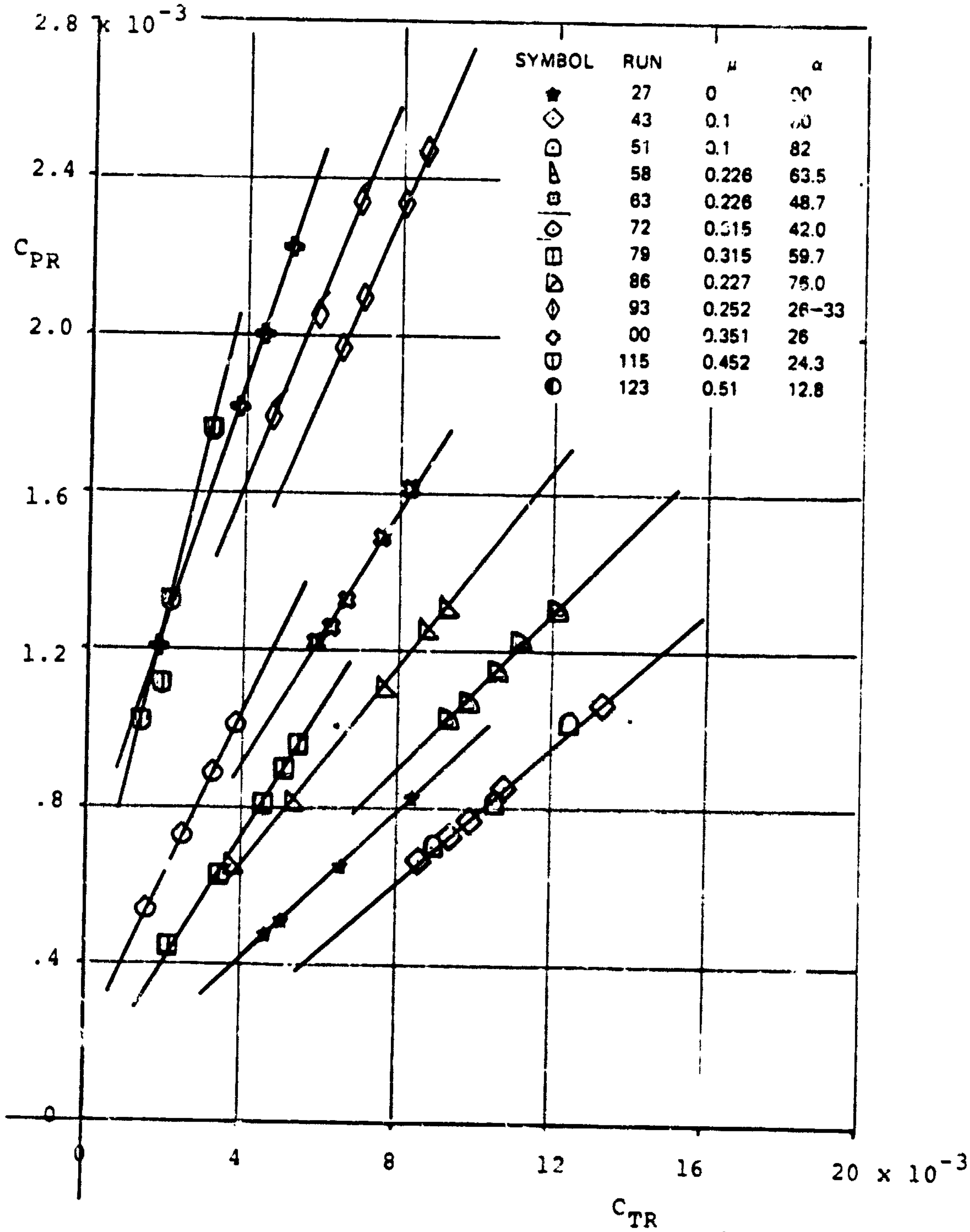

Figure 3.40. Corrected Power Coefficient versus Corrected Thrust Coefficient

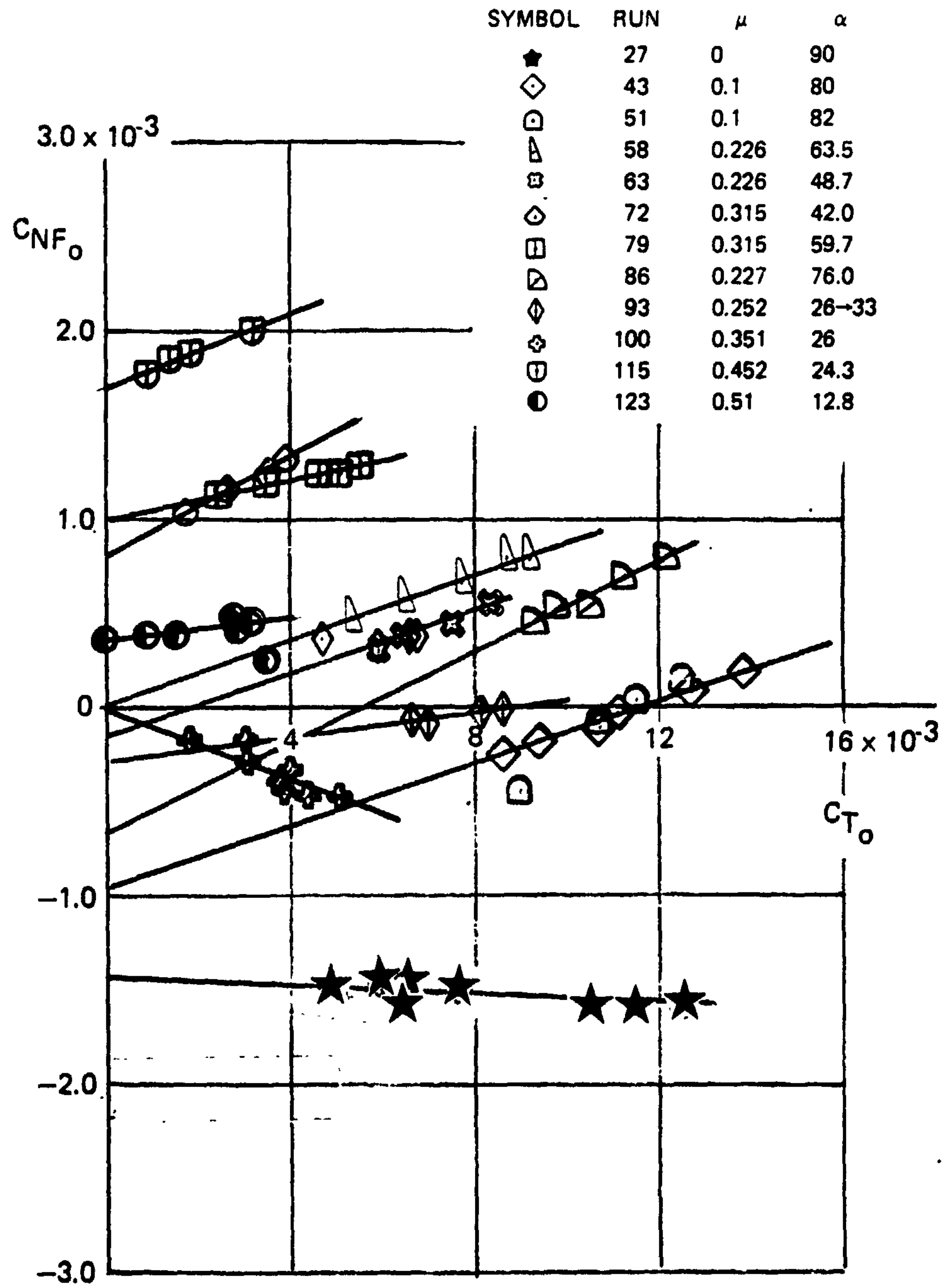

Figure 3.41. Corrected Normal Force Coefficient Versus Corrected Thrust Coefficient

C-2

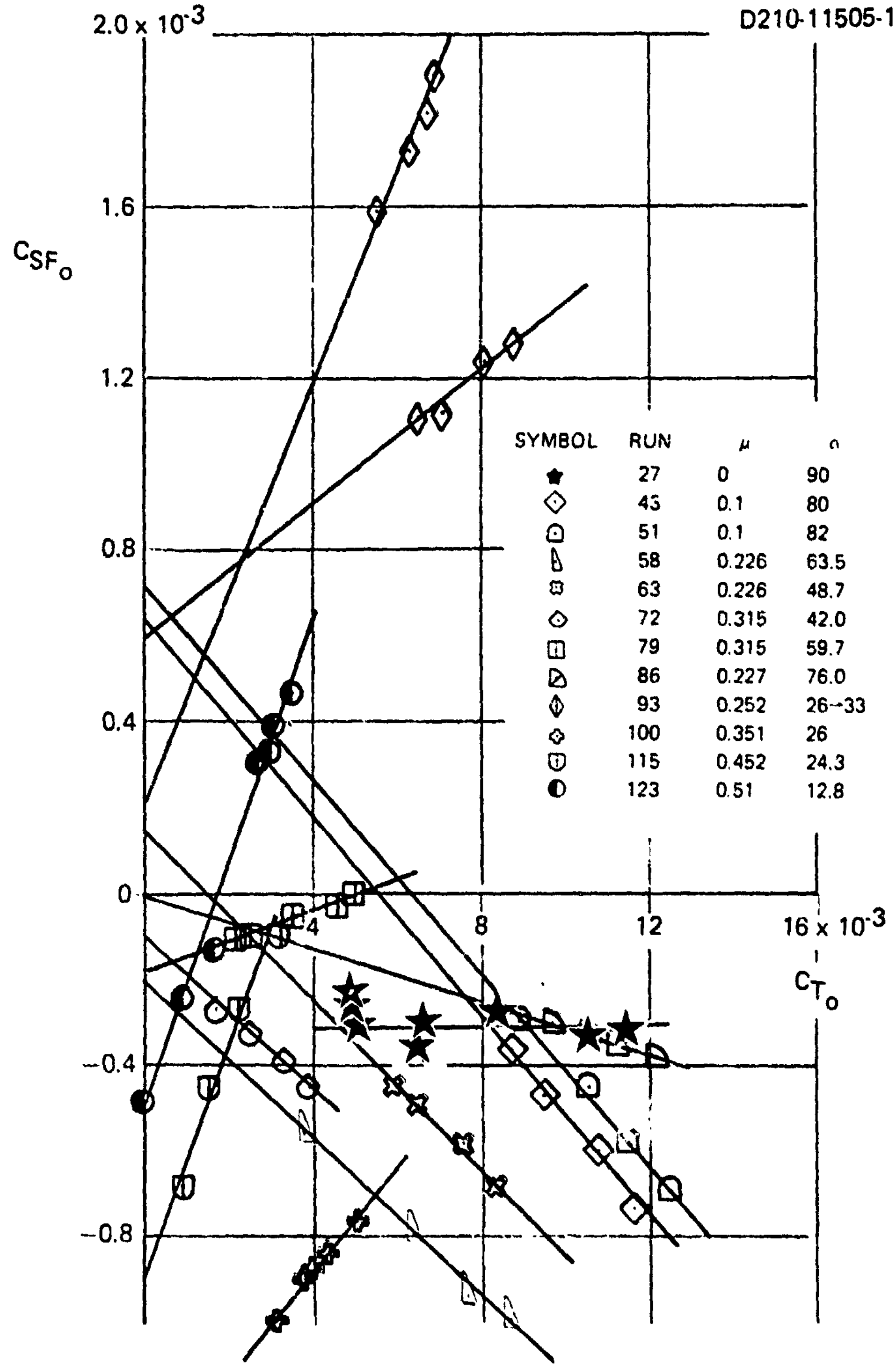

Figure 3.42. Corrected Sideforce Coefficient Versus Corrected Thrust Coefficient

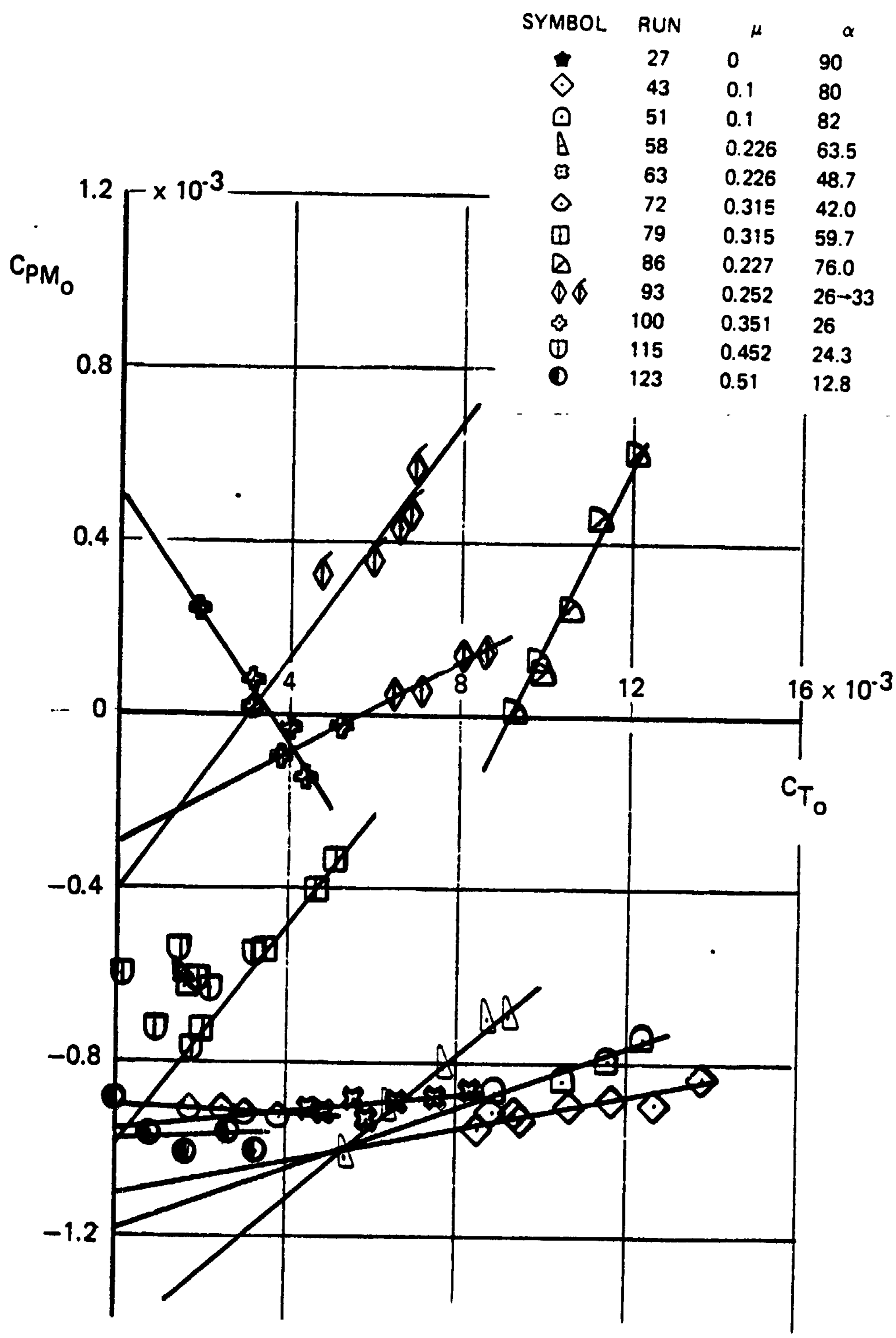

Figure 3.43. Corrected Pitching Moment Coefficient Versus Corrected Thrust Coefficient

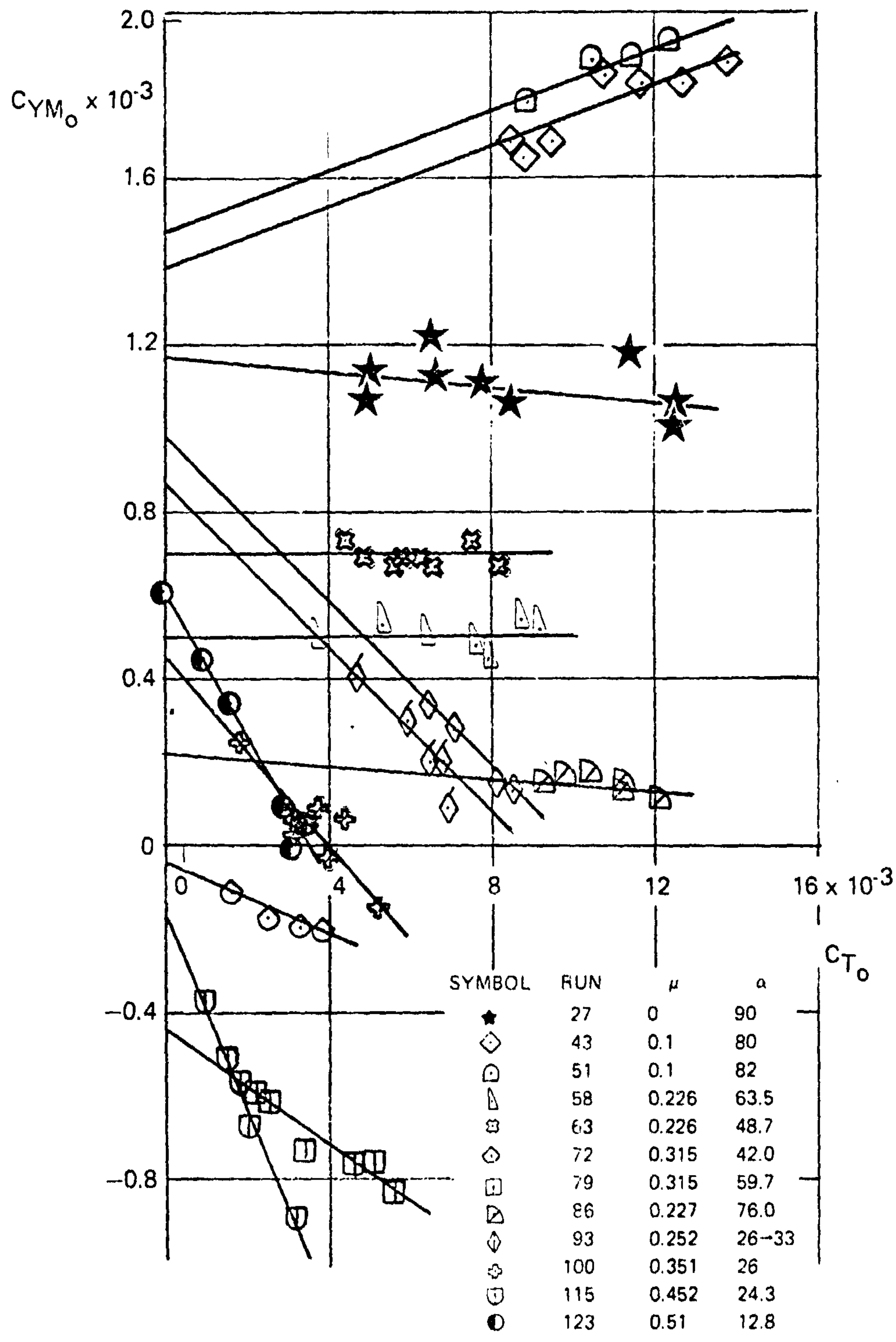

Figure 3.44. Corrected Yawing Moment Coefficient Versus Corrected Thrust Coefficient

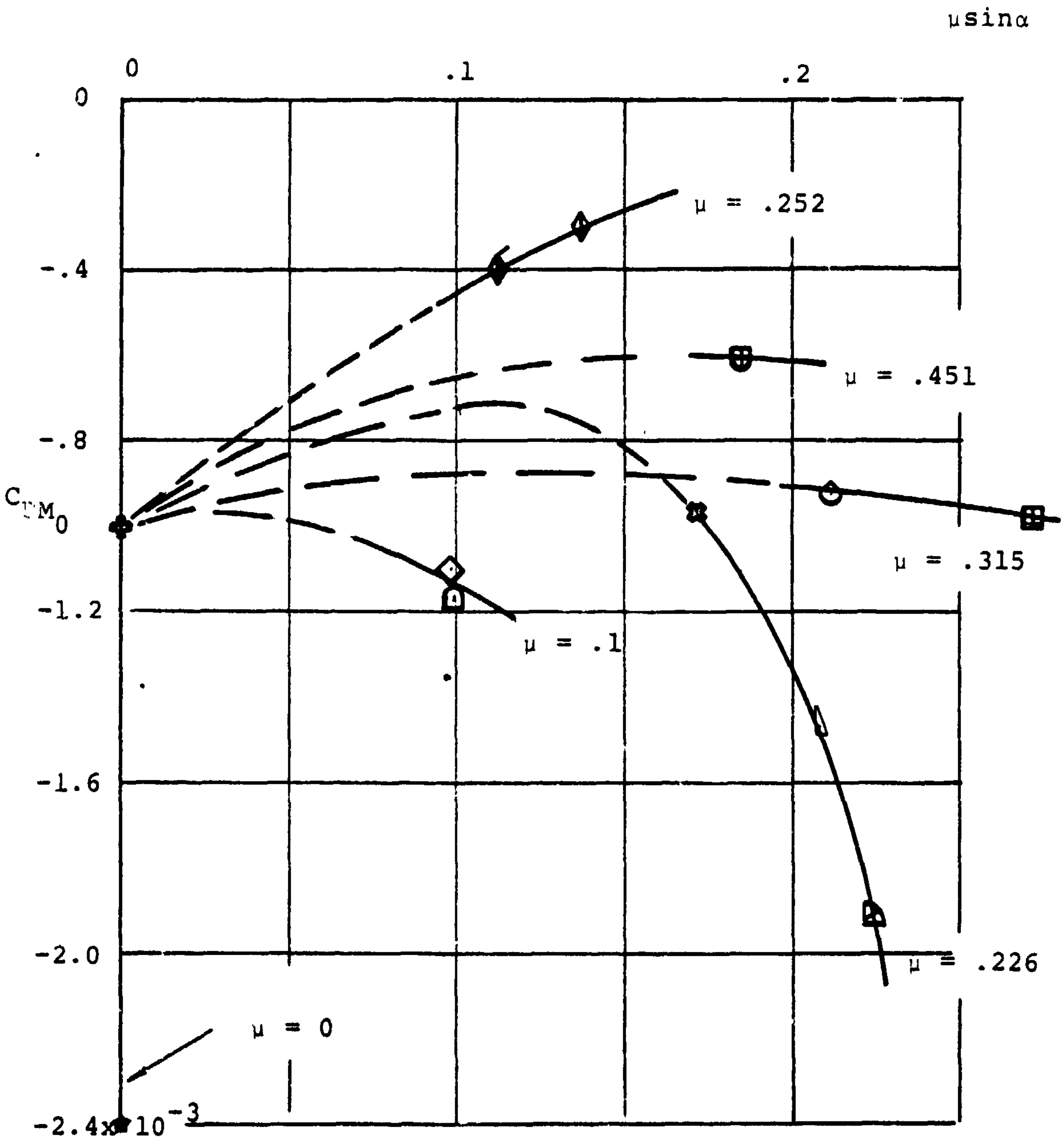

Figure 3.45. Variations of the Reduced Pitching Moment Coefficient at Zero Thrust with μsinα

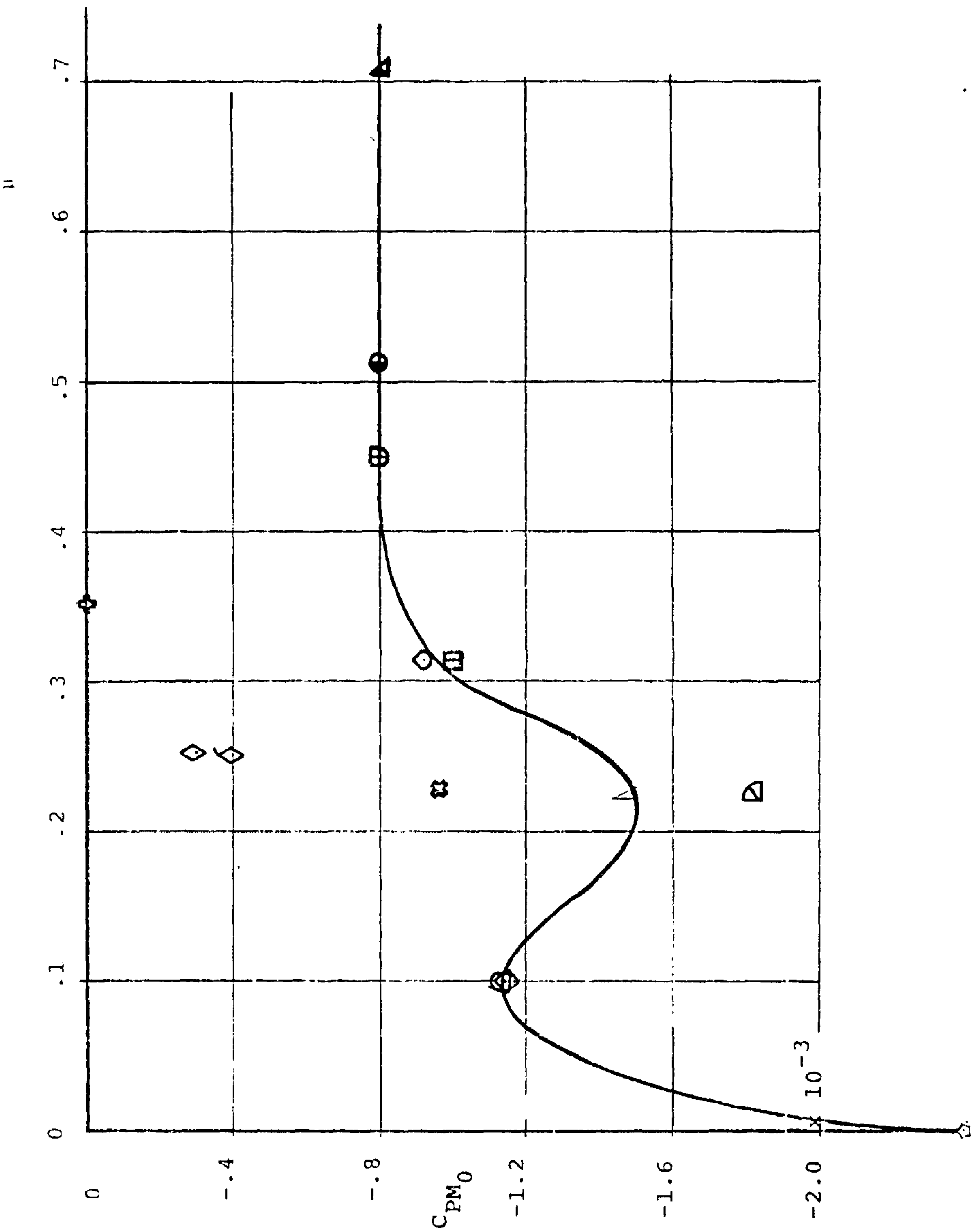

Figure 3.46. Illustration of Method of Fitting the Reduced Data.

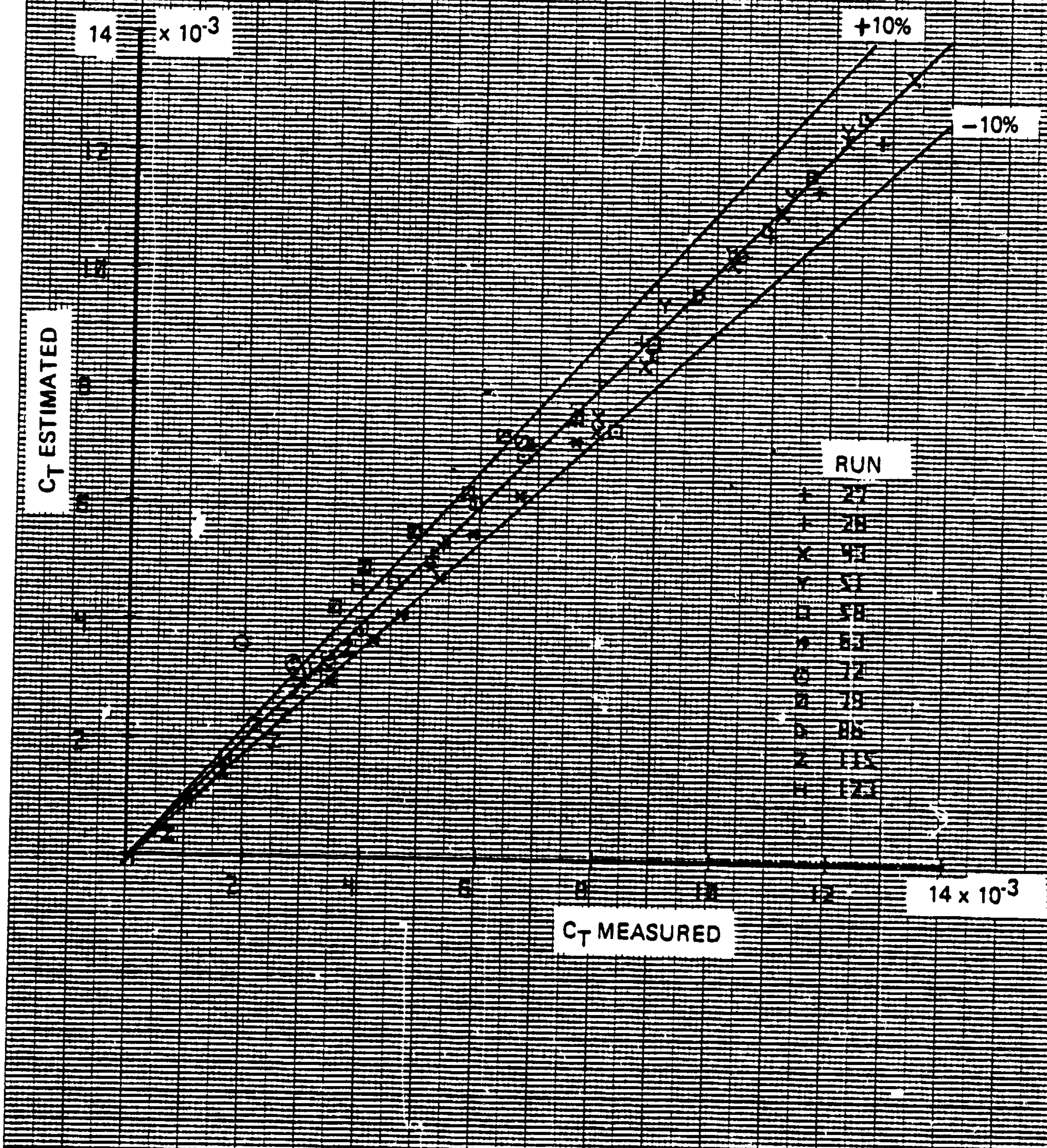

Figure 3.47. Thrust Coefficient Correlation - Collective Sweeps

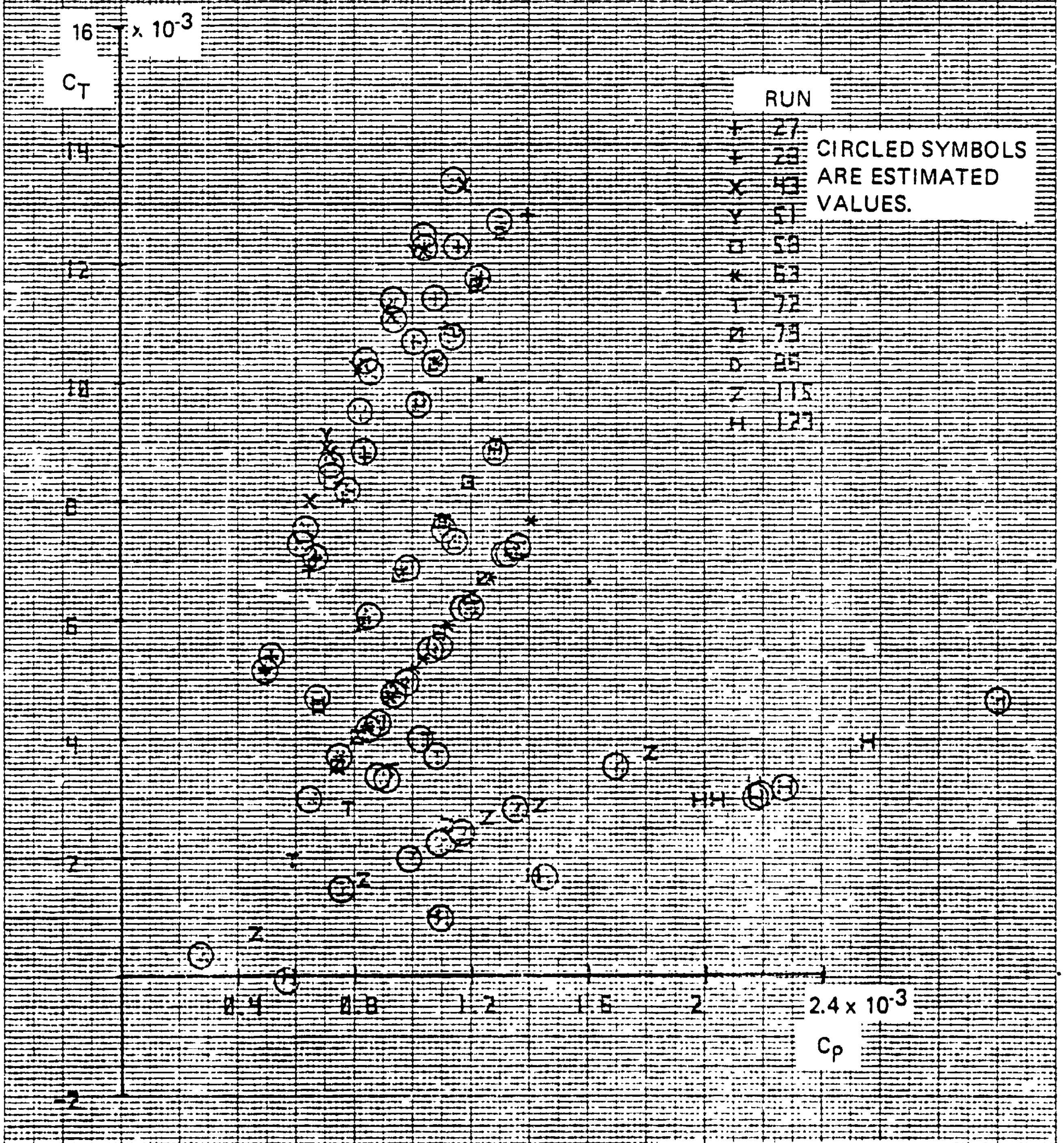

Figure 3.48. Variation of Estimated and Test Values of Power Coefficient With Thrust Coefficient

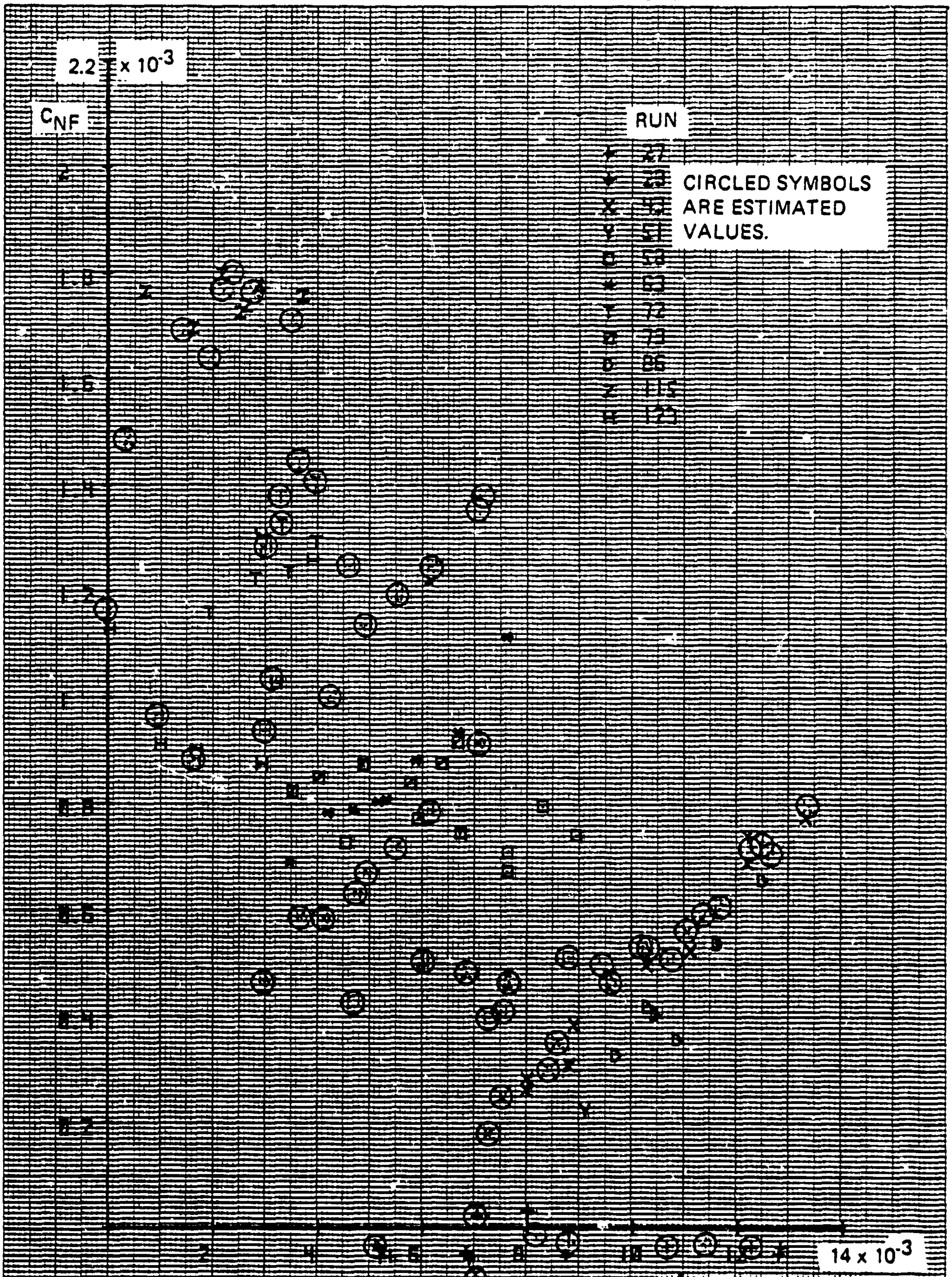

Figure 3.49. Variation of Estimated and Test Values of Normal Force Coefficient With Thrust Coefficient

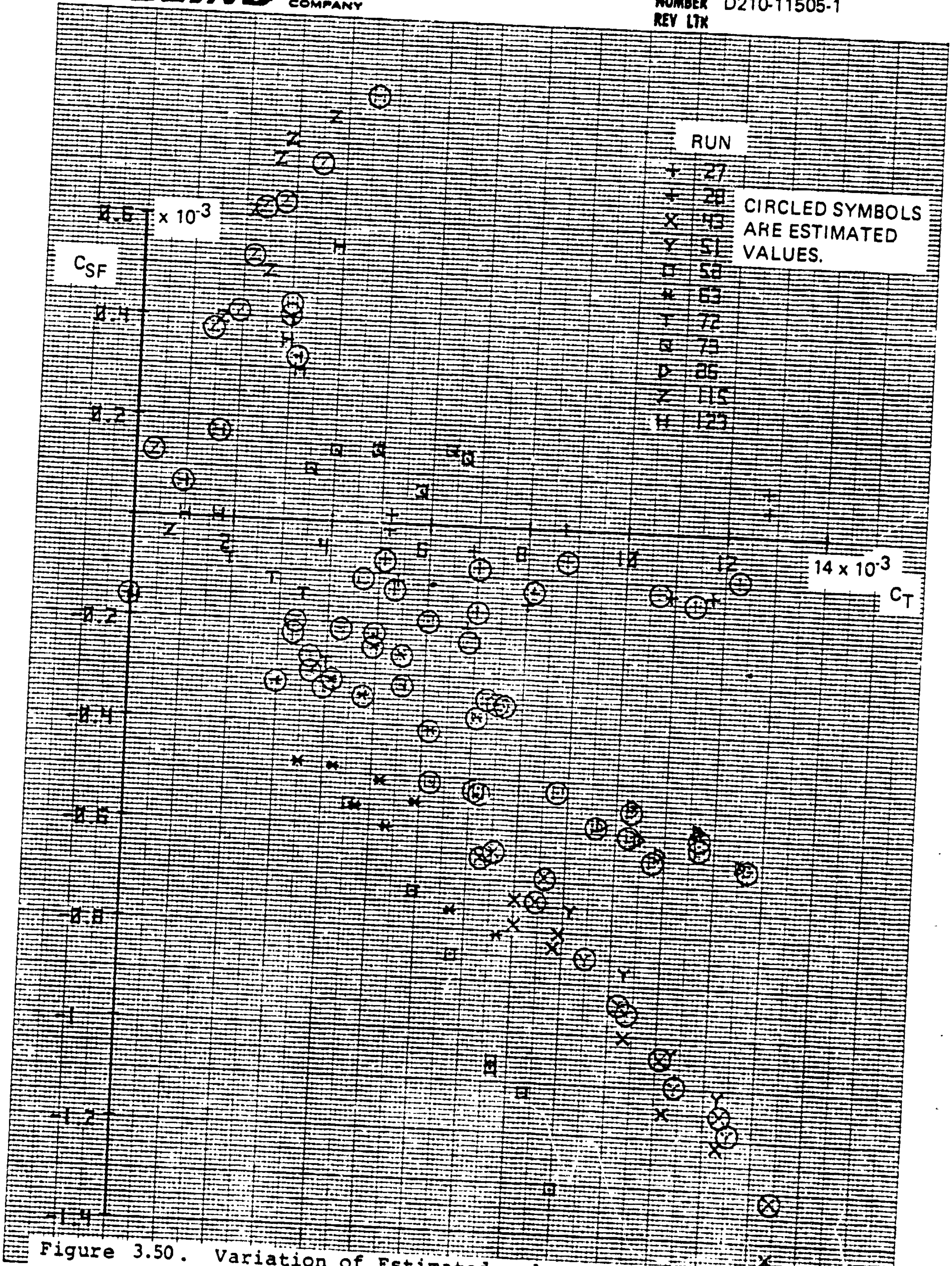

Figure 3.50. Variation of Estimated and Test Values of Sideforce Coefficient With Thrust Coefficient

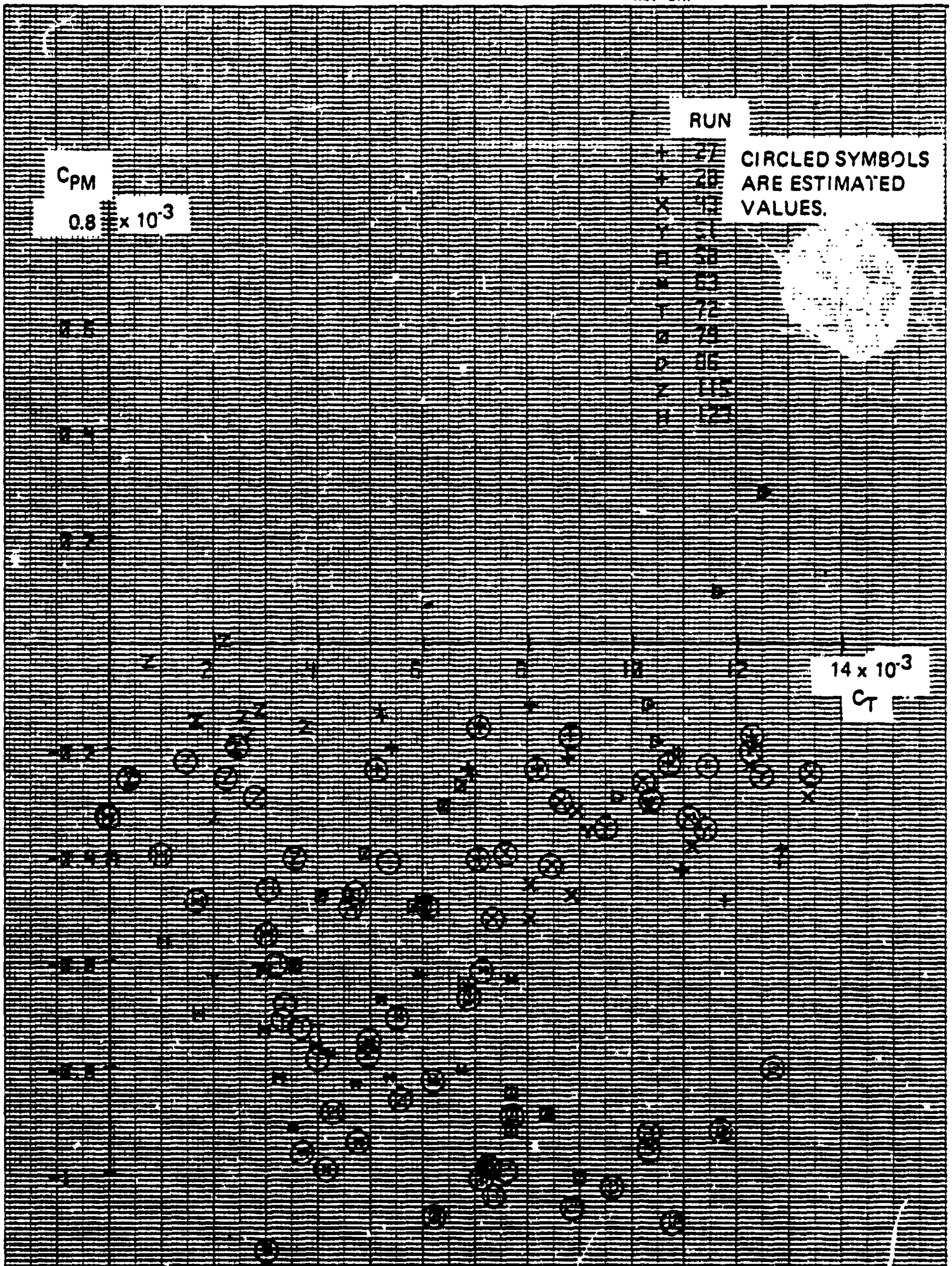

Figure 3.51. Variation of Estimated and Test Values of Pitching Moment Coefficient with Thrust Coefficient

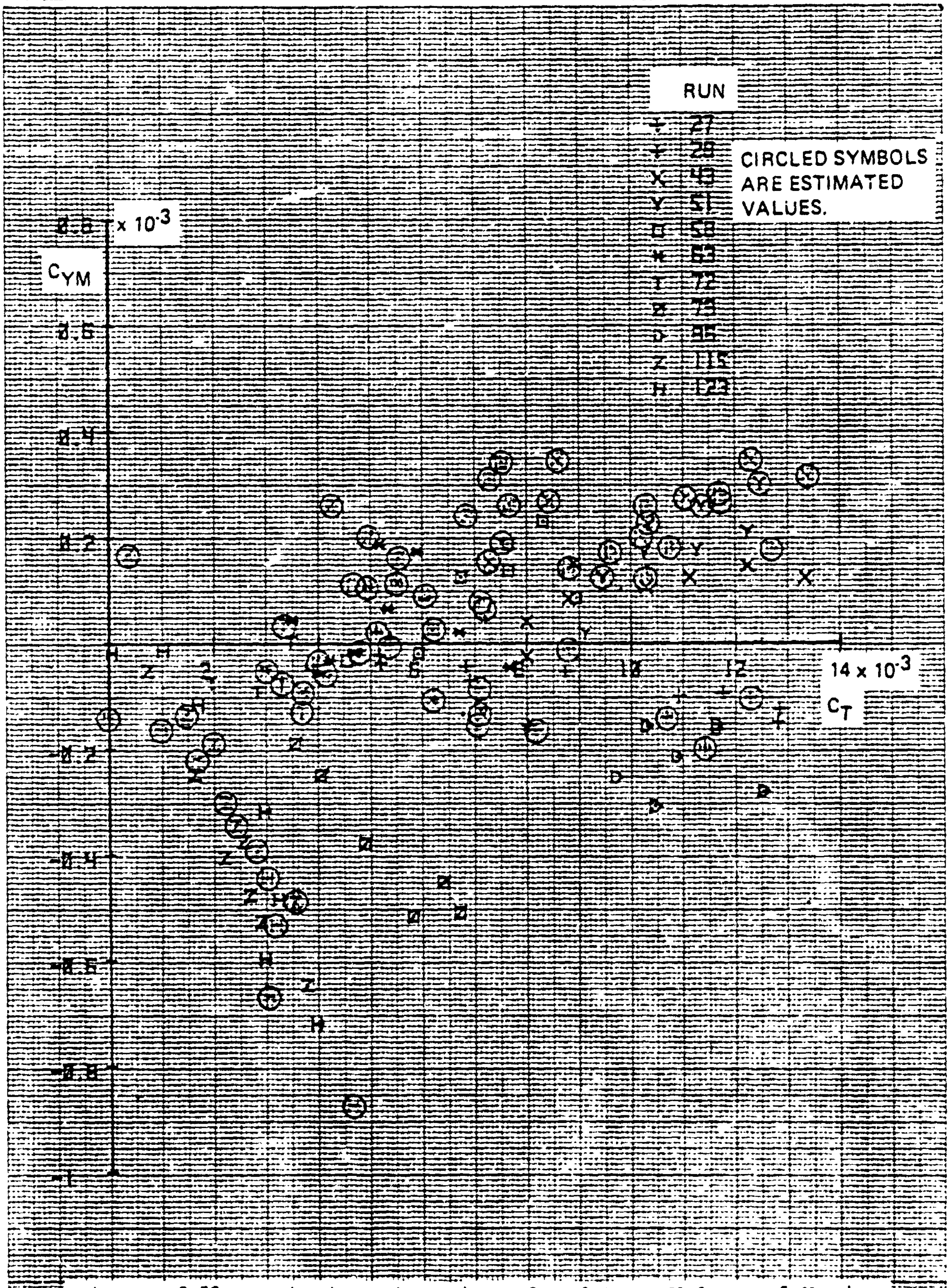

Figure 3.52. Variation of Estimated and Test Values of Yawing Moment Coefficient With Thrust Coefficient

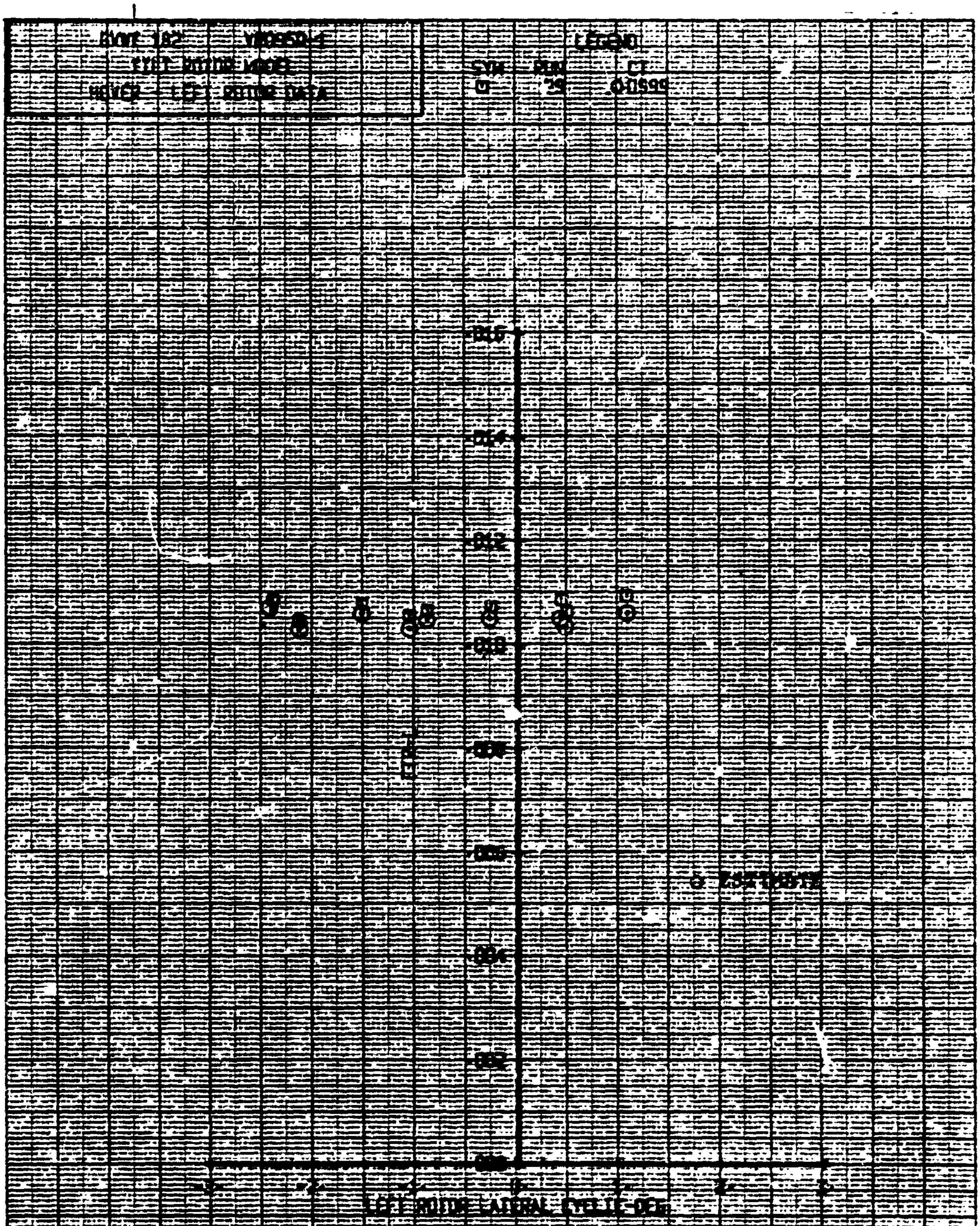

Figure 3.53. Left Rotor Thrust Coefficient Versus Lateral Cyclic Pitch. I_N = 90° Hover.

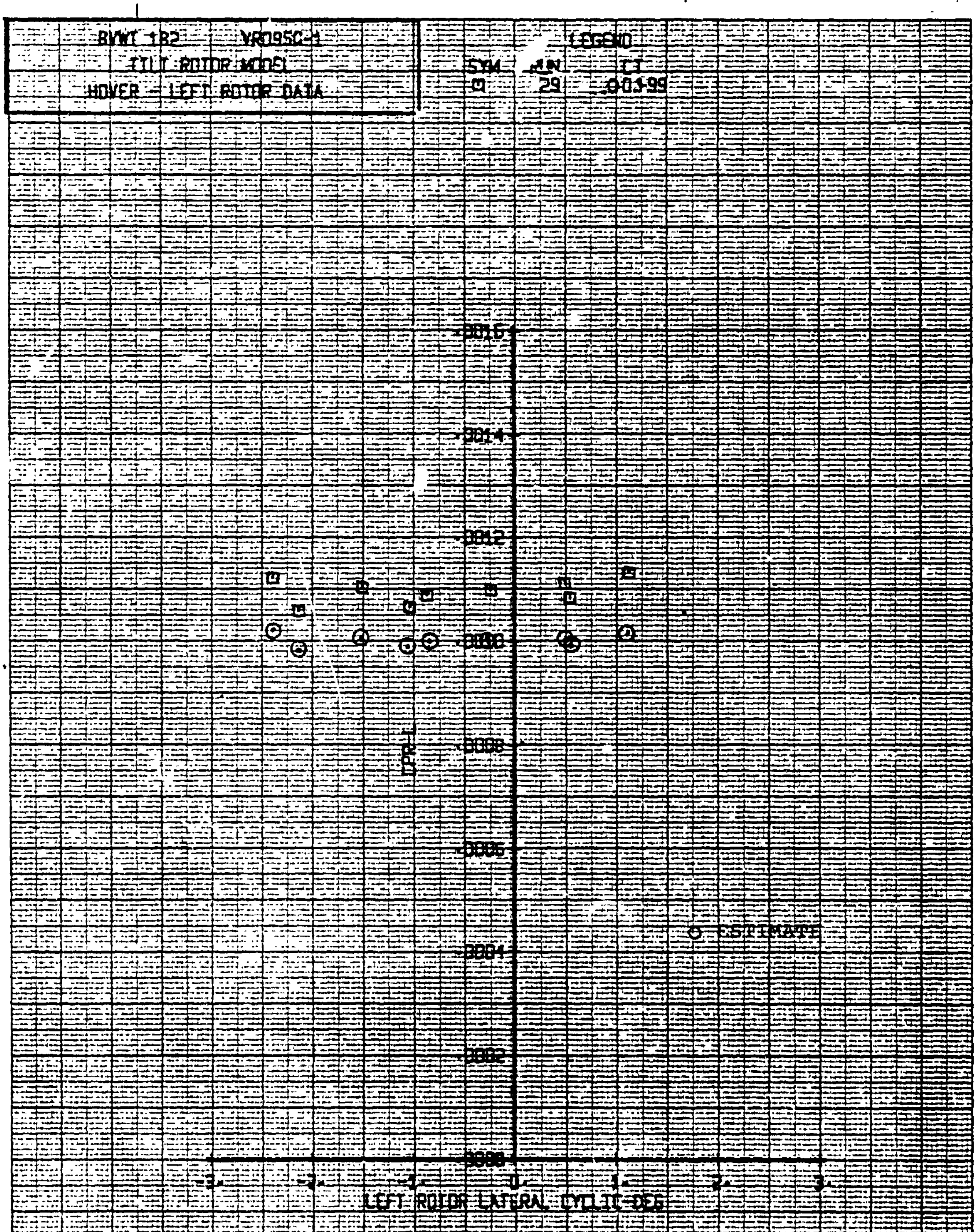

Figure 3.54. Left Rotor Power Coefficient Versus Lateral Cyclic Pitch. I_N = 90° Hover.

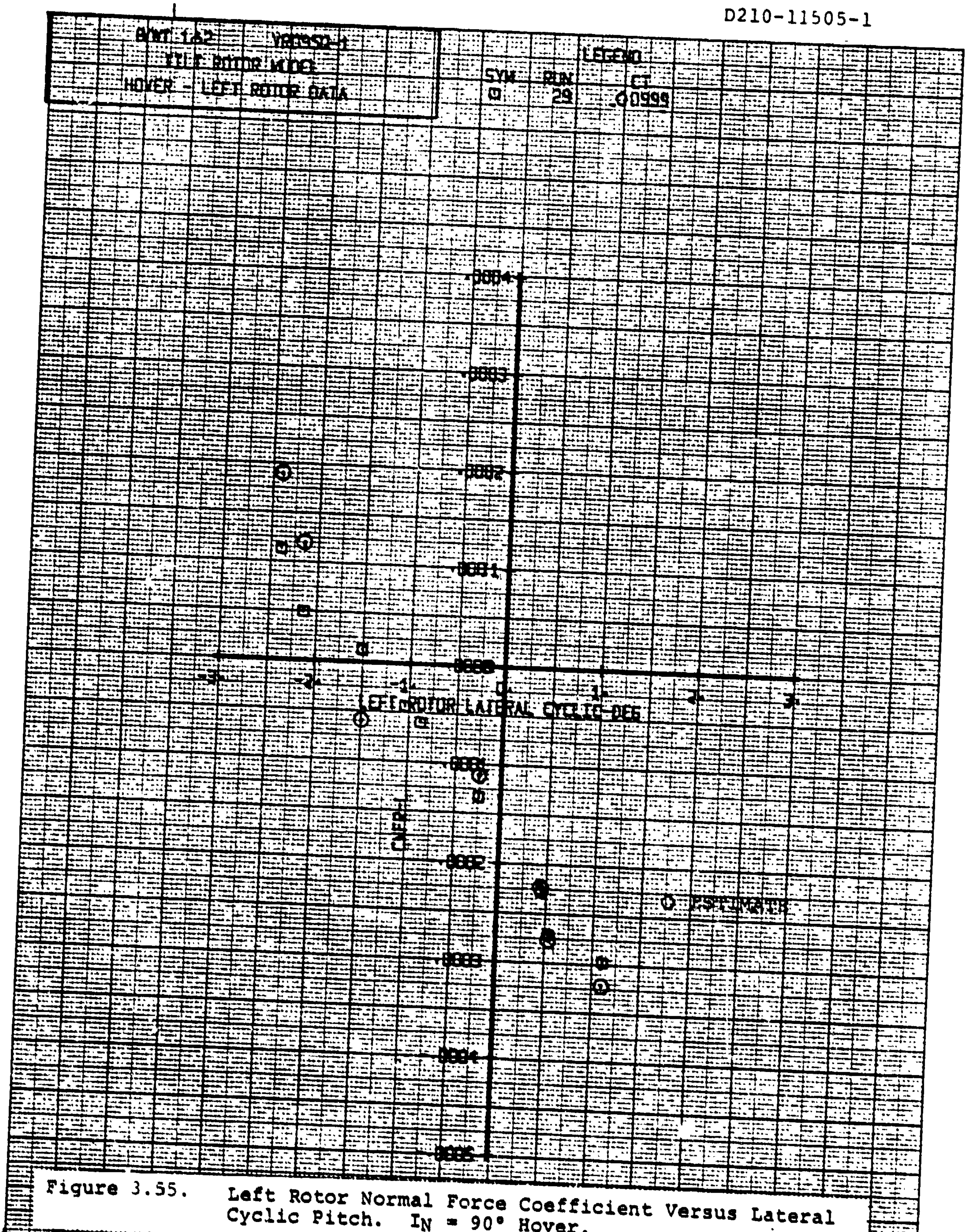

Figure 3.55. Left Rotor Normal Force Coefficient Versus Lateral Cyclic Pitch. $I_N = 90°$ Hover.

SET 117
BVWT 182

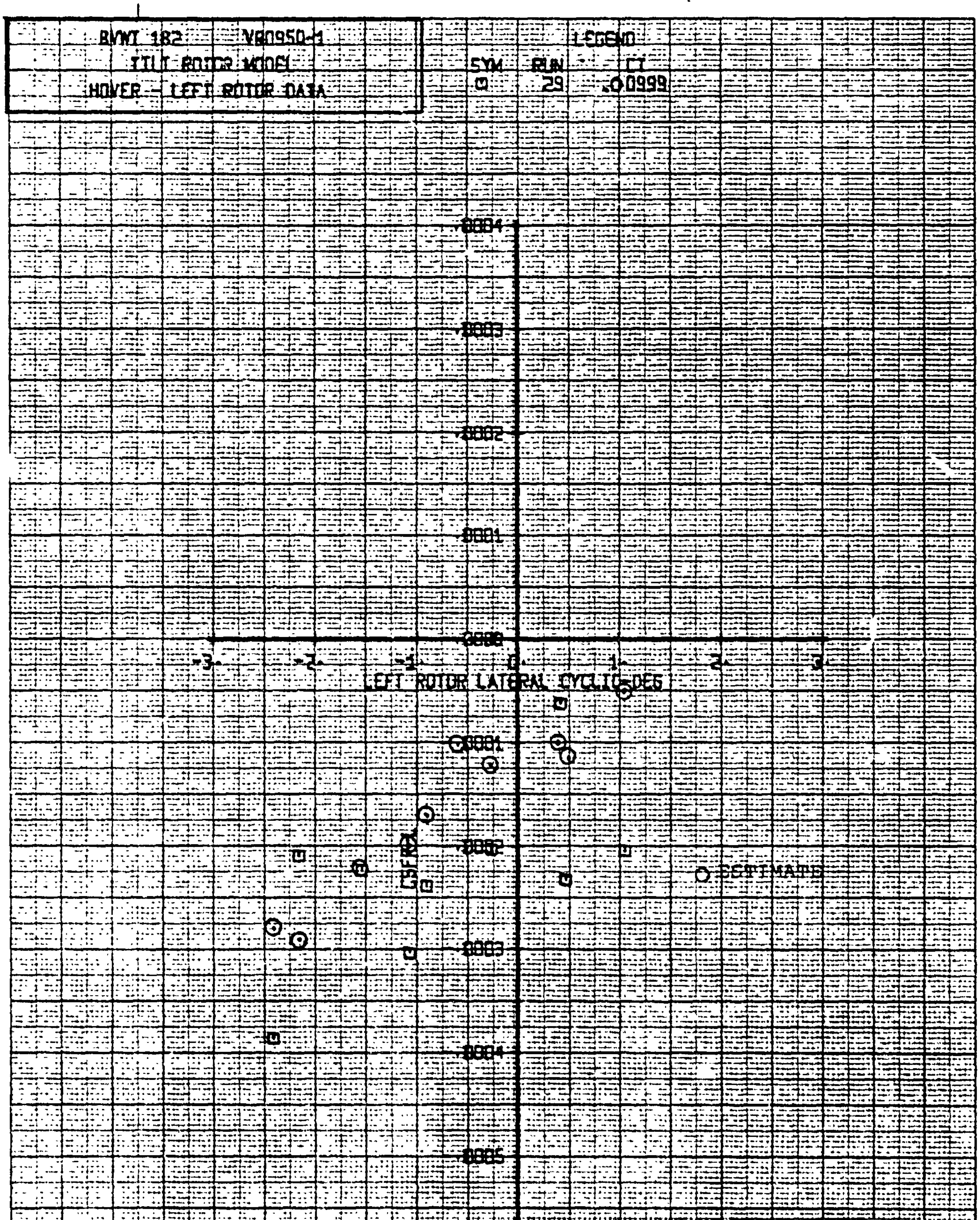

Figure 3.56. Left Rotor Side Force Coefficient Versus Lateral Cyclic Pitch. I_N = 90° Hover.

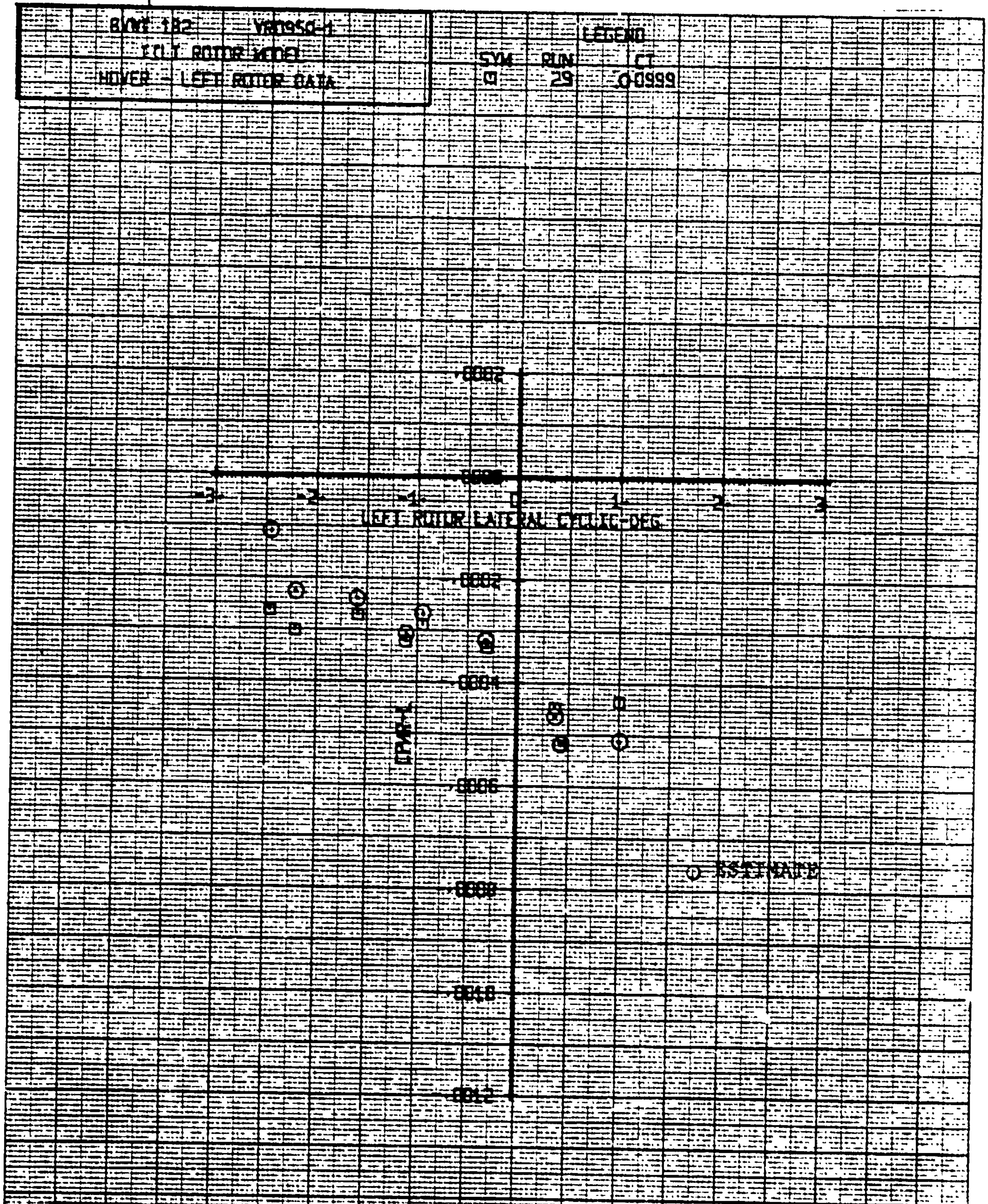

Figure 3.57. Left Rotor Pitch Moment Coefficient Versus Lateral Cyclic Pitch. $I_N = 90°$ Hover.

SET 117
BVWT 182

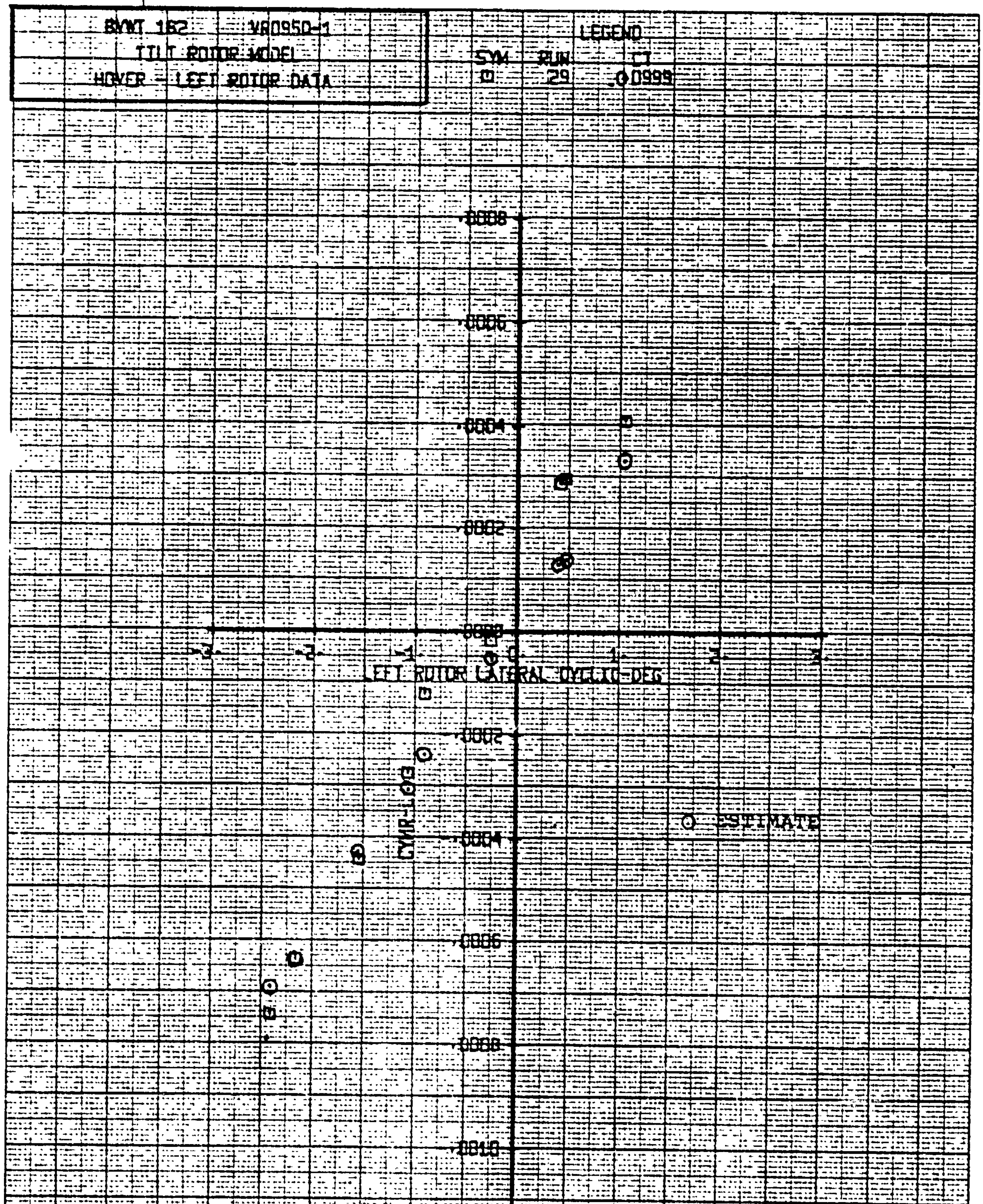

Figure 3.58. Left Rotor Yaw Moment Coefficient Versus Lateral Cyclic Pitch. I_N = 90° Hover.

117
182

SET 117
BVWT 182

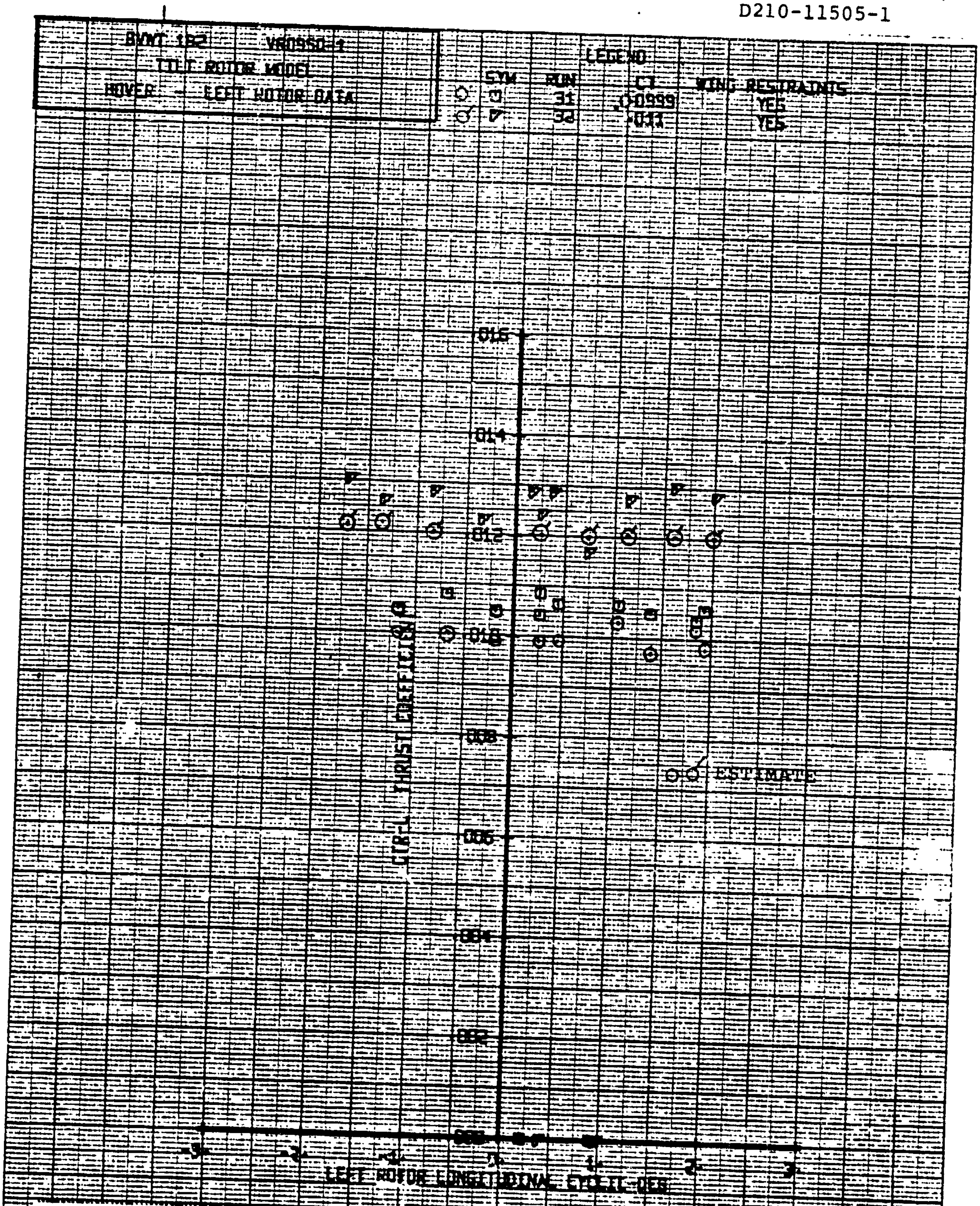

Figure 3.59. Left Rotor Thrust Coefficient Versus Longitudinal Cyclic Pitch. $I_N = 90°$ Hover.

119
182

SET 119
BVWT 182

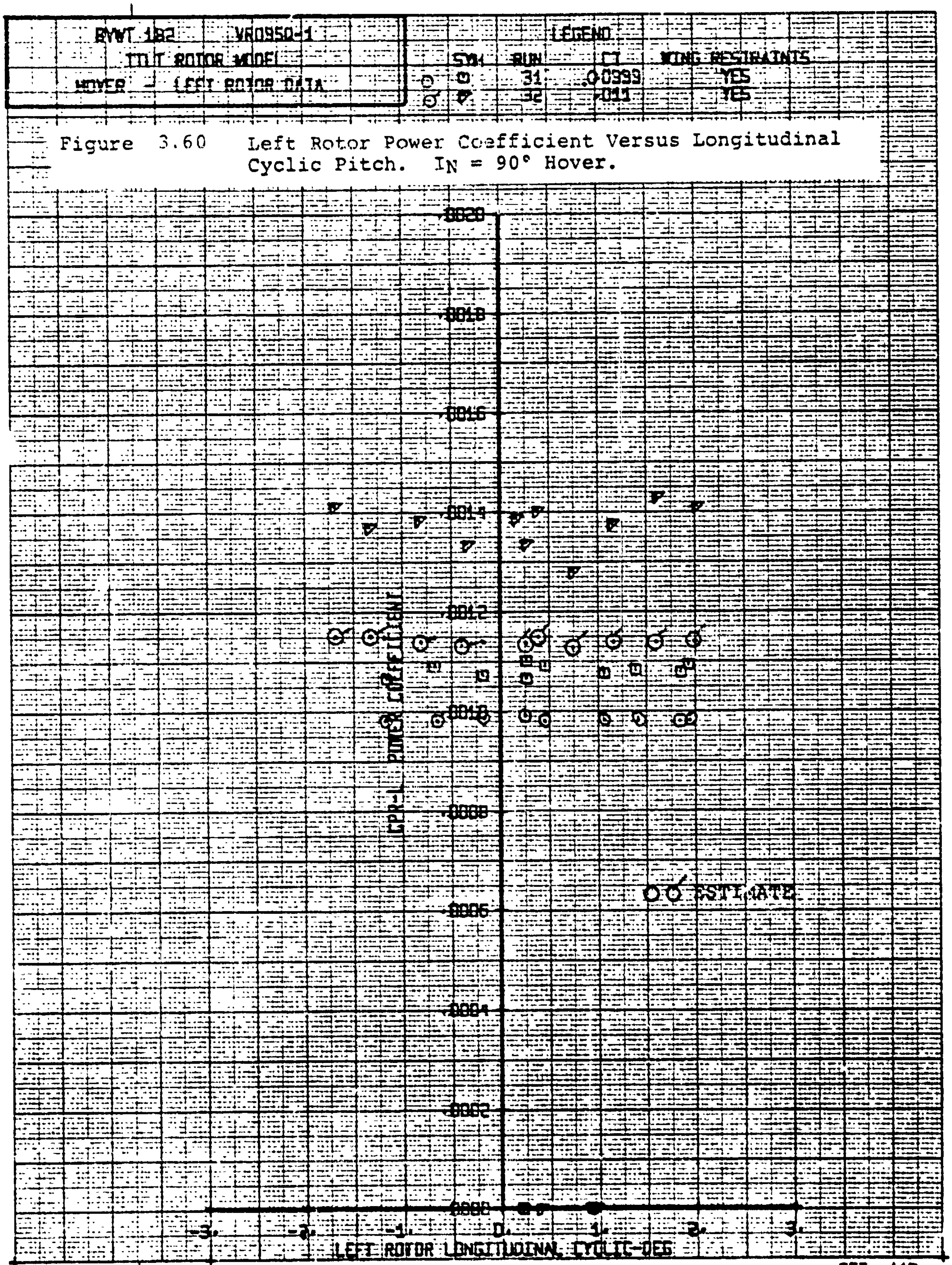

Figure 3.60 Left Rotor Power Coefficient Versus Longitudinal Cyclic Pitch. I_N = 90° Hover.

119
182

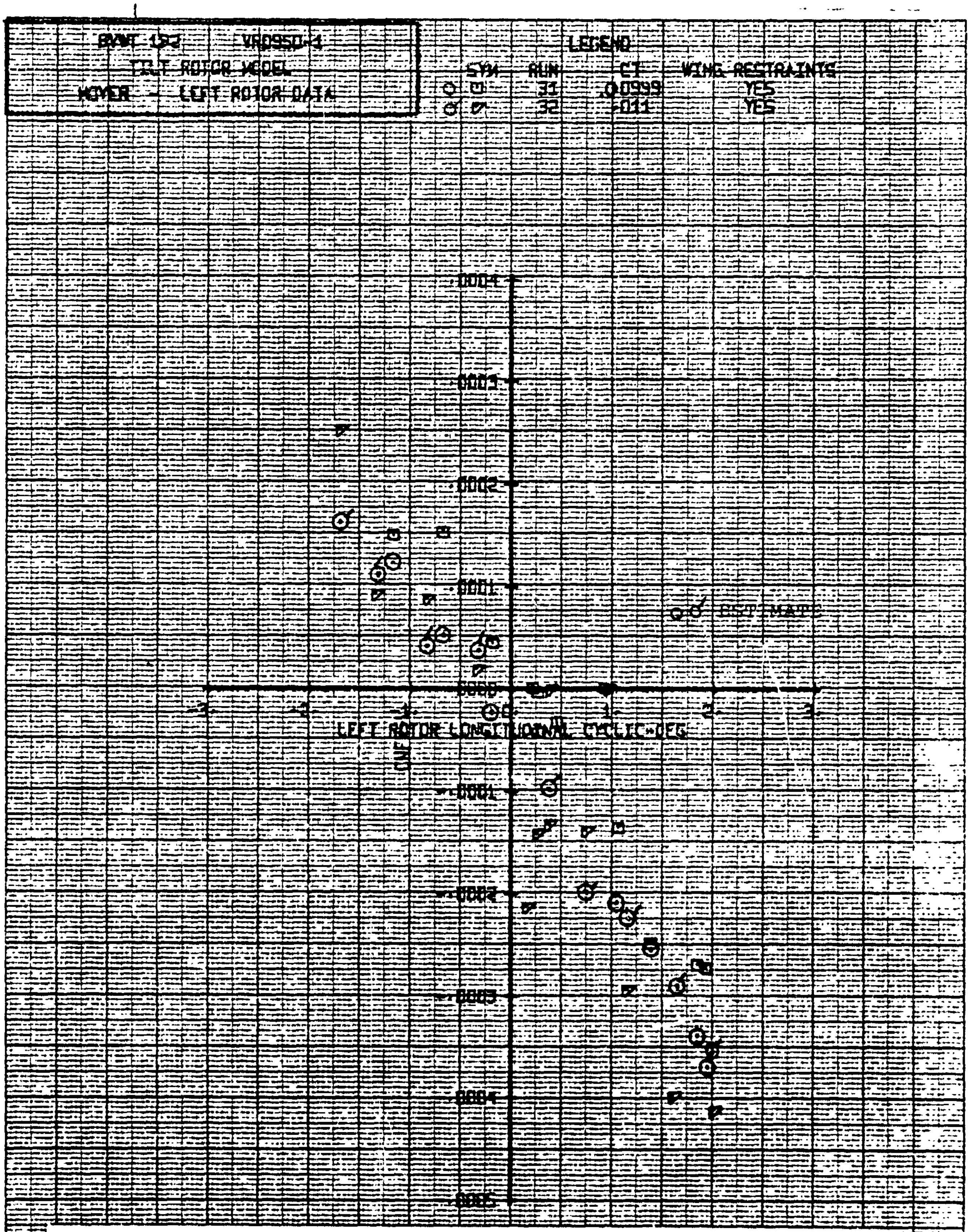

Figure 3.61. Left Rotor Normal Force Coefficient Versus Longitudinal Cyclic Pitch. I_N = 90° Hover.

119
192

SET 119
BVWT 192

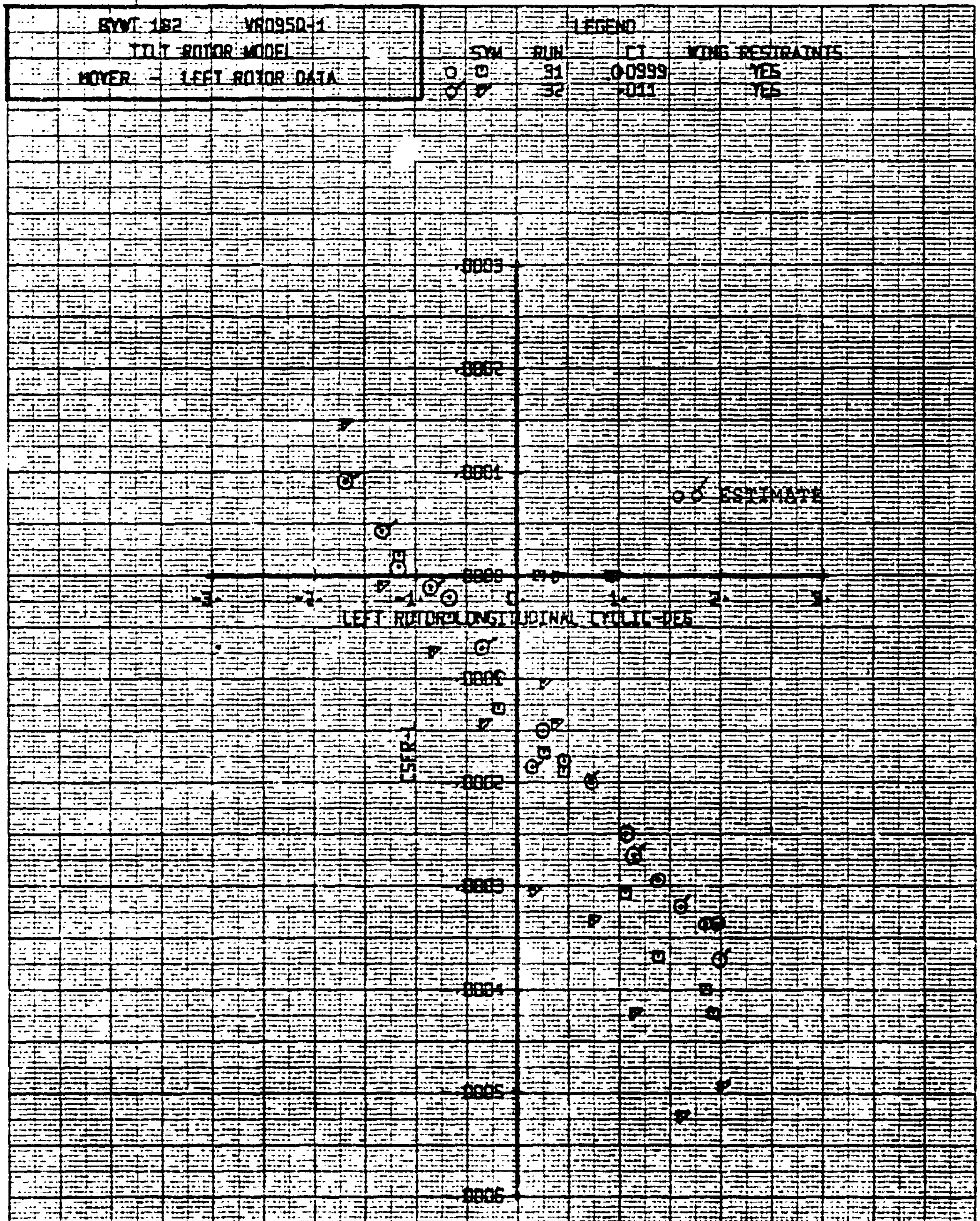

Figure 3.62. Left Rotor Side Force Coefficient Versus Longitudinal Cyclic Pitch. $I_N = 90°$ Hover.

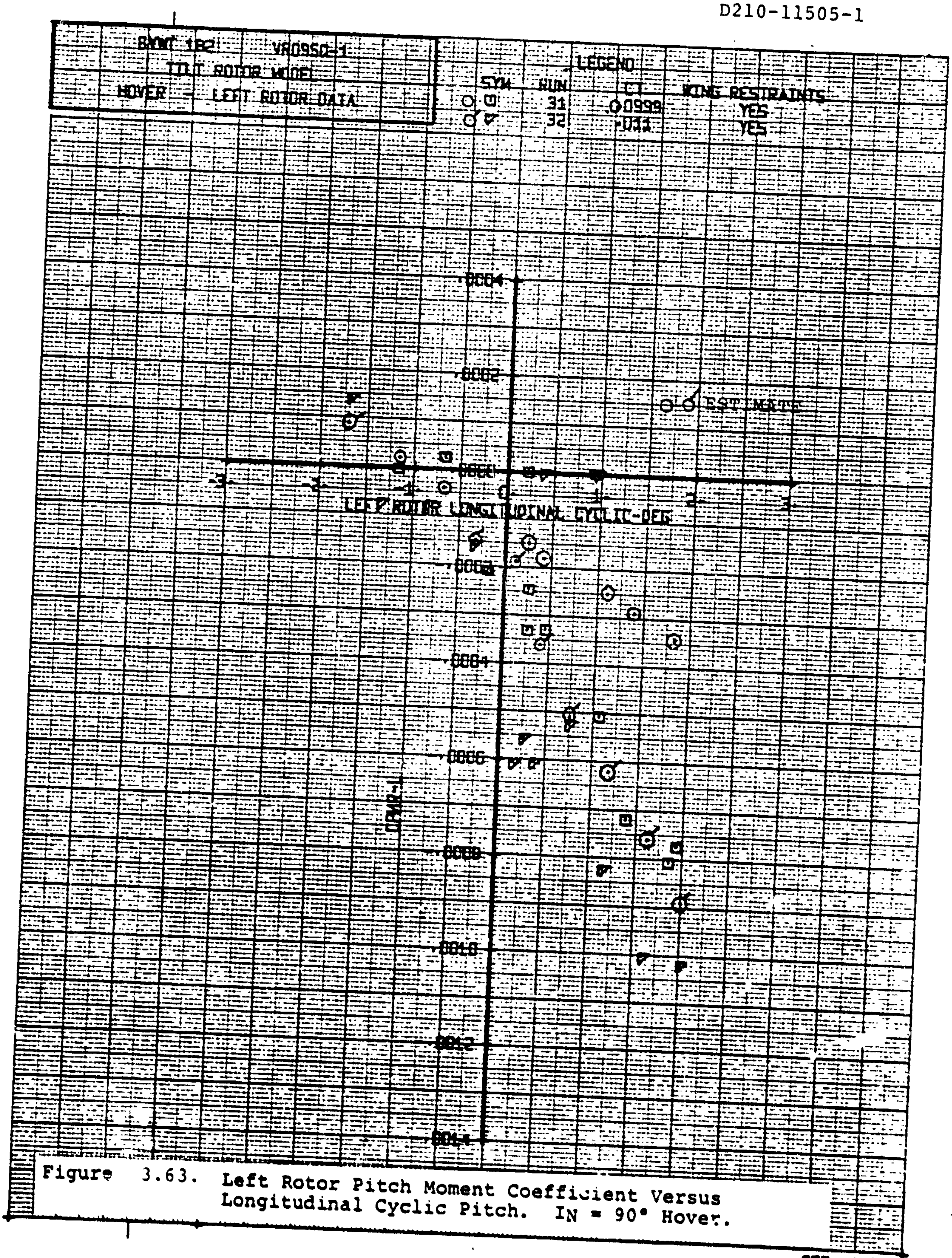

Figure 3.63. Left Rotor Pitch Moment Coefficient Versus Longitudinal Cyclic Pitch. I_N = 90° Hover.

119
182

SET 119
BVWT 182

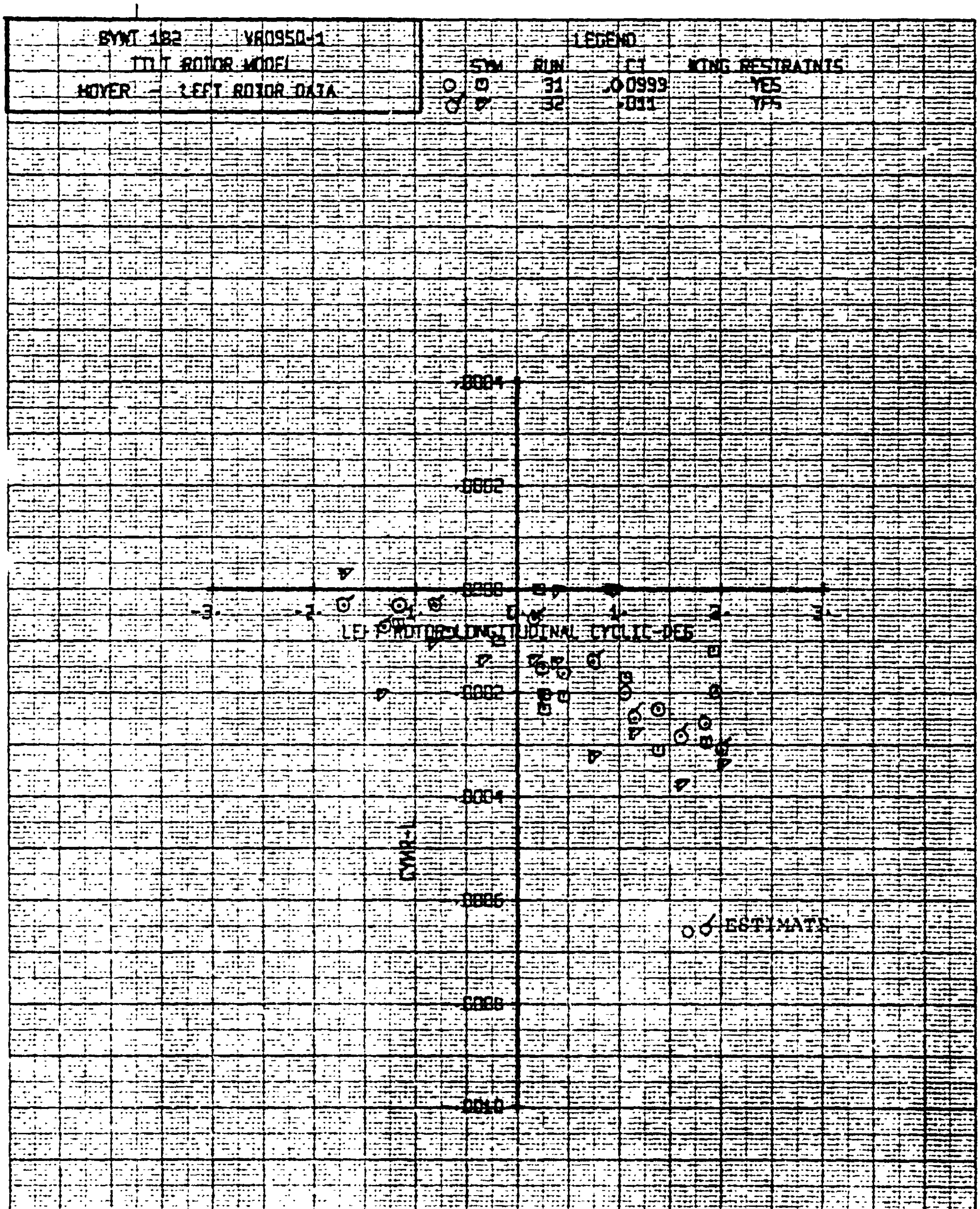

Figure 3.64. Left Rotor Yaw Moment Coefficient Versus Longitudinal Cyclic Pitch. $I_N = 90°$ Hover.

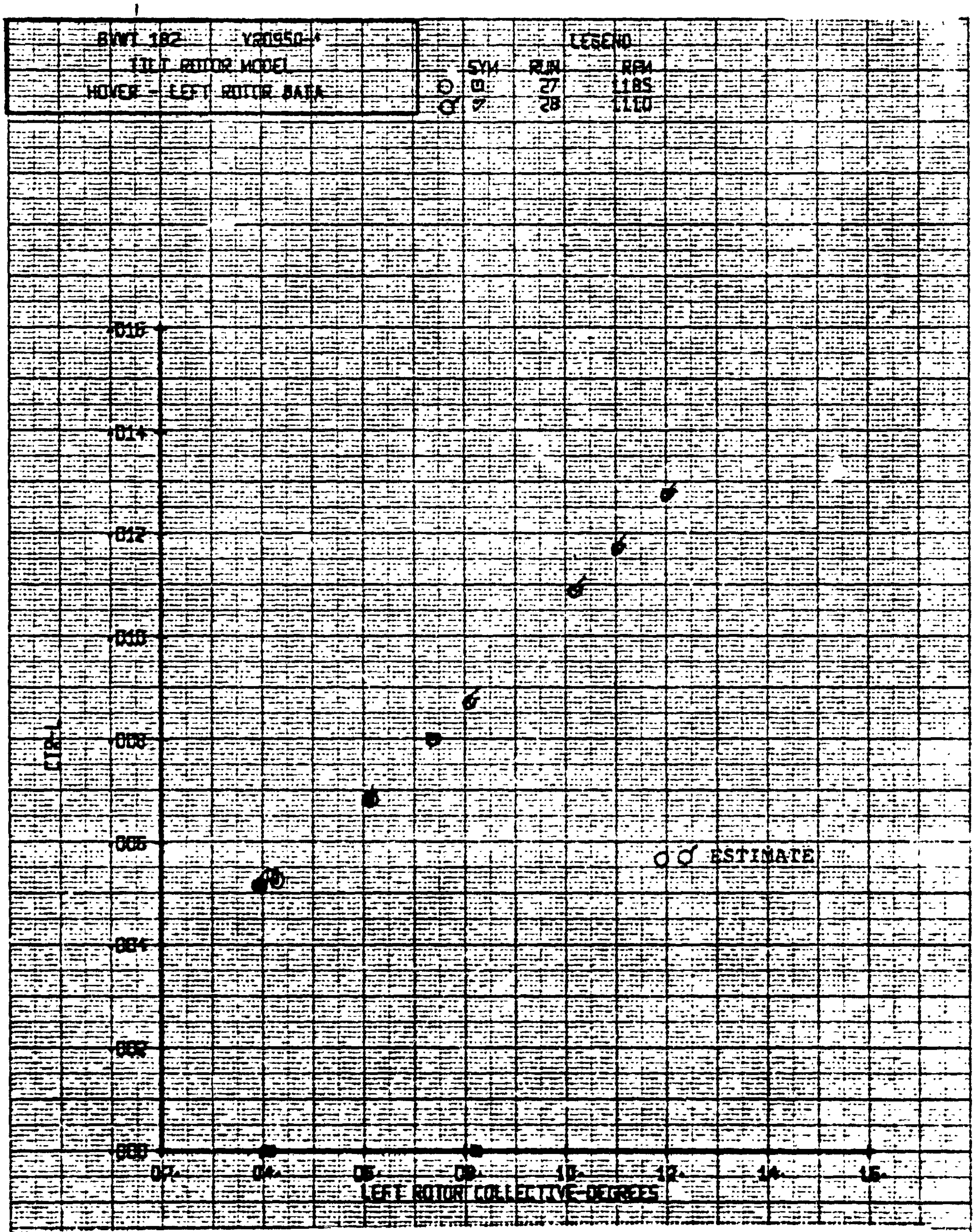

Figure 3.65. Left Rotor Thrust Coefficient Versus Collective Pitch. I_N = 90° Hover.

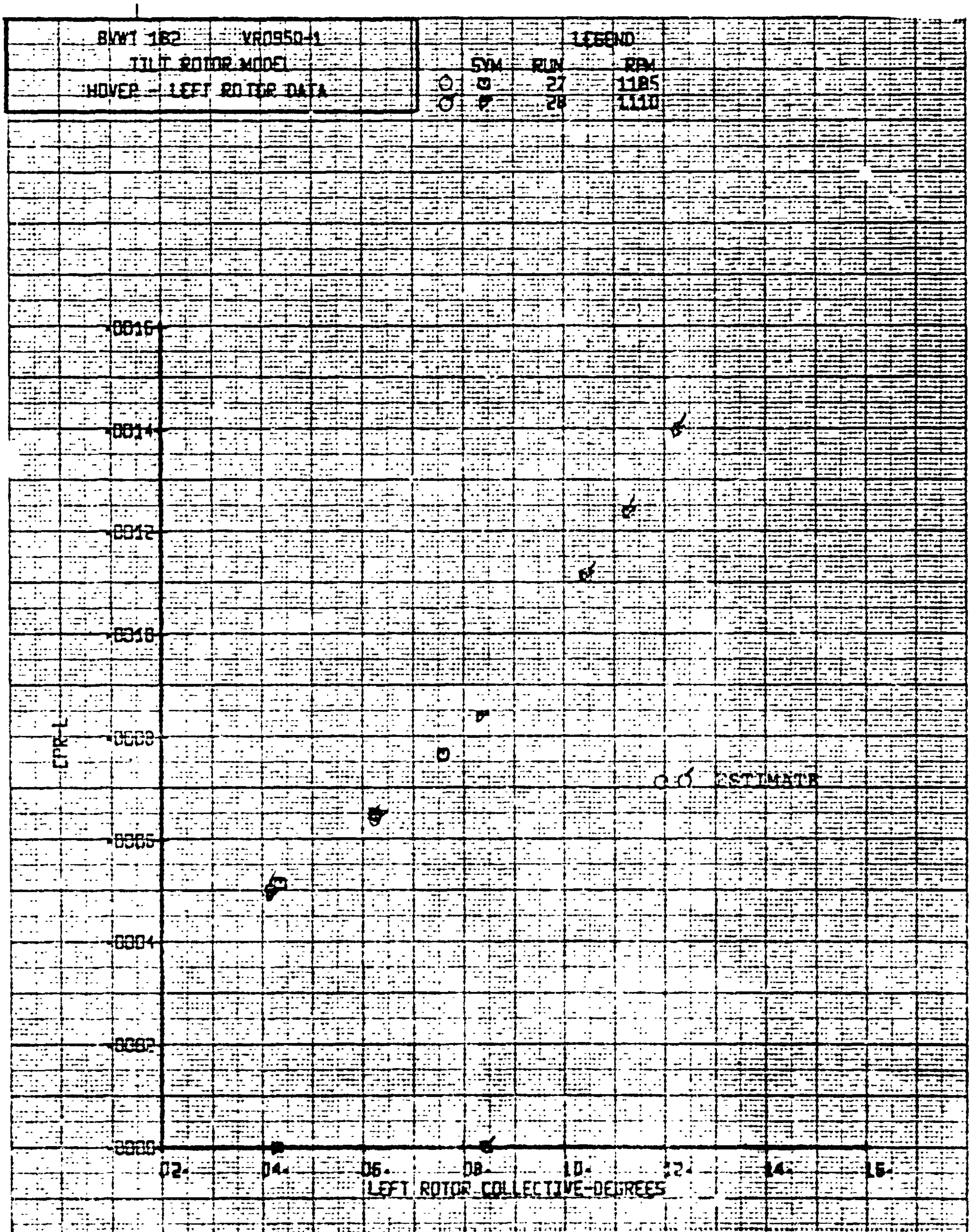

Figure 3.66. Left Rotor Power Coefficient Versus Collective Pitch. I_N = 90° Hover.

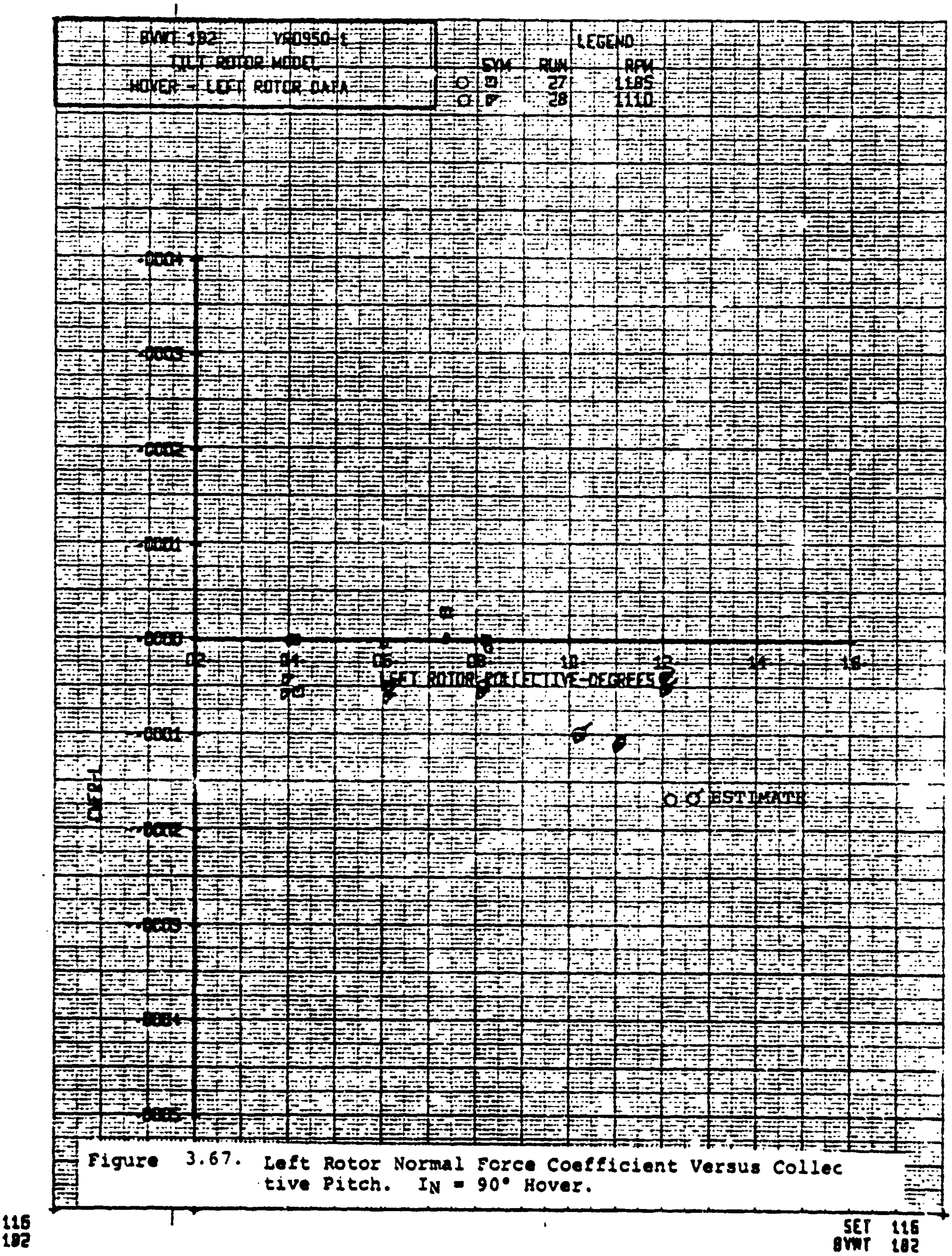

Figure 3.67. Left Rotor Normal Force Coefficient Versus Collective Pitch. I_N = 90° Hover.

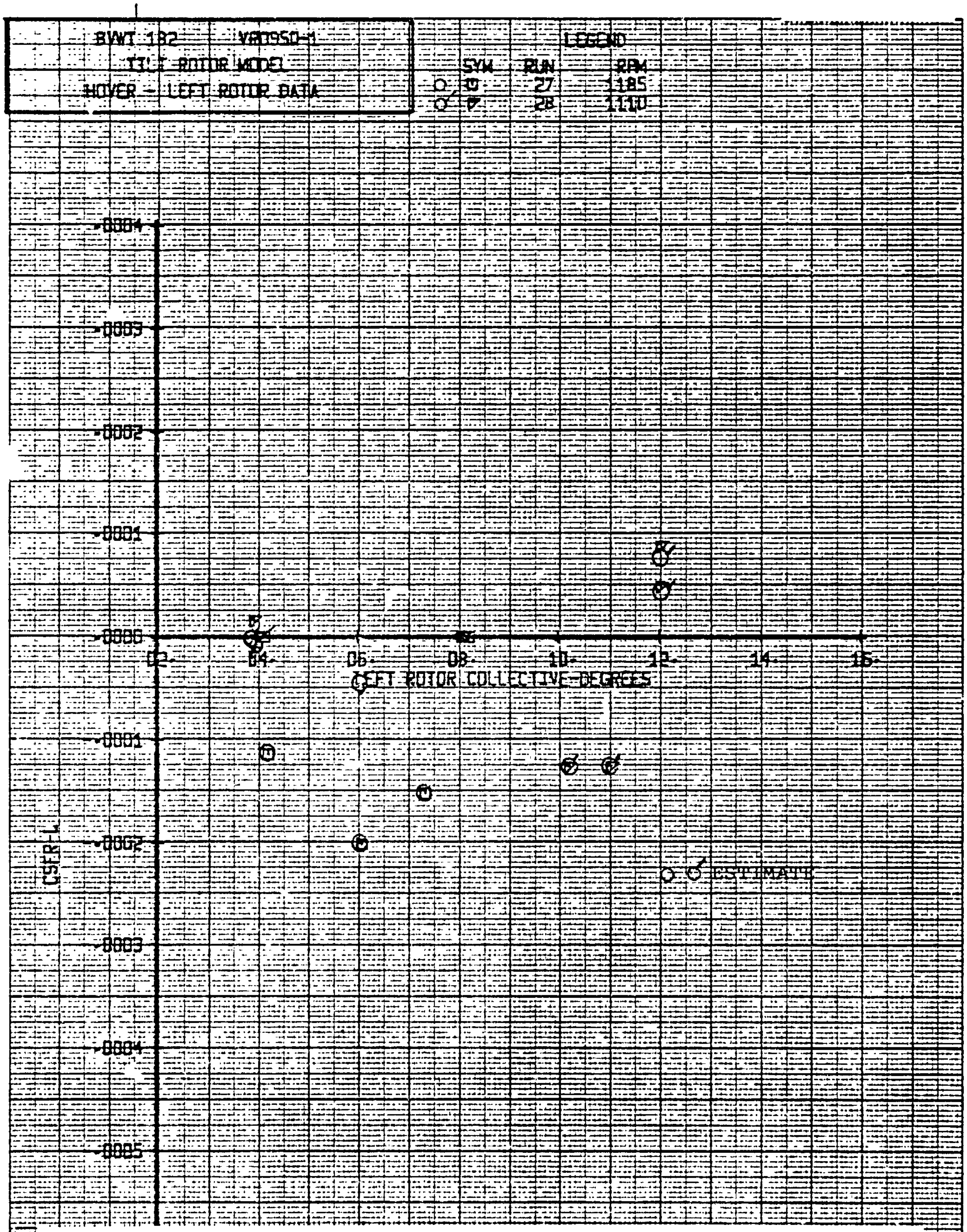

Figure 3.68. Left Rotor Side Force Coefficient Versus Colle tive Pitch. I_N = 90° Hover.

116
182

SET 116
BVWT 182

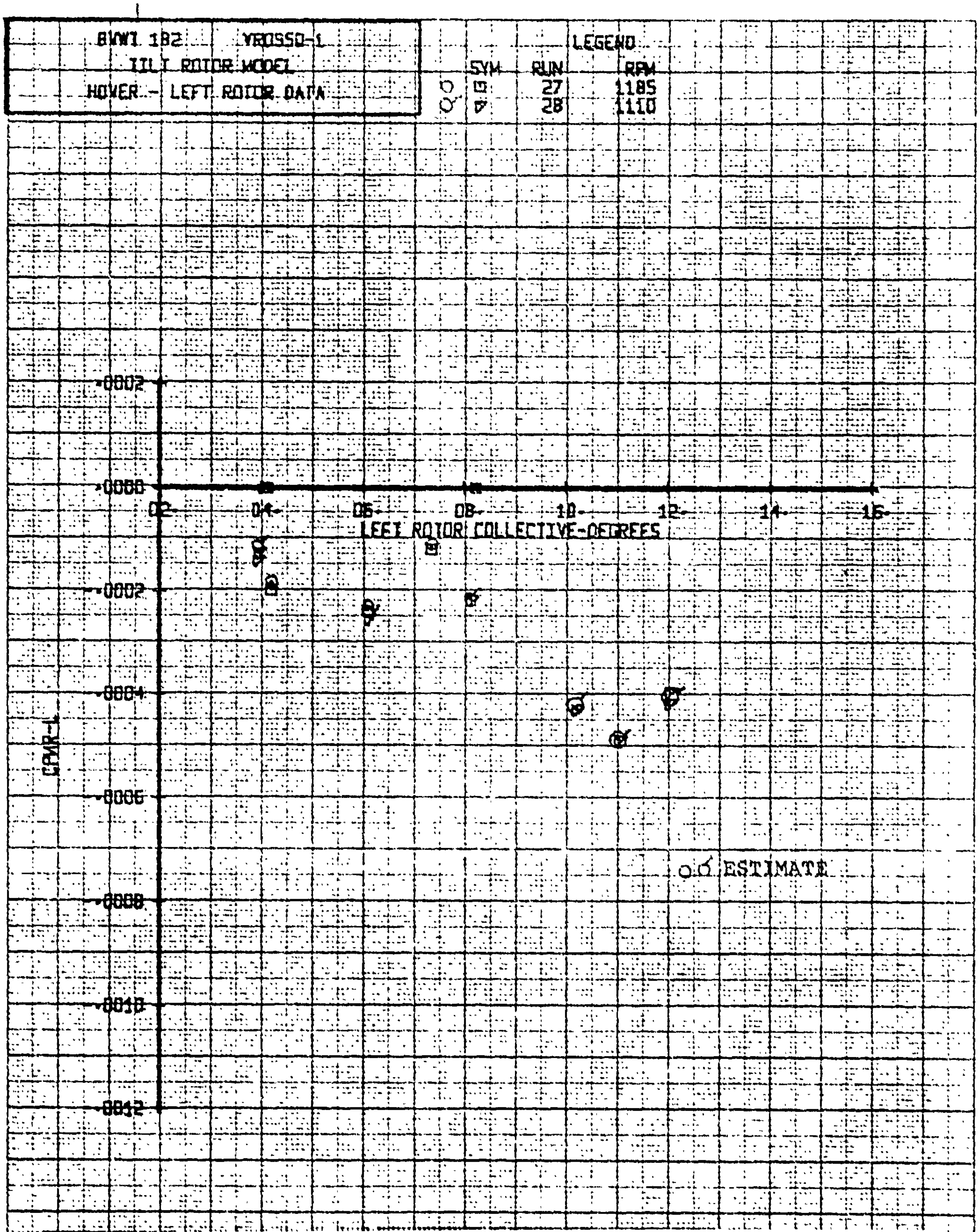

Figure 3.69. Left Rotor Pitching Moment Coefficient Versus Collective Pitch. I_N = 90° Hover.

116
182

SET 116
BVWT 182

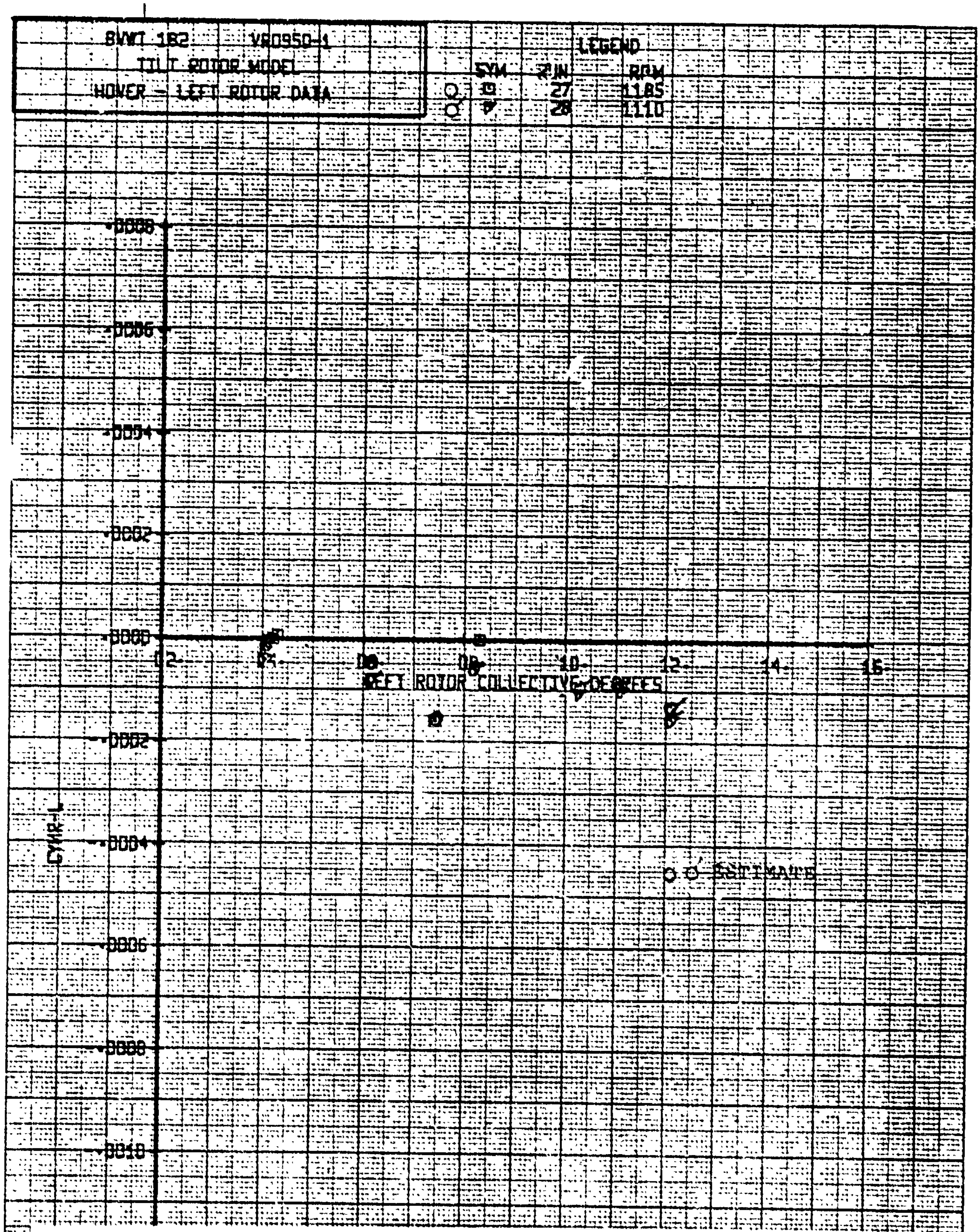

Figure 3.70. Left Rotor Yaw Moment Coefficient Versus Collective Pitch. I_N = 90° Hover.

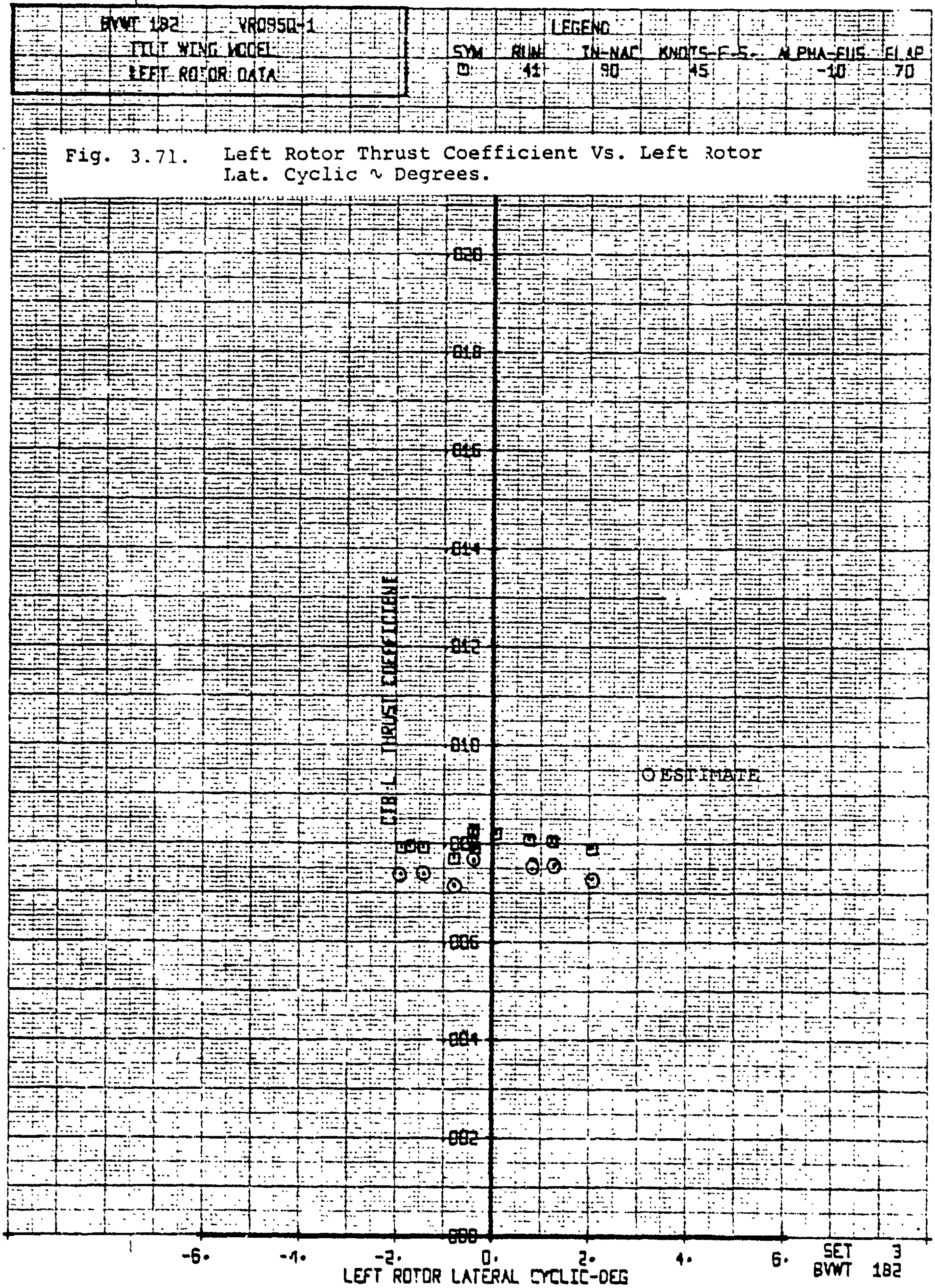

Fig. 3.71. Left Rotor Thrust Coefficient Vs. Left Rotor Lat. Cyclic ∿ Degrees.

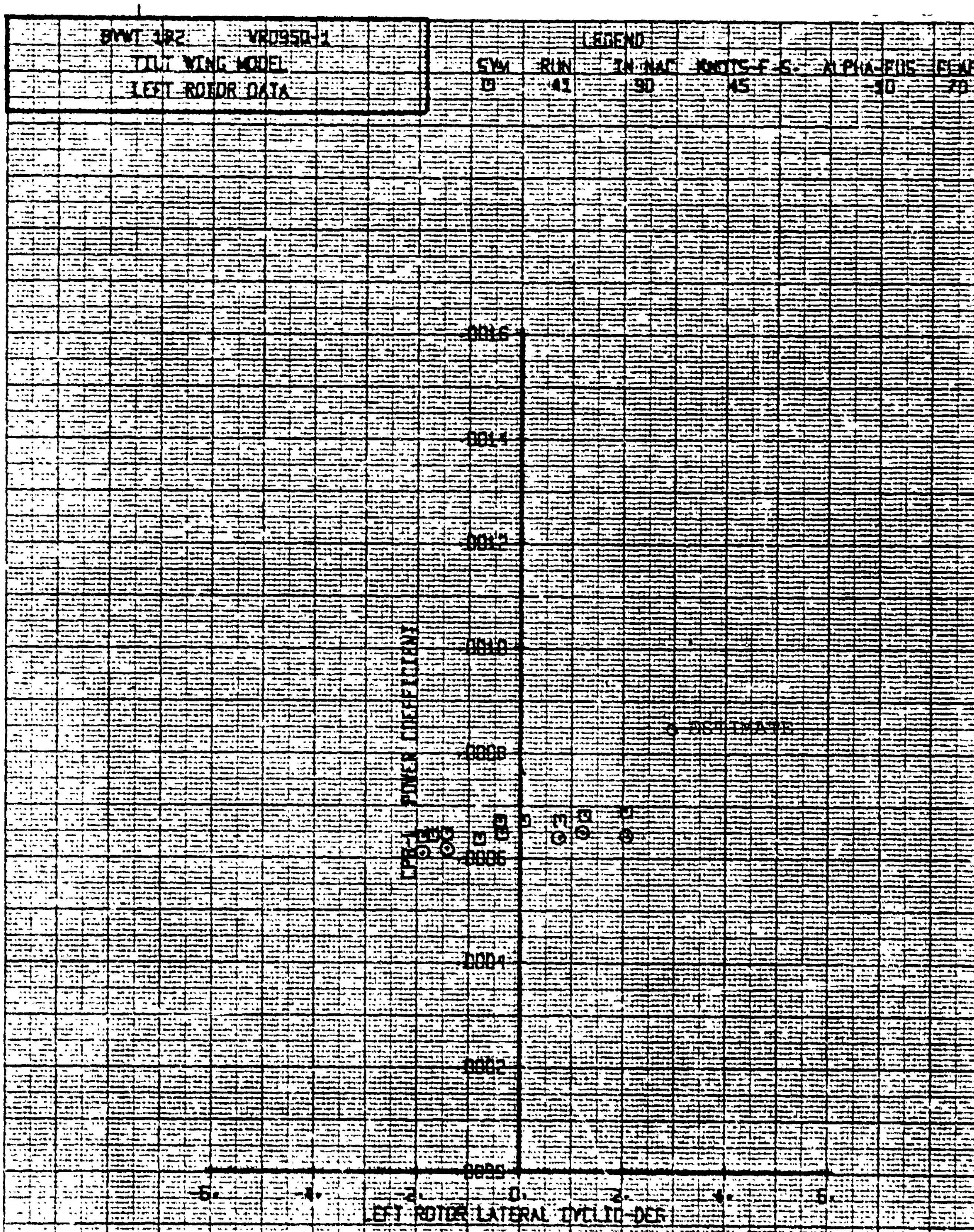

Fig. 3.72. Left Rotor Power Coefficient Vs. Left Rotor Lat. Cyclic ∿ Degrees.

3
182

SET 3
BVWT 182

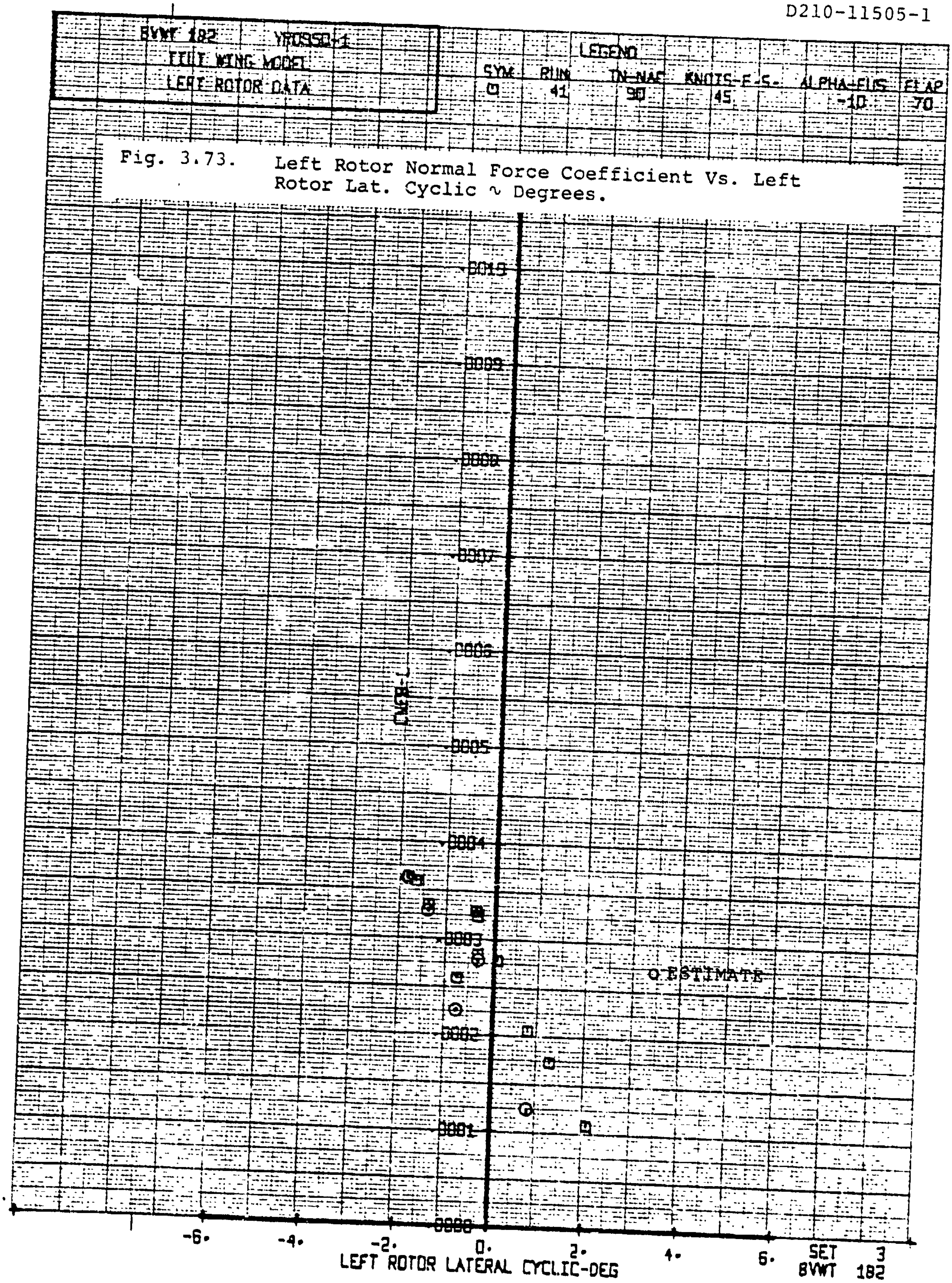

Fig. 3.73. Left Rotor Normal Force Coefficient Vs. Left Rotor Lat. Cyclic ∿ Degrees.

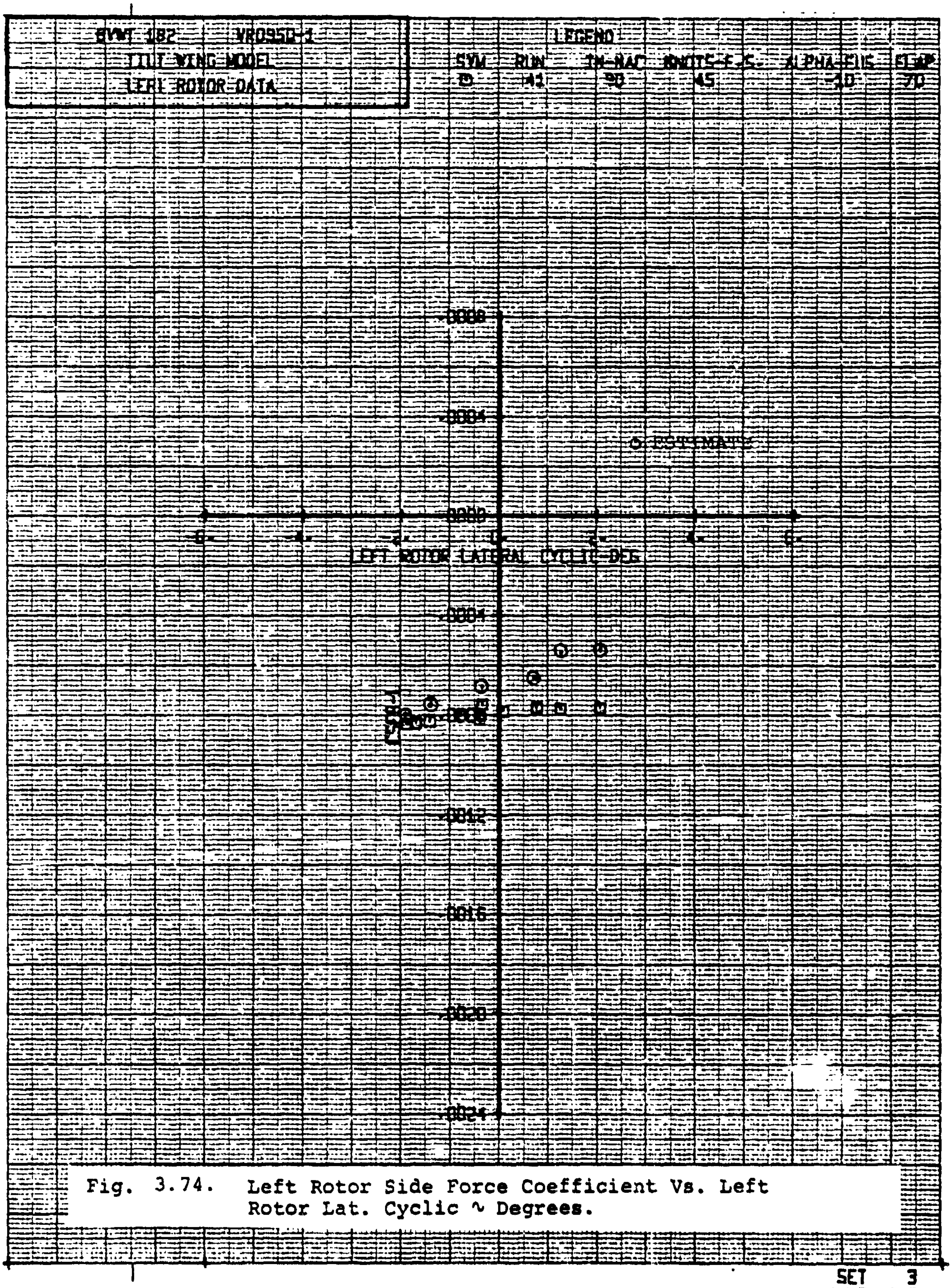

Fig. 3.74. Left Rotor Side Force Coefficient Vs. Left Rotor Lat. Cyclic ∿ Degrees.

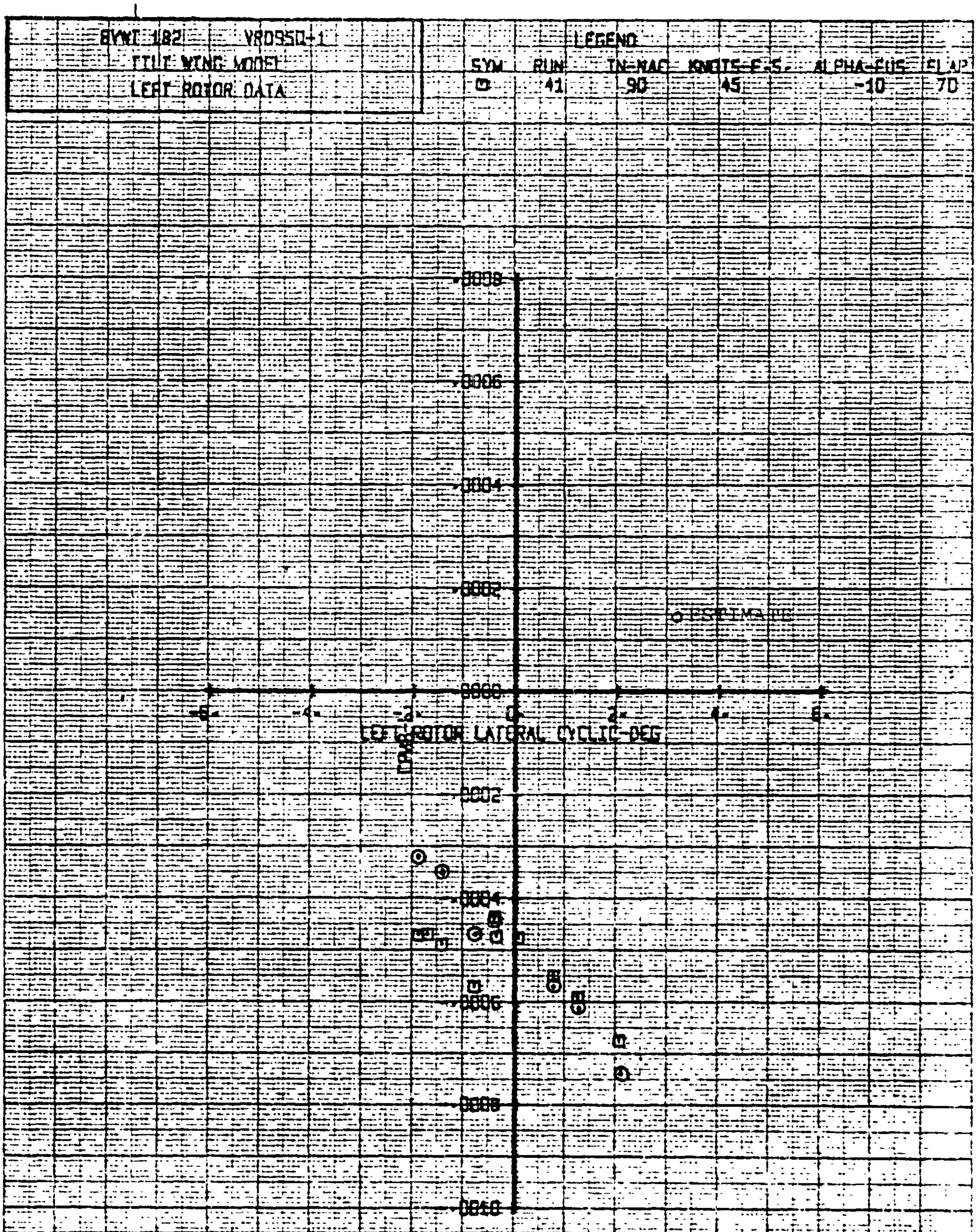

Fig. 3.75. Left Rotor Pitching Moment Coefficient Vs. Left Rotor Lat. Cyclic ~ Degrees.

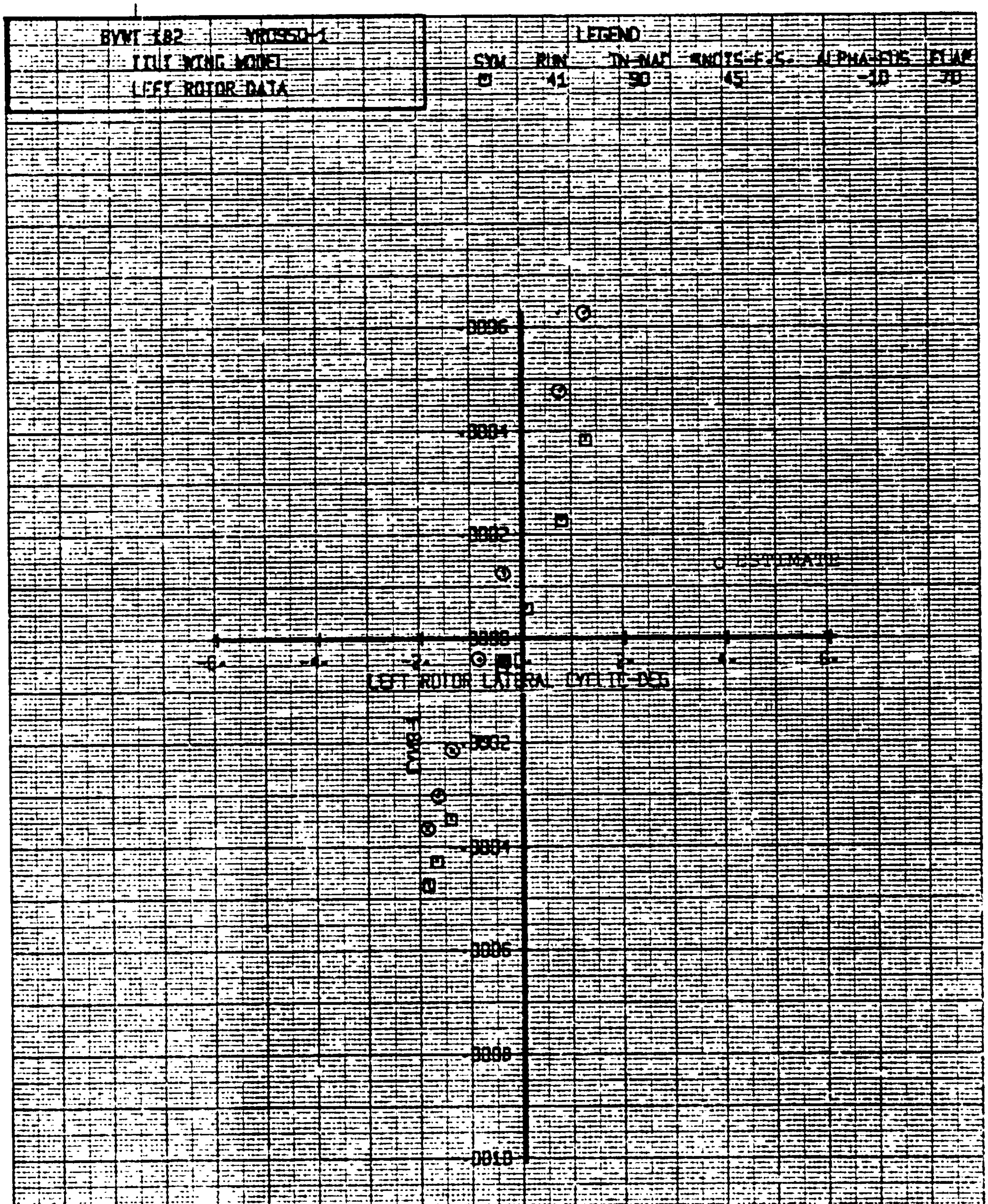

Fig. 3.76. Left Rotor Yawing Moment Coefficient Vs. Left Rotor Lat. Cyclic ∿ Degrees.

3
182

SET 3
BVWT 182

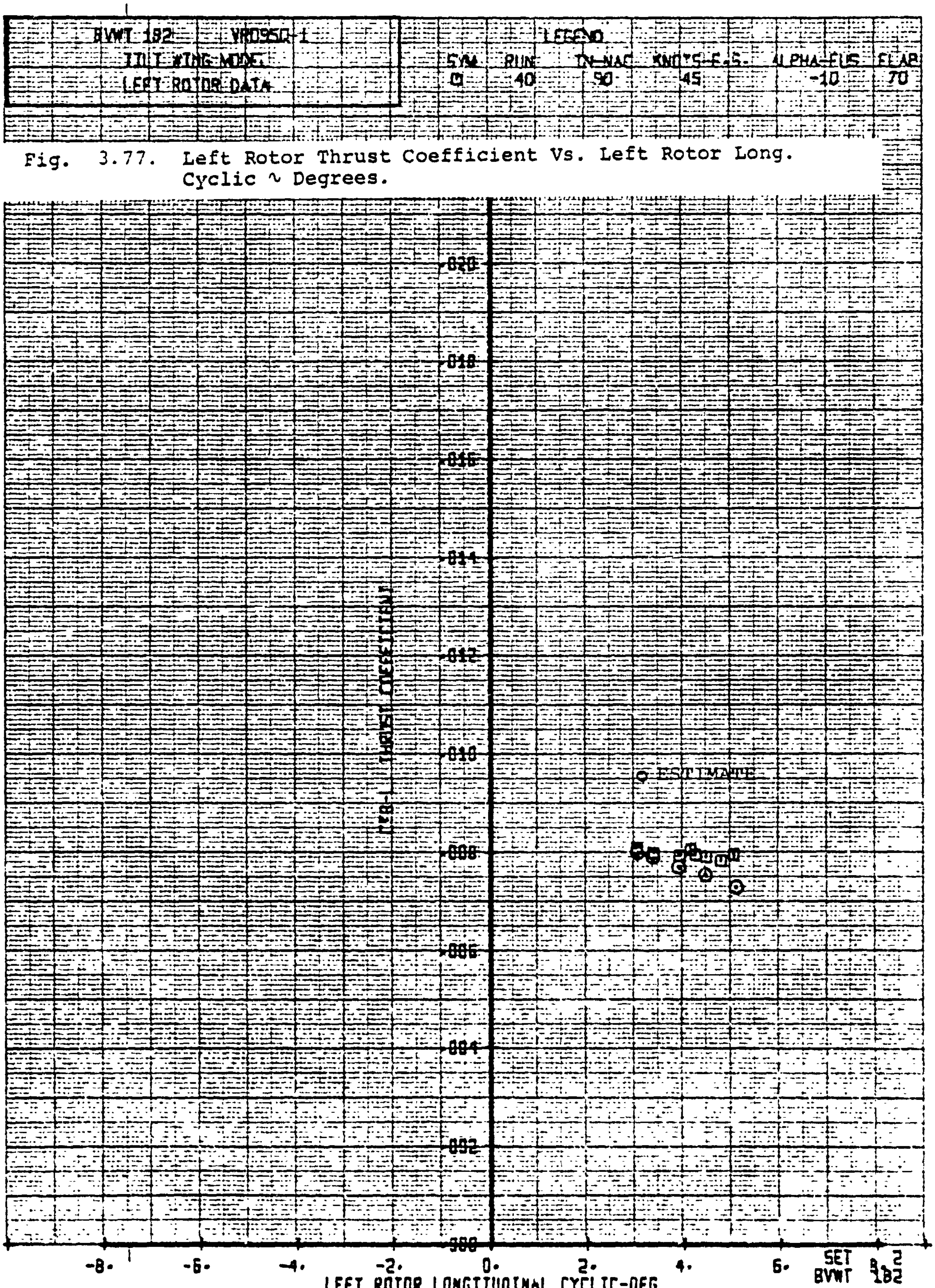

Fig. 3.77. Left Rotor Thrust Coefficient Vs. Left Rotor Long. Cyclic ~ Degrees.

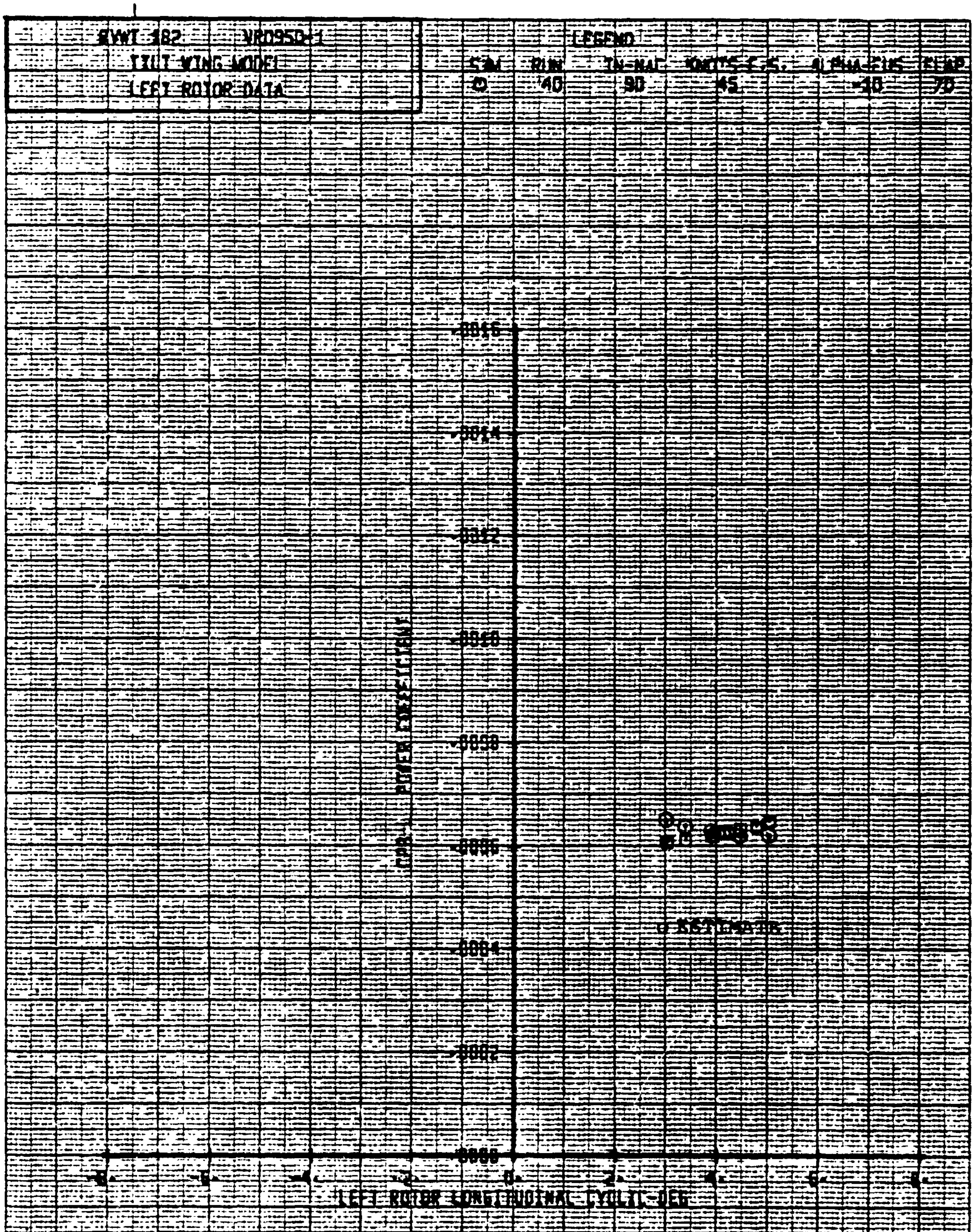

Fig. 3.78. Left Rotor Power Coefficient Vs. Left Rotor Long. Cyclic ∿ Degrees.

2
182

SET 2
BVWT 182

Fig. 3.79. Left Rotor Normal Force Coefficient Vs. Left Rotor Long. Cyclic ~ Degrees.

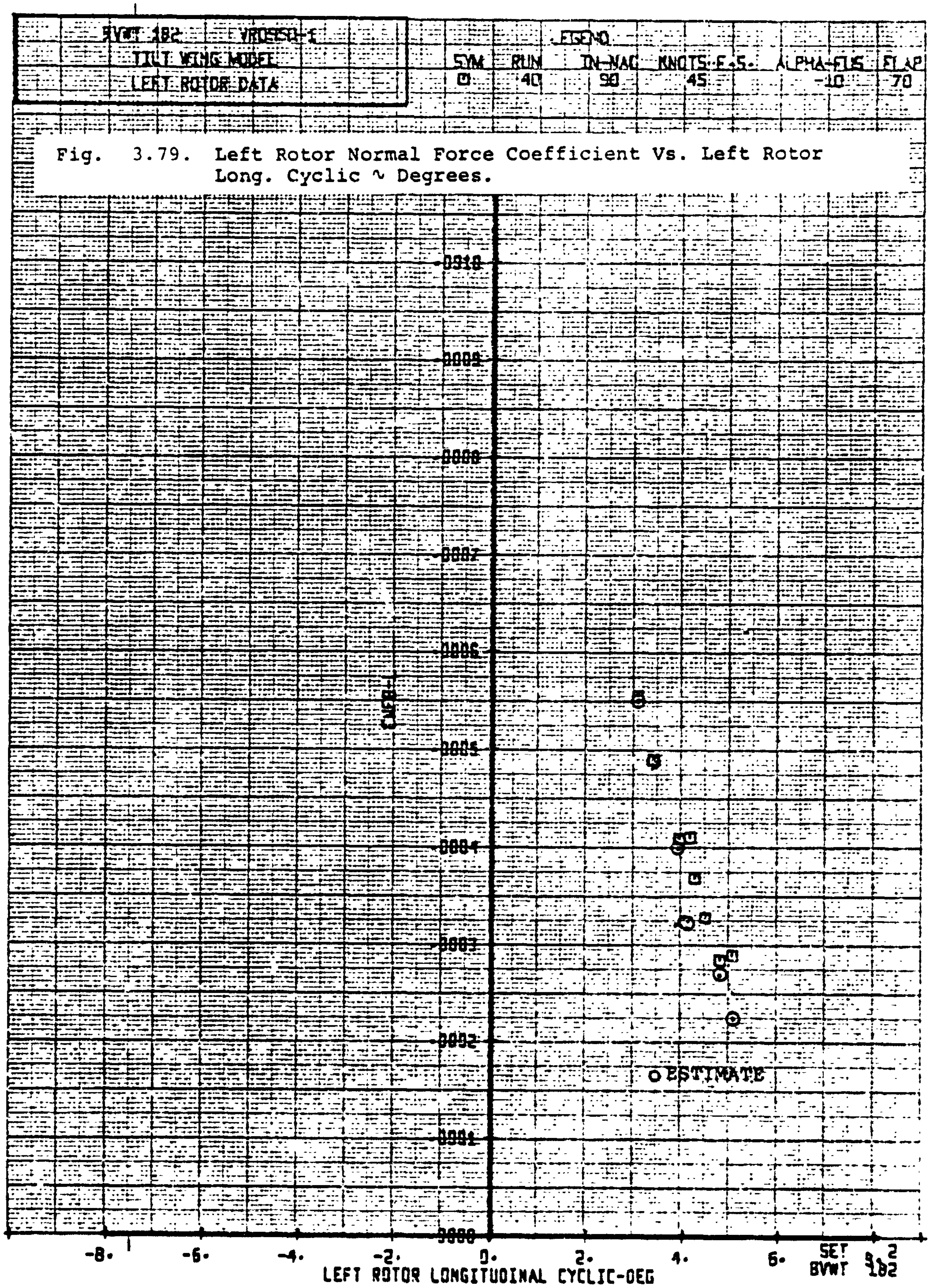

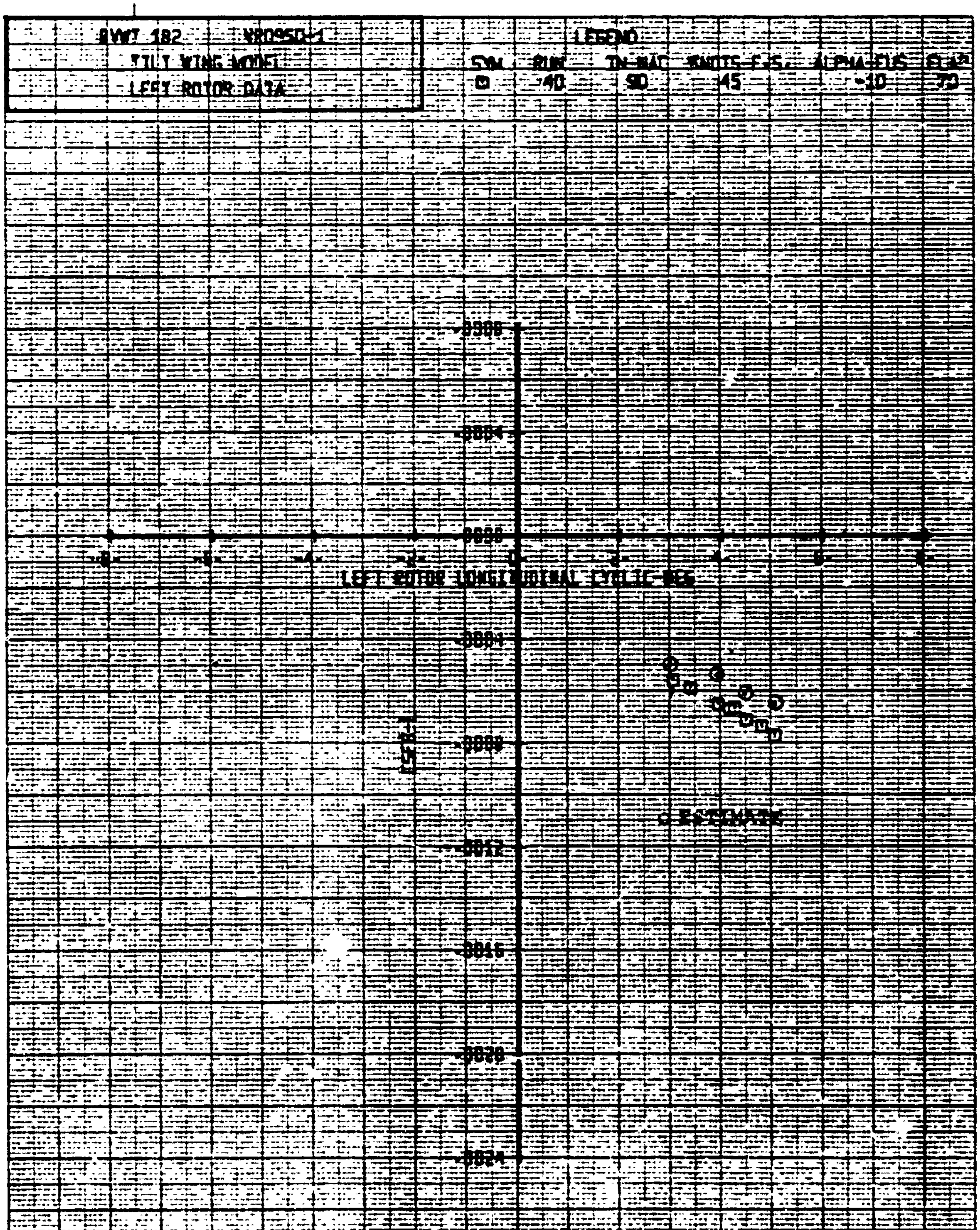

Fig. 3.80. Left Rotor Side Force Coefficient Vs. Left Rotor Long. Cyclic ~ Degrees.

2
182

SET 2
BVWT 182

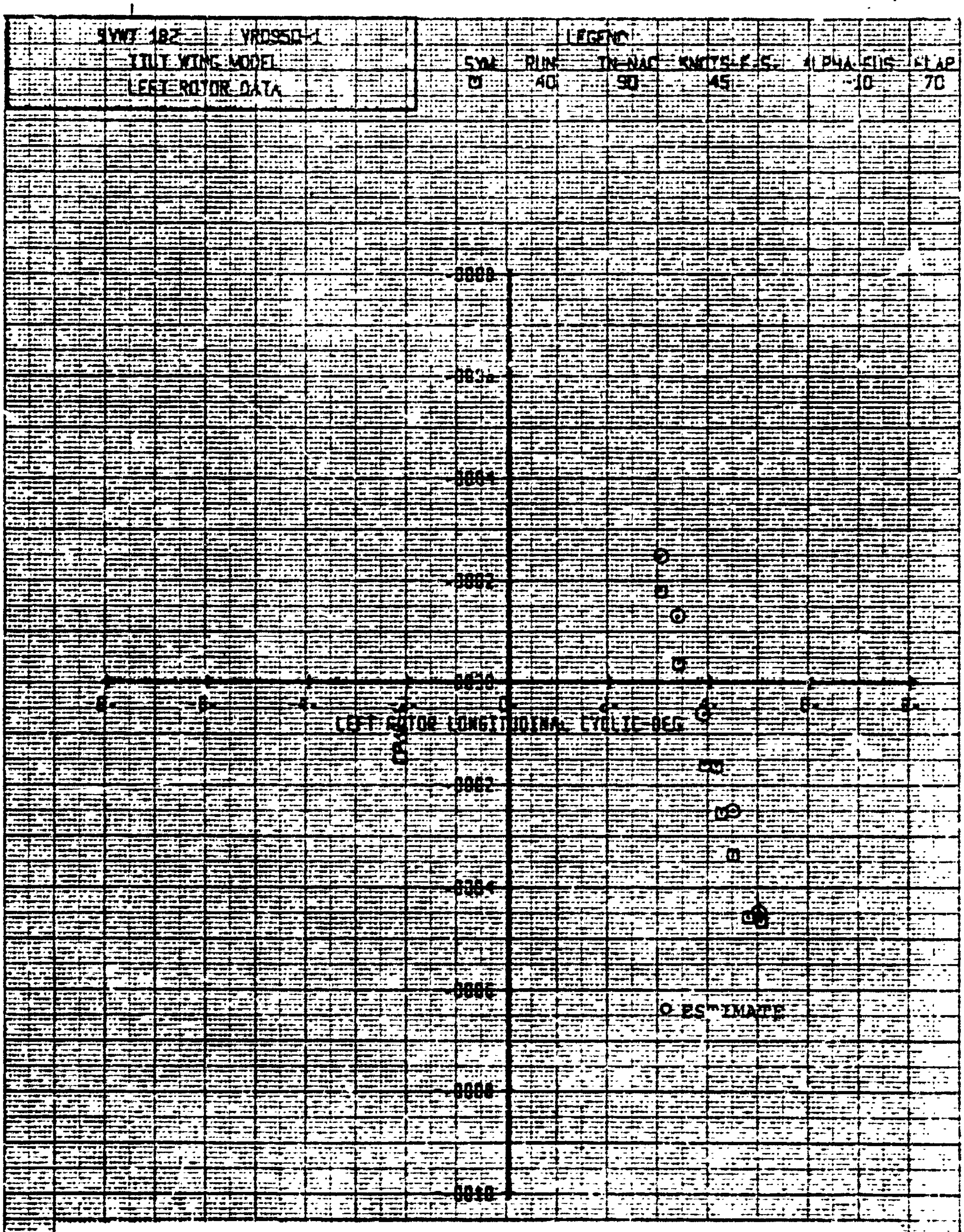

Fig. 3.81. Left Rotor Pitching Moment Vs. Left Rotor Long. Cyclic ~ Degrees.

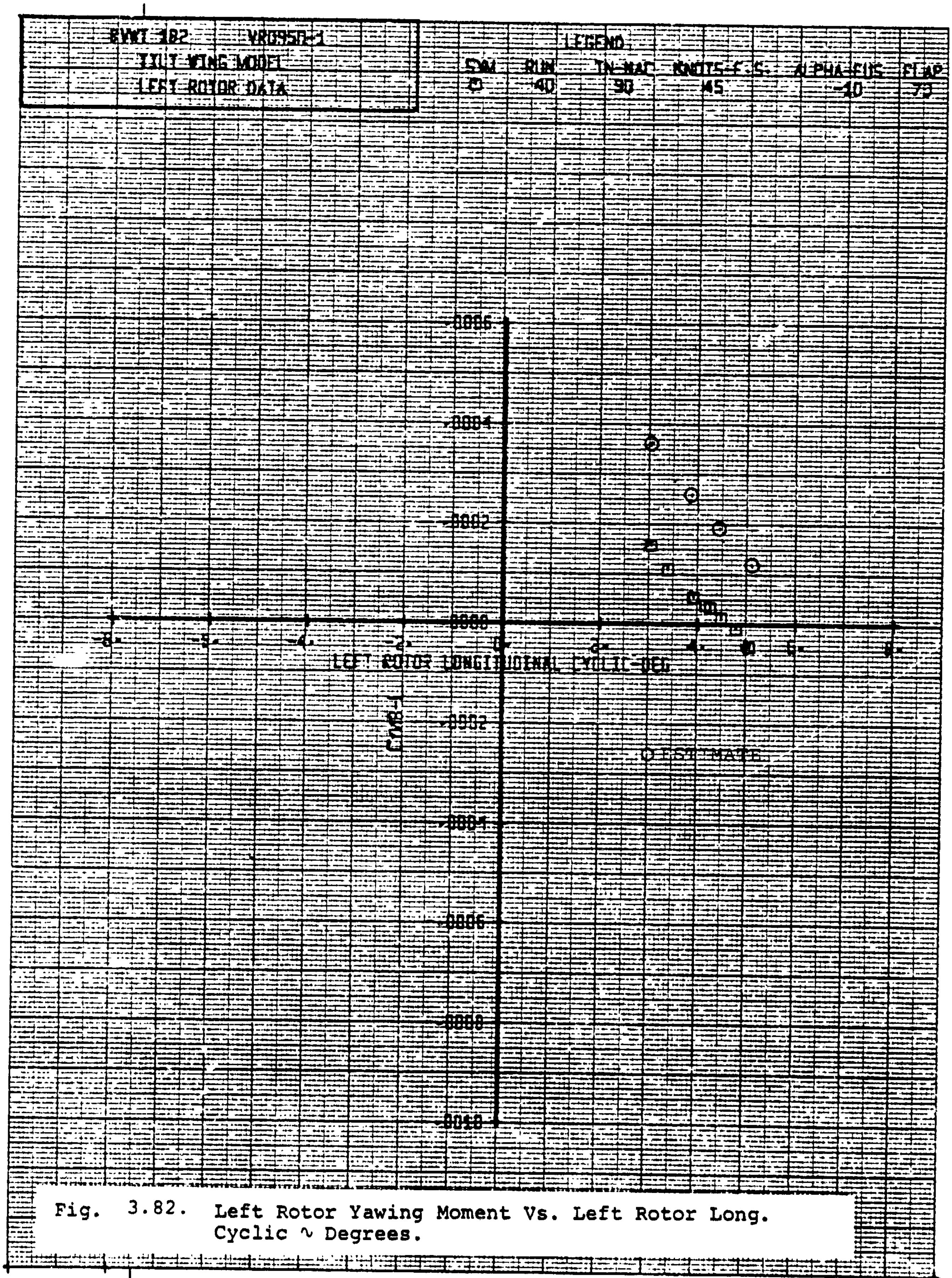

Fig. 3.82. Left Rotor Yawing Moment Vs. Left Rotor Long. Cyclic ∿ Degrees.

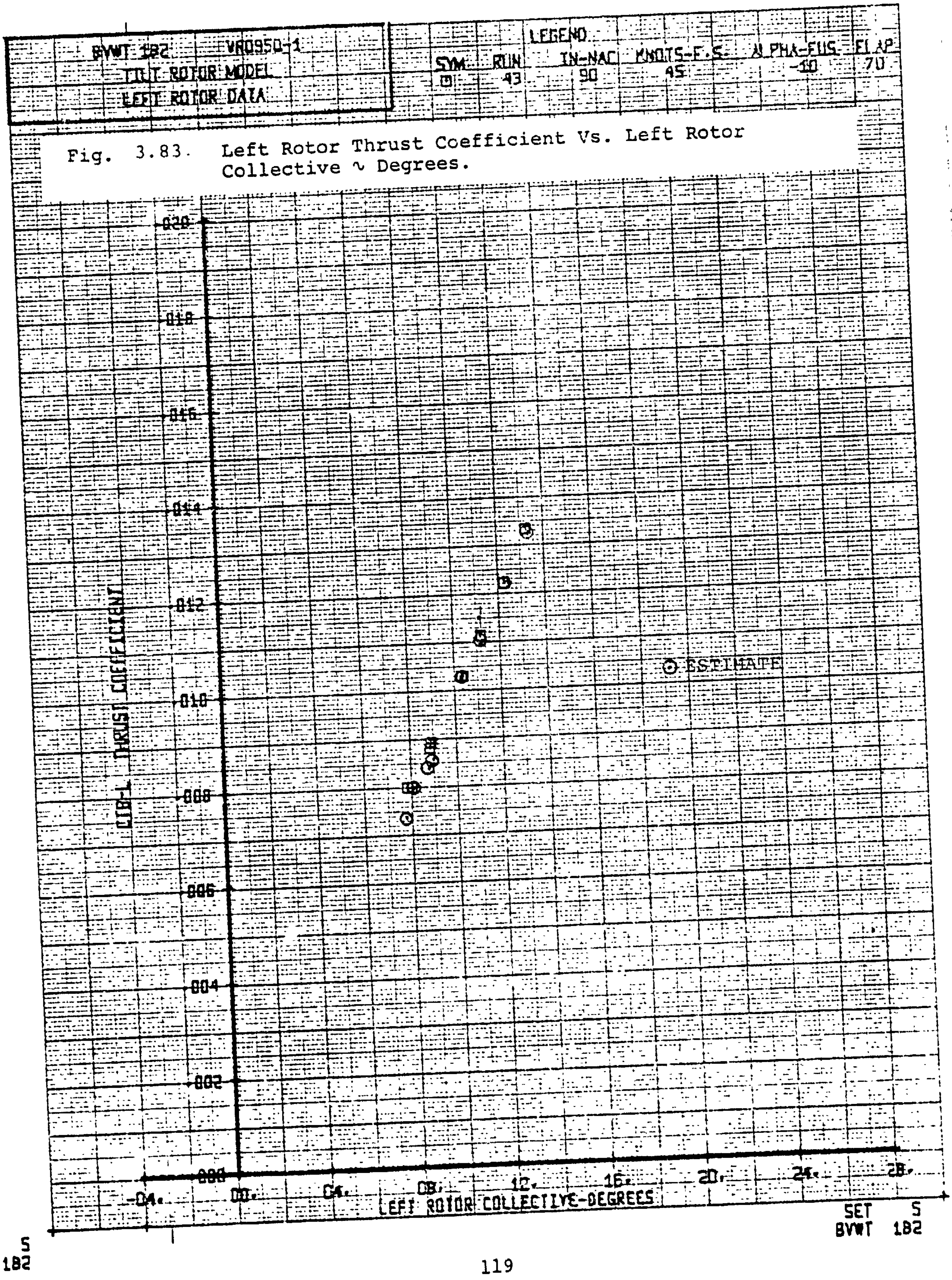

Fig. 3.83. Left Rotor Thrust Coefficient Vs. Left Rotor Collective ~ Degrees.

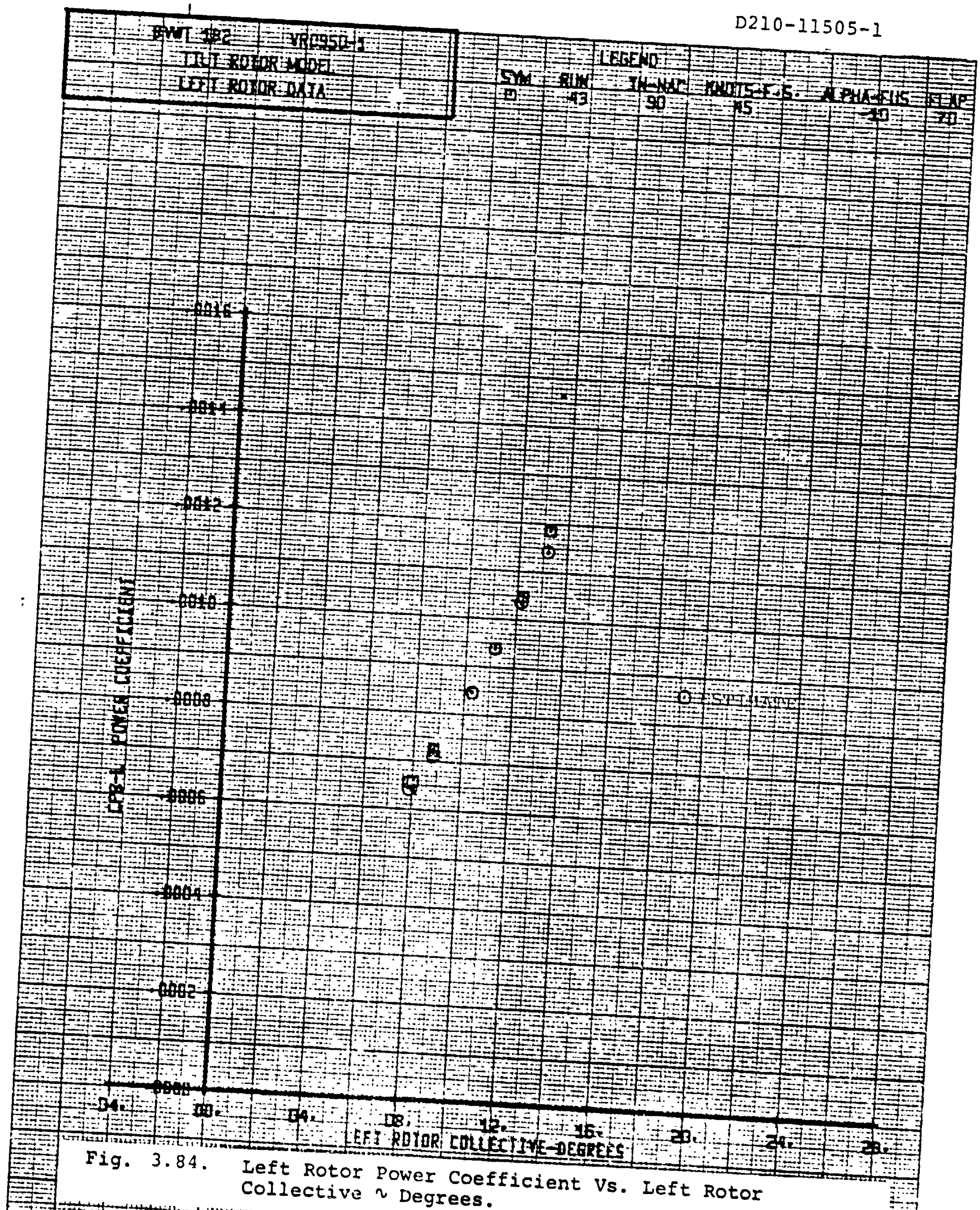

Fig. 3.84. Left Rotor Power Coefficient Vs. Left Rotor Collective ~ Degrees.

S
182

SET S
BVWT 182

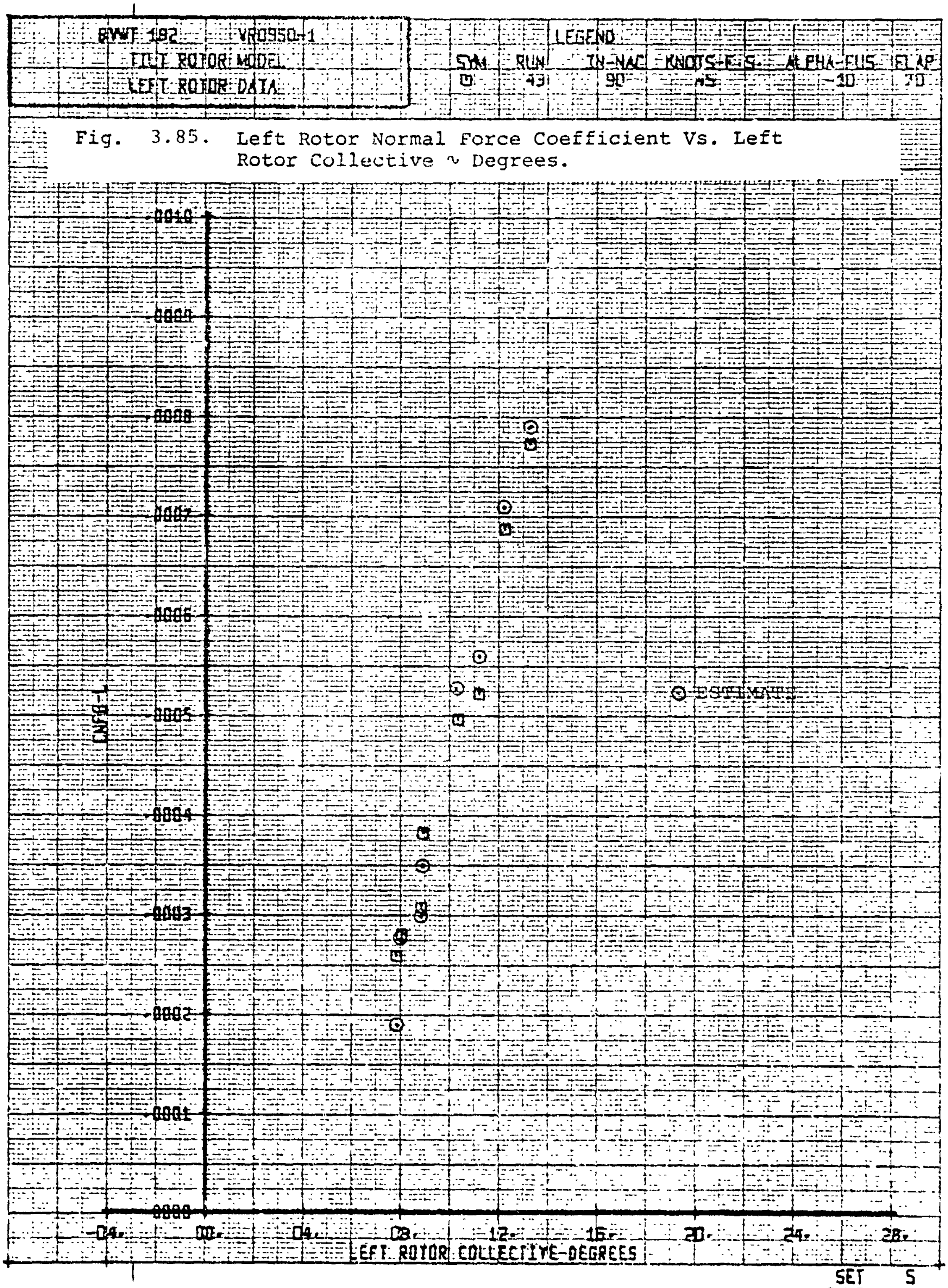

Fig. 3.85. Left Rotor Normal Force Coefficient Vs. Left Rotor Collective ∿ Degrees.

S 182

SET BVWT S 182

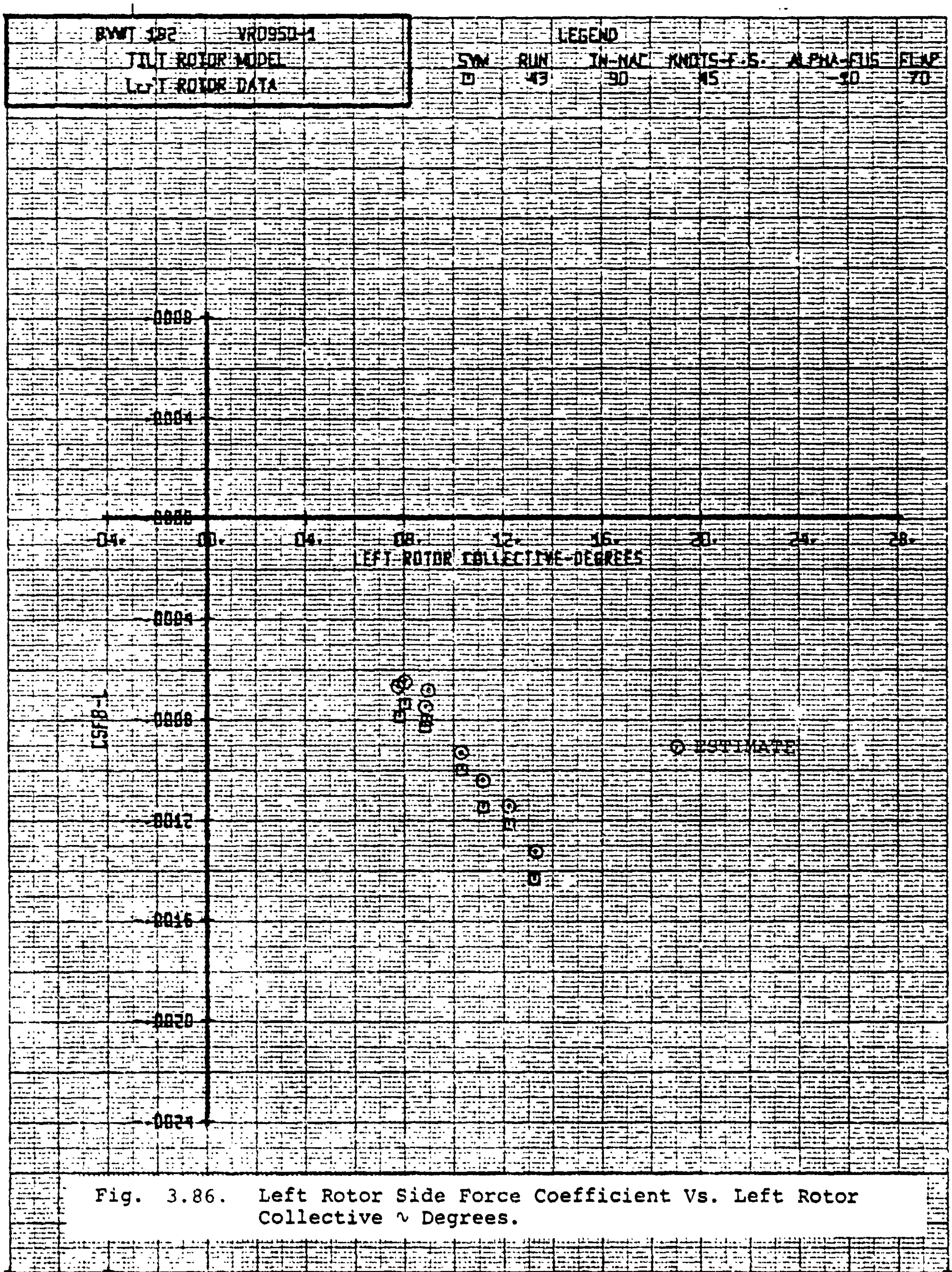

Fig. 3.86. Left Rotor Side Force Coefficient Vs. Left Rotor Collective ∿ Degrees.

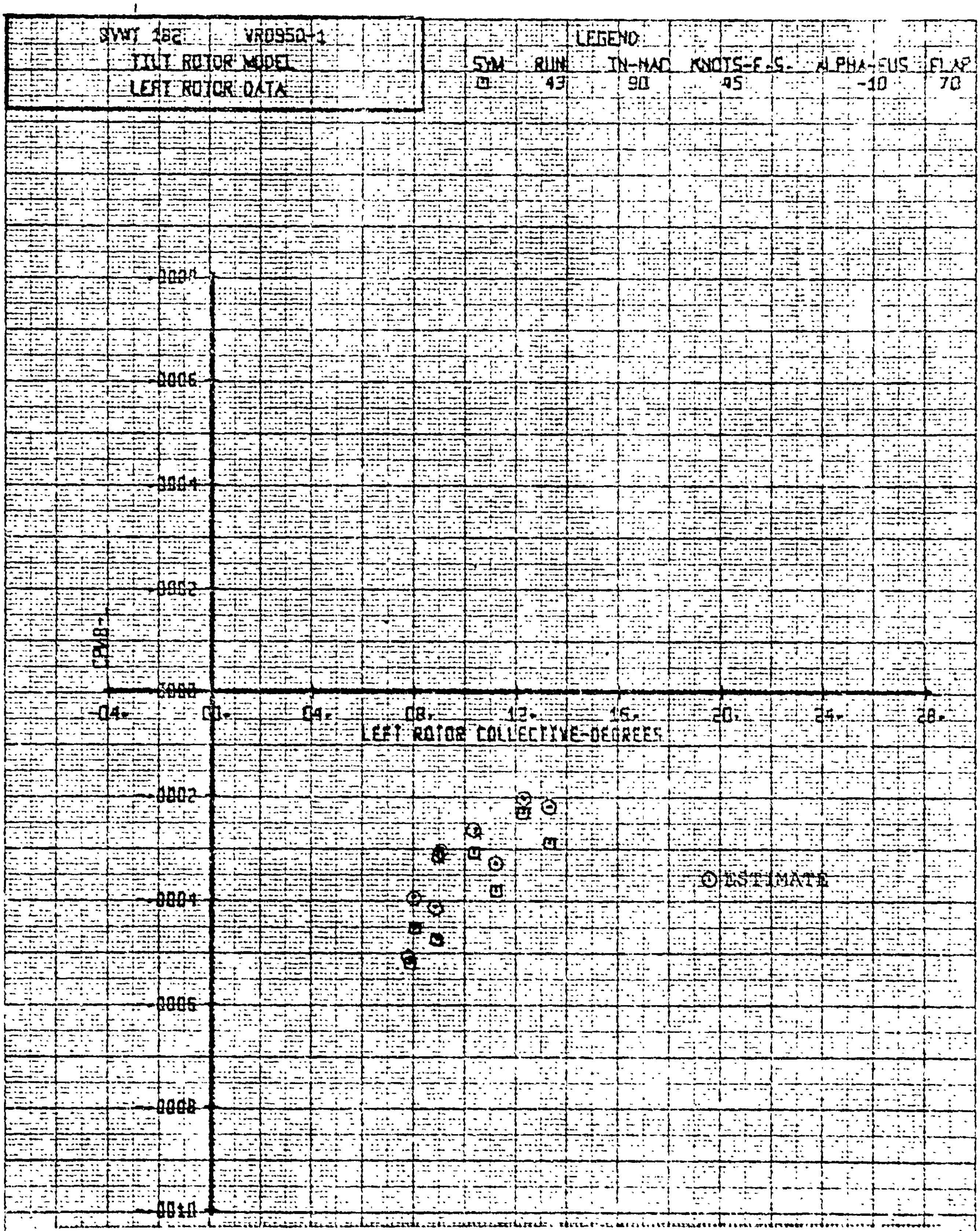

Fig. 3.87. Left Rotor Pitching Moment Coefficient Vs. Left Rotor Collective ~ Degrees.

S
182

SET S
BVWT 182

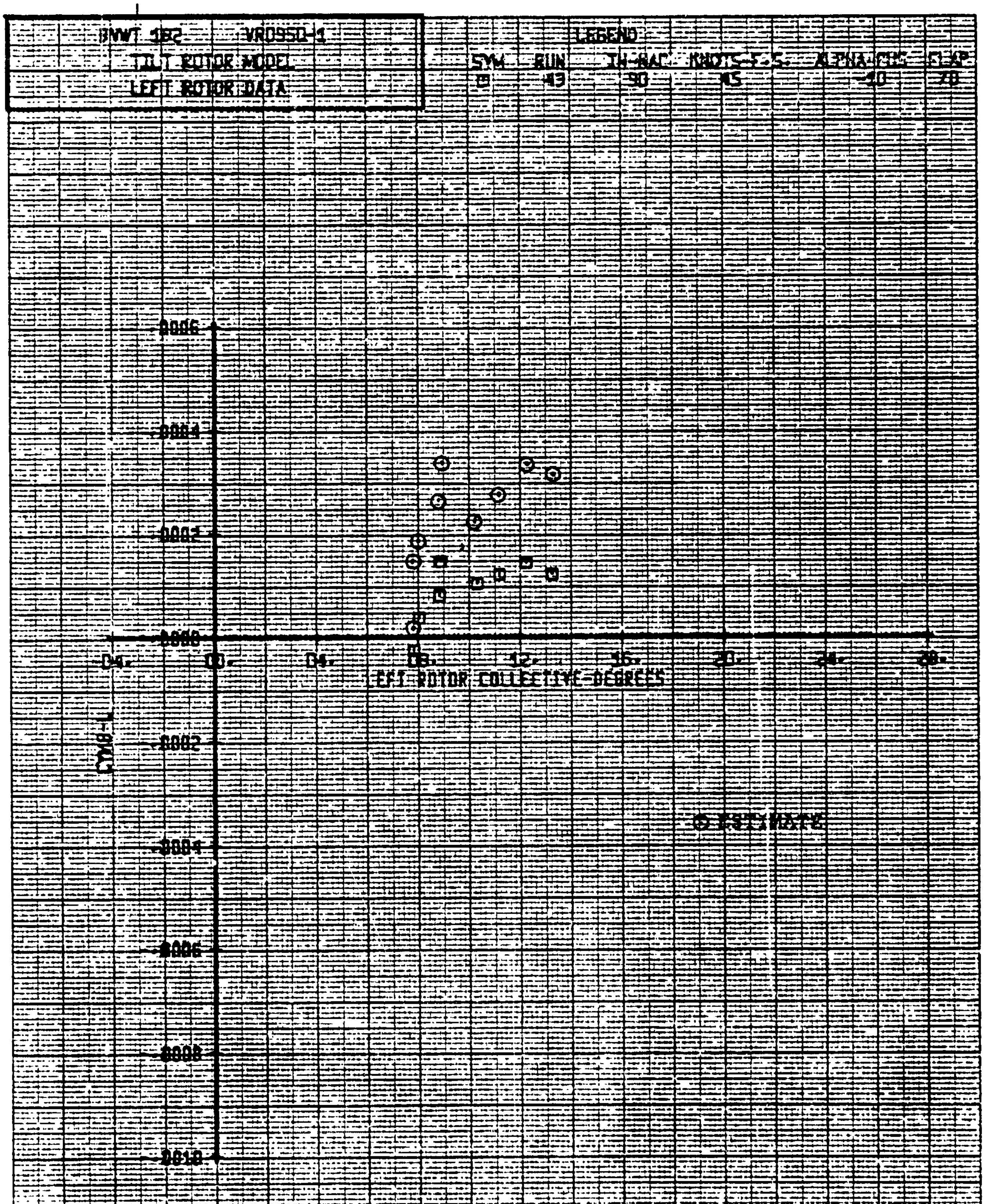

Fig. 3.88. Left Rotor Yawing Moment Coefficient Vs. Left Rotor Collective ∿ Degrees.

5
182

SET 5
BVWT 182

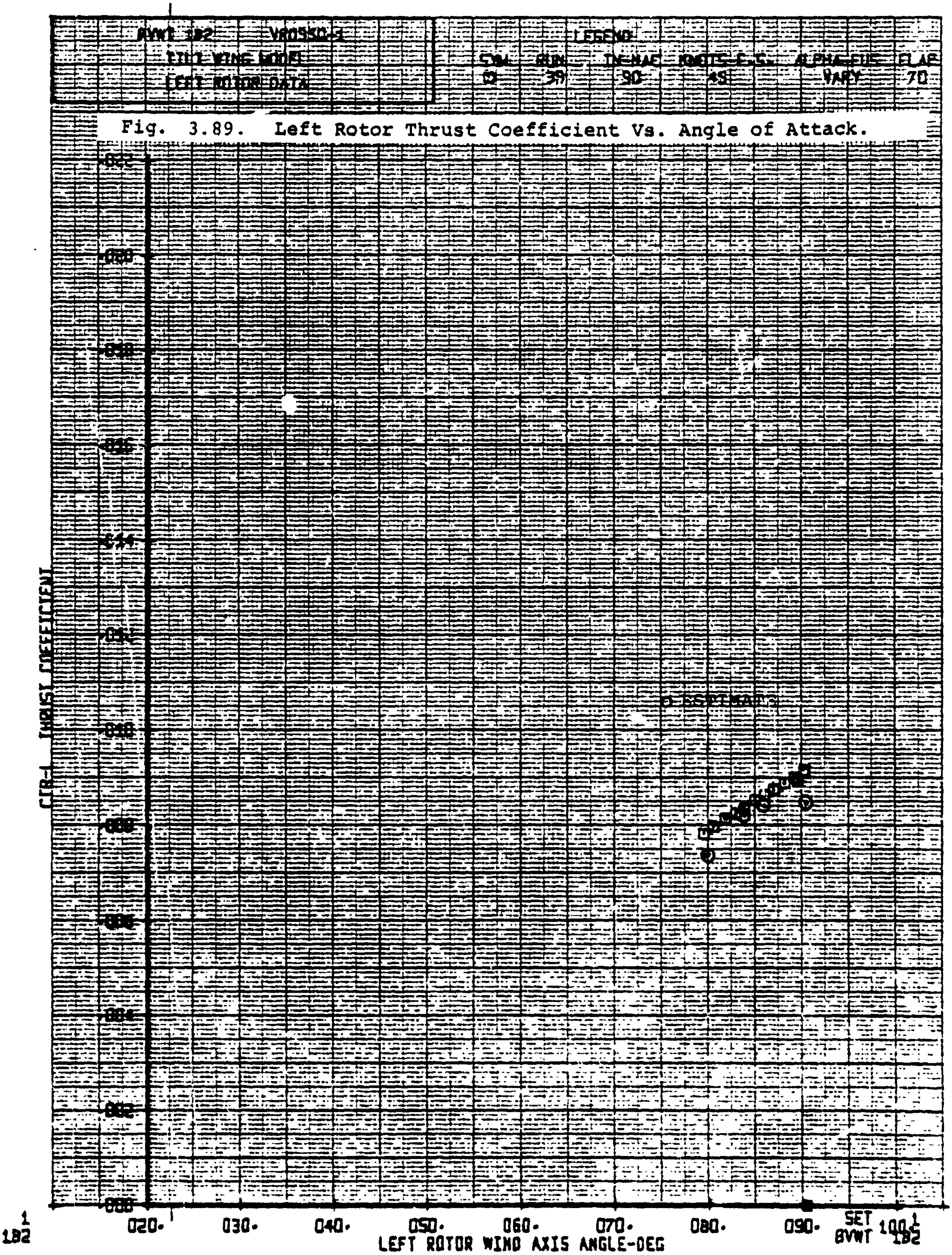

Fig. 3.89. Left Rotor Thrust Coefficient Vs. Angle of Attack.

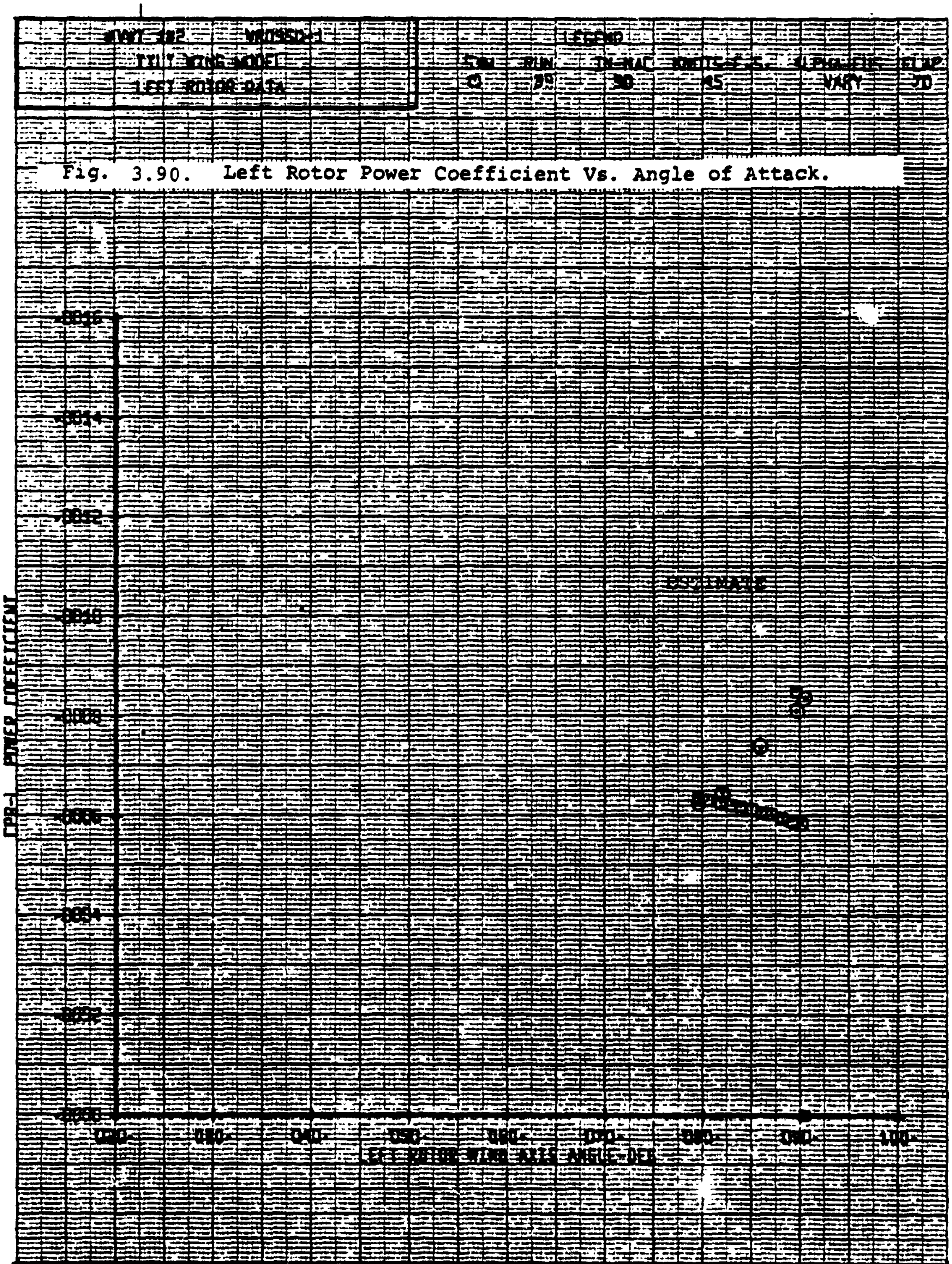

Fig. 3.90. Left Rotor Power Coefficient Vs. Angle of Attack.

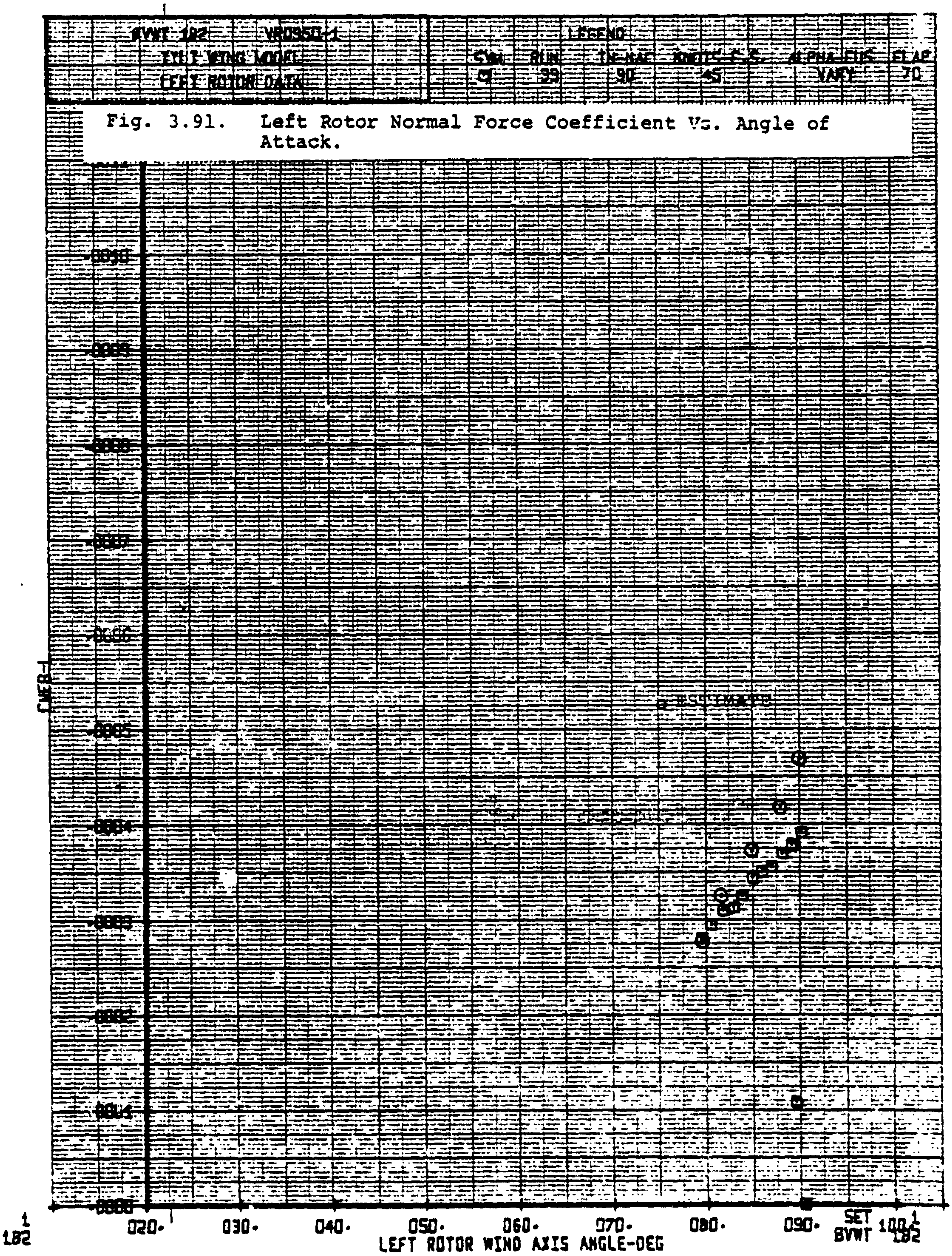

Fig. 3.91. Left Rotor Normal Force Coefficient Vs. Angle of Attack.

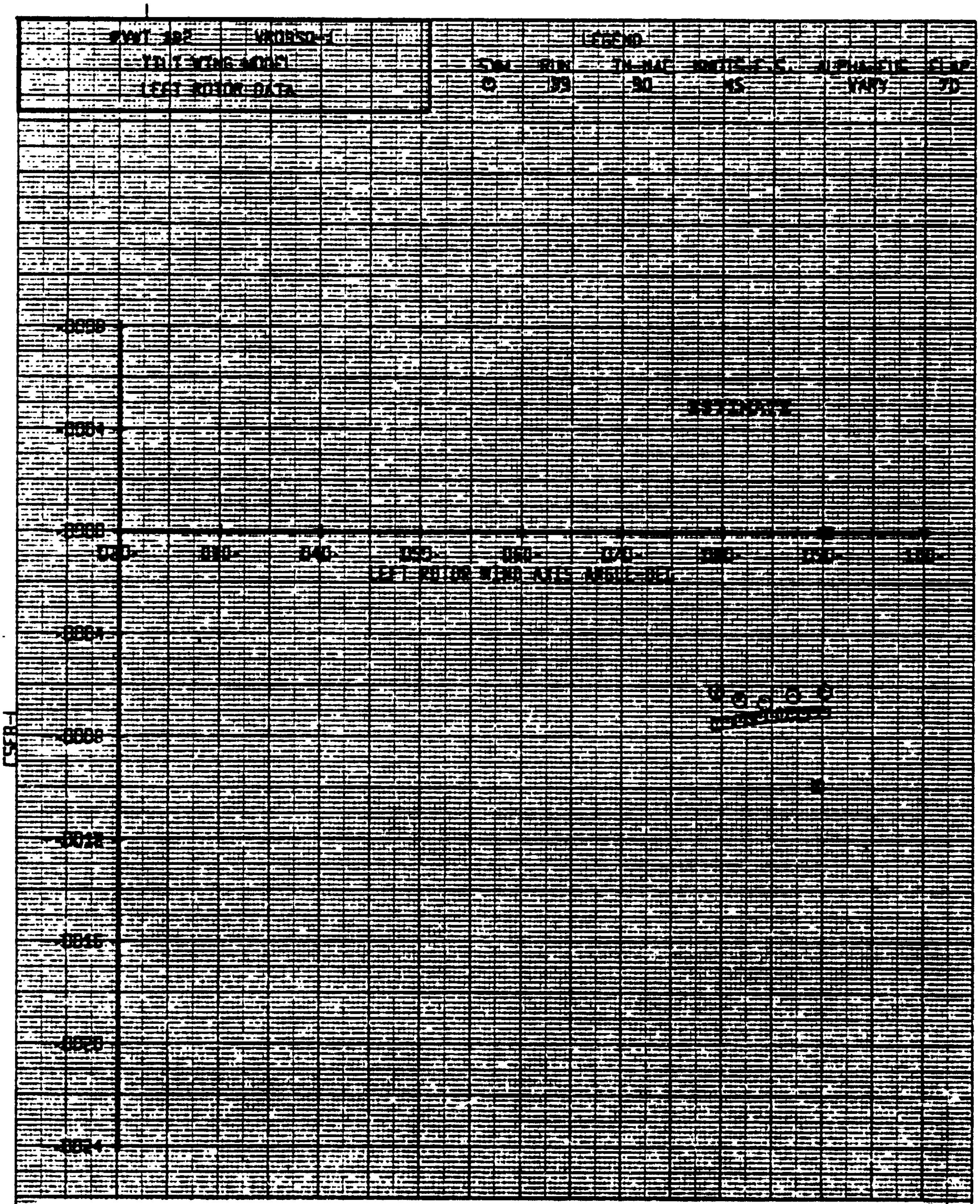

Fig. 3.92. Left Rotor Side Force Coefficient Vs. Angle of Attack.

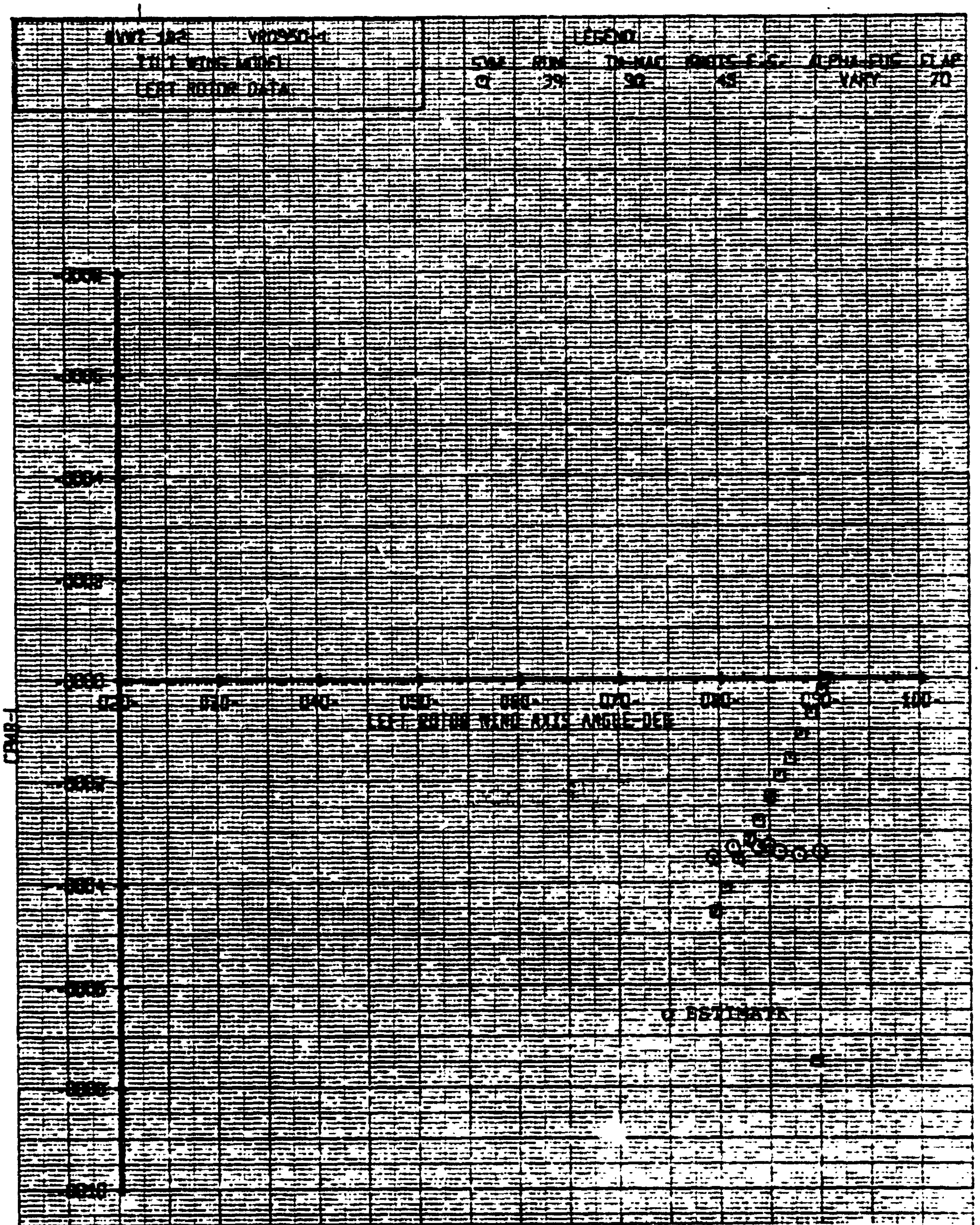

Fig. 3.93. Left Rotor Pitching Moment Vs. Angle of Attack.

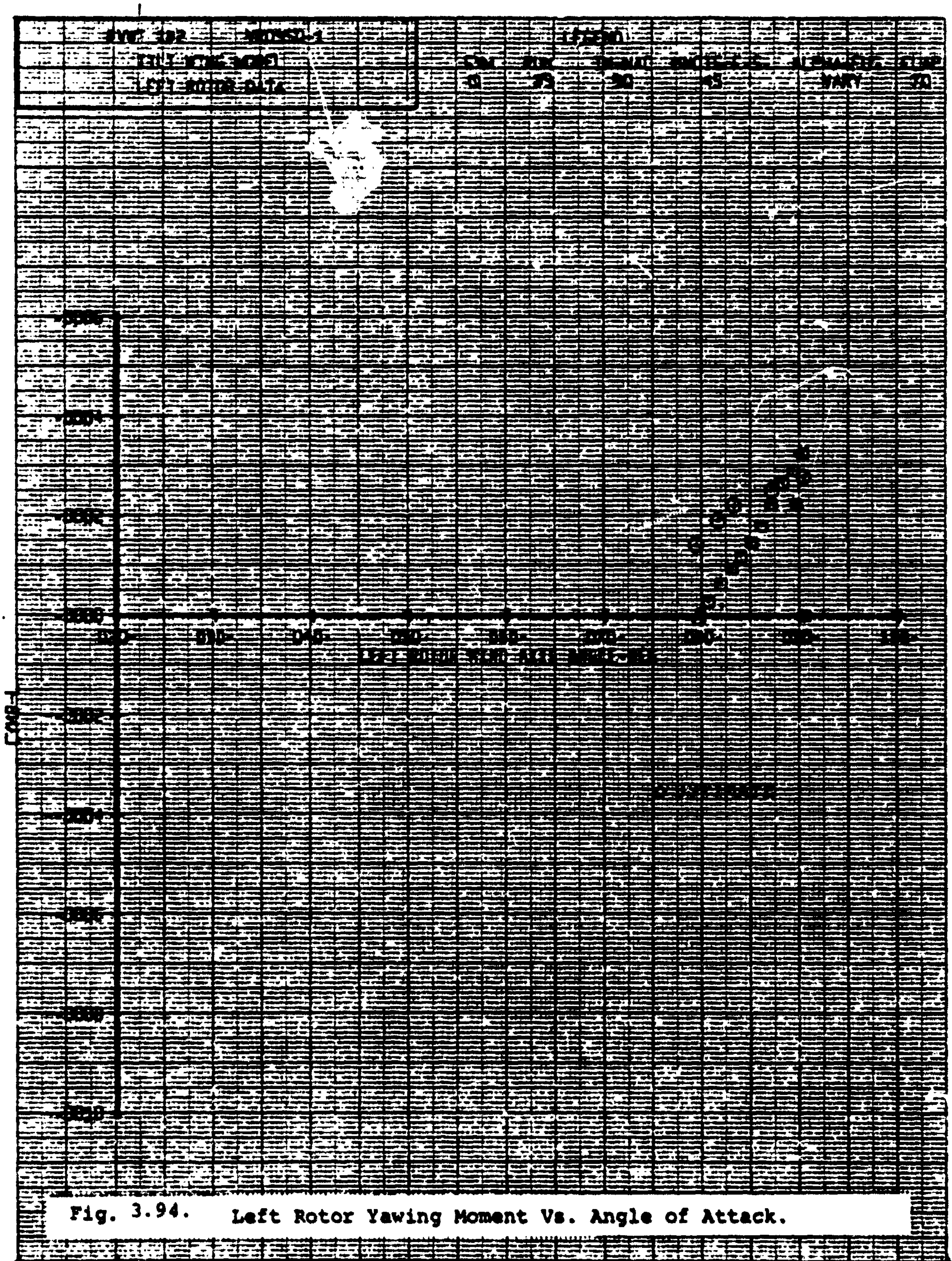

Fig. 3.94. Left Rotor Yawing Moment Vs. Angle of Attack.

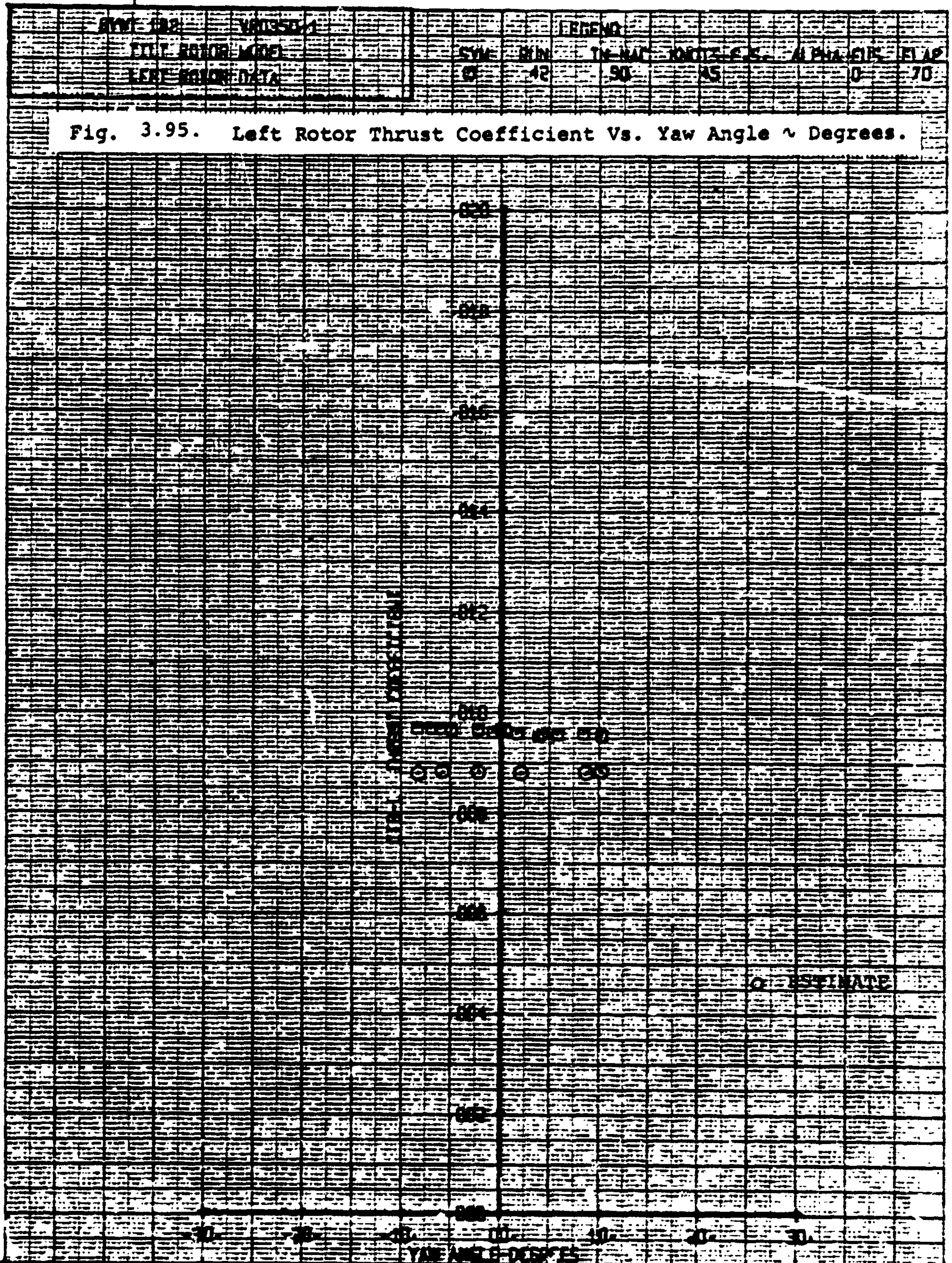

Fig. 3.95. Left Rotor Thrust Coefficient Vs. Yaw Angle ~ Degrees.

4
82

SET 4
BVWT 182

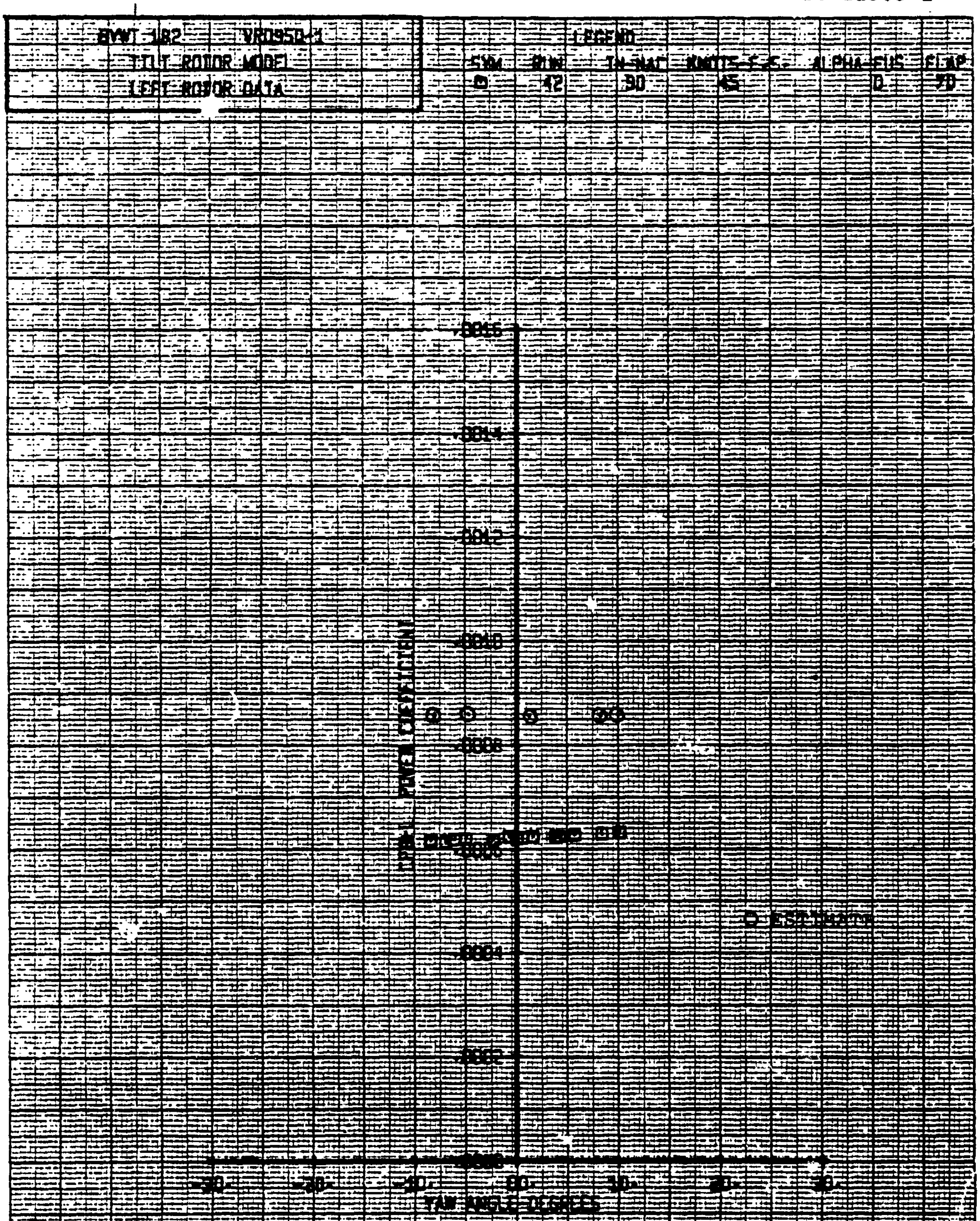

Fig. 3.96. Left Rotor Power Coefficient Vs. Yaw Angle ~ Degrees.

4
182

SET 4
BVWT 182

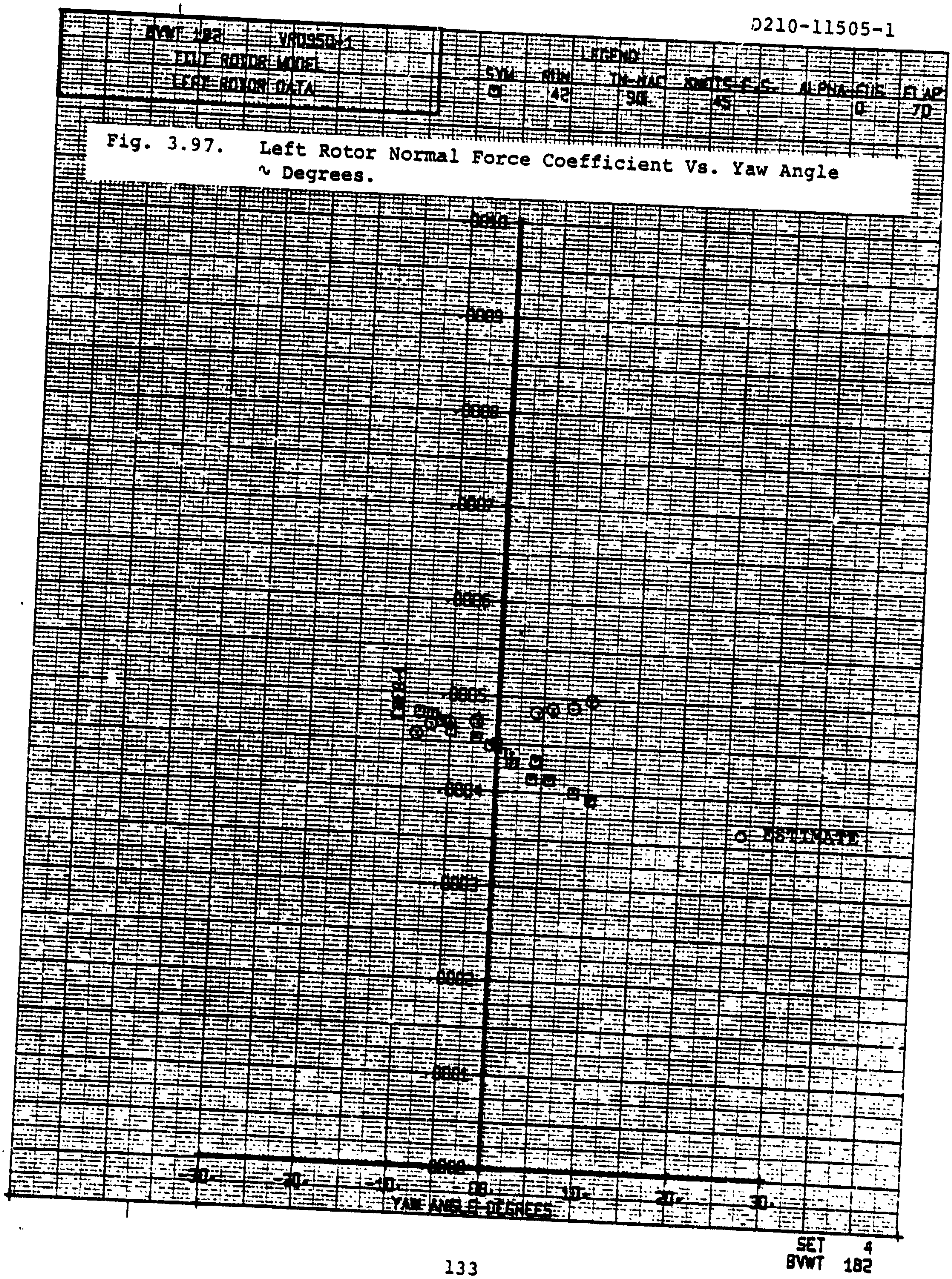

Fig. 3.97. Left Rotor Normal Force Coefficient Vs. Yaw Angle ~ Degrees.

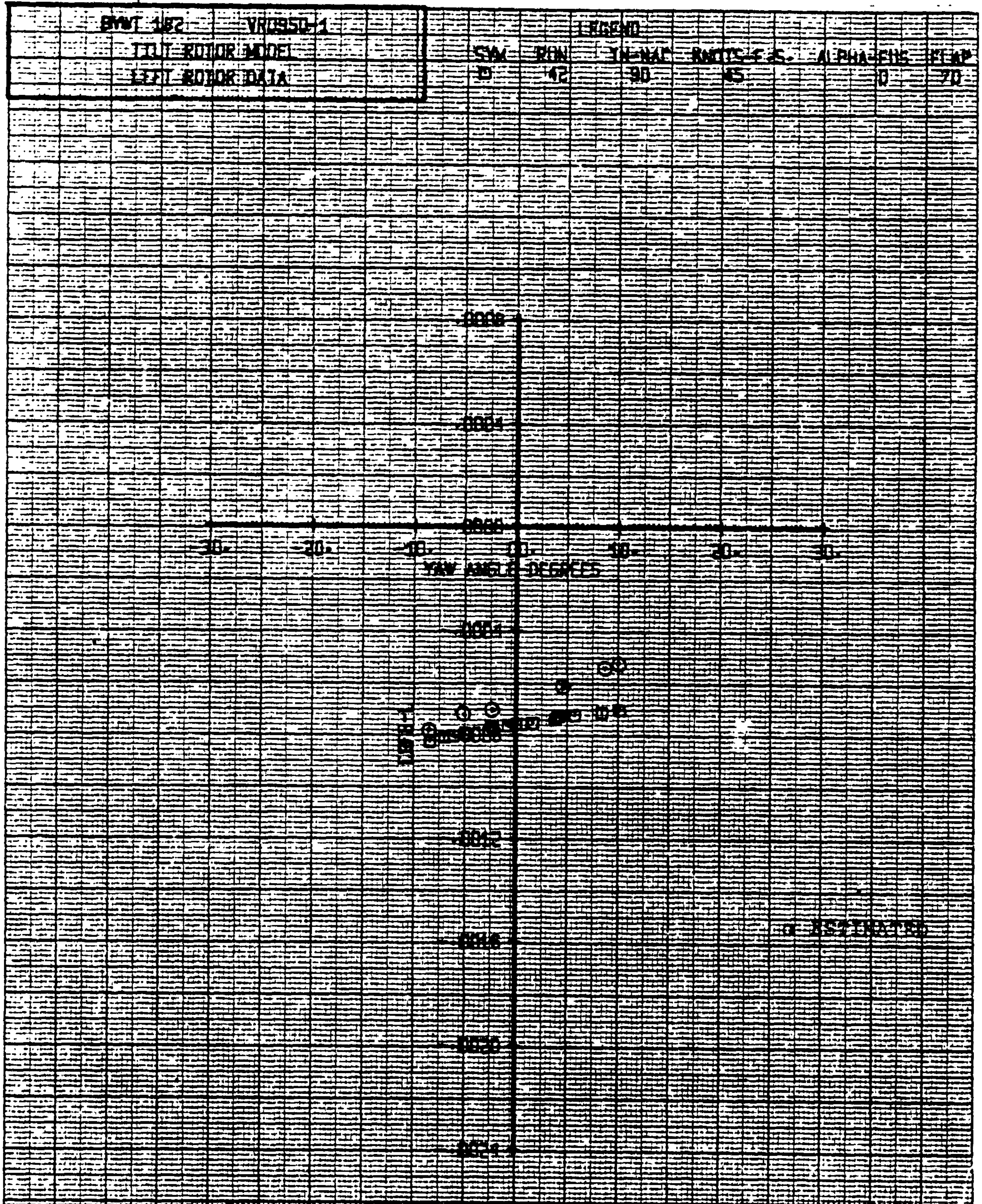

Fig. 3.98. Left Rotor Side Force Coefficient Vs. Yaw Angle ∿ Degrees.

4
1B2

SET 4
BVWT 1B2

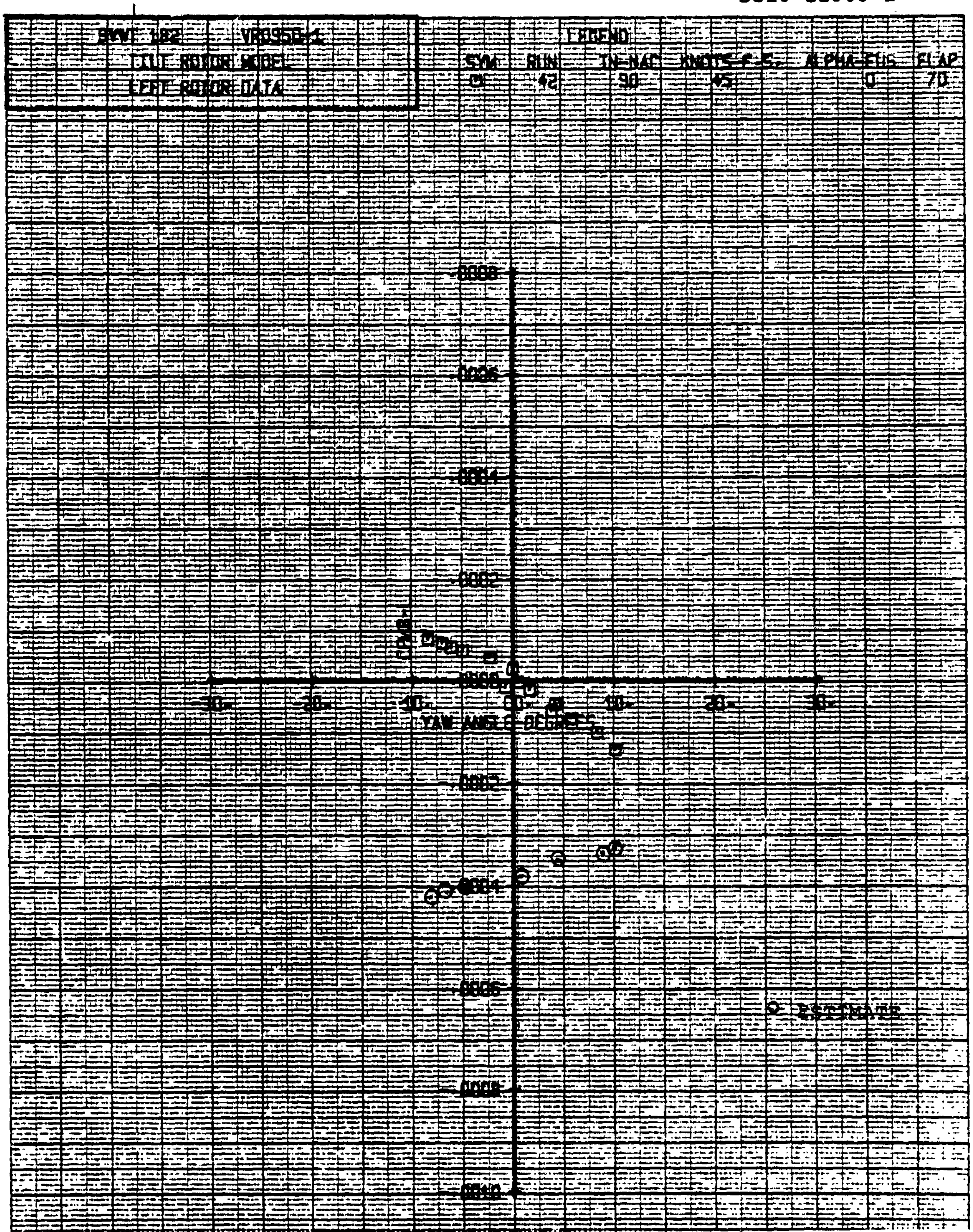

Fig. 3.99. Left Rotor Pitching Moment Vs. Yaw Angle ~ Degrees.

4
82

SET 4
BVWT 182

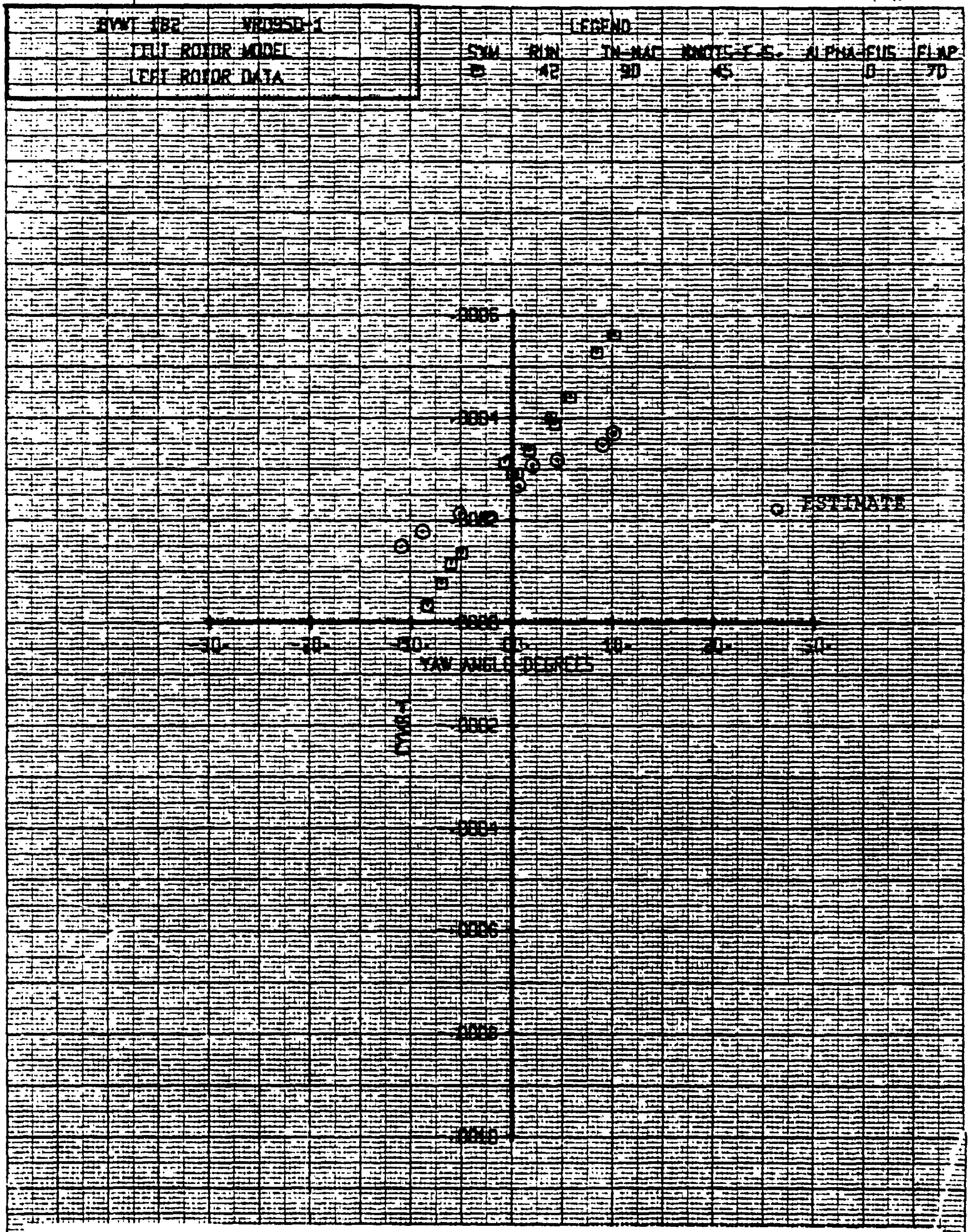

Fig. 3.100. Left Rotor Yawing Moment Vs. Yaw Angle ~ Degrees.

4
182

SET 4
BVWT 182

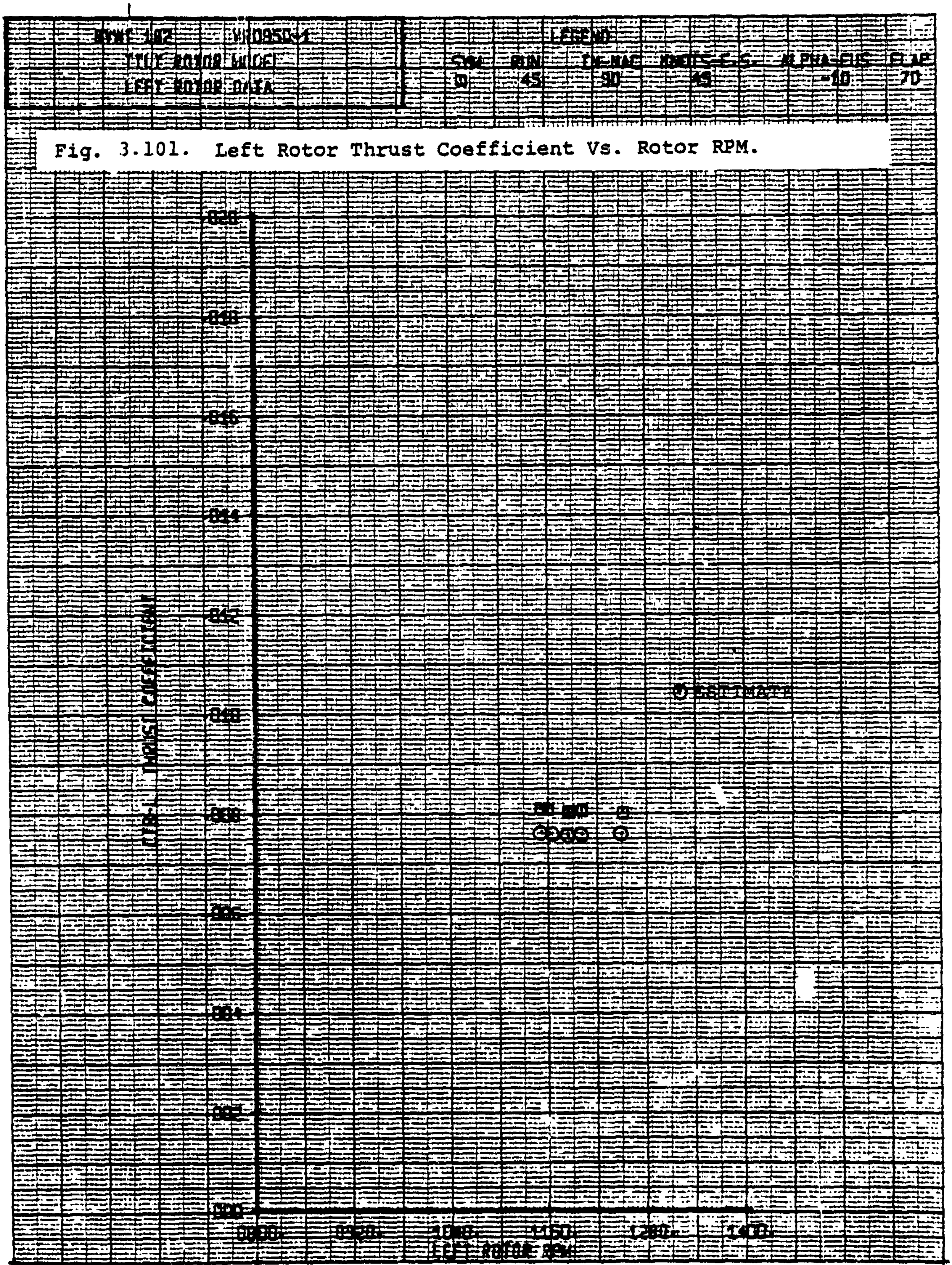

Fig. 3.101. Left Rotor Thrust Coefficient Vs. Rotor RPM.

7
182

SET 7
BVWT 182

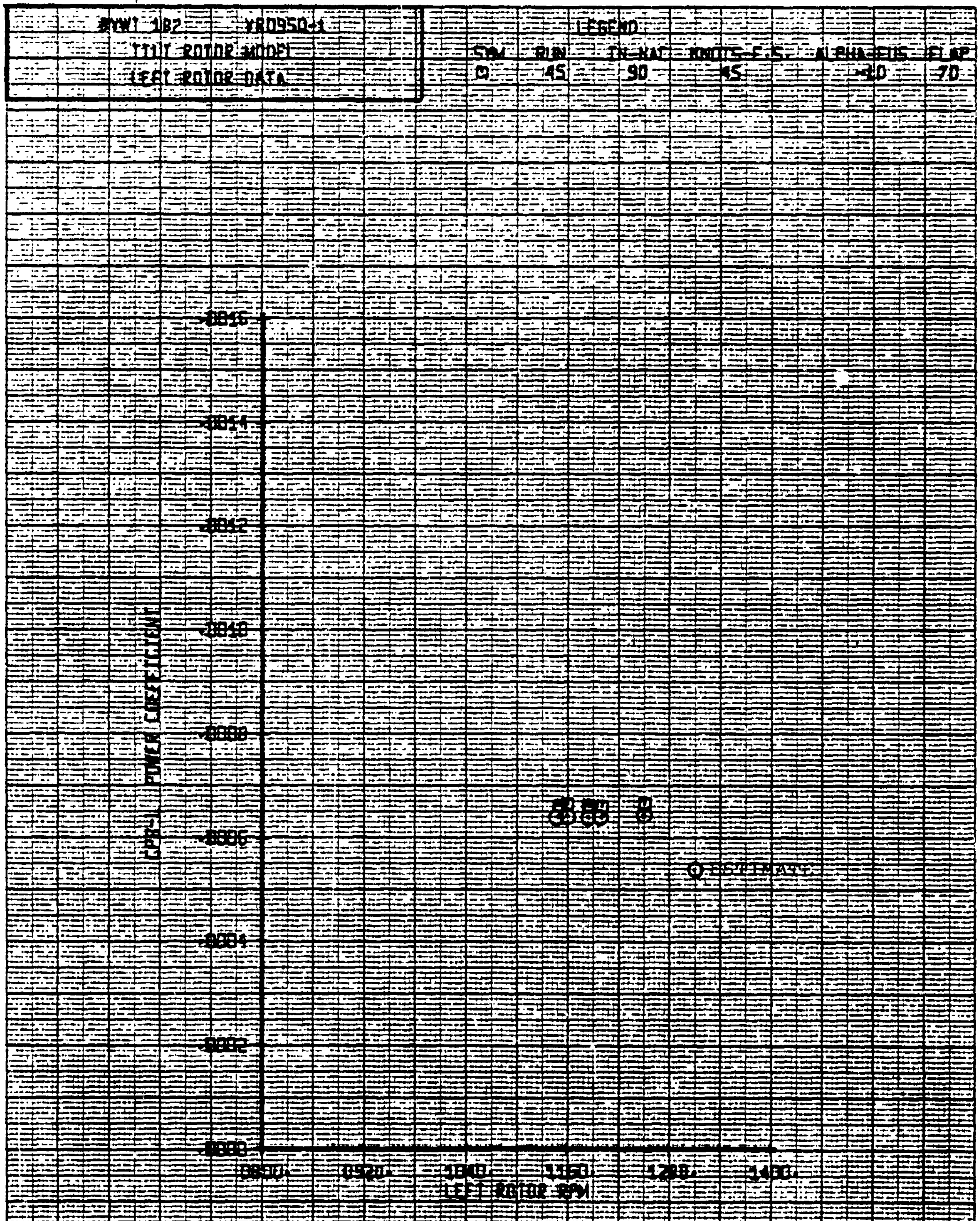

Fig. 3.102. Left Rotor Power Coefficient Vs. Rotor RPM.

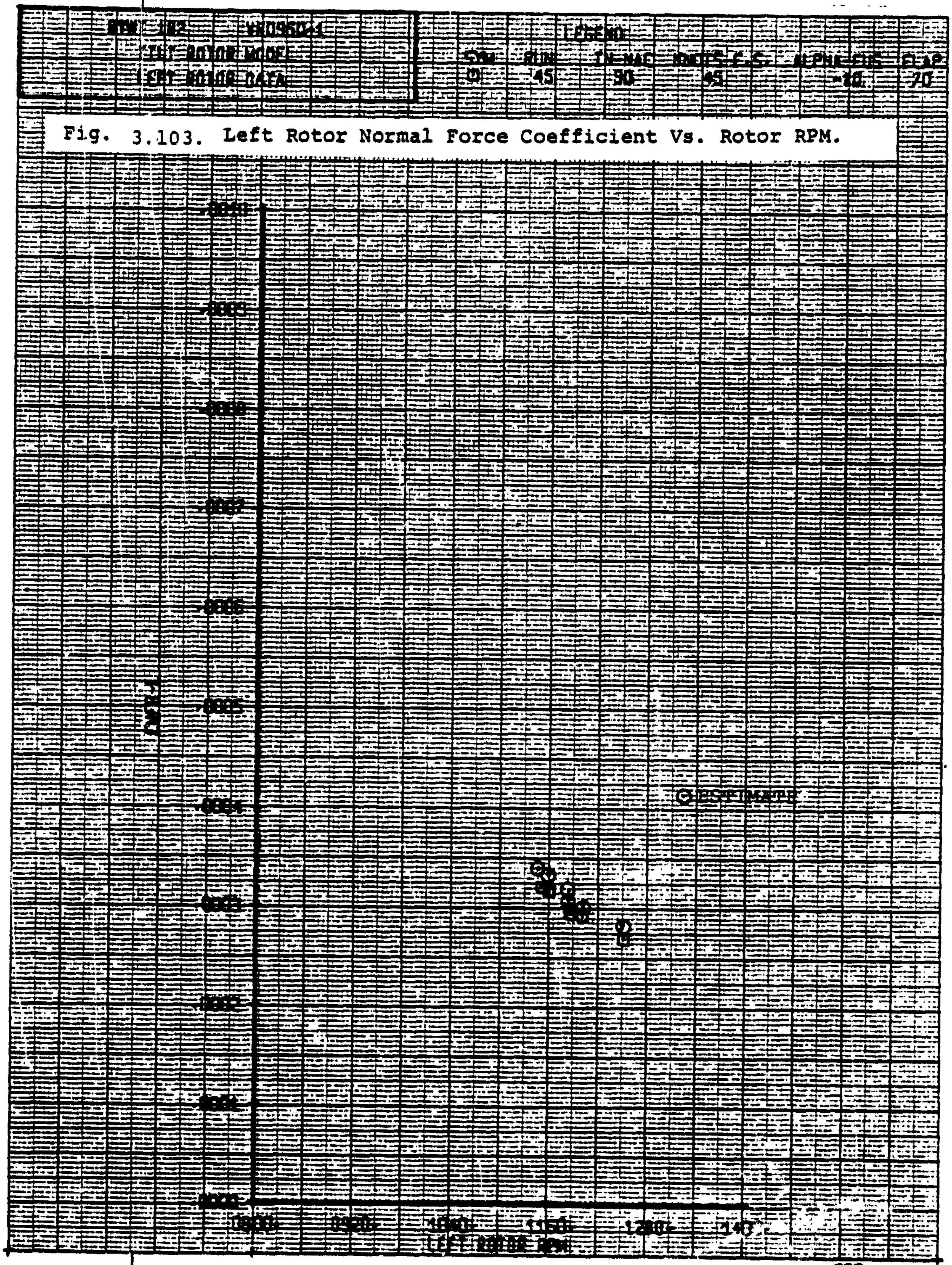

Fig. 3.103. Left Rotor Normal Force Coefficient Vs. Rotor RPM.

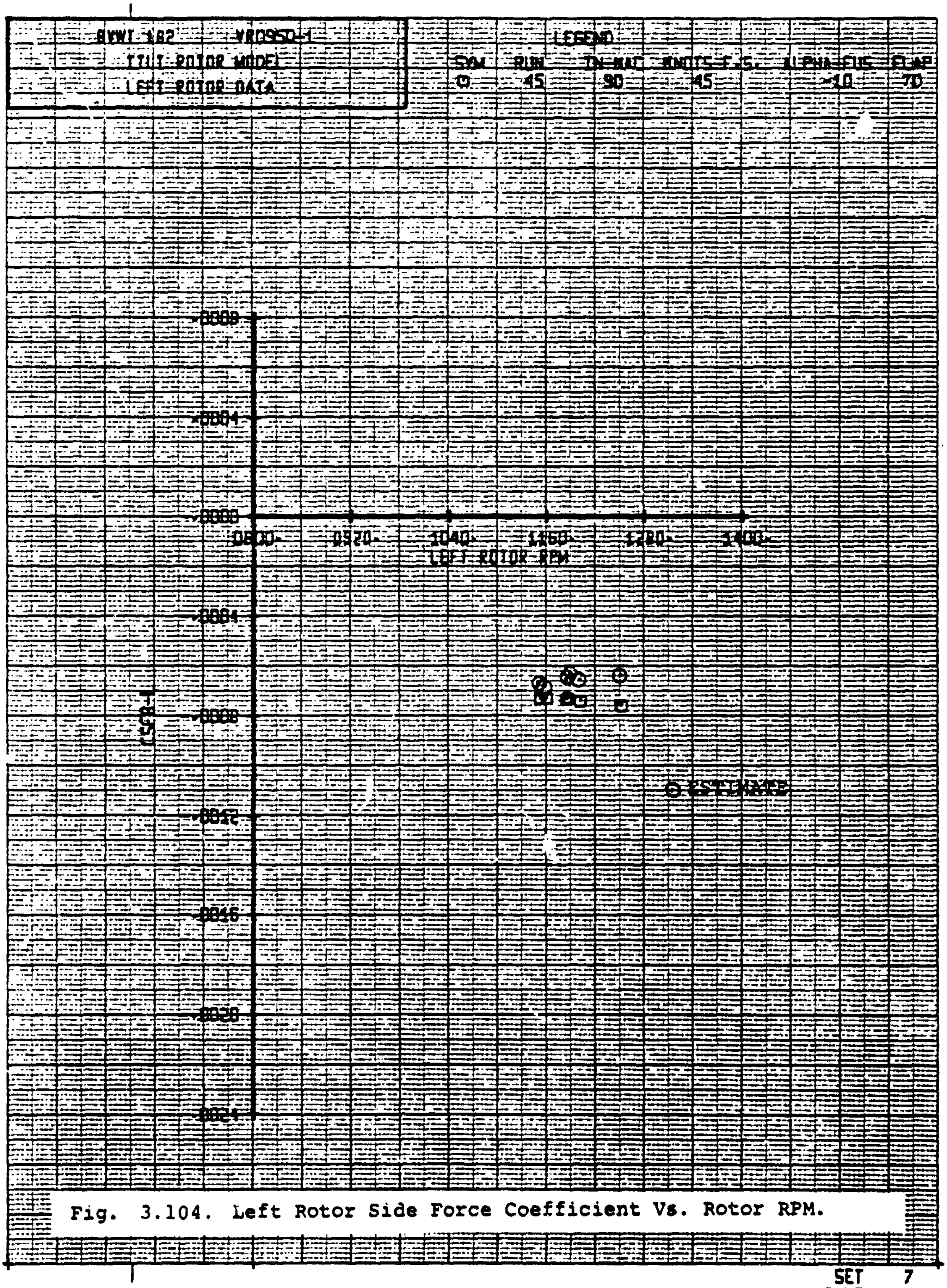

Fig. 3.104. Left Rotor Side Force Coefficient Vs. Rotor RPM.

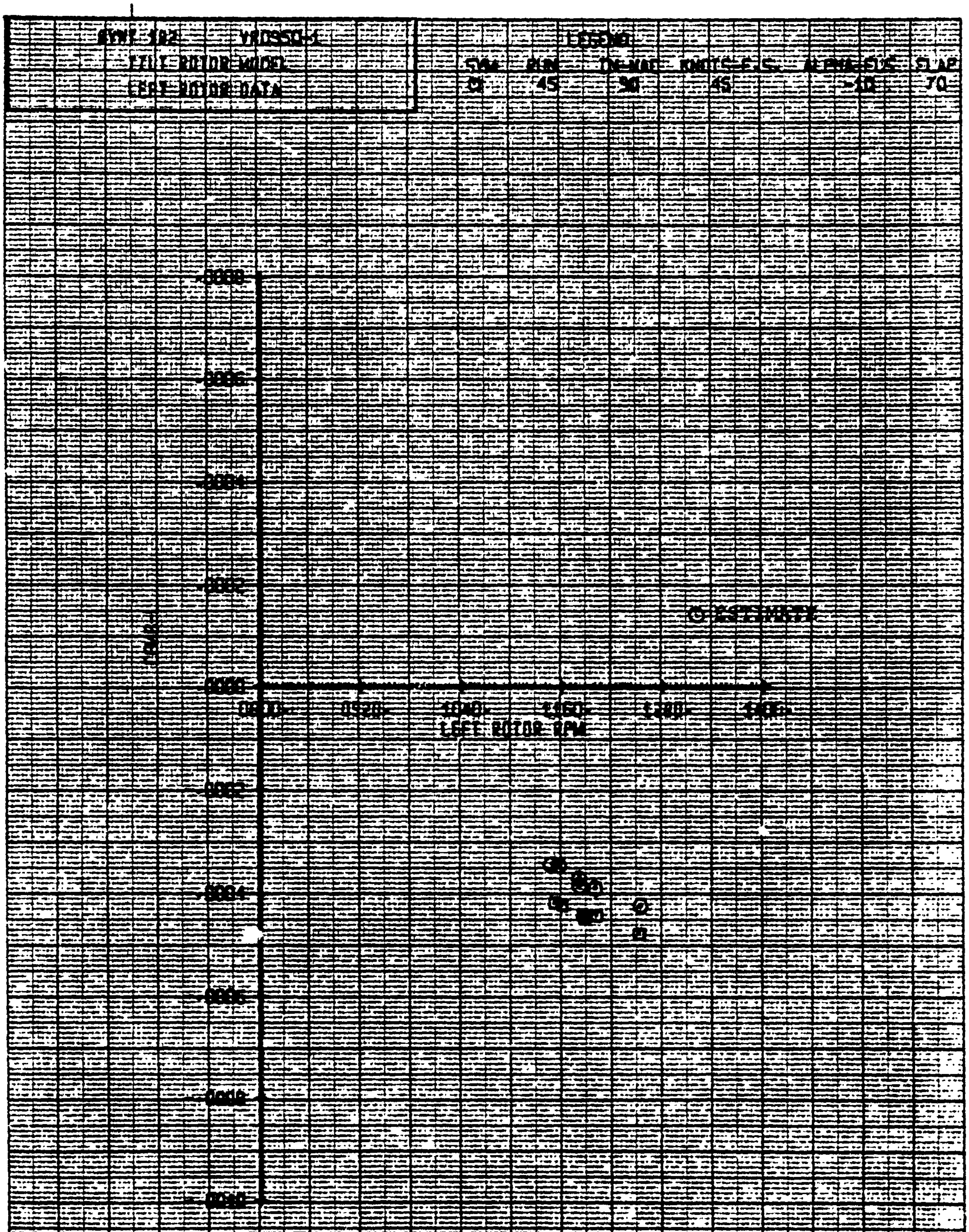

Fig. 3.105. Left Rotor Pitching Moment Coefficient Vs. Rotor RPM.

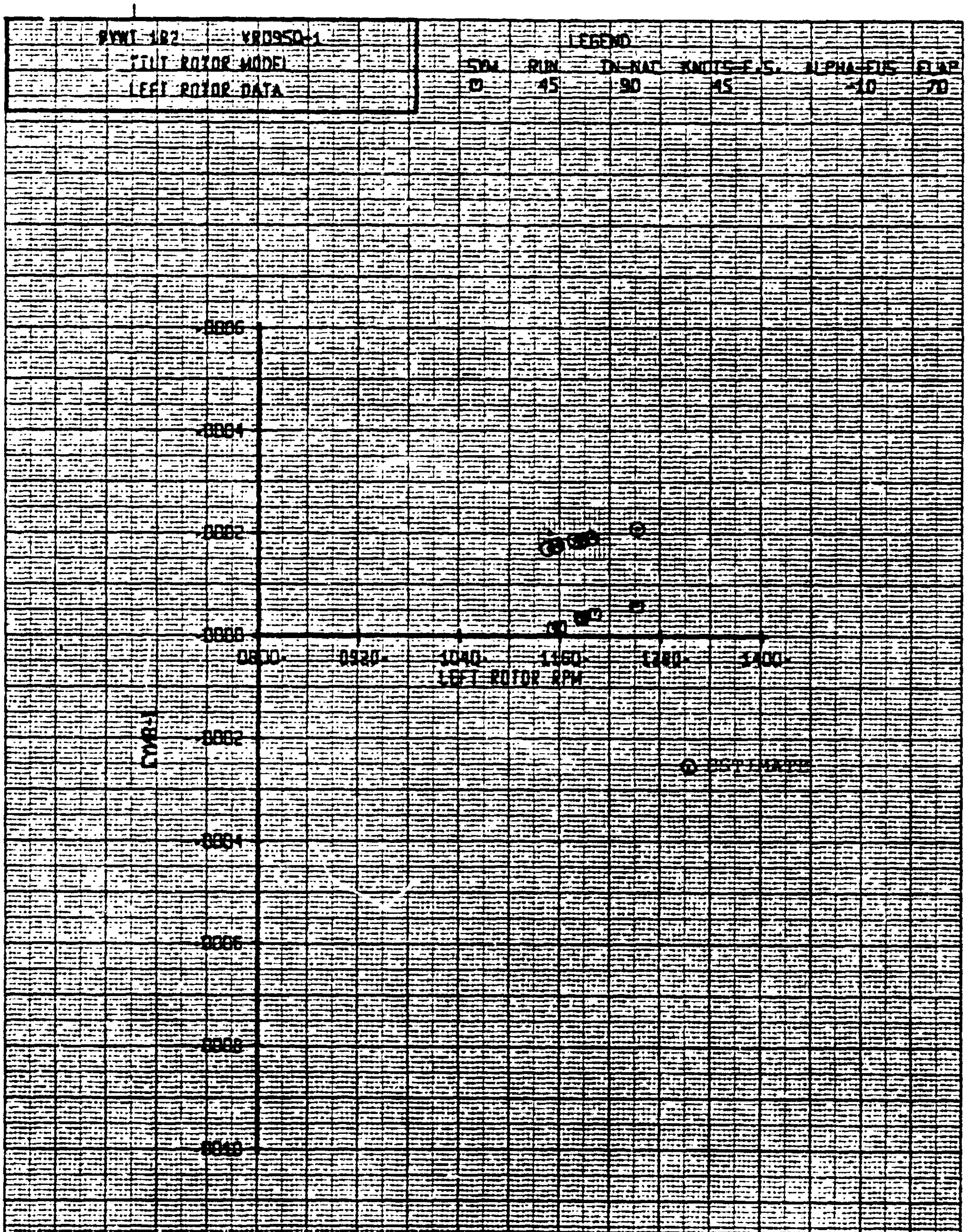

Fig. 3.106. Left Rotor Yawing Moment Coefficient Vs. Rotor RPM.

7 182 SET BVWT 7 182

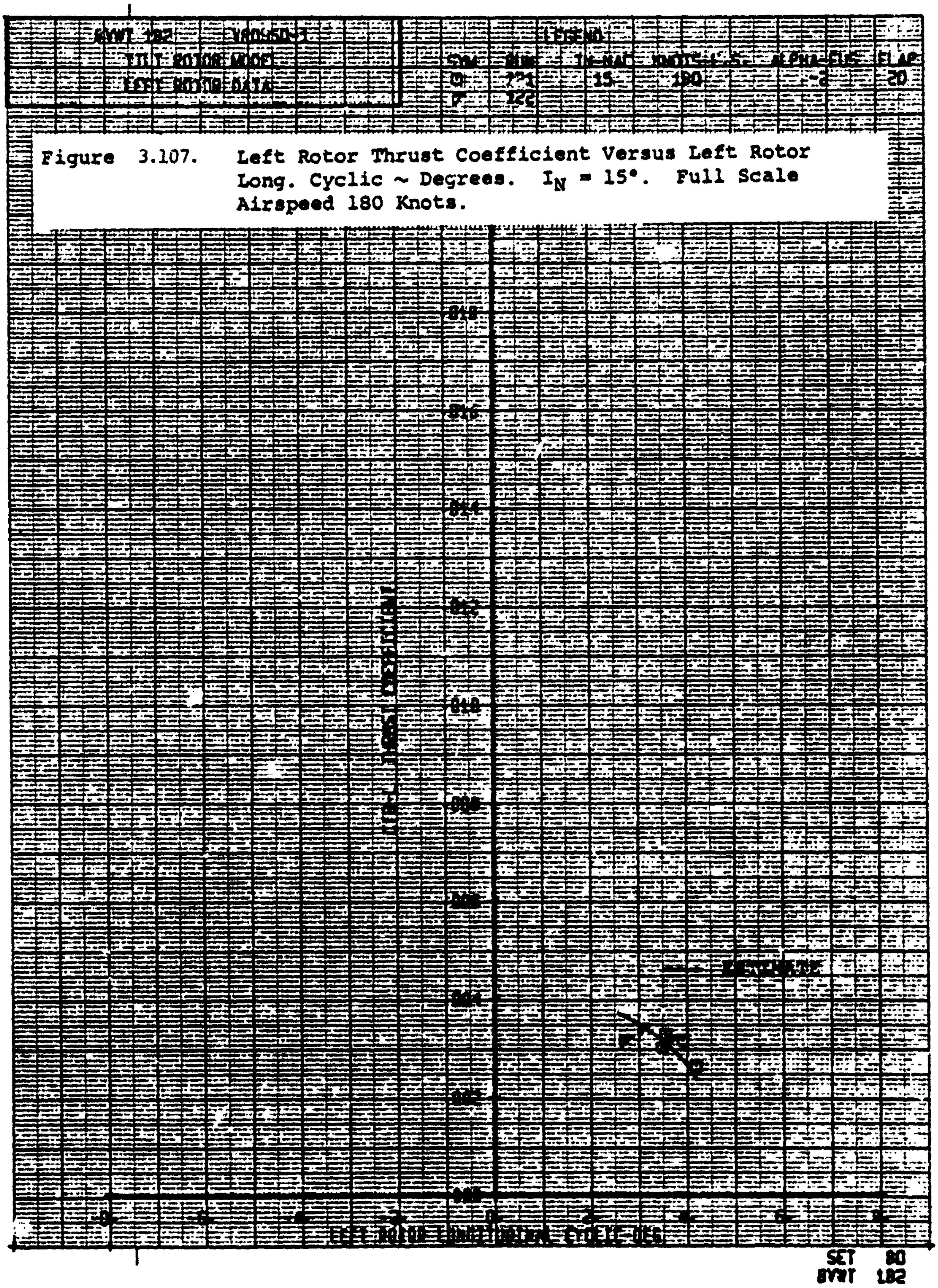

Figure 3.107. Left Rotor Thrust Coefficient Versus Left Rotor Long. Cyclic ~ Degrees. $I_N = 15°$. Full Scale Airspeed 180 Knots.

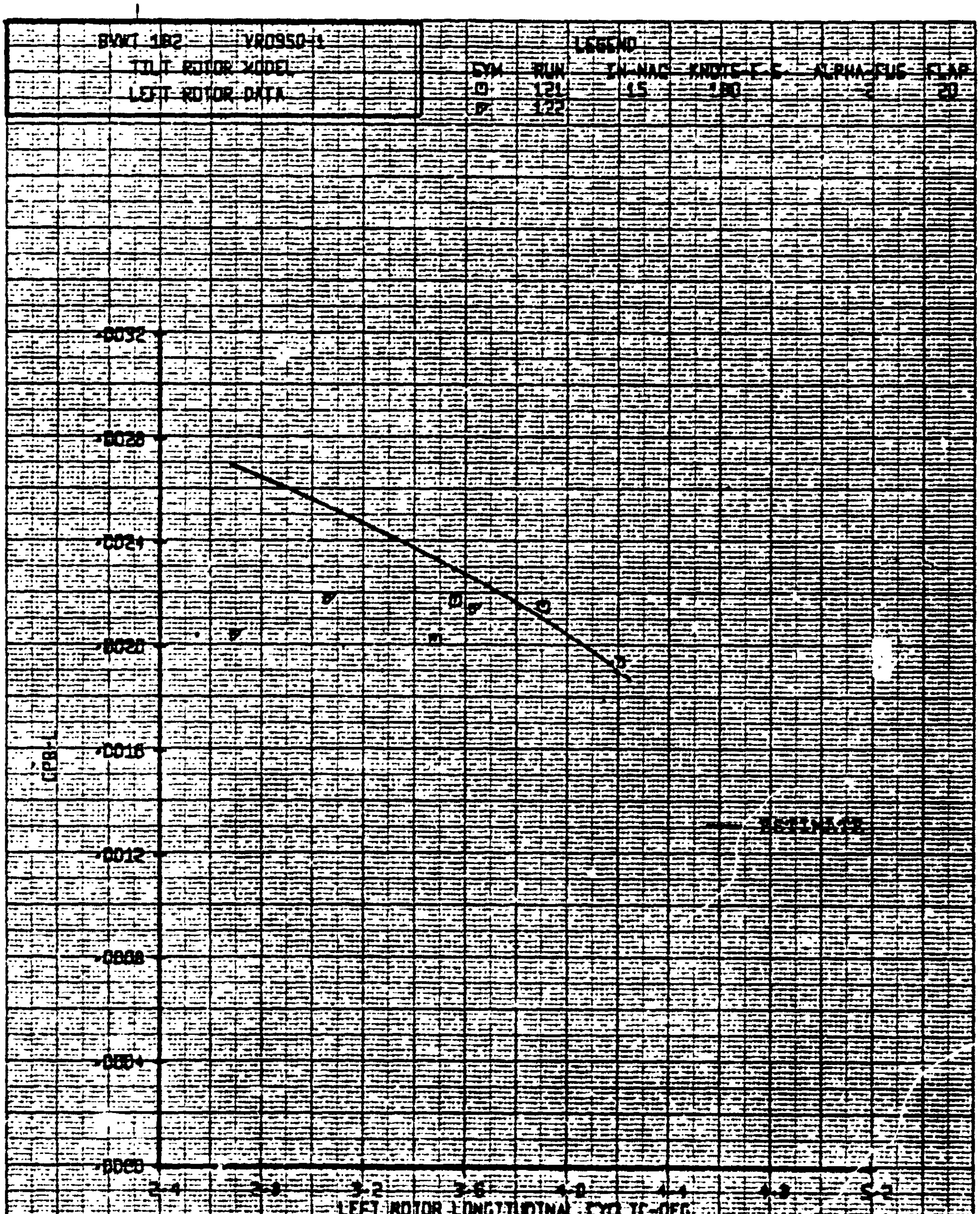

Figure 3.108. Left Rotor Power Coefficient Versus Left Rotor Long. Cyclic ~ Degrees. $I_N = 15°$. Full Scale Airspeed 180 Knots.

BD 182

SET BD BVWT 182

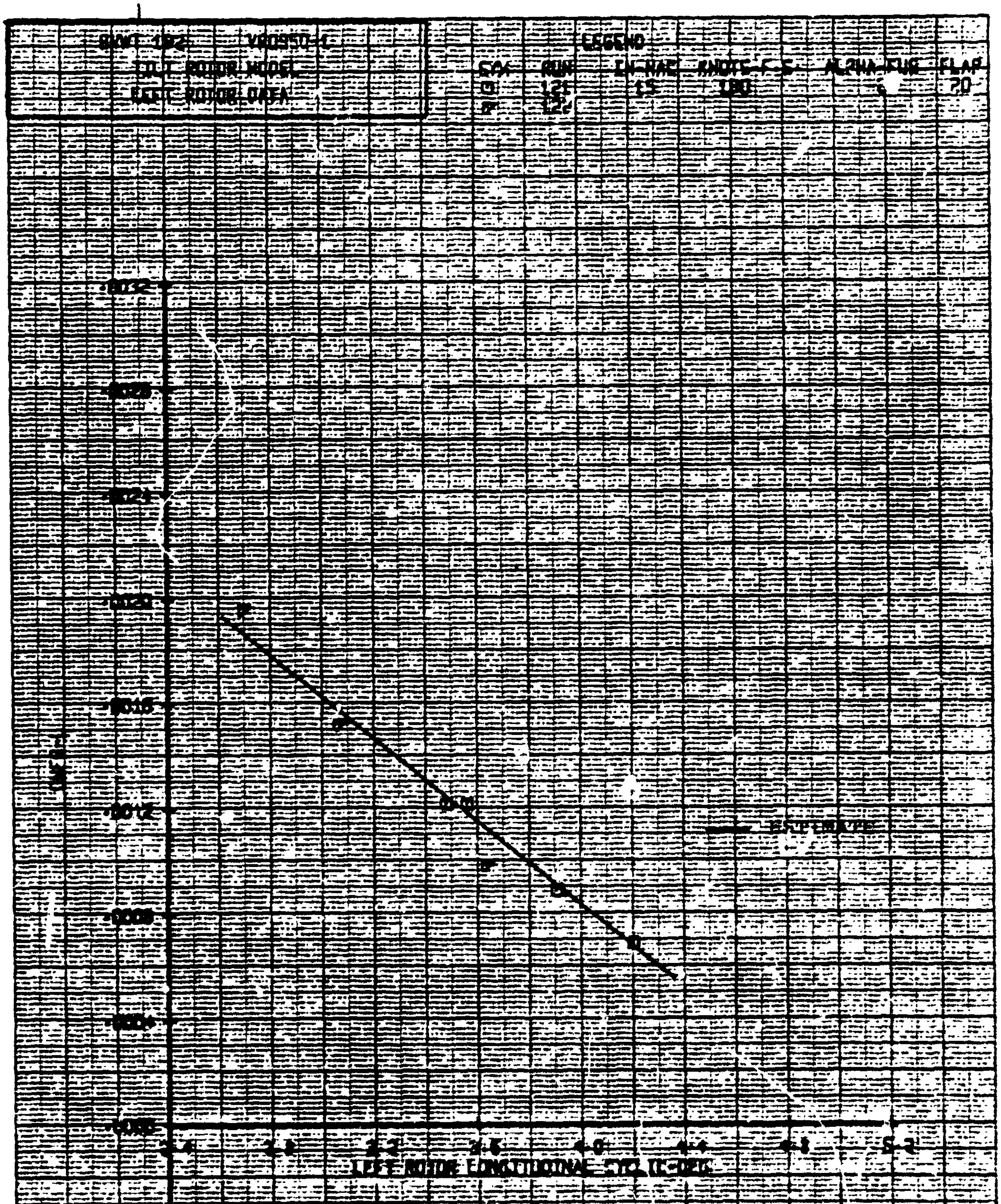

Figure 3.109. Left Rotor Normal Force Coefficient Versus Left Rotor Long. Cyclic – Degrees. $I_N = 15°$. Full Scale Airspeed 180 Knots.

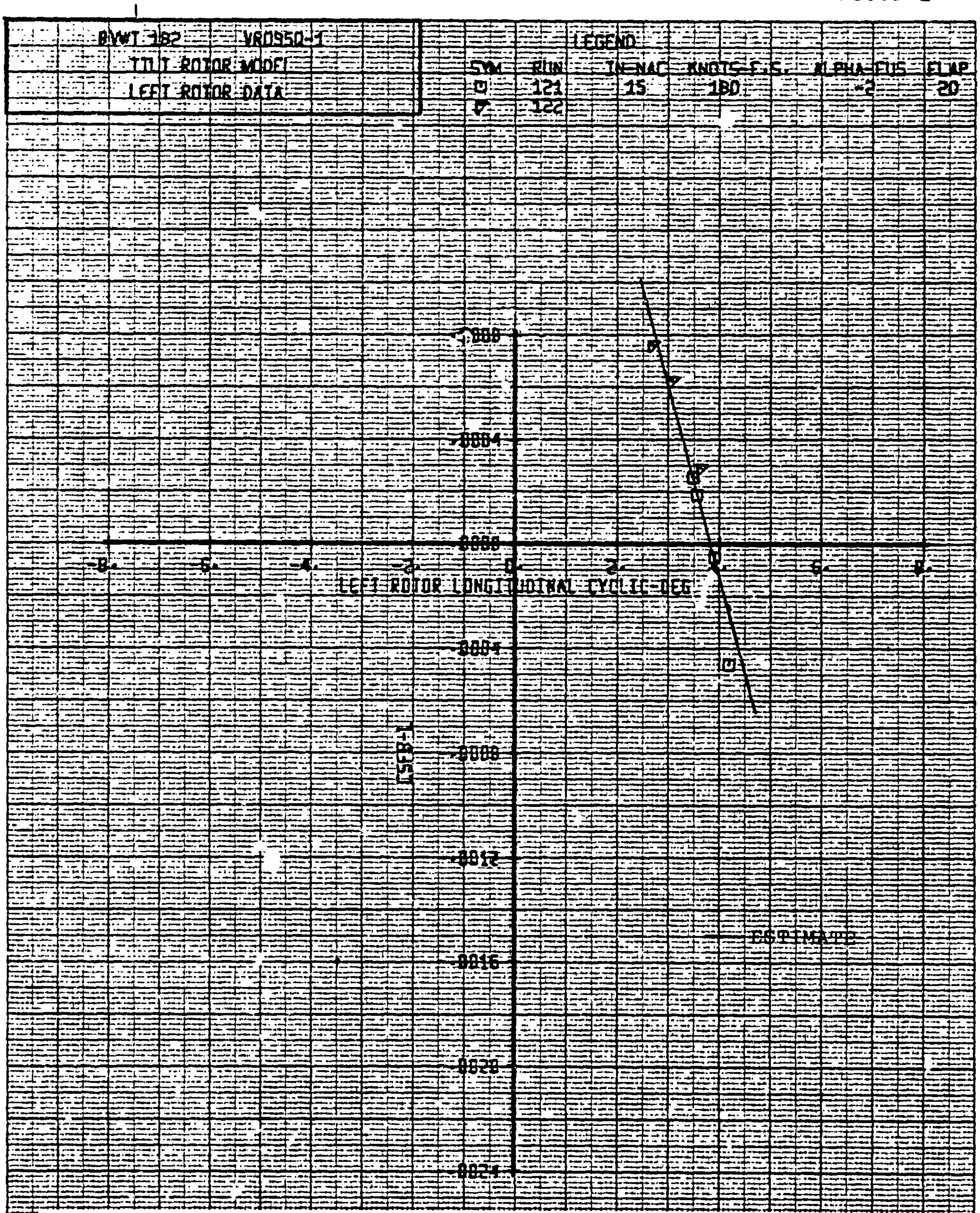

Figure 3.110. Left Rotor Side Force Coefficient Versus Left Rotor Long. Cyclic ~ Degrees. $I_N = 15°$. Full Scale Airspeed 180 Knots.

BD 182

SET BD BVWT 182

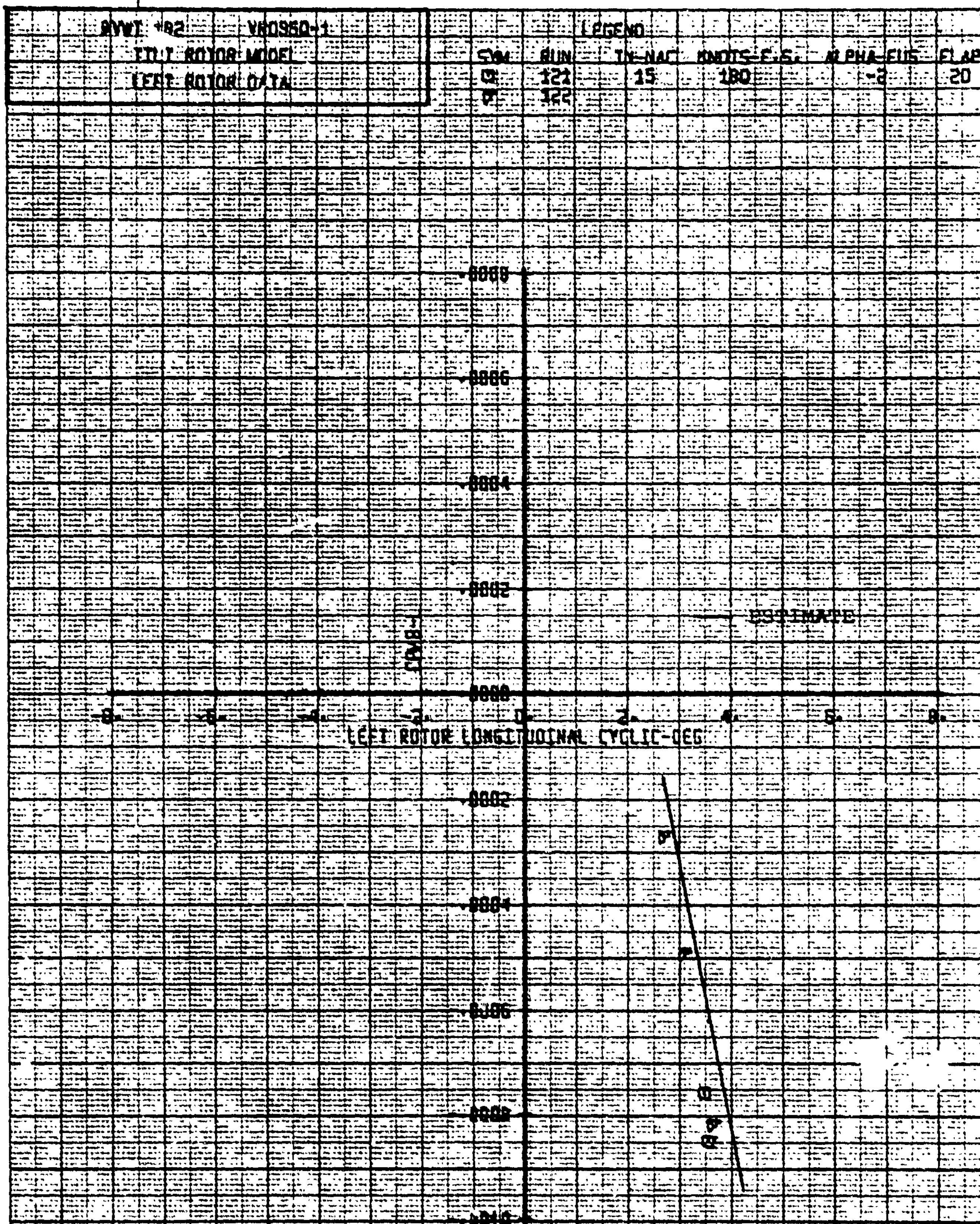

Figure 3.111. Left Rotor Pitching Moment Versus Left Rotor Long. Cyclic ~ Degrees. I_N = 15°. Full Scale Airspeed 180 Knots.

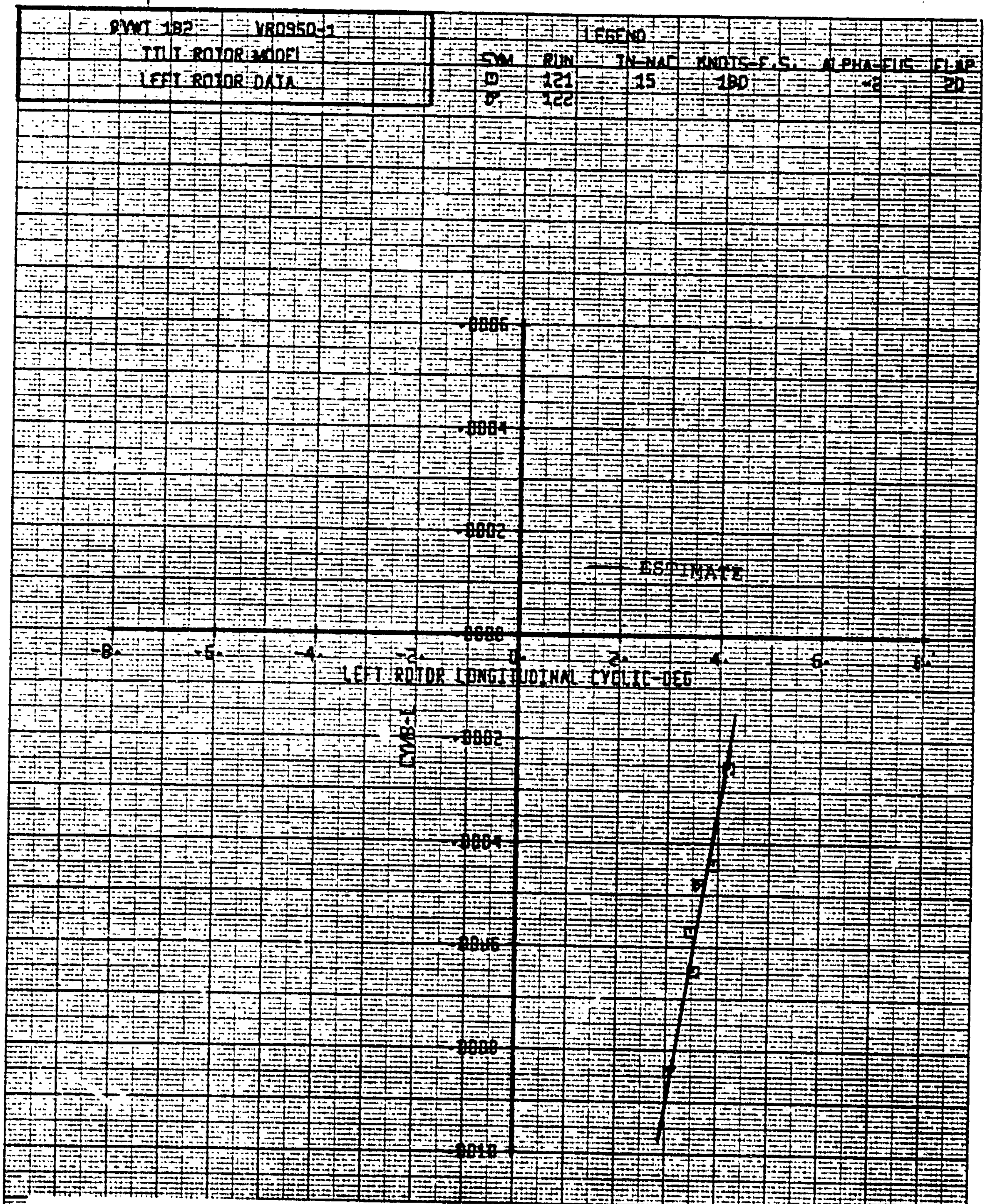

Figure 3.112. Left Rotor Yawing Moment Versus Left Rotor Long. Cyclic ~ Degrees. $I_N = 15°$. Full Scale Airspeed 180 Knots.

80
182

SET 80
BVWT 182

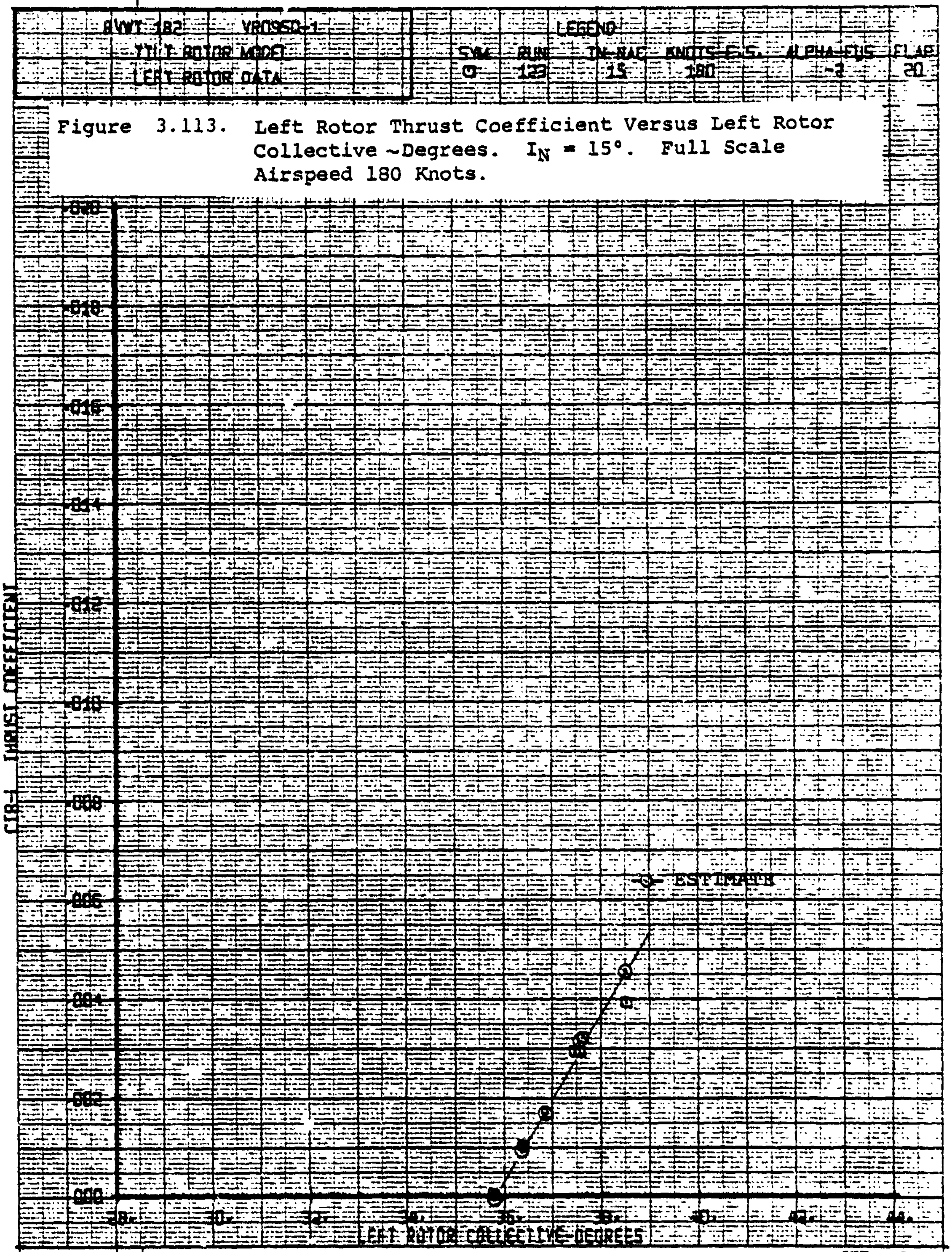

Figure 3.113. Left Rotor Thrust Coefficient Versus Left Rotor Collective ~Degrees. $I_N = 15°$. Full Scale Airspeed 180 Knots.

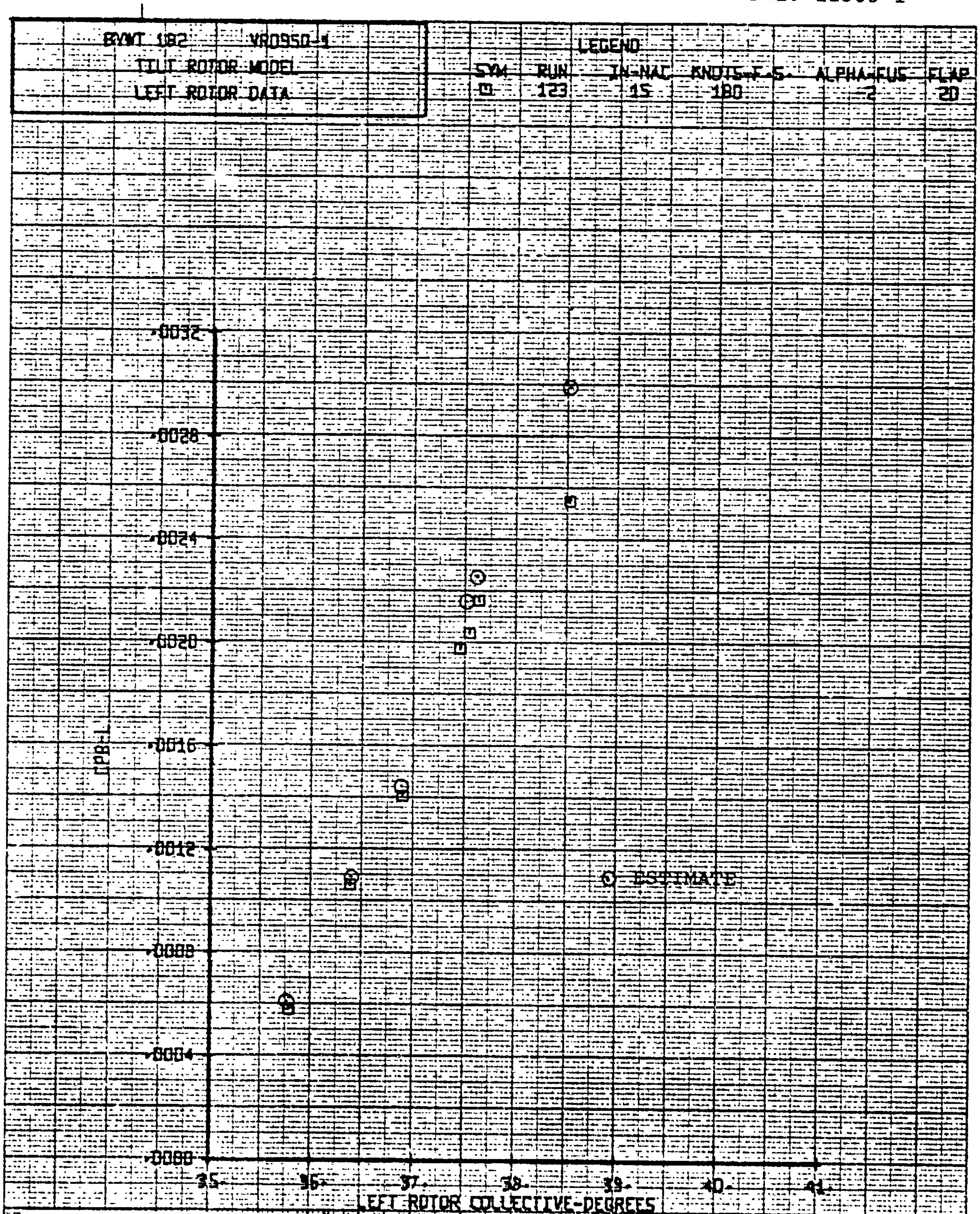

Figure 3.114. Left Rotor Power Coefficient Versus Left Rotor Collective ~ Degrees. $I_N = 15°$. Full Scale Airspeed 180 Knots.

81
182

SET 81
BVWT 182

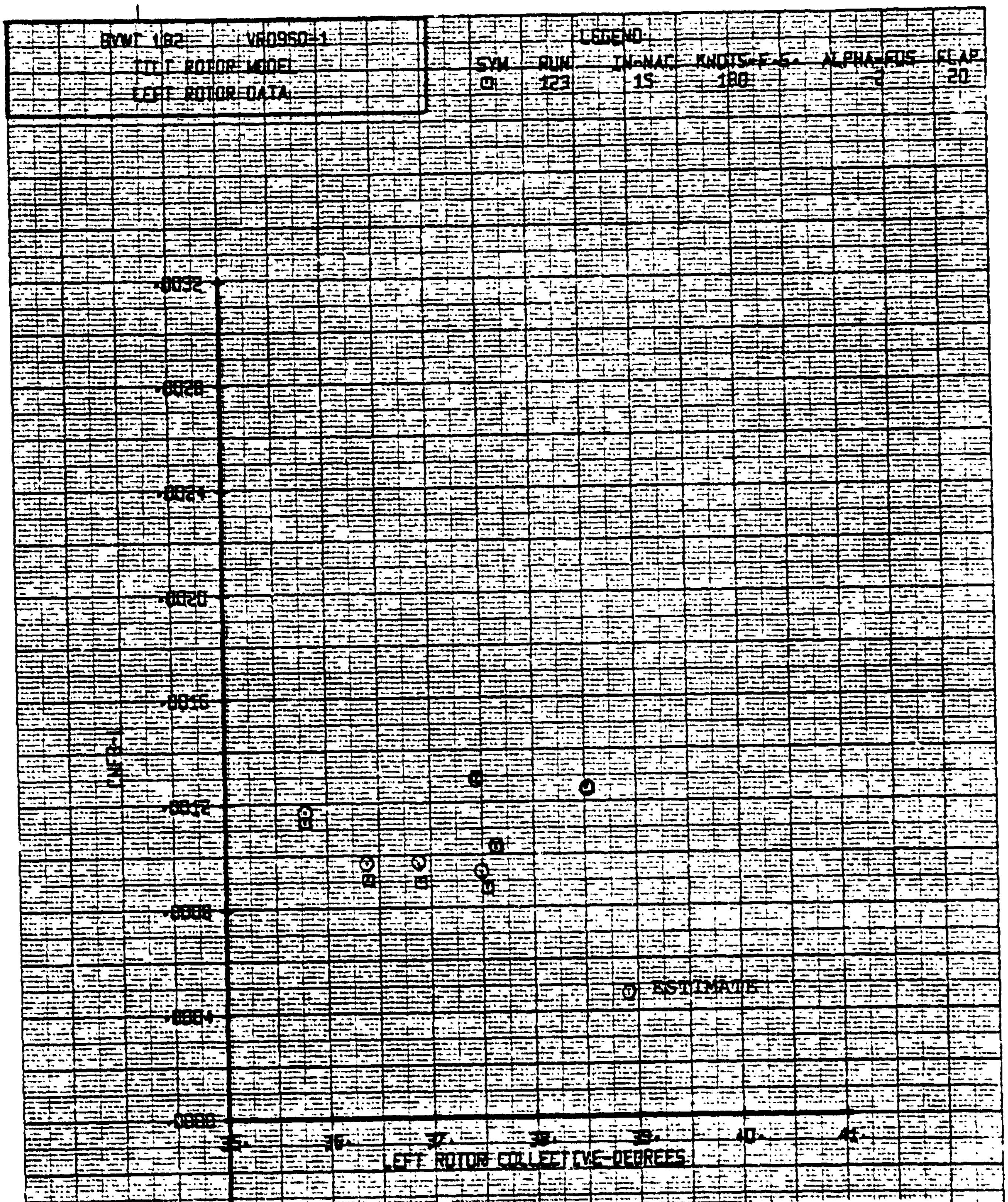

Figure 3.115. Left Rotor Normal Force Coefficient Versus Left Rotor Collective ~ Degrees. $I_N = 15°$. Full Scale Airspeed 180 Knots.

81 182

SET 81 BVWT 182

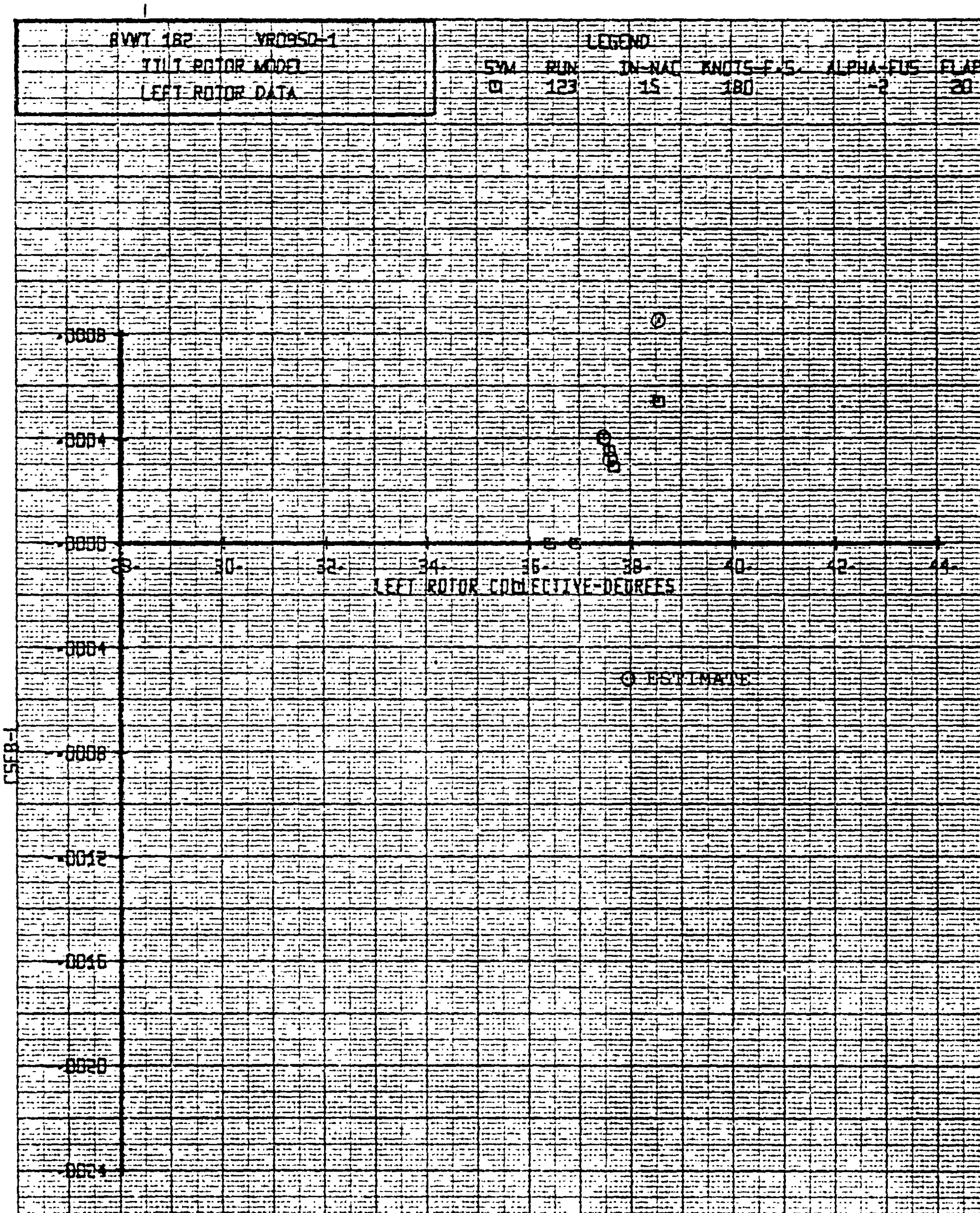

Figure 3.116. Left Rotor Side Force Coefficient Versus Left Rotor Collective ~ Degrees. $I_N = 15°$. Full Scale Airspeed 180 Knots.

81
182

SET 81
BVWT 182

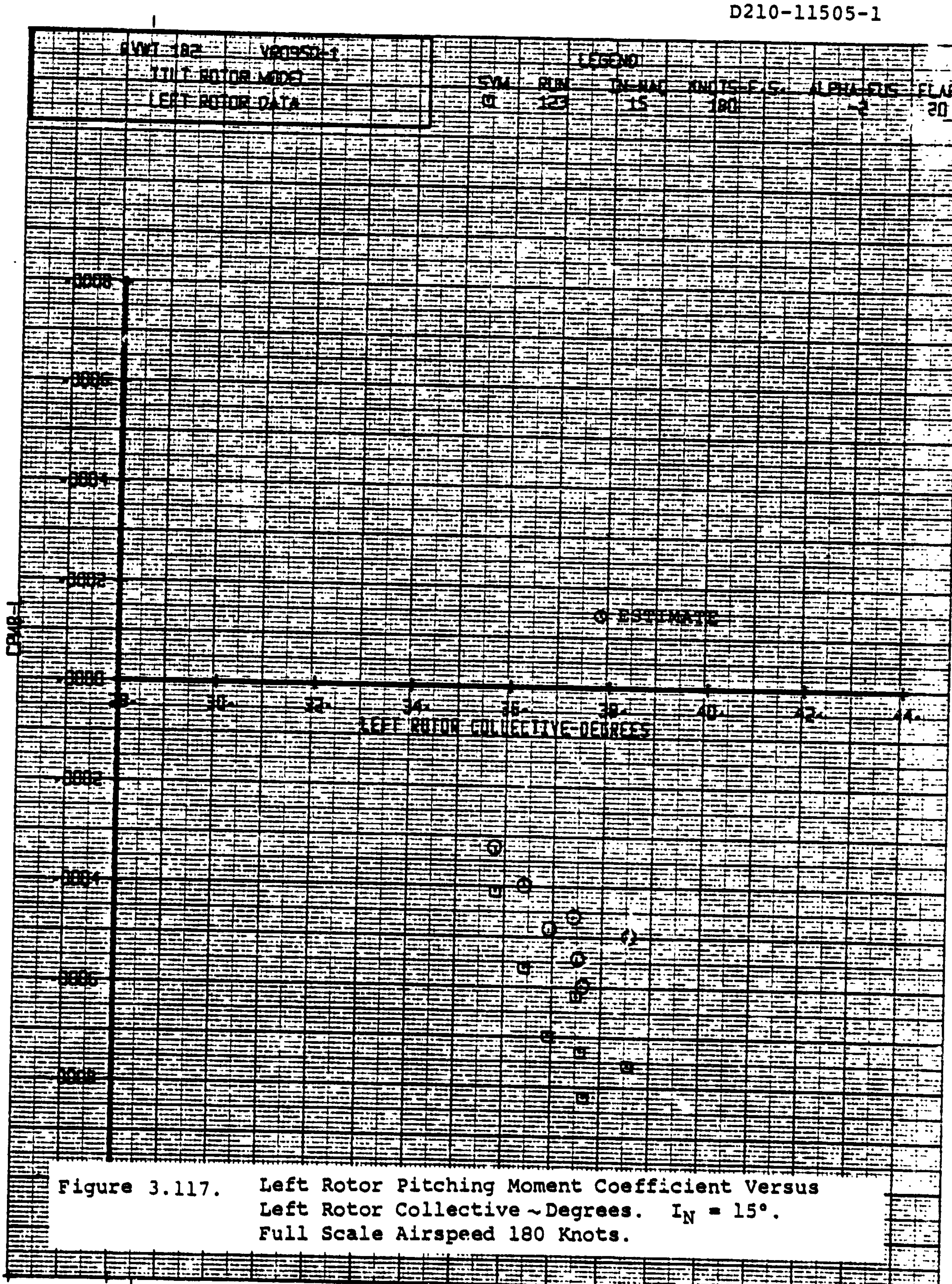

Figure 3.117. Left Rotor Pitching Moment Coefficient Versus Left Rotor Collective ~ Degrees. $I_N = 15°$. Full Scale Airspeed 180 Knots.

81
182

SET 81
RVWT 182

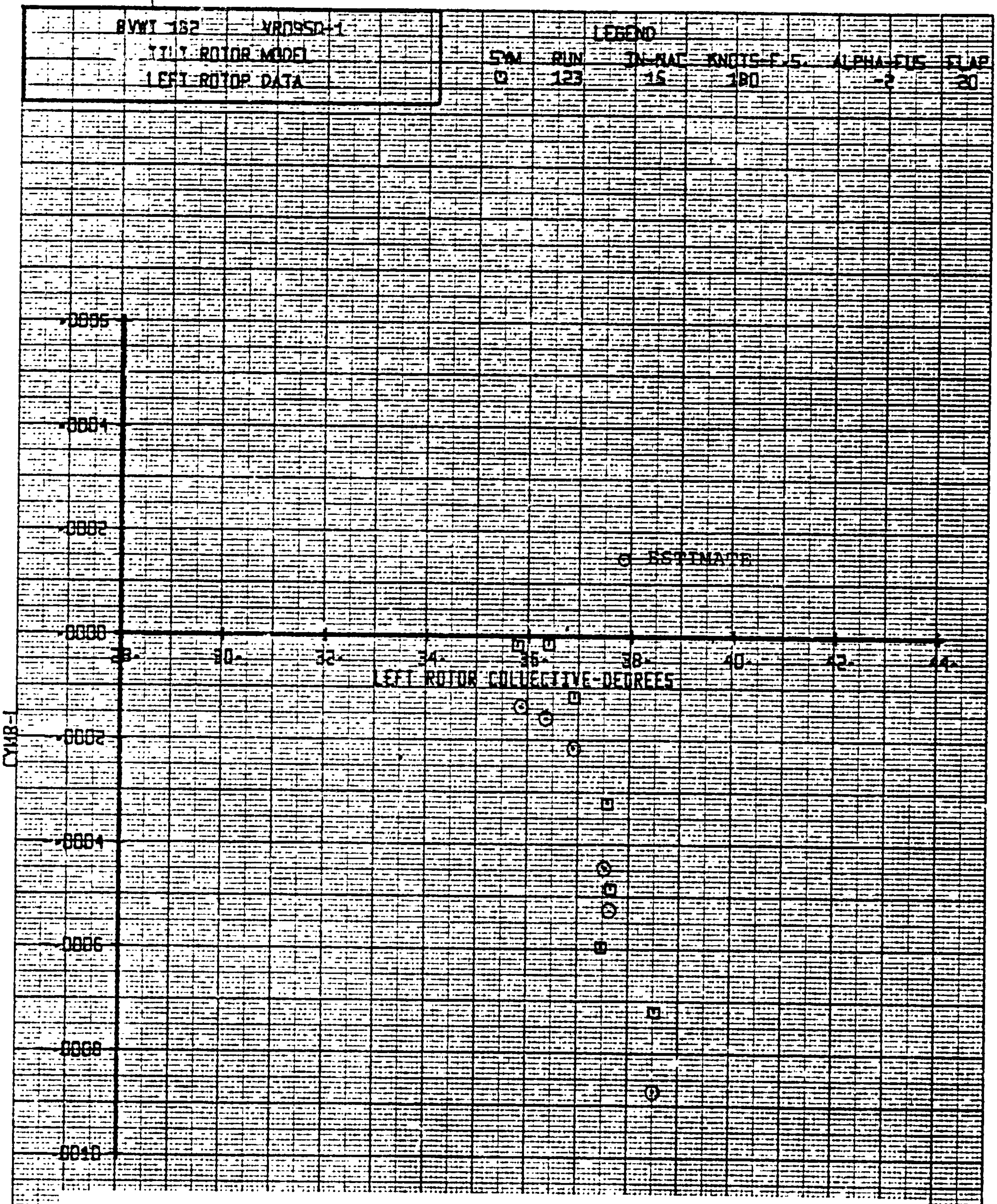

Figure 3.118. Left Rotor Yawing Moment Coefficient Versus Left Rotor Collective ~ Degrees. $I_N = 15°$. Full Scale Airspeed 180 Knots.

B1 182

SET BVWT B1 182

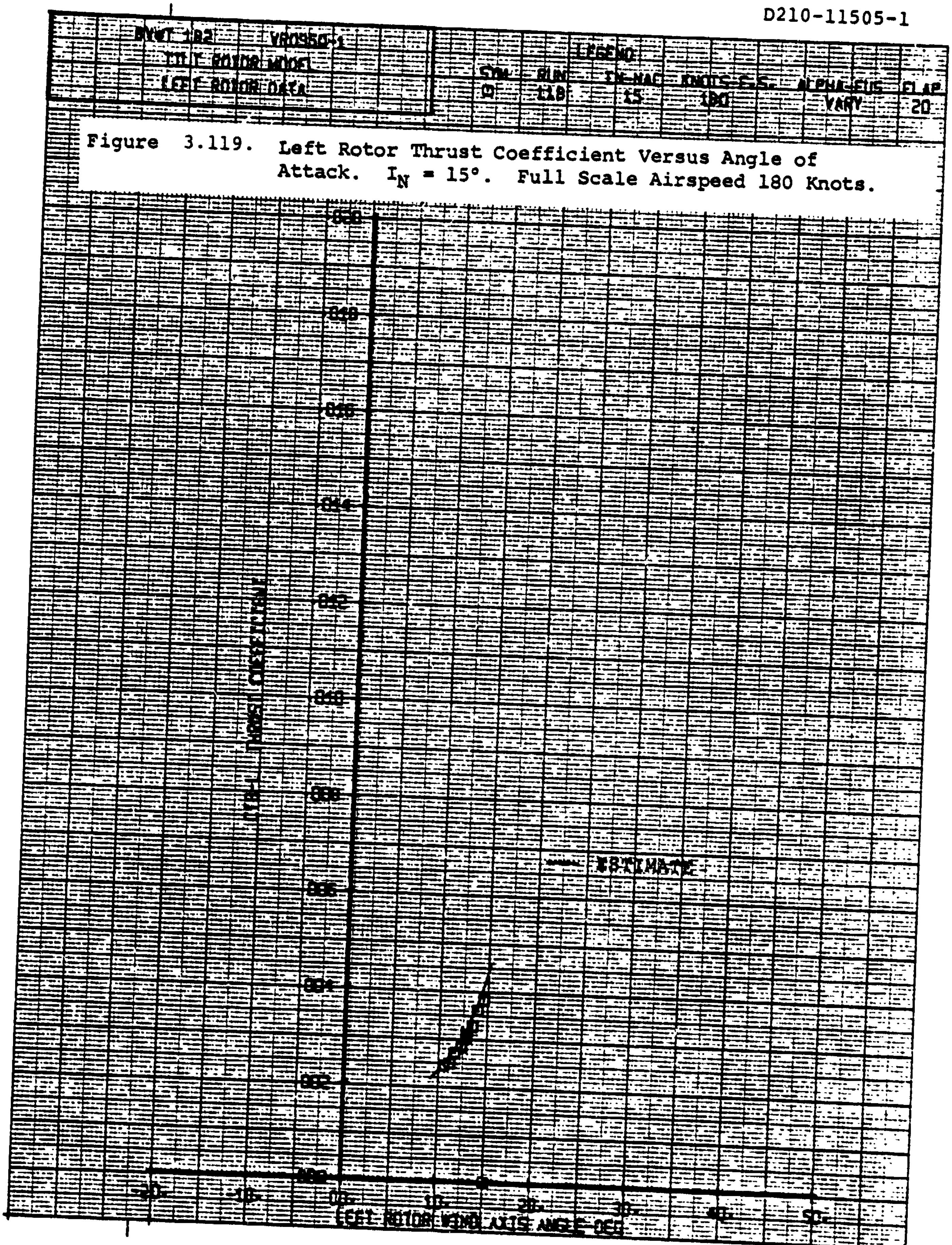

Figure 3.119. Left Rotor Thrust Coefficient Versus Angle of Attack. $I_N = 15°$. Full Scale Airspeed 180 Knots.

77
182

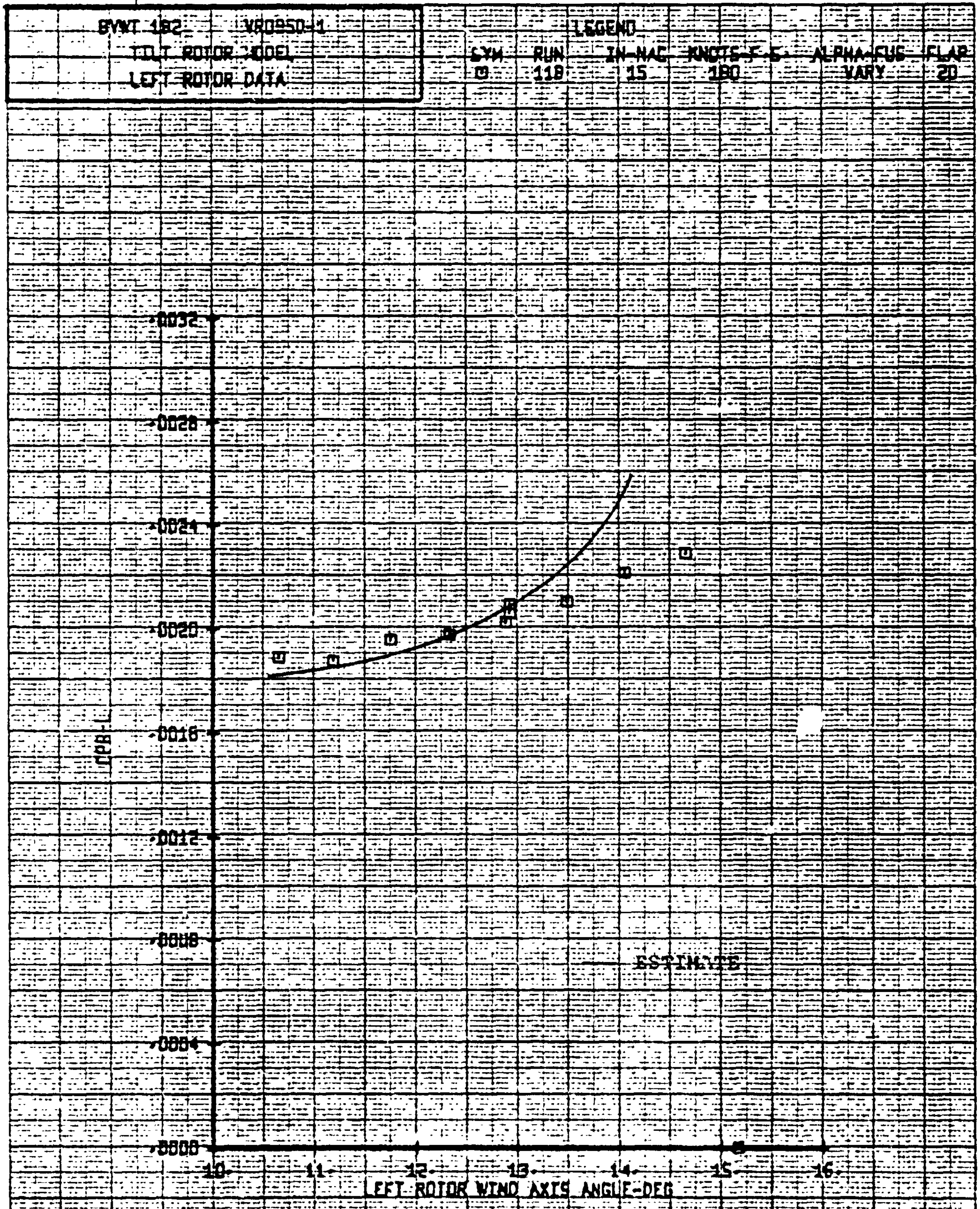

Figure 3.120. Left Rotor Power Coefficient Versus Angle of Attack. $I_N = 15°$. Full Scale Airspeed 180 Knots.

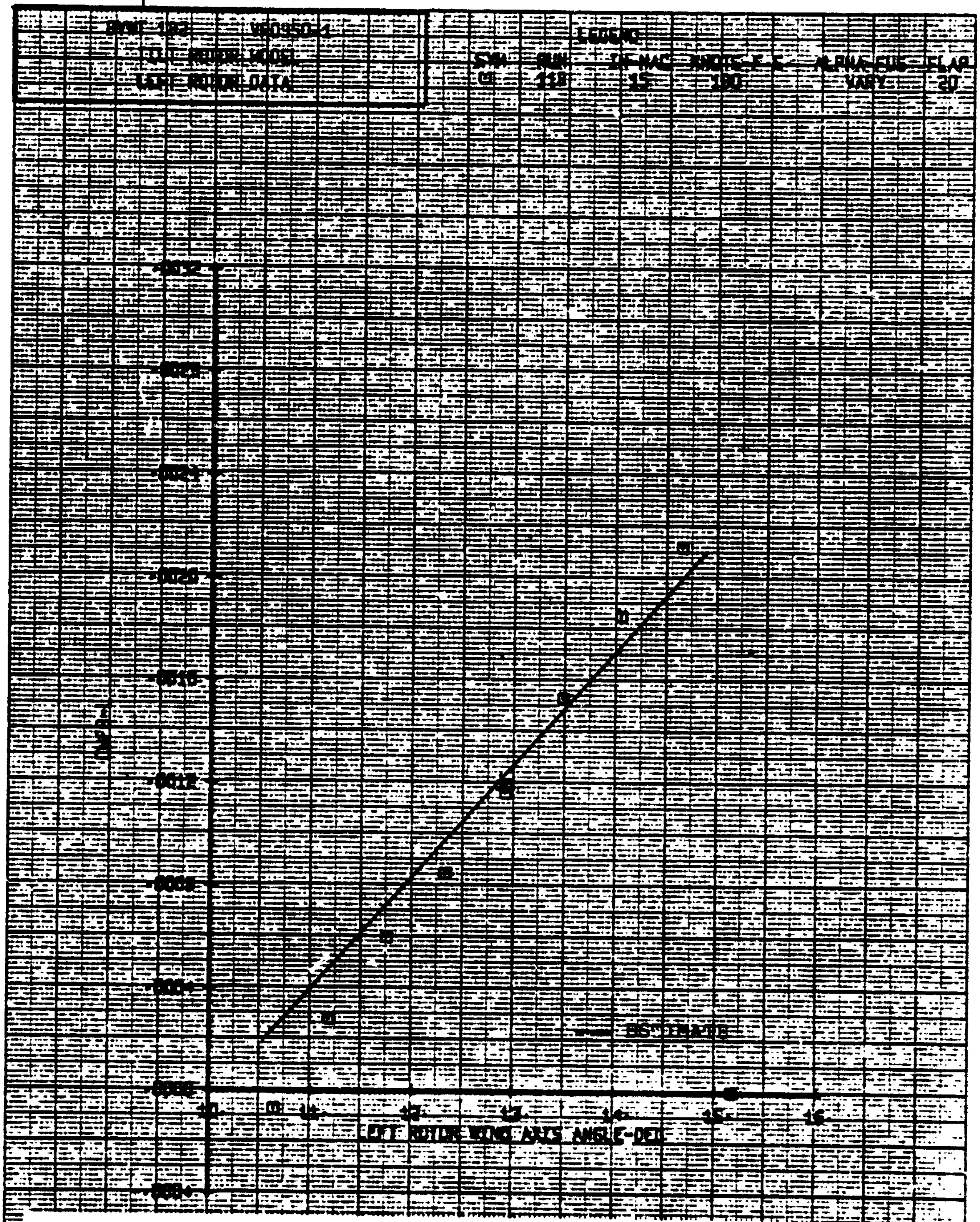

Figure 3.121. Left Rotor Normal Force Coefficient Versus Angle of Attack. $I_N = 15°$. Full Scale Airspeed 180 Knots.

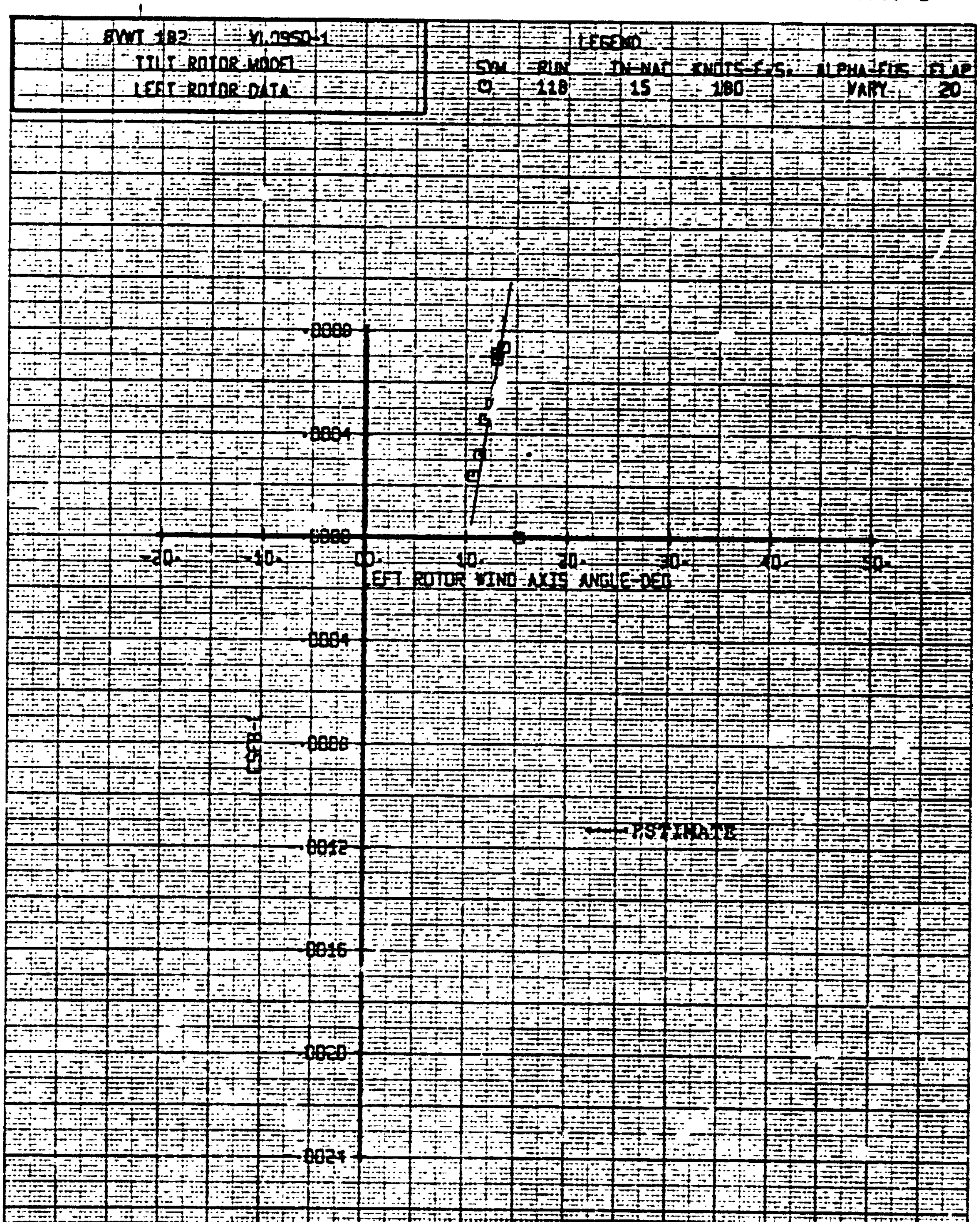

Figure 3.122. Left Rotor Side Force Coefficient Versus Angle of Attack. $I_N = 15°$. Full Scale Airspeed 180 Knots.

77
182

SET 77
BVWT 182

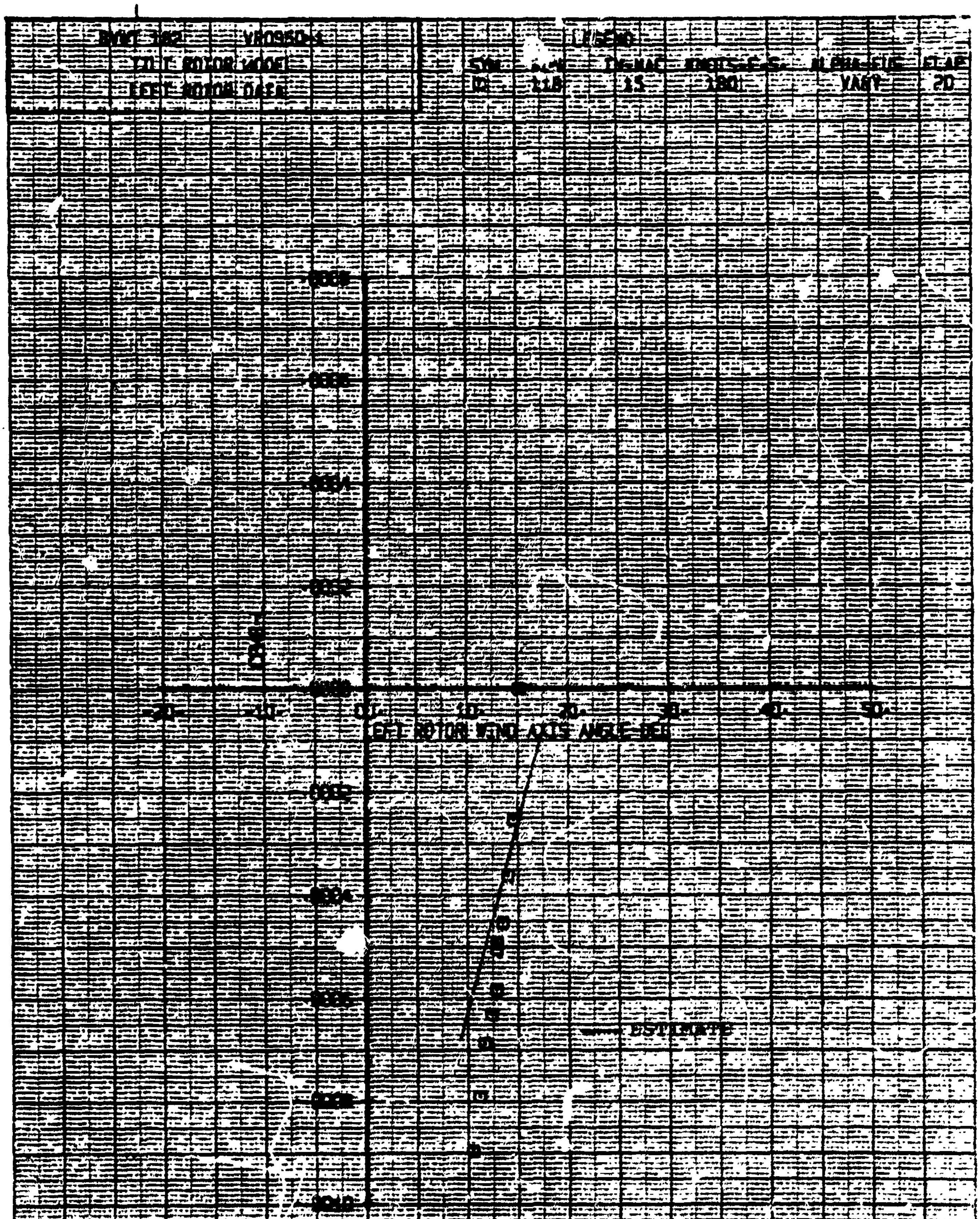

Figure 3.123. Left Rotor Pitching Moment Versus Angle of Attack. i_N = 15°. Full Scale Airspeed 180 Knots.

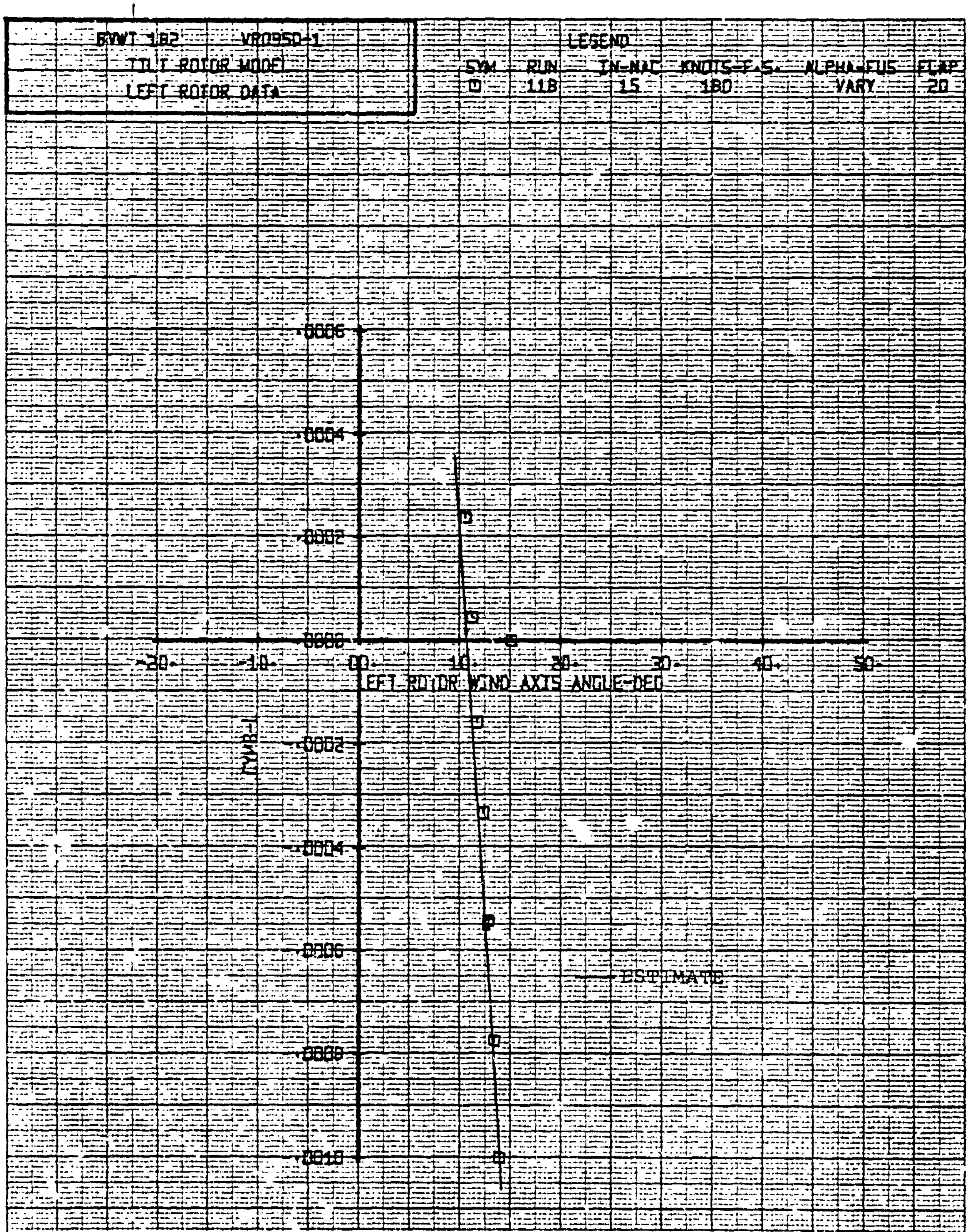

Figure 3.124. Left Rotor Yawing Moment Versus Angle of Attack. $I_N = 15°$. Full Scale Airspeed 180 Knots.

77
182

SET 77
BVWT 182

BVWT 182 VR0950-1
TILT ROTOR MODEL
LEFT ROTOR DATA

SYM	RUN	IN-NAC	KNOTS-F.S.	ALPHA-FUS	FLAP
⊡	119	15	180	-2	20

Figure 3.125. Left Rotor Thrust Coefficient Versus Yaw Angle–Degrees. $I_N = 15°$. Full Scale Airspeed 180 Knots.

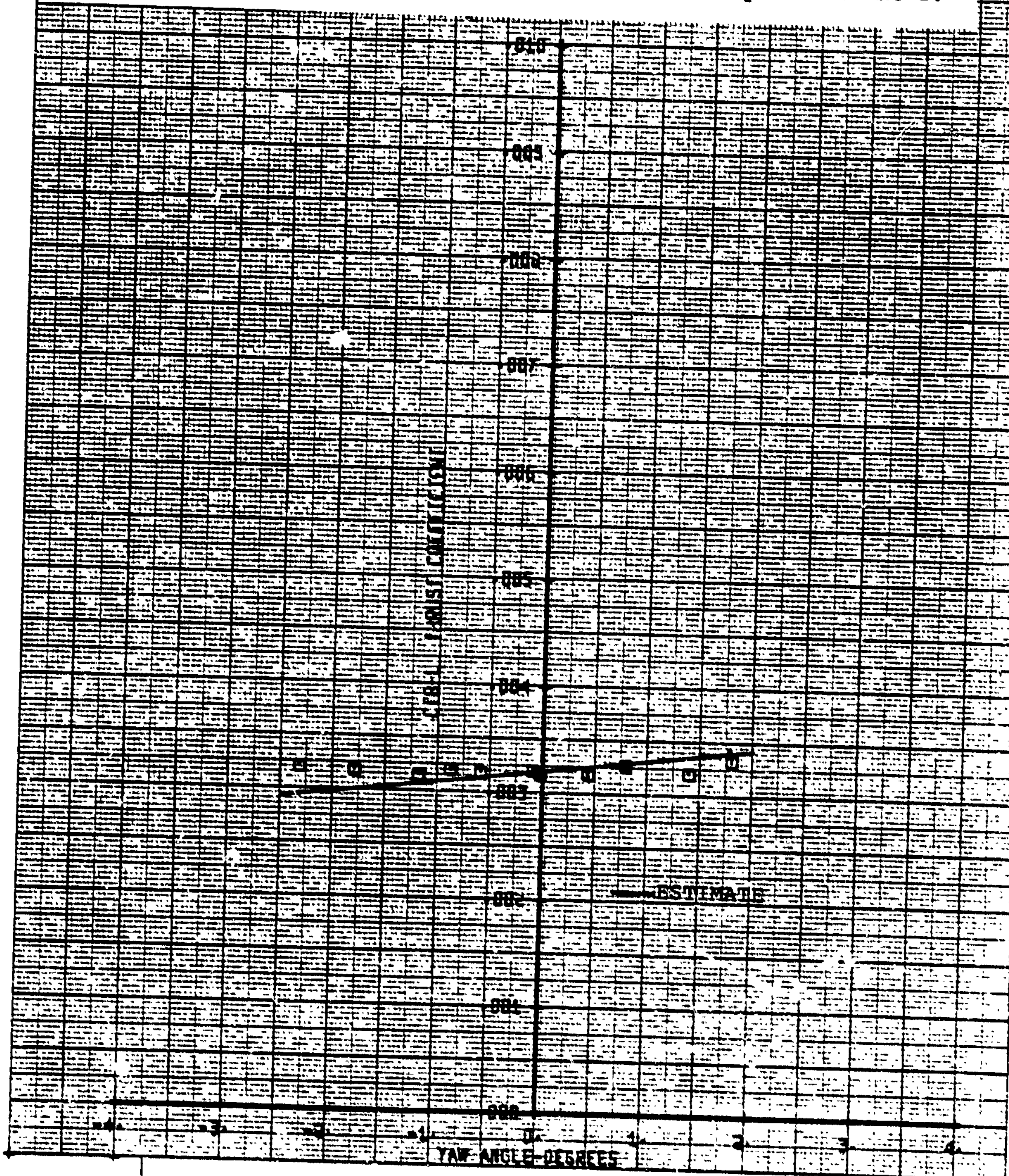

79
182

SET 79
BVWT 182

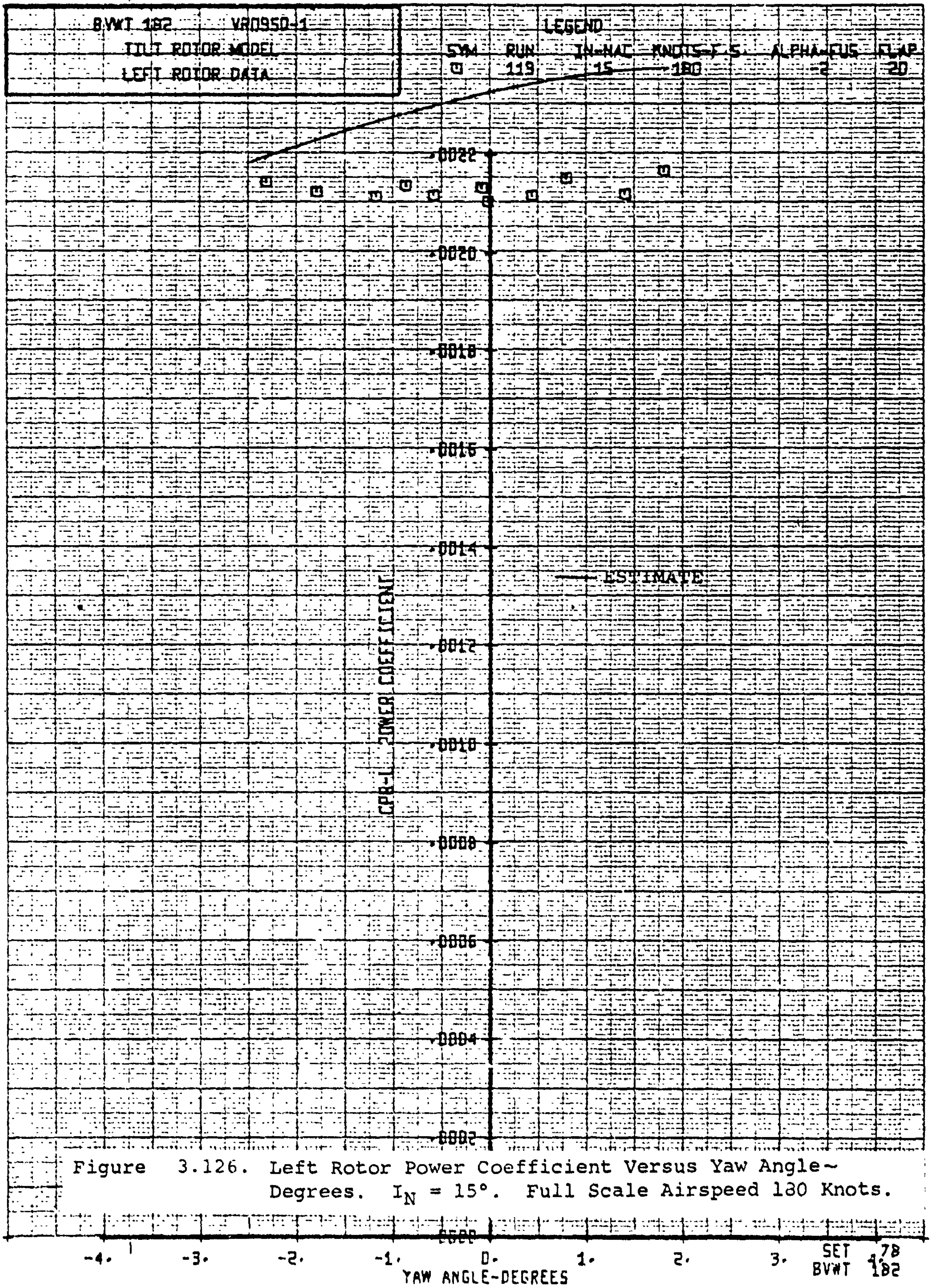

Figure 3.126. Left Rotor Power Coefficient Versus Yaw Angle ~ Degrees. $I_N = 15°$. Full Scale Airspeed 180 Knots.

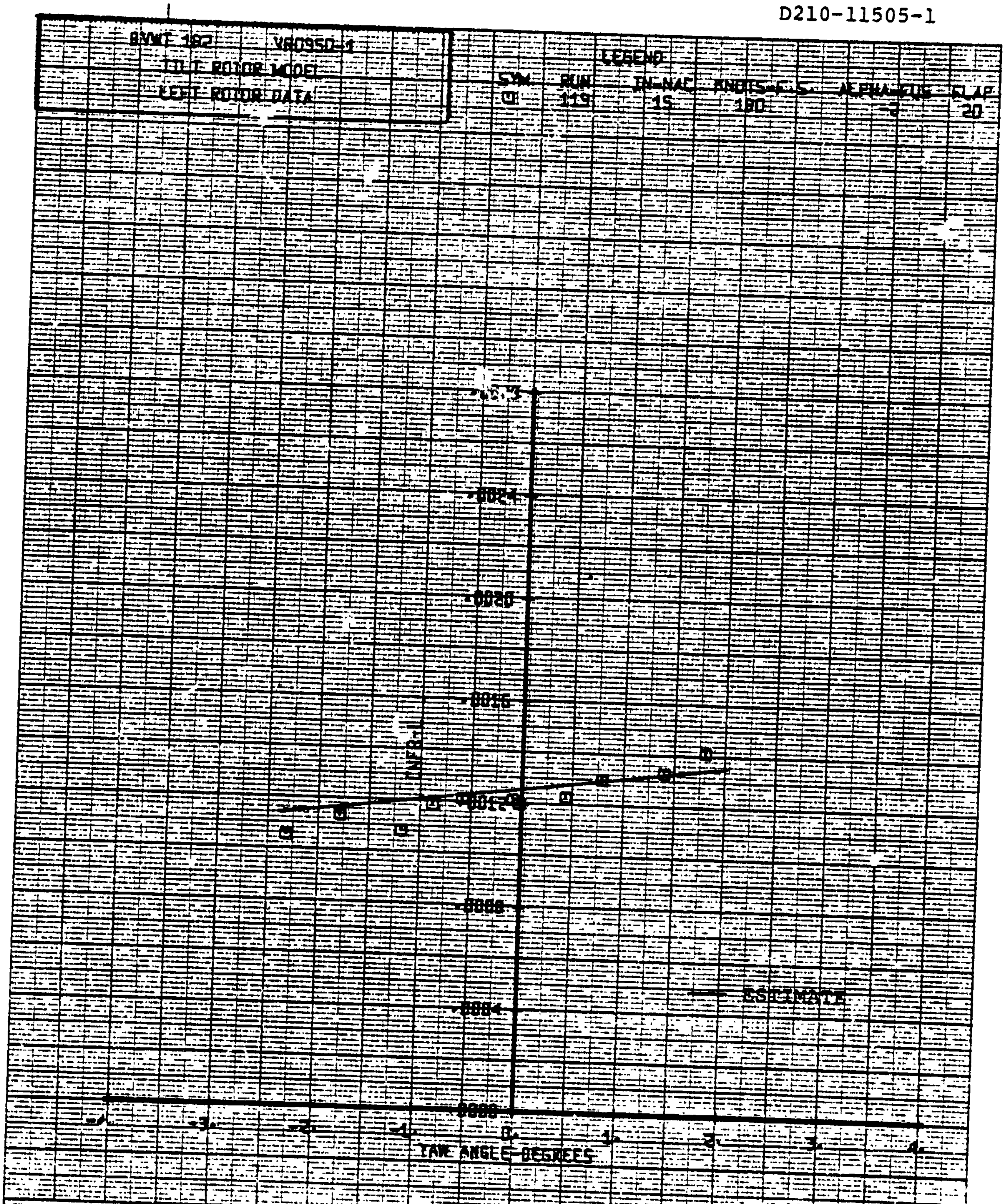

Figure 3.127. Left Rotor Normal Force Coefficient Versus Yaw Angle ~ Degrees. $I_N = 15°$. Full Scale Airspeed 180 Knots.

7B
182

SET 7D
BVWT 182

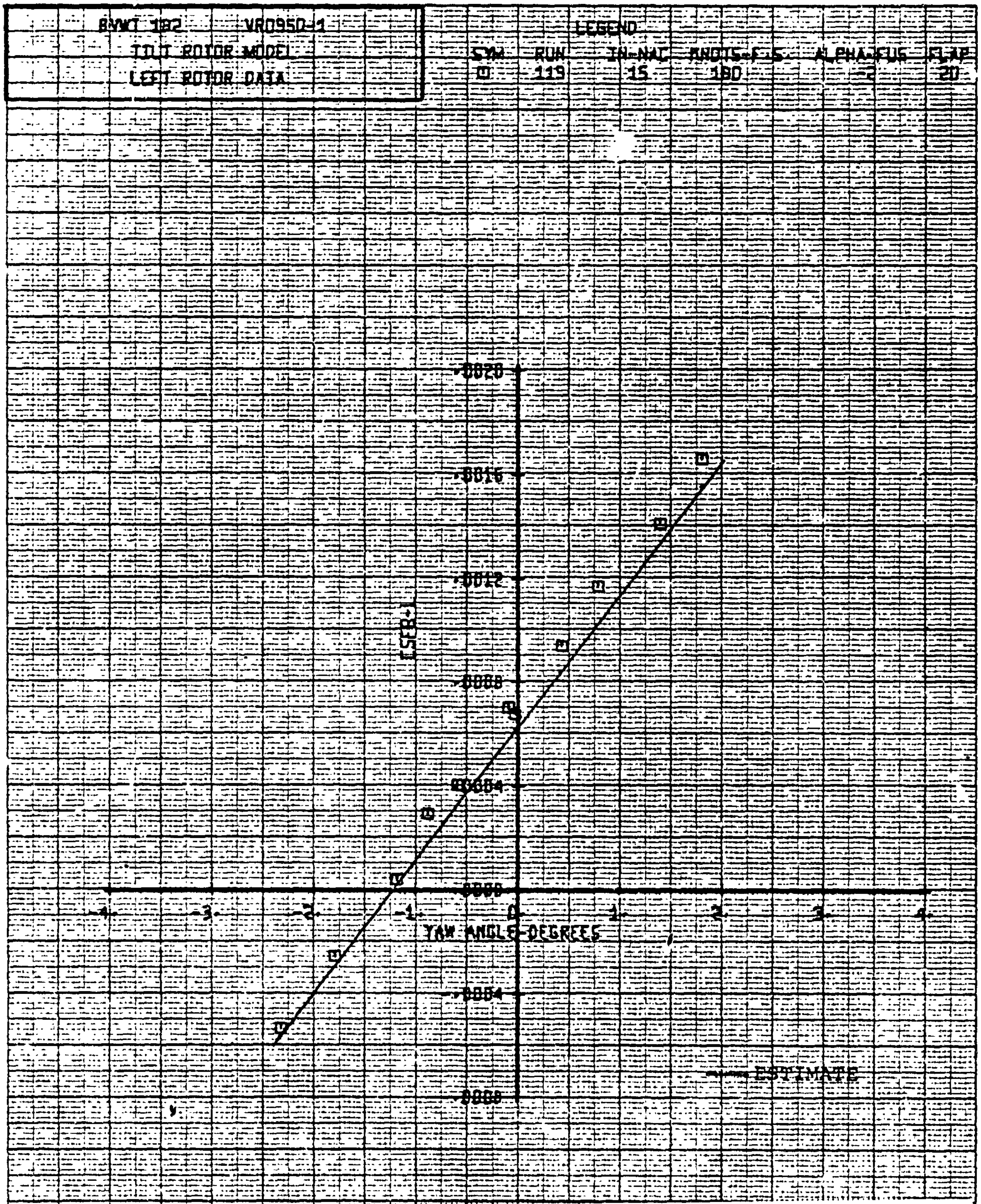

Figure 3.128. Left Rotor Side Force Coefficient Versus Yaw Angle~ Degrees. $I_N = 15°$. Full Scale Airspeed 180 Knots.

78 182

SET 78 BVWT 182

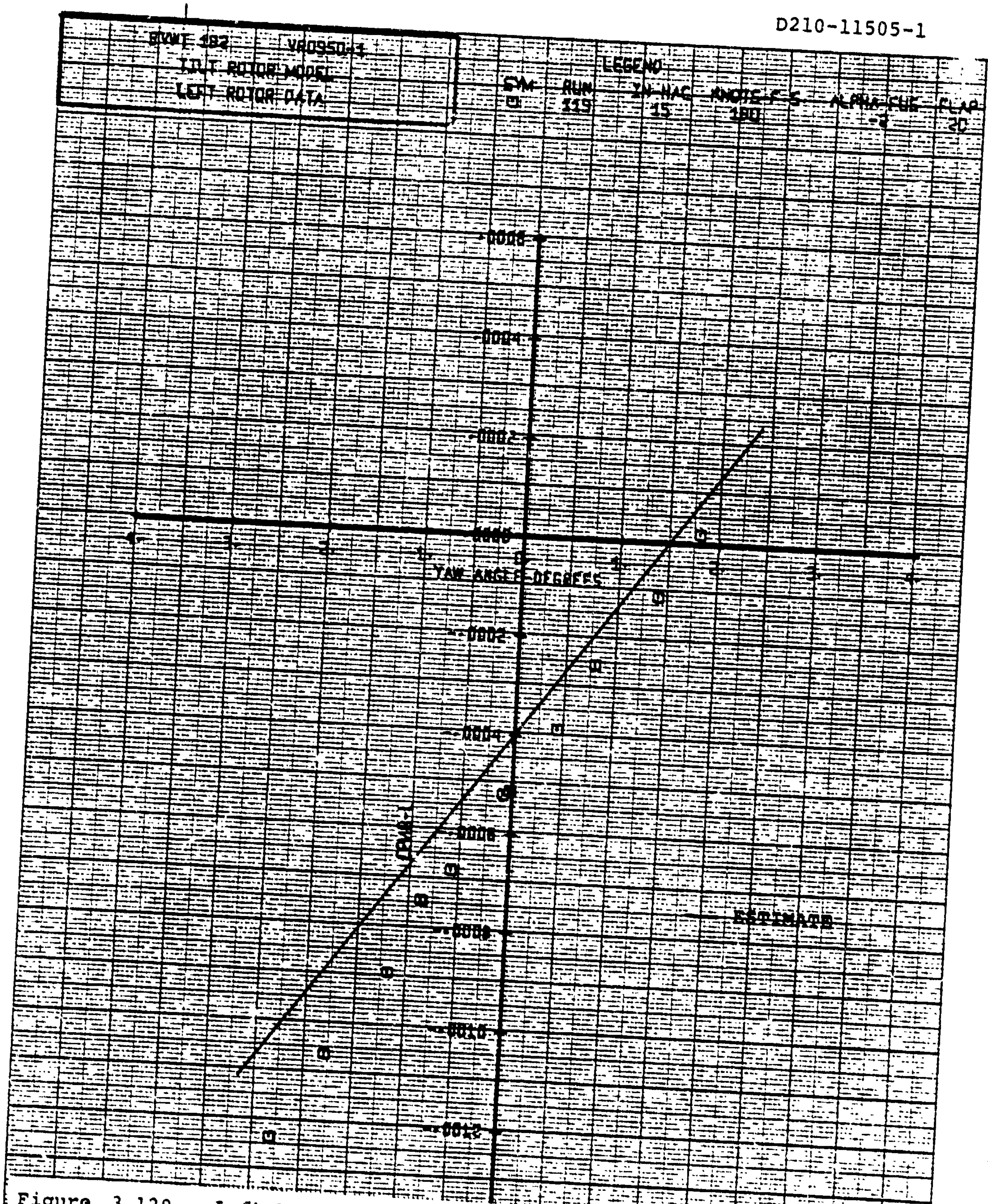

Figure 3.129. Left Rotor Pitching Moment Versus Yaw Angle~ Degrees. $I_N = 15°$. Full Scale Airspeed 180 Knots.

SET 79
BVWT 182

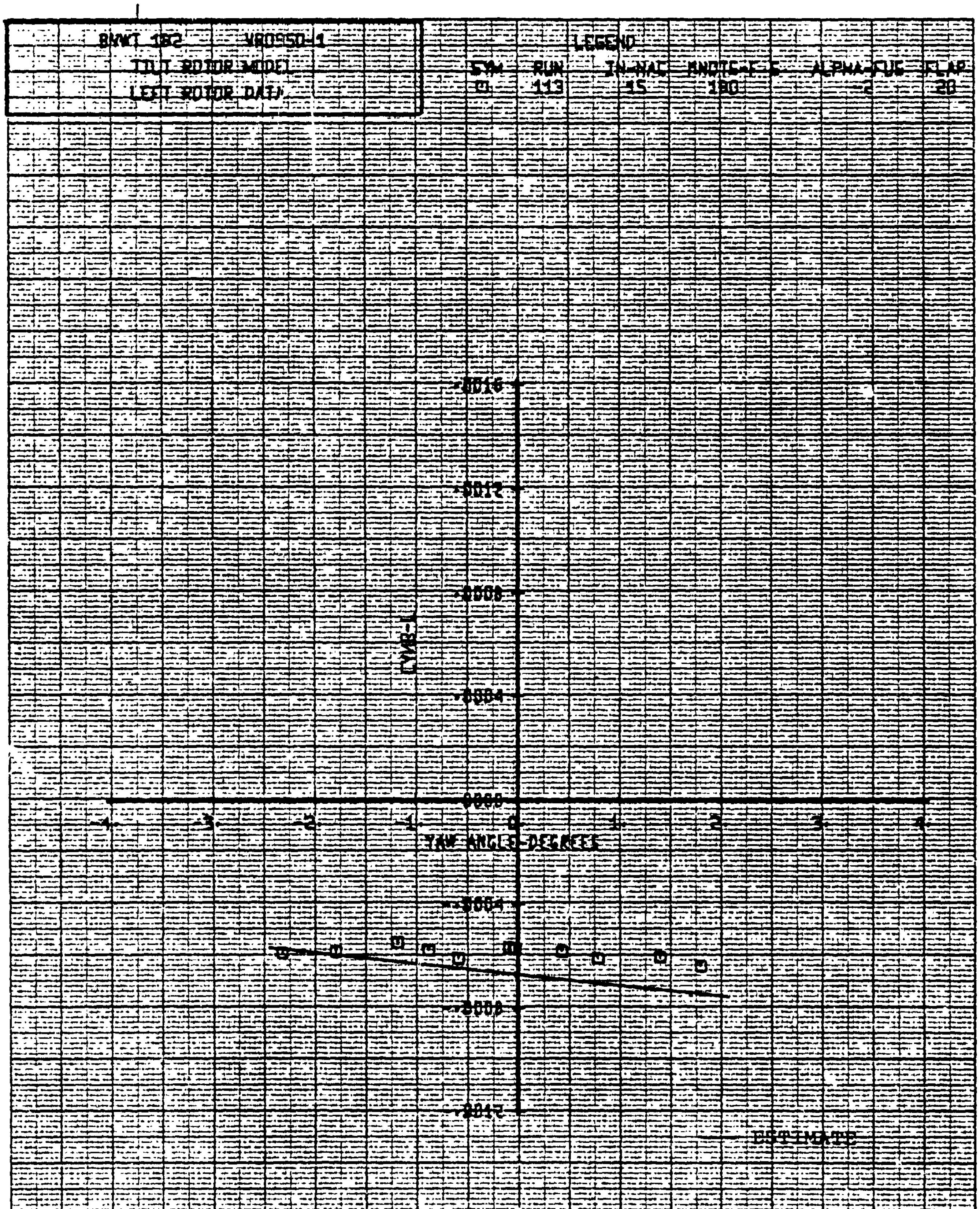

Figure 3.130 Left Rotor Yawing Moment Versus Yaw Angle ~ Degrees. $I_N = 15°$. Full Scale Airspeed 180 Knots.

78 182

SET 78 BVWT 182

Figure 3.131. Left Rotor Thrust Coefficient Versus Rotor RPM. $I_N = 15°$. Full Scale Airspeed 180 Knots.

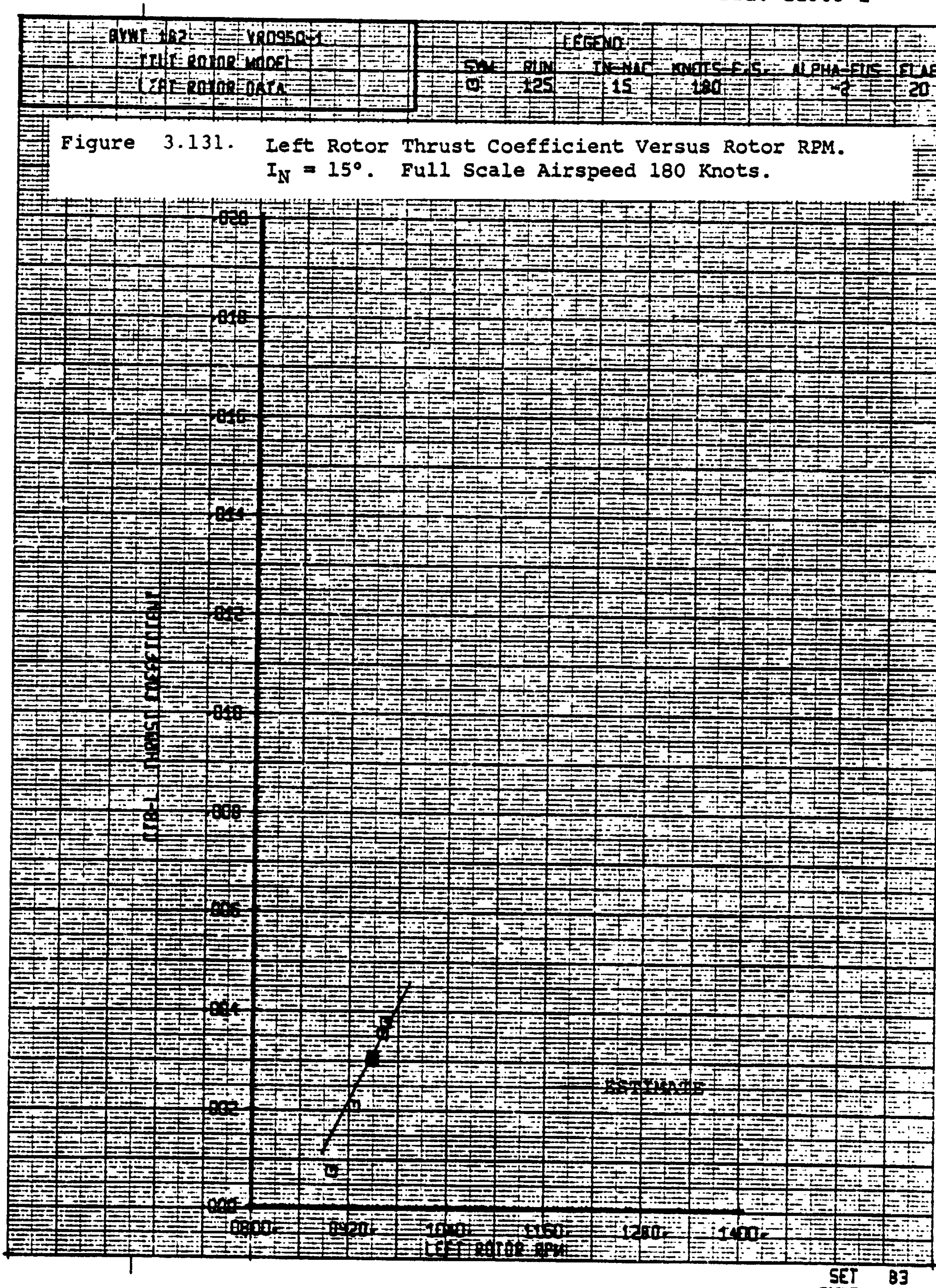

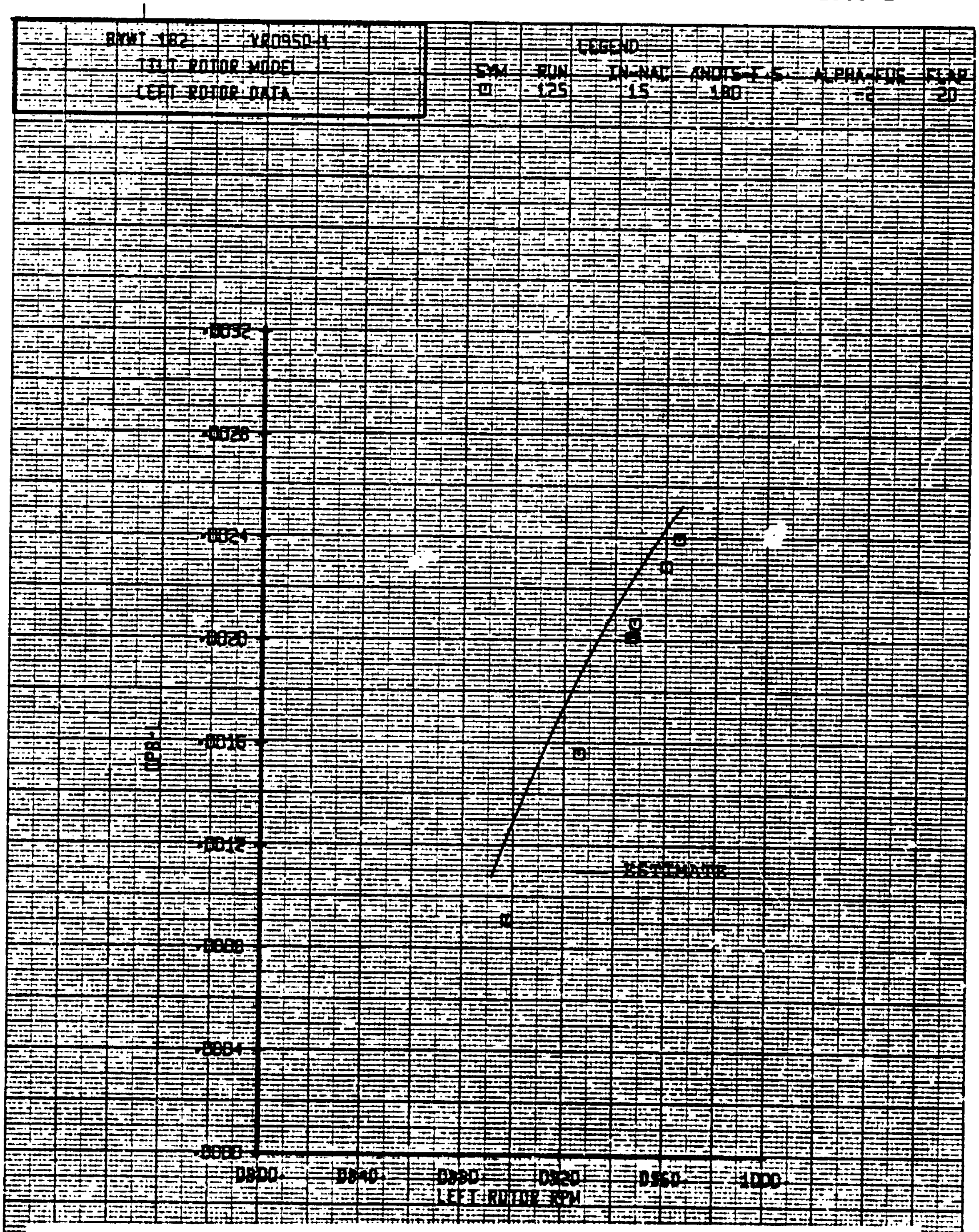

Figure 3.132. Left Rotor Power Coefficient Versus Rotor RPM. $I_N = 15°$. Full Scale Airspeed 180 Knots.

83
182

SET 83
BVWT 182

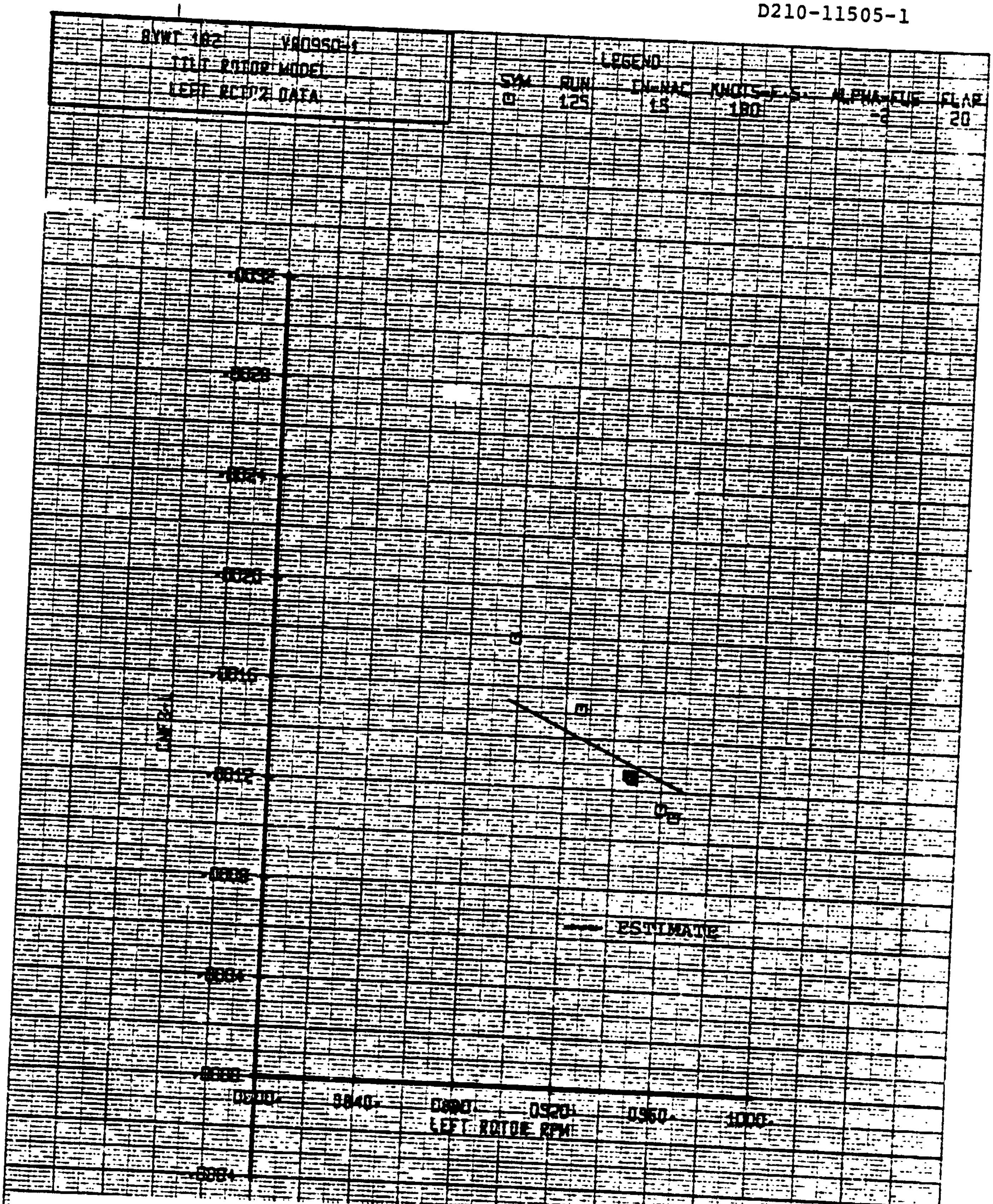

Figure 3.133. Left Rotor Normal Force Coefficient Versus Rotor RPM. $I_N = 15°$. Full Scale Airspeed 180 Knots.

83
182

SET 83
BVWT 182

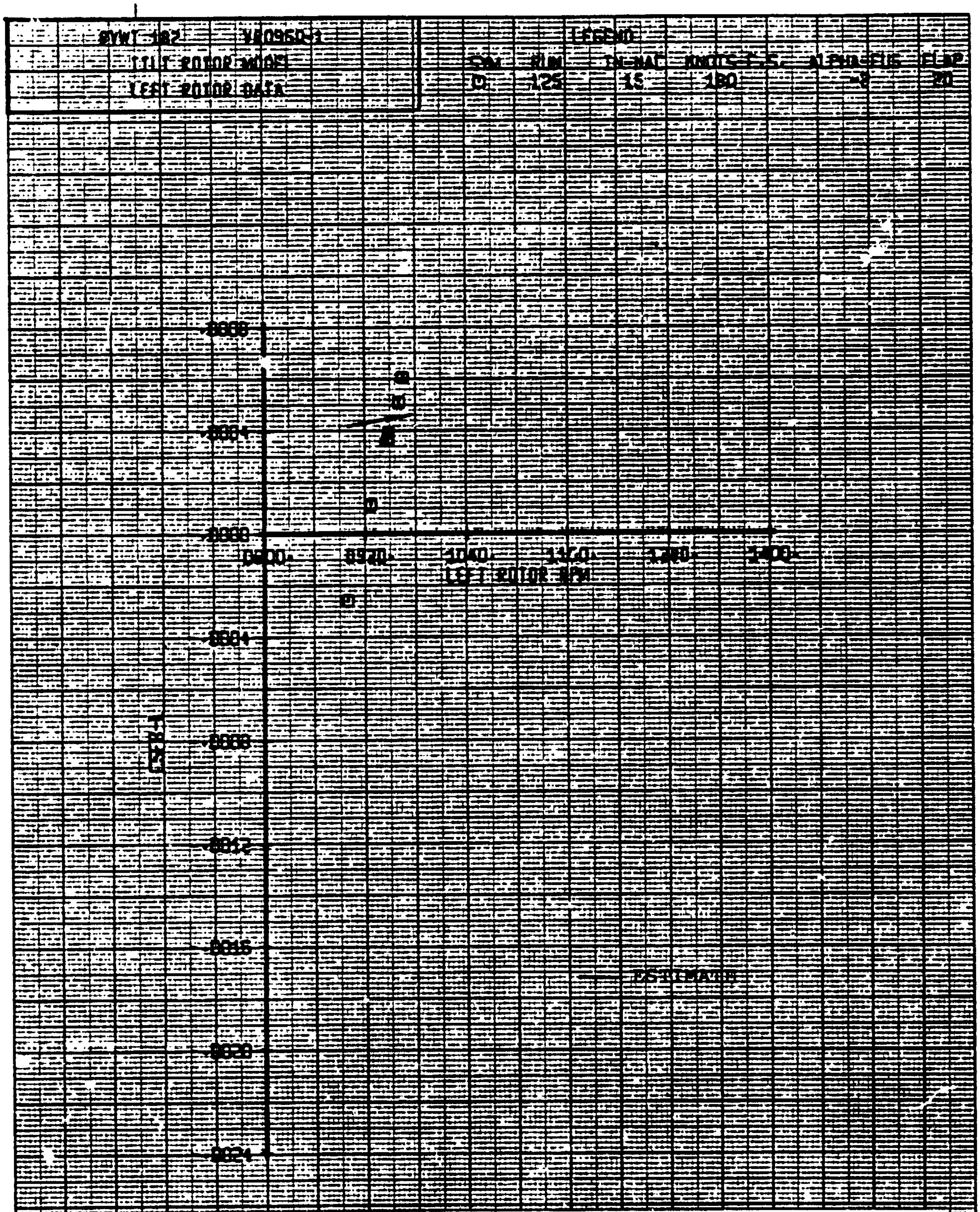

Figure 3.134 Left Rotor Side Force Coefficient Versus Rotor RPM. $I_N = 15°$. Full Scale Airspeed 180 Knots.

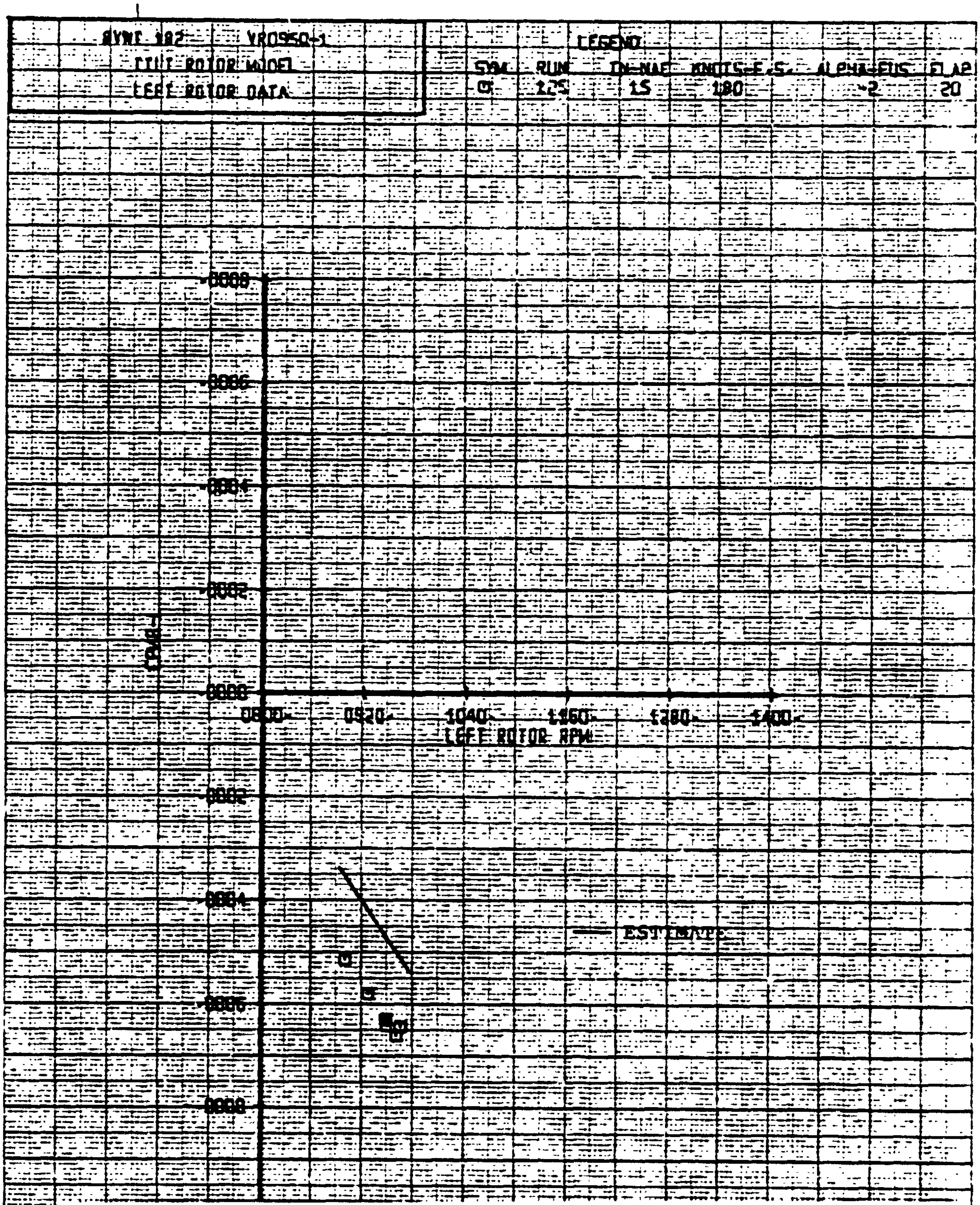

Figure 3.135. Left Rotor Pitching Moment Coefficient Versus Rotor RPM. $I_N = 15°$. Full Scale Airspeed 180 Knots.

APPENDIX A. APPLICATION OF LINEAR REGRESSION TECHNIQUES

As mentioned in the Introduction, an attempt was made to apply multivariable linear regression techniques to the data. This was motivated by the need to process the large amount of data available in the shortest time A brief description of the procedure and the results is given here.

The basis of the approach was that each component of force or moment was functionally of the form

$$C_F = C_{F0}\ (\alpha,\ \mu,\ \Omega,\ \theta_{.75},\ A_1,\ B_1) + \frac{\partial C_F}{\partial A_1} A_1 + \frac{\partial C_F}{\partial B_1} B_1 \qquad \text{(A-1)}$$

where $\frac{\partial C_F}{\partial A_1}, \frac{\partial C_F}{\partial B_1}$ were, in turn, functions of the independent variables, i.e.,

$$\frac{\partial C_F}{\partial A_1} = \quad (\alpha,\ \mu,\ \Omega,\ \theta_{.75},\ A_1,\ B_1) \qquad \text{(A-2)}$$

Thus each component was to be represented as the sum of the force or moment at zero cyclic, and perturbations in that force produced by the application of the cyclic controls. In principle it appeared possible to read all the wind tunnel data into a data file, specify likely parameters for correlation (for example, $\mu\cos\alpha$, μC_T) and use the linear regression option of a statistical package (STATPAK) to determine how well a linear combination of the selected parameters fitted the data.

The first step in this process was obviously to use the linear regression feature of STATPAK to find the values of the cyclic derivatives $\partial C_F/\partial A_1$, $\partial C_F/\partial B_1$ since this would be faster than calculating the slopes from the wind tunnel data plots. Accordingly those runs in which μ, α, $\theta_{.75}$, and RPM were fixed and A_1 or B_1 varied, were processed by the statistical package. The equation for a particular force coefficient was therefore

$$C_F = a + b\ A_1$$

where the slope, b, and the intercept, a, were given by the linear regression. The slopes were then plotted against $\mu\cos\alpha$. An inspection of these plots showed considerable scatter in some areas. The wind tunnel data was reviewed and it was then observed that small but significant changes in the values of cyclic and collective (that were nominally fixed) had occurred in a number of the runs. In view of these deviations it was decided to combine the A_1 and B_1 sweep data and introduce thrust coefficient as a variable in the regression equations. The equation form chosen was

$$CF = CF_0 + CF_1 C_T + CF_2 A_1 + CF_3 B_1 + CF_4 A_1 C_T + CF_5 B_1 C_T \tag{A-3}$$

Using this form in the regression analysis resulted in extremely good correlation being achieved. Figure A-1 presents a comparison of sideforce coefficient computed using equation (A-3) with the measured sideforce, as produced by variations in A and B cyclic at $\mu = .1$ and $\alpha = 80°$. Agreement is to within 5% of the measured values. Figure A-2 shows similar agreement measured and computed normal forces at $\mu = .314$ and $\alpha = 42°$.

Since good correlation was achieved using equation A-3 it was anticipated that those portions of the final rotor math model equations which were to represent changes due to cyclic pitch would be written

$$\frac{\partial C_F}{\partial A_1} = CF_2 + CF_4\ CT$$

$$\frac{\partial C_F}{\partial B_1} = CF_3 + CF_5\ CT$$

The next step was then to determine how the coefficients CF_2 through CF_5 varied with μ, α, Ω, $\theta_{.75}$ and hence obtain general equations for $\partial C_{NF}/\partial A_1$, $\partial C_{NF}/\partial B_1$, etc., covering all flight conditions. It was at this point that difficulties were encountered in finding suitable combinations of parameters that would achieve this. The coefficients could not be represented by a simple function of $\mu\cos\alpha$ as is shown by Figure A-3 which presents the variation of the coefficients in the normal force derivative. Combinations of likely parameters such as $\mu\sin\alpha$, $\mu \sin \alpha$, μC_T etc. were tried to no avail and it was therefore concluded that some theoretical guidance was required. This led to the development of the analysis described in Appendix B.

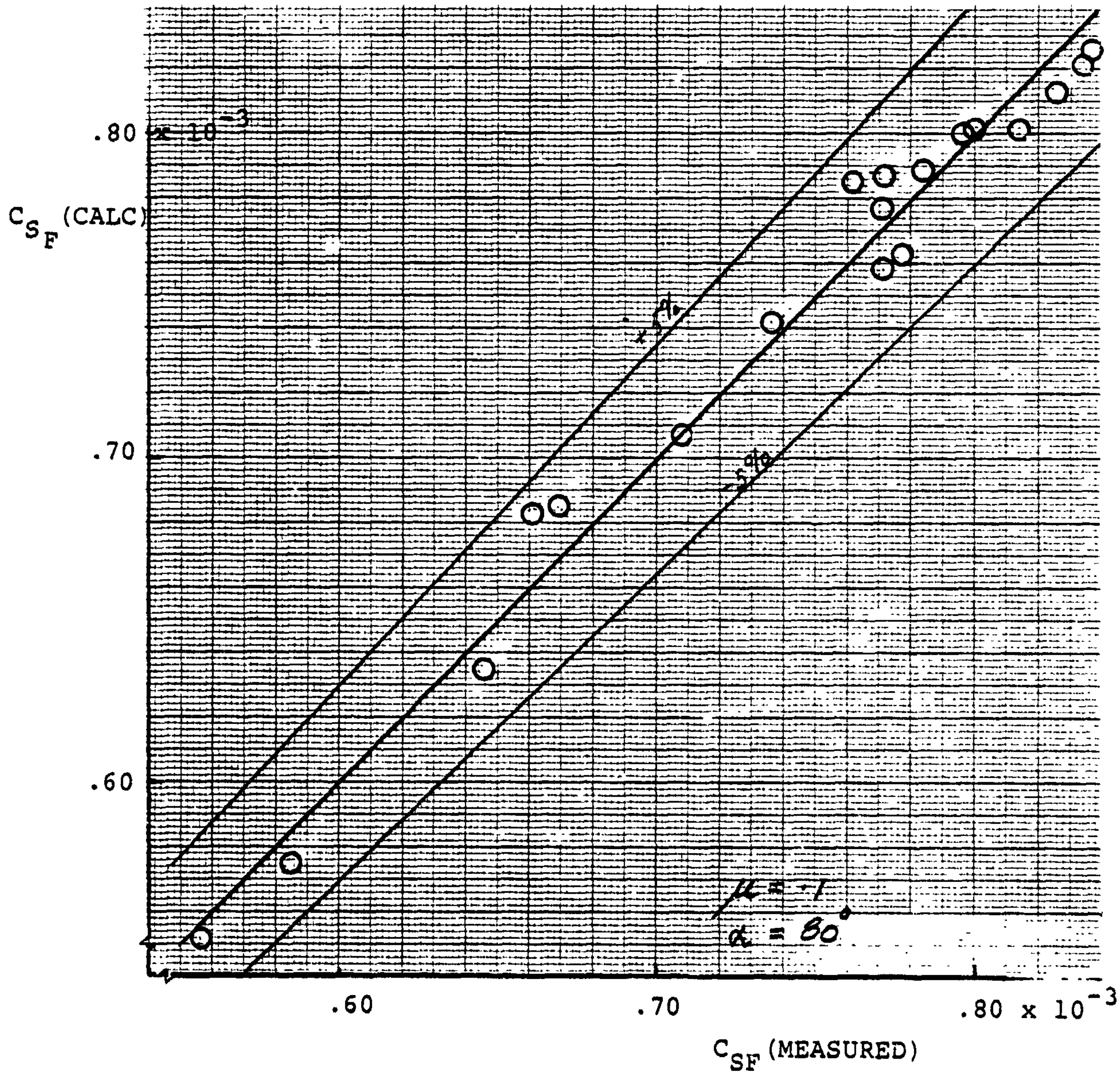

FIGURE A-1. COMPARISON OF MEASURED AND CALCULATED SIDEFORCE COEFFICIENTS USING THE REGRESSION TECHNIQUE

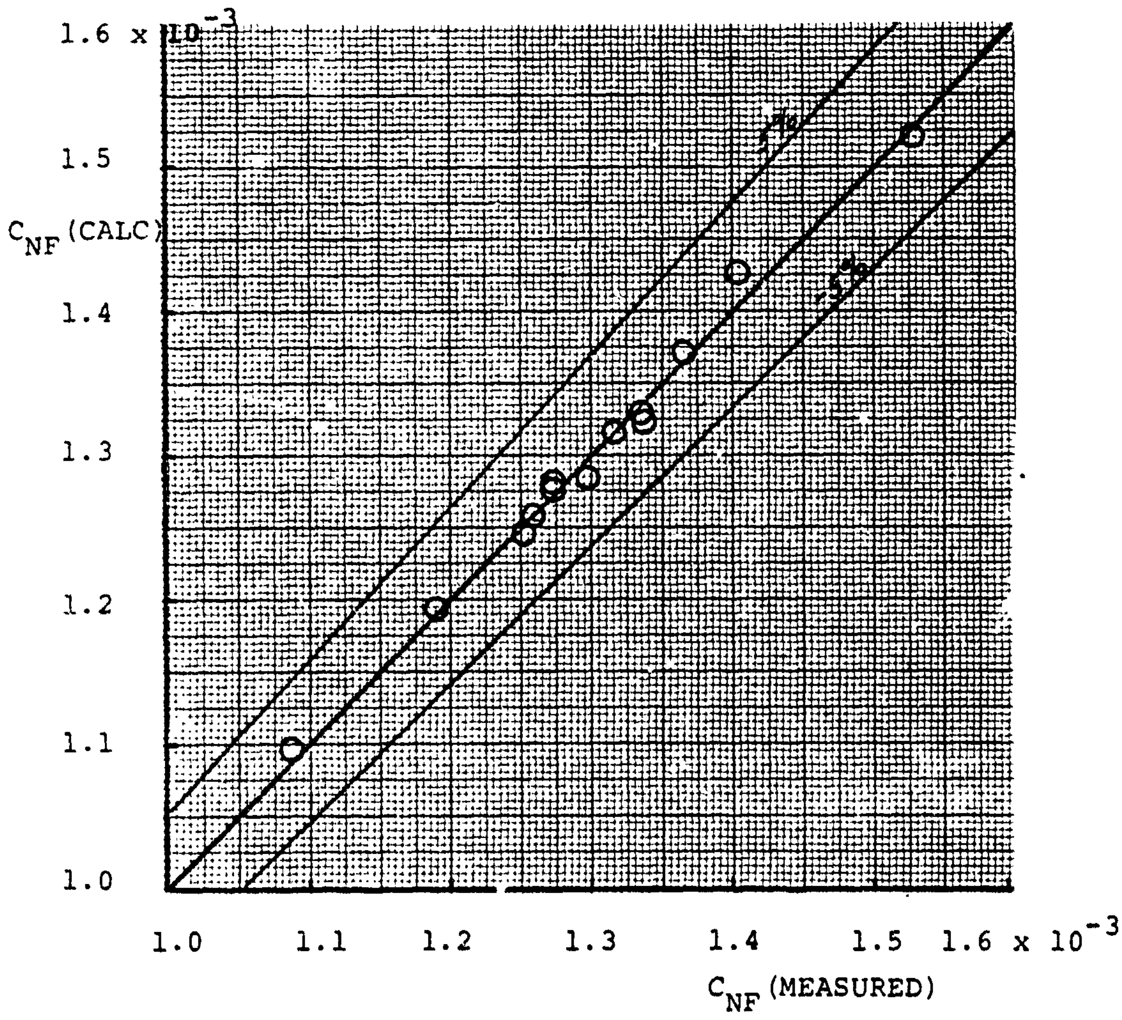

FIGURE A-2. COMPARISON OF MEASURED AND CALCULATED NORMAL FORCE COEFFICIENTS USING THE REGRESSION METHOD.

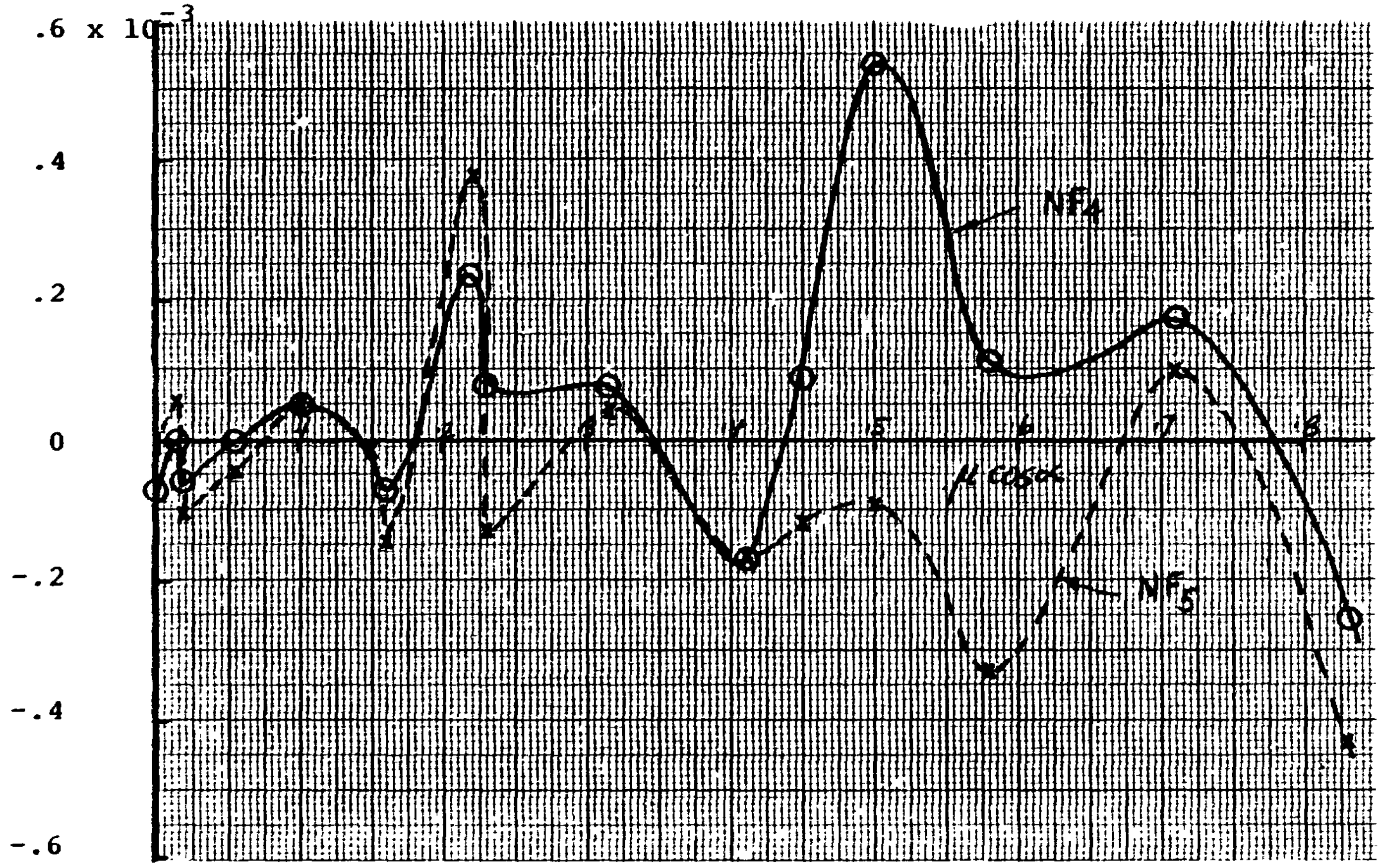

FIGURE A-3. VARIATIONS OF COEFFICIENTS IN THE NORMAL FORCE EQUATION WITH $\mu COS\alpha$.

APPENDIX B
SIMPLIFIED ROTOR ANALYSIS

Introduction

As described in Section 1.0 an analysis was developed to help provide some guidance in choosing basic parameters for use in the regression approach. Later the analysis was expanded in the expectation that the analytical estimates could be simply related to the measured data and hence provide a means for predicting the rotor behavior. While this approach met with only limited success, the analysis and the results are presented here and may be used as a starting point for a more refined treatment. The objective was to obtain some closed-form expressions for the rotor forces and moments that could be rapidly evaluated by a computer. Closed form was desired since the resulting expressions could be inspected to see the significance of each term and identify simplifications. The analysis is developed based upon the following assumptions:

(1) uniform induced velocity across the disc

(2) linear twist

(3) constant blade chord

(4) first flap bending mode only

(5) no in-plane motion considered

(6) no elastic torsion

(7) linear section aerodynamics

Because the analysis must apply to a highly-twisted prop-rotor at large axial advance ratio, the conventional small-angle approximation to the inflow angle at a blade section cannot be made. This results in a very lengthy development of the analysis and the resulting equations are also lengthy. The treatment is an extension of that given by Dommasch in Reference 4 and makes use of some results presented in Reference 5. The final equations are presented in full with no simplifications made other than those stated. An assessment of the relative importance of each term was postponed.

The analysis is developed in rotor wind axes i.e., at zero sideslip and at a resultant angle of attack related to the wind tunnel pitch and yaw angles by

$$\alpha_R = \text{Cos}^{-1}\ (\text{Cos}\,\alpha_T \text{Cos}\,\psi_T).$$

ANALYSIS

Referring to Figure B.1 let the deflected blade shape be represented by

$$z = r C_0 + R S(x) f(\psi) \tag{1}$$

where S(x) is the first flap bending mode shape and $f(\psi)$ is a first harmonic variation with azimuth i.e.

$$z = r C_0 + R S(x) \left(a_0 - a_1 \cos\psi - a_2 \sin\psi \right) \tag{2}$$

Taking moments about the blade root, the centrifugal, inertial and gravity forces acting on the element of mass dm yield

$$dM_{cf} + dM_i + dM_W = \left[r\Omega^2 z + r(\ddot{z} + g \sin\alpha_s) \right] \rho' dr \tag{3}$$

where $\rho' = dm/dr$ is the mass per unit length and α_s is the shaft angle measured from the horizontal.

The aerodynamic contribution to the root moment is approximated by

$$dM_a = r\, dT$$

The total externally-applied moment is therefore

$$M = M_a - M_{cf} - M_i - M_W$$

and the existing elastic moment is

$$M_e = \left[EI \frac{d^2 z}{dr^2} \right]_{r=0} = \left[EI\, R\, f(\psi) \frac{d^2 S}{dr^2} \right]_{r=0} \tag{4}$$

Now

$$dM_i = r \ddot{z} \rho' dr = \Omega^2 R f_1 S \rho' r dr$$

$$dM_{cf} = z r \Omega^2 \rho' dr = \Omega^2 r \rho' dr \left(r C_0 + R S f \right)$$

where

$$f_1 = a_1 \cos\psi + a_2 \sin\psi$$

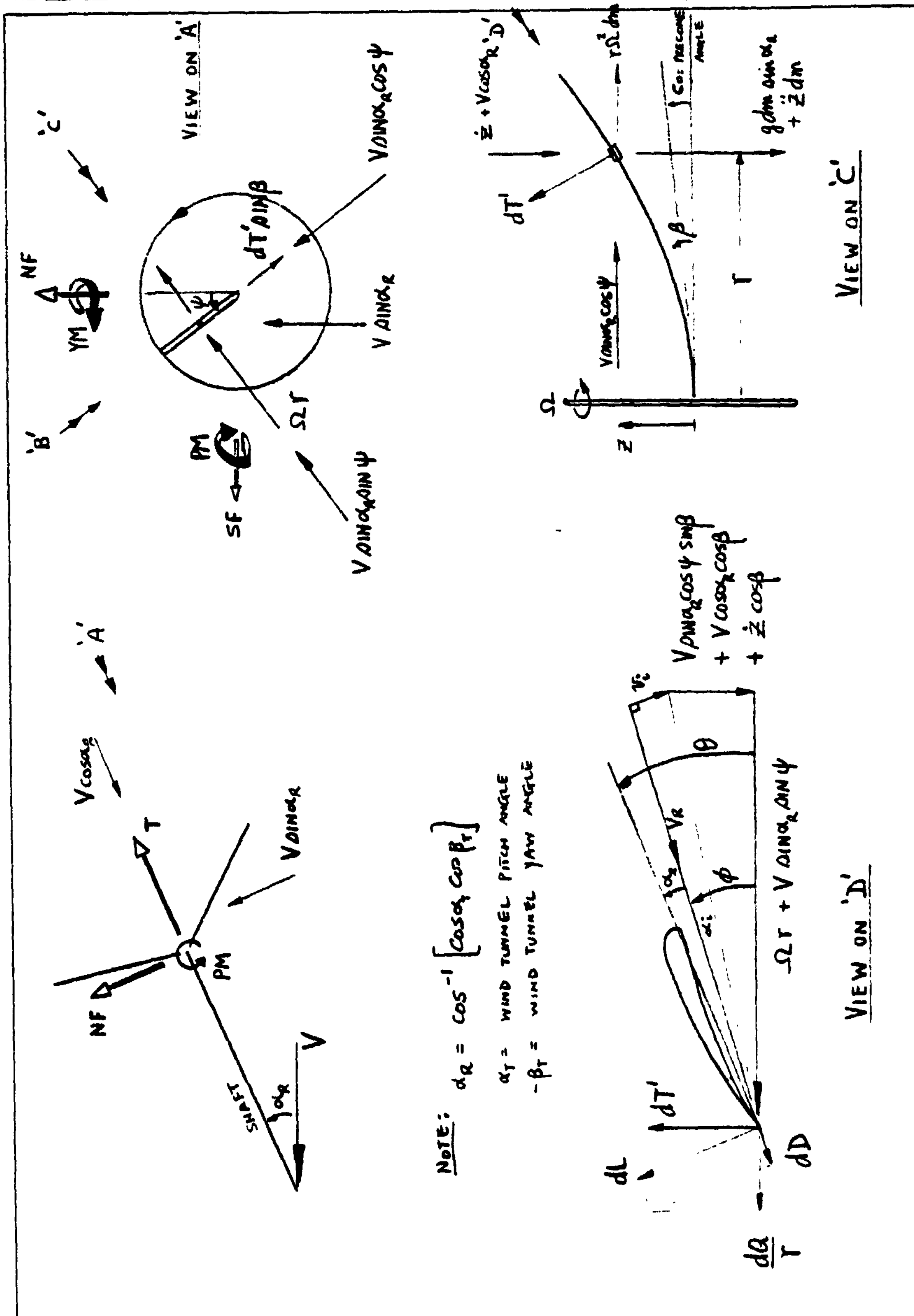

FIGURE B-1. Definition of Axes Systems and Quantities used in the Analysis.

$$\therefore \quad dM_i + dM_{cf} = \Omega^2 R^3 \left[f_1 S x + x^2 c_0 + x^2 S f \right] \rho' dx$$

and

$$M_I = \int_0^R \left(\frac{dM_i}{dr} + \frac{dM_{cf}}{dr} \right) dr = \Omega^2 R^3 \left(a_0 I_1 + c_0 I_0 \right) \quad (5)$$

where $\quad I_0 = \int_0^1 \rho' x^2 dx \quad ; \quad I_1 = \int_0^1 S x \rho' dx$

$$M_W = \int_0^R g r \sin\alpha_R \rho' dr = M_W \sin\alpha_R \quad (6)$$

where M_W is the blade weight moment.

The aerodynamic contribution to the moment is now required. With reference to Figure B.1, assuming small angles for the <u>induced</u> inflow, the tangential and perpendicular components of velocity are

$$\bar{U}_P = \lambda + \beta \mu \cos\psi + \dot{z}/\Omega R \quad (7)$$

$$\bar{U}_T = \mu \sin\psi + x \quad (8)$$

where $\quad \lambda = \dfrac{V \cos\alpha_R + v_i}{\Omega R}$

and $\quad \mu = V/\Omega R \sin\alpha_R$

With $\quad f_3 = a_1 \sin\psi - a_2 \cos\psi \quad$ and $\quad S' = dS/dx$

these components become

$$\bar{U}_P = \lambda + (c_0 + f S')\mu \cos\psi + S f_3 = \bar{V}_R \sin\phi$$

$$\bar{U}_T = \mu \sin\psi + x = \bar{V}_R \cos\phi$$

The elemental thrust is

$$dT = dL\cos\phi - dD\sin\phi \tag{9}$$

Now $dL = \frac{1}{2}\rho V_R^2 a c \alpha_e dr$ $\quad a = dC_\ell/d\alpha$

$dD = \frac{1}{2}\rho V_R^2 c C_d dr$

and $\alpha_e = \theta - \phi \doteq \sin(\theta-\phi)$ for unstalled flow.

Therefore we have

$$dT = K_T\left\{ \bar{U}_T^2 \sin\theta - (1 + C_d')\bar{U}_T\bar{U}_P\cos\theta - C_d'\bar{U}_P^2\sin\theta \right\} dx \tag{10}$$

Where $K_T = \frac{1}{2}\rho a c \Omega^2 R^3$

$C_d' = C_d/a$

This form for the thrust allows the high inflow conditions of the tilting rotor to be treated in a straightforward manner. When calculating the thrust force the drag contribution to the thrust will be retained since in high speed cruise this can be a significant portion of the total. For the present purpose of calculating the aerodynamic moment, however, the drag will be neglected.

The local value of blade angle, θ, is

$$\theta = \theta_0 - \theta_T x - A_1\cos\psi - B_1\sin\psi \tag{11}$$

$$= \theta' - \Delta\theta$$

Where $\theta' = \theta_0 - \theta_T x$

$\Delta\theta = A_1\cos\psi + B_1\sin\psi$

A_1 and B_1 are the lateral and longitudinal values of cyclic, θ_0 the root blade angle, and θ_T is the net linear twist.

Thus

$$\sin\theta \doteq \sin\theta' - \Delta\theta\cos\theta' \qquad (12)$$

$$\cos\theta \doteq \cos\theta' + \Delta\theta\sin\theta' \qquad (13)$$

for normal values of cyclic pitch.

The aerodynamic moment about the blade root at aximuth ψ is, therefore,

$$M_a = K_T R \int_0^1 x \frac{dT}{dx} dx$$

$$= K_T R \int_0^1 \Big\{ \sin\theta \left(x\mu^2 \sin^2\psi + 2\mu x^2 \sin\psi + x^3 \right) - \cos\theta \Big[x\lambda\mu \sin\psi + \mu^2 \frac{\sin 2\psi}{2} (c_0 x + x f S') + \mu S f_3 x \sin\psi + x^2\lambda + x^2 \mu \cos\psi (c_0 + f S') + x^2 S f_3 \Big] \Big\} dx \qquad (14)$$

When performing the integration, integrals of the form

$$\int_0^1 x^n \sin\theta' \, dx \quad , \quad \int_0^1 x^n \cos\theta' \, dx$$

$$\int_0^1 \frac{ds}{dx} S x^n \sin\theta' \, dx \quad , \quad \int_0^1 S x^n \cos\theta' \, dx$$

are encountered. The following notation is introduced to represent these twist integrals.

Let

$$T_{nc}^{ij} = \int_0^1 \left(\frac{ds}{dx}\right)^i S^j x^n \cos\theta' \, dx$$

$$T_{ns}^{ij} = \int_0^1 \left(\frac{ds}{dx}\right)^i S^j x^n \sin\theta' \, dx$$

where, for example,

$$T^{00}_{nc} = \int_0^1 x^n \cos\theta' \, dx$$

$$T^{12}_{3c} = \int_0^1 \frac{ds}{dx} s^2 x^3 \cos\theta' \, dx$$

Now

$$T^{ij}_{nc} = \int_0^1 \left(\frac{ds}{dx}\right)^i s^j x^n \left(\cos\theta_0 \cos\overline{\theta_T x} + \sin\theta_0 \sin\overline{\theta_T x}\right) dx$$

$$= \cos\theta_0 \int_0^1 \left(\frac{ds}{dx}\right)^i s^j x^n \cos\overline{\theta_T x} \, dx + \sin\theta_0 \int_0^1 \left(\frac{ds}{dx}\right)^i s^j x^n \sin\overline{\theta_T x} \, dx$$

$$= \cos\theta_0 \, I^{ij}_{nc} + \sin\theta_0 \, I^{ij}_{ns} \qquad (15)$$

Similarly $$T^{ij}_{ns} = \sin\theta_0 \, I^{ij}_{nc} - \cos\theta_0 \, I^{ij}_{ns} \qquad (16)$$

The values of I^{ij}_{nc}, I^{ij}_{ns} are constants for a given mode shape and twist.

With this notation equation (14) may be integrated. The resulting expression when simplified to include only steady and first harmonic terms is

$$\frac{M^a_\psi}{RK_T} = \frac{1}{2}\mu^2 T^{00}_{1s} + T^{00}_{3s} - \mu B_1 T^{00}_{2c} - \frac{1}{2}\mu a_1 T^{01}_{1c} - \lambda T^{00}_{2c} + \frac{1}{2} a_1 \mu T^{10}_{2c}$$
$$- \frac{1}{2}\lambda\mu B_1 T^{00}_{1s} - \frac{1}{2}\mu c_0 T^{00}_{2s} A_1 - \frac{1}{2}\mu a_0 T^{10}_{2s} A_1 - \frac{1}{2} a_1 B_1 T^{01}_{2s}$$

$$+ \frac{1}{2} a_2 A_1 T_{2s}^{01} - \cos\psi \Big\{ \frac{1}{4}\mu^2 T_{1c}^{00} A_1 + A_1 T_{3c}^{00} - \frac{1}{4}\mu^2 a_2 T_{1c}^{10}$$

$$+ \mu c_0 T_{2c}^{00} - a_2 T_{2c}^{01} + a_0 \mu T_{2c}^{10} + \frac{1}{4}\mu^2 c_0 B_1 T_{1s}^{00} + \frac{1}{4}\mu^2 a_0 B_1 T_{1s}^{10}$$

$$+ \frac{1}{4}\mu a_1 A_1 T_{1s}^{01} - \frac{1}{4}\mu a_2 T_{1s}^{01} B_1 + \lambda T_{2s}^{00} A_1 - \frac{3}{4}\mu a_1 A_1 T_{2s}^{10}$$

$$- \frac{1}{4}\mu a_2 B_1 T_{2s}^{10} \Big\} - \sin\psi \Big\{ -2\mu T_{2s}^{00} + \frac{3}{4}\mu^2 B_1 T_{1c}^{00} + B_1 \ldots$$

$$+ \lambda\mu T_{1c}^{00} - \frac{1}{4}\mu^2 a_1 T_{1c}^{10} + a_1 T_{2c}^{01} + \frac{1}{4}\mu^2 c_0 T_{1s}^{00} A_1$$

$$+ \frac{1}{4}\mu^2 a_0 A_1 T_{1s}^{10} - \frac{1}{4}\mu a_2 A_1 T_{1s}^{01} + \frac{3}{4}\mu a_1 B_1 T_{1s}^{01} + \lambda T_{2s}^{00} B_1$$

$$- \frac{1}{4}\mu a_2 A_1 T_{2s}^{10} - \frac{1}{4}\mu a_1 B_1 T_{2s}^{10} \Big\} \qquad (17)$$

Equating this expression for the aerodynamic moment to the moments due to inertia, centrifugal force, weight and elastic bending it is possible to obtain the coefficients a_0, a_1 and a_2 of the first harmonic flapping by solving the following set of equations.

$$\begin{aligned} C_{11} a_0 + C_{12} a_1 + C_{13} a_2 &= R_1 \\ C_{21} a_0 + C_{22} a_1 + C_{23} a_2 &= R_2 \\ C_{31} a_0 + C_{32} a_1 + C_{33} a_2 &= R_3 \end{aligned} \qquad (18)$$

where

$$C_{11} = \frac{\pi^2 EI}{4R^2 K_T} + \frac{\Omega^2 R^2 I_1}{K_T} + \frac{1}{2}\mu A_1 T_{2s}^{10}$$

$$C_{12} = \frac{1}{2}\mu \left(T_{1c}^{01} - T_{2c}^{10} \right) + \frac{1}{2} B_1 T_{2s}^{01}$$

$$C_{13} = -\frac{1}{2} A_1 T_{2s}^{01}$$

$$R_1 = \frac{1}{2}\mu T_{1s}^{00} \left(\mu - \lambda B_1 \right) + T_{3s}^{00} - \left(\mu B_1 + \lambda \right) T_{2c}^{00} - \frac{1}{2}\mu c_0 A_1 T_{2s}^{00}$$

$$- \frac{M_W}{RK_T} \sin \alpha_R - \frac{\Omega^2 R^2 c_0 I_0}{K_T}$$

$$C_{21} = -\mu T_{2c}^{10} - \frac{1}{4}\mu^2 B_1 T_{2s}^{10}$$

$$C_{22} = \frac{\pi^2 EI}{4R^2 K_T} - \frac{1}{4}\mu A_1 \left(T_{1s}^{01} - 3 T_{2s}^{10} \right)$$

$$C_{23} = \frac{1}{4}\mu^2 T_{1c}^{10} + T_{2c}^{01} + \frac{1}{4}\mu B_1 \left(T_{1s}^{01} + T_{2s}^{10} \right)$$

$$R_2 = \frac{1}{4}\mu^2 A_1 T_{1c}^{00} + A_1 T_{3c}^{00} + \mu c_0 T_{2c}^{00} + \frac{1}{4}\mu^2 c_0 B_1 T_{1s}^{00} + \lambda T_{2s}^{00} A_1$$

$$C_{31} = -\frac{1}{4}\mu^2 A_1 T_{1s}^{10}$$

$$C_{32} = \frac{1}{4}\mu^2 T_{1c}^{10} - T_{2c}^{01} - \frac{1}{4}\mu B_1 \left(3 T_{1s}^{01} - T_{2s}^{10} \right)$$

$$C_{33} = \frac{\pi^2 EI}{4R^2 K_T} + \frac{1}{4}\mu A_1 \left(T_{1s}^{01} + T_{2s}^{10} \right)$$

$$R_3 = -2\mu T_{2s}^{00} + \frac{3}{4}\mu^2 B_1 T_{1c}^{00} + B_1 T_{3c}^{00} + \lambda\mu T_{1c}^{00} + \frac{1}{4}\mu^2 c_0 T_{1s}^{00} A_1 + \lambda B_1 T_{2s}^{00}$$

FORM 10284 (2/66)

Expressions for the Rotor Forces and Moments

Because of the very lengthy manipulations involved in obtaining expression for the rotor forces and moments, only the first few steps in each development will be given and then the final result will be presented.

Thrust

Retaining the drag contribution, the thrust on an element is, from equations (10) and (11), and neglecting squares and products of the flapping coefficients -

$$
\begin{aligned}
dT = K_T \Big\{ & (\sin\theta' - \Delta\theta\cos\theta')(\mu^2\sin^2\psi + 2\mu x\sin\psi + x^2) \\
& - (1+C_d)\Big[(\cos\theta' + \Delta\theta\sin\theta')(\lambda\mu\sin\psi + \tfrac{1}{2}c_0\mu^2\sin 2\psi \\
& + \tfrac{1}{2}\mu^2\sin 2\psi\, f S' + \mu S f_3\sin\psi + x\lambda + c_0 x\mu\cos\psi \\
& + x\mu f S'\cos\psi + x S f_3)\Big] - C_d\Big[(\sin\theta' - \Delta\theta\cos\theta')(\lambda^2 \\
& + \mu^2 c_0^2\cos^2\psi + 2c_0\mu^2 f S'\cos^2\psi + 2\lambda c_0\mu\cos\psi \\
& + 2\lambda\mu f S'\cos\psi + 2\lambda S f_3 + 2c_0\mu\cos\psi\, S f_3\Big]\Big\}\, dx
\end{aligned}
\qquad (20)
$$

Integrating around the azimuth and along the blade the final expression for the thrust is

$$
\begin{aligned}
\frac{2C_T}{\sigma a} = \; & \tfrac{1}{2}\mu^2 T_{0s}^{00} + T_{2s}^{00} - \mu B_1 T_{1c}^{00} - \left(\frac{1+C_d}{2}\right)\Big[a_1\mu T_{0c}^{01} + 2\lambda T_{1c}^{00} \\
& - a_1\mu T_{1c}^{10} + B_1\lambda\mu T_{0s}^{00} - \tfrac{1}{4}(A_1 a_2 + B_1 a_1)\mu^2 T_{0s}^{1c} \\
& + A_1 c_0\mu T_{1s}^{00} + A_1 a_0\mu T_{1s}^{10} + (a_1 B_1 - a_2 A_1) T_{1s}^{01}\Big] \\
& - C_d\Big[\lambda^2 T_{0s}^{00} + \tfrac{1}{2}\mu^2 c_0^2 T_{0s}^{00} + a_0 c_0\mu^2 T_{0s}^{10} - a_1\lambda\mu T_{0s}^{10}
\end{aligned}
$$

FORM 46284 (2/66)

$$- a_2 c_0 \mu T_{0s}^{01} + \frac{1}{4}(3A_1a_1 + B_1a_2) c_0\mu^2 T_{00}^{10} - A_1\lambda\mu c_0 T_{0c}^{00}$$
$$- A_1 a_0 \lambda\mu T_{0c}^{10} - (B_1a_1 - A_1a_2)\lambda T_{0c}^{01} \Big] \quad (21)$$

This equation is solved in the usual manner by using momentum theory to obtain a value of λ consistent with the thrust.

Rotor Power

At blade radius r the contribution of the element dr to the rotor power is

$$dP = \Omega r \left[dL \sin\phi + dD \cos\phi \right] dr$$
$$= K_T \Omega R \left[(1 + C_d)\bar{U}_P \bar{U}_T \sin\theta - \bar{U}_P^2 \cos\theta + C_d \bar{U}_T^2 \cos\theta \right] x\,dx$$

Performing the same kind of substitutions, simplifications and integrations as were required to obtain C_T, the final equation for rotor power coefficient is

$$\frac{2C_P}{\sigma a} = (1 + C_d)\Big[\lambda T_{2s}^{00} + \frac{1}{2}a_1\mu(T_{1s}^{01} - T_{2s}^{10}) - \frac{1}{2}\lambda\mu B_1 T_{1c}^{00}$$
$$- \frac{1}{2}c_0\mu A_1 T_{2c}^{00} + \frac{1}{8}\mu^2(a_1B_1 + a_2A_1)T_{1c}^{10} - \frac{1}{2}\mu a_0 A_1 T_{2c}^{10}$$
$$- \frac{1}{2}(a_1B_1 - a_2A_1)T_{2c}^{01}\Big] + C_d\left[\frac{1}{2}\mu^2 T_{1c}^{00} + T_{3c}^{00} + \mu B_1 T_{2s}^{00}\right]$$
$$- \lambda^2 T_{1c}^{00} + \frac{1}{2}c_0^2\mu^2 T_{1c}^{00} - a_0c_0\mu^2 T_{1c}^{10} + a_1\mu\lambda T_{1c}^{10}$$
$$+ a_2c_0\mu T_{1c}^{01} + \frac{1}{4}c_0\mu^2(3a_1A_1 + a_2B_1)T_{1s}^{10} - \lambda\mu c_0 A_1 T_{1s}^{00}$$
$$- \lambda\mu a_0 A_1 T_{1s}^{10} - \lambda(a_1B_1 - a_2A_1)T_{1s}^{01} \quad (22)$$

Rotor Pitching Moment and Yawing Moment

In Reference 5 a particularly simple set of equations are obtained for the pitching moment and yawing moment coefficients in terms of the first harmonic flapping coefficients. Defining an analog of the Lock number as

$$\gamma_1 = \frac{\rho a c R}{\int_0^1 \rho' S x \, dx} \tag{23}$$

the pitching moment coefficient is

$$\frac{2 C_{PM}}{\sigma a} = \frac{(\lambda_1^2 - 1) a_1}{\gamma_1} \tag{24}$$

and the yawing moment coefficient is

$$\frac{2 C_{YM}}{\sigma a} = \frac{(\lambda_1^2 - 1) \dot{a}_2}{\gamma_1} \tag{25}$$

where λ_1 is the (nondimensional) first flap frequency and the directions for positive moments are defined in Figure B-1.

Rotor Normal Force

Referring to Figure B-1 the elementary contribution to the normal force at station r on a blade is

$$dNF = (dD \cos\phi + dL \sin\phi) \sin\psi - (dL \cos\phi - dD \sin\phi) \cos\psi \sin\beta$$

With the approximation

$$\sin\beta = \tan\beta = dz/dr = c_0 + Rf \, dS/dr = c_0 + f S'$$

the normal force coefficient may be obtained (after some considerable labor) as the sume of fi~~v~~e terms

$$\frac{2 C_{NF}}{\sigma a} = \frac{2 C_{NF1}}{\sigma a} + \frac{2 C_{NF2}}{\sigma a} + \frac{2 C_{NF3}}{\sigma a} + \frac{2 C_{NF4}}{\sigma a} + \frac{2 C_{NF5}}{\sigma a}$$

where

$$\frac{2C_{NF1}}{\sigma a} = \left(\frac{1+C_d'}{8}\right)\left\{ 4a_1 T_{1S}^{01} - 4\lambda B_1 T_{1C}^{00} + \mu\left[4\lambda T_{0S}^{00} - a_1\mu T_{0S}^{10} - A_1\mu\left(c_0 T_{0C}^{00} + a_0 T_{0C}^{10}\right) + \left(A_1 a_2 - B_1 a_1\right)T_{1C}^{10} - \left(3B_1 a_1 - A_1 a_2\right)T_{0C}^{01}\right]\right\}$$
$$+ \frac{C_d'}{8}\left\{4B_1 T_{2S}^{00} + \mu\left(8T_{1C}^{00} + 3B_1\mu T_{0S}^{00}\right)\right\} - \lambda\left\{a_1 T_{0C}^{01} + \frac{B_1}{2}\lambda T_{0S}^{00}\right\}$$
$$+ \frac{\mu}{4}\left\{\left(A_1 a_2 + B_1 a_1\right)\lambda T_{0S}^{10} - \left(A_1 a_1 - B_1 a_2\right)c_0 T_{0S}^{01} + c_0\mu\left(a_2 T_{0C}^{10} - \frac{1}{2}B_1 T_{0S}^{00} - B_1 a_0 T_{0S}^{10}\right)\right\} \quad (26)$$

$$\frac{2C_{NF2}}{\sigma a} = -c_0\left\{\left(\frac{1+C_d'}{8}\right)\left[4a_2 T_{1C}^{01} - 4\lambda A_1 T_{1S}^{00} + \mu\left(a_2\mu T_{0C}^{10} - B_1\mu c_0 T_{0S}^{00} - B_1 a_0\mu T_{0S}^{10} - \left(A_1 a_1 - B_1 a_2\right)T_{0S}^{01} - 4c_0 T_{1C}^{00} - 4a_0 T_{1C}^{10} + \left(3A_1 a_1 + B_1 a_2\right)T_{1S}^{10}\right)\right] + \frac{C_d'}{4}\left[4\lambda a_2 T_{0S}^{01} + 2A_1\lambda^2 T_{0C}^{00}\right.\right.$$
$$\left. + \mu\left(3\mu c_0 a_1 T_{0S}^{10} - 4\lambda c_0 T_{0S}^{00} - 4\lambda a_0 T_{0S}^{10} + 3\mu c_0 A_1 a_2 T_{0C}^{10} - \left(3A_1 a_1 + B_1 a_2\right)\lambda T_{0C}^{10} - \left(3A_1 a_2 - B_1 a_1\right)c_0 T_{0C}^{01}\right)\right]$$
$$\left. - \frac{A_1}{8}\left(\mu^2 T_{0C}^{00} + 4T_{2C}^{00}\right)\right\} \quad (27)$$

$$
\begin{aligned}
\frac{2C_{NF3}}{\sigma a} = a_0 \Bigg\{ & \left(\frac{1+C_d}{8}\right)\Big[4a_2 T^{11}_{1c} - 4\lambda A_1 T^{10}_{1s} + \mu\Big(a_2\mu T^{11}_{0c} - \\
& B_1 \mu c_0 T^{10}_{0s} - B_1 a_0 \mu T^{11}_{0s} - (A_1 a_1 - B_1 a_2) T^{11}_{0s} - 4c_0 T^{10}_{1c} \\
& - 4a_0 T^{11}_{1c} + 3(A_1 a_1 + B_1 a_2) T^{11}_{1s}\Big)\Big] + \frac{C_d}{4}\Big[4\lambda a_2 T^{11}_{0s} + \\
& 2A_1\lambda^2 T^{10}_{0c} + \mu\Big(3\mu c_0 a_1 T^{11}_{0s} - 4\lambda c_0 T^{10}_{0s} - 4\lambda a_0 T^{11}_{0s} \\
& + 3\mu c_0 A_1 a_2 T^{11}_{0c} - (3A_1 a_1 + B_1 a_2)\lambda T^{11}_{0c} - (3A_1 a_2 - \\
& B_1 a_1) c_0 T^{11}_{0c}\Big)\Big] - \frac{A_1}{8}\left(\mu^2 T^{10}_{0c} + 4T^{10}_{2c}\right)\Bigg\} \qquad (28)
\end{aligned}
$$

$$
\begin{aligned}
\frac{2C_{NF4}}{\sigma a} = a_1 \Bigg\{ & \left(\frac{1+C_d}{8}\right)\Big[(3A_1 a_2 - B_1 a_1) T^{11}_{1s} - 4\lambda T^{10}_{1c} + \mu\Big(\frac{1}{2}(\\
& A_1 a_2 + B_1 a_1) T^{11}_{0s} - \lambda B_1 T^{10}_{0s} + 3a_1 T^{11}_{1c} - 3A_1 c_0 T^{10}_{1s} \\
& - 3A_1 a_2 T^{11}_{1s}\Big)\Big] + \frac{C_d}{4}\Big[3\mu\Big(a_2 c_0 \mu T^{11}_{0s} + \lambda A_1 a_2 T^{11}_{0c} \\
& + A_1 \lambda c_0 T^{10}_{0c} - a_1 \lambda T^{11}_{0s} - a_0 c_0 \mu T^{11}_{0s}\Big) - \lambda\Big(2\lambda T^{10}_{0s} \\
& + (3A_1 a_2 - B_1 a_1) T^{11}_{0c}\Big)\Big] + \frac{\mu}{8}\left(\mu T^{10}_{0s} - 2B_1 T^{10}_{1c}\right) \\
& + \frac{1}{2} T^{10}_{2s}\Bigg\} \qquad (29)
\end{aligned}
$$

FORM 46284 (2/66)

$$\frac{2C_{NF5}}{\sigma a} = a_2 \left\{ \left(1+\frac{\delta}{8}\right) \left[(B_1 a_2 - A_1 a_1) T_{1s}^{11} + \mu \left(a_2 T_{0c}^{11} + \frac{1}{2}(A_1 a_1 + B_1 a_2) \mu T_{0s}^{11} - \mu c_0 T_{0c}^{10} - \mu a_0 T_{0c}^{11} - a_1 T_{1c}^{11} - A_1 \lambda T_{0s}^{10} - B_1 c_0 T_{1s}^{10} - B_1 a_0 T_{1s}^{11} \right) \right] + \frac{\delta}{2} \left[(A_1 a_1 - B_1 a_2) \lambda T_{0c}^{11} + \mu \left(a_2 \lambda T_{0s}^{11} - a_1 c_0 T_{0s}^{11} + B_1 \lambda (c_0 T_{0c}^{10} + a_0 T_{0c}^{11}) + \frac{1}{2}(A_1 a_2 + B_1 a_1) c_0 \mu T_{0c}^{11} \right) \right] - \frac{1}{4} A_1 \mu T_{1c}^{10} \right\} \qquad (3u)$$

Rotor Sideforce

The elementary contribution to rotor sideforce is

$$-dSF = (dD \cos\phi + dL \sin\phi)\cos\psi + (dL \cos\phi - dD \sin\phi)\sin\psi \sin\beta$$

and, as for the normal force, the sideforce is given by

$$\frac{2C_{SF}}{\sigma a} = 2\frac{C_{SF1}}{\sigma a} + 2\frac{C_{SF2}}{\sigma a} + \frac{2C_{SF3}}{\sigma a} + 2\frac{C_{SF4}}{\sigma a} + 2\frac{C_{SF5}}{\sigma a}$$

where

$$\frac{2C_{SF1}}{\sigma a} = \left(1+\frac{\delta}{8}\right) \left\{ -4 A_1 \lambda T_{1c}^{00} + \mu \left[4 c_0 T_{1s}^{00} - a_2 \mu T_{0s}^{10} + 4 a_0 T_{1s}^{10} - B_1 \mu (c_0 T_{0c}^{00} + a_0 T_{0c}^{10}) + (3A_1 a_1 + B_1 a_2) T_{1c}^{10} - (A_1 a_1 - B_1 a_2) T_{0c}^{01} \right] \right\} - \frac{\delta}{8} \left[A_1 \mu^2 T_{0s}^{00} + 4 A_1 T_{2s}^{00} \right] - \lambda \left[\frac{A_1 \lambda}{2} T_{0s}^{00} - a_1 T_{0c}^{01} \right] +$$

$$\frac{\mu}{4}\Big[(3A_1a_1+B_1a_2)\lambda T_{0s}^{10} + (3A_1a_2-B_1a_1)c_0T_{0s}^{01}$$

$$+ c_0\mu\Big(3a_1T_{0c}^{10} - \frac{3}{2}A_1T_{0s}^{00}\Big) - 3A_1a_2T_{0s}^{10}\Big)\Big] - \lambda\mu\big(c_0T_{0c}^{00}$$

$$+ a_0T_{0c}^{10}\big) \qquad (31)$$

$$\frac{2C_{SF2}}{\sigma a} = c_0\Big\{\frac{(1+d)}{8}\Big[-4a_1T_{1c}^{01} - 4\lambda B_1T_{1s}^{00} + \mu\Big(a_2\mu T_{0c}^{10} - A_1c_0\mu T_{0s}^{00}$$

$$- A_1a_0\mu T_{0s}^{10} + (A_1a_2-B_1a_1)T_{1s}^{10} - (3B_1a_1-A_1a_2)T_{0s}^{01}$$

$$- 4\lambda T_{0c}^{00}\Big)\Big] + \frac{d}{4}\Big[-4\lambda a_1T_{0s}^{01} + 2\lambda^2B_1T_{0c}^{00} + \mu\Big(a_2c_0\mu T_{0s}^{10}$$

$$+ a_0c_0\mu B_1T_{0c}^{10} - \lambda(A_1a_2+B_1a_1)T_{0c}^{10} + c_0(A_1a_1 -$$

$$B_1a_2)T_{0c}^{01}\Big)\Big] - \frac{B_1}{8}\big(4T_{2c}^{00} + 3\mu^2T_{0c}^{00}\big) + \mu T_{1s}^{00}\Big\} \qquad (32)$$

$$\frac{2C_{SF3}}{\sigma a} = a_0\Big\{\frac{(1+d)}{8}\Big[-4a_1T_{1c}^{11} - 4\lambda B_1T_{1s}^{10} + \mu\Big(a_2\mu T_{0c}^{11} -$$

$$A_1c_0\mu T_{0s}^{10} - A_1a_0\mu T_{0s}^{11} + (A_1a_2-B_1a_1)T_{1s}^{11}$$

$$- (3B_1a_1-A_1a_2)T_{0s}^{11} - 4\lambda T_{0c}^{10}\Big)\Big] + \frac{d}{4}\Big[-4\lambda a_1T_{0s}^{11} + 2\lambda^2B_1T_{0c}^{10}$$

$$+ \mu\Big(a_2c_0\mu T_{0s}^{11} + a_0c_0\mu B_1T_{0c}^{11} - \lambda(A_1a_2+B_1a_1)T_{0c}^{11}$$

$$+ c_0(A_1a_1-B_1a_2)T_{0c}^{11}\Big)\Big] - \frac{B_1}{8}\big(4T_{2c}^{10} + 3\mu^2T_{0c}^{10}\big)$$

$$+ \mu T_{1s}^{10}\Big\} \qquad (33)$$

$$\frac{2C_{SF4}}{\sigma a} = -a_1 \Big\{ \frac{(1+c_l)}{8} \Big[(A_1 a_1 - B_1 a_2) T_{1s}^{11} + \mu \Big(\frac{1}{2}(A_1 a_1 + B_1 a_2) \mu T_{0s}^{11} - \lambda A_1 T_{0s}^{10} + a_2 T_{0c}^{11} + a_2 T_{1c}^{11} - B_1 c_0 T_{1s}^{10} - B_1 a_0 T_{1s}^{11} - \mu c_0 T_{0c}^{10} - \mu a_0 T_{0c}^{11} \Big) \Big] + \frac{c_l}{4} \Big[\mu \Big(-a_1 c_0 T_{0s}^{11} + \lambda B_1 a_0 T_{0c}^{11} + B_1 \lambda c_0 T_{0c}^{10} + a_2 \lambda T_{0s}^{11} + \frac{1}{2}(A_1 a_2 + B_1 a_1) c_0 \mu T_{0c}^{11} \Big) + (A_1 a_1 - B_1 a_2) \lambda T_{0c}^{11} \Big] - \frac{1}{4} A_1 \mu T_{1c}^{10} \Big\} \tag{34}$$

$$\frac{2C_{SF5}}{\sigma a} = -a_2 \Big\{ \frac{(1+c_l)}{8} \Big[(A_1 a_2 - 3B_1 a_1) T_{1s}^{11} - 4\lambda T_{1c}^{10} + \mu \Big(a_1 T_{1c}^{11} + \frac{1}{2}(B_1 a_1 + A_1 a_2) \mu T_{0s}^{11} - 3A_1 T_{0c}^{11} - 3B_1 \lambda T_{0s}^{10} - A_1 c_0 T_{1s}^{10} - A_1 a_0 T_{1s}^{11} \Big) \Big] + \frac{c_l}{4} \Big[(3B_1 a_1 - A_1 a_2) \lambda T_{0c}^{11} - 2\lambda^2 T_{0s}^{10} + \mu \Big(a_1 \lambda T_{0s}^{11} - a_0 c_0 \mu T_{0s}^{11} + a_2 c_0 T_{0s}^{11} + A_1 \lambda (c_0 T_{0c}^{10} + a_0 T_{0c}^{11}) + \frac{1}{2}(A_1 a_1 + B_1 a_2) c_0 \mu T_{0c}^{11} \Big) \Big] + \frac{3}{8} \mu (\mu T_{0s}^{10} - 2B_1 T_{1c}^{10}) + \frac{1}{2} T_{2s}^{10} \Big\} \tag{35}$$

Comparison of the Analytical Predictions with the Wind Tunnel Data

At each wind tunnel test point, the test values of collective pitch, cyclic, shaft angle of attack, yaw angle, advance ratio and rpm were used in the analysis to calculate the rotor forces and moments. The first flap bending mode shape was computed using the model blade properties presented in Reference 3. The frequencies of the first flap bending mode were obtained from the rotating blade frequency measurements given in that Reference. The average value of blade drag coefficient, C_d, was obtained by extrapolation of the hover power coefficient to zero thrust and using the approximation

$$C_d = 8C_{P_0}/\sigma \tag{36}$$

The results are presented in Figures B-2 through B-6 which show the calculated and measured forces and moments. The calculated values are plotted using the same symbol as the test value but marked by a flag. A guide to the test runs is provided in Tables B-1 and B-2.

In general the predictions are in fairly good agreement with thetest data considering the simplifying assumptions that are made in the analysis. In cruise flight the predicted slope of sideforce coefficient with collective pitch is opposite to the test data. This may indicate the need for a lead-lag degree of freedom in the analysis. Further work is required in this area. It should be noted that the execution time of the program incorporating the analysis is short, about the same as the curve-fit equations.

It was hoped that the analytical results would be linearly related to the measured data i.e.

$$C_{F_{THEORY}} = a + b\, C_{F_{TEST}} \tag{37}$$

where a and b would be functions of effective advance ratio, $\mu\cos\alpha$. If this had been the case, then estimated values for the rotor forces could be obtained from

$$C_{F_{TEST}} = \frac{1}{b}\,(C_{F_{THEORY}} - a) \tag{38}$$

In other words the analysis would be used to predict the forces and moments, and equation (38) used to correct them to provide estimates. While linear relationships were found for thrust and power, the remaining quantities were not linearly related and the approach was abandoned in favor or direct curve fitting as described in Section 3.0.

RUN #	SYMBOL	RUN TYPE	μ	α	RPM	$\theta_{.75}$
27,28		$\theta_{.75}$	0	90.	1185	10.0
39		α	.1	VARY		7.9
42		ψ		90		8.2
43		$\theta_{.75}$		80		VARY
45		RPM			VARY	8.9
46		α		VARY		
50		ψ		82		
51		$\theta_{.75}$				VARY
53		RPM			VARY	8.9
54		α	.226	VARY		13.5
55		ψ		65		13.5
58		$\theta_{.75}$				VARY
59		RPM			VARY	13.5
61		α		VARY		16.0
62		ψ		49.0		16.0
63		$\theta_{.75}$				VARY
67		RPM	VARY		VARY	16.0
68		α	.315	VARY		22.6
69		ψ		42.0		22.6
72		$\theta_{.75}$				VARY
74		RPM			VARY	22.6
75		α		VARY		18.2
76		ψ		59		18.2
79		$\theta_{.75}$				VARY
81		RPM	VARY		VARY	18.2
82		α	.226	VARY		12.10
83		ψ		76.0		12.10
86		$\theta_{.75}$				VARY
88		RPM	VARY		VARY	12.10
89		α	.252	VARY	1065	20.7
90		ψ		26		20.7
93		$\theta_{.75}$				VARY
95		RPM	VARY		VARY	20.7
96		α	.351	VARY		29.0
97		ψ				29.0
100		$\theta_{.75}$				VARY
102		RPM	VARY		VARY	29.0
111		α	.451	VARY		32.0
112		ψ		24.0		32.0
115		$\theta_{.75}$				VARY
117		RPM	VARY		VARY	32.0
118		α	.510	VARY	946	36.0
119		ψ		13		36.0
123		$\theta_{.75}$				36.0
125		RPM	VARY		VARY	37.5
128		α	.58	VARY	830	41.5
132		ψ	.58	0		41.5
138		α	.707			47.2
141		ψ	.707			47.2
146		α	.836			52.0
148		ψ	.836			52.0
153		α	.97	0	830	56.3
154		ψ	.97			56.4
159		α	.448			33.8
162		ψ	.448			34.2

TABLE B-1. List of Runs in which Cyclic was Fixed

RUN #	SYMBOL	RUN TYPE	μ	α	RPM	$\theta_{.75}$
29		A1	0	90.0	1111	10.0
31		B1	0	90.0	1110	9.9
32		B1	0	90.0	1110	11.8
40		B1	.1	80.0	1183	7.9
41		A1	.1	79.3	1183	8.0
84		A1	.23	76.0	1185	12.0
85		B1	.23	76.0	1186	11.9
46		B1	.09	82.2	1186	8.6
49		A1	.1	81.7	1185	9.0
56		A1	.23	64.0	1185	13.3
57		B1	.23	63.5	1185	13.4
77		A1	.32	59.5	1184	18.0
78		B1	.31	60.0	1185	17.9
64		A1	.23	48.6	1185	16.0
65		B1	.23	48.6	1185	16.3
70		A1	.31	42.0	1186	22.5
71		B1	.31	41.8	1185	22.6
91		A1	.25	31.0	1065	20.7
92		B1	.25	31.0	1065	20.8
98		A1	.35	26.5	1065	29.0
99		B1	.35	26.5	1065	29.0
113		A1	.45	24.3	1065	32.0
114		B1	.45	24.3	1066	31.9
120		A1	.51	12.8	943	37.7
121		B1	.51	12.7	944	37.6
122		B1	.51	12.9	945	37.7
163		A1	.45	14.0	830	34.1
164		B1	.44	13.7	830	33.6
133		A1	.58	15.0	830	41.8
134		B1	.58	14.3	830	41.7
142		A1	.71	14.5	830	47.0
143		B1	.71	14.5	830	47.1
149		A1	.84	14.3	830	51.8
150		B1	.84	14.0	828	51.9
155		A1	.97	14.4	827	56.2
156		B1	.97	14.7	826	56.3

TABLE B-2. List of Runs in which Cyclic was Varied

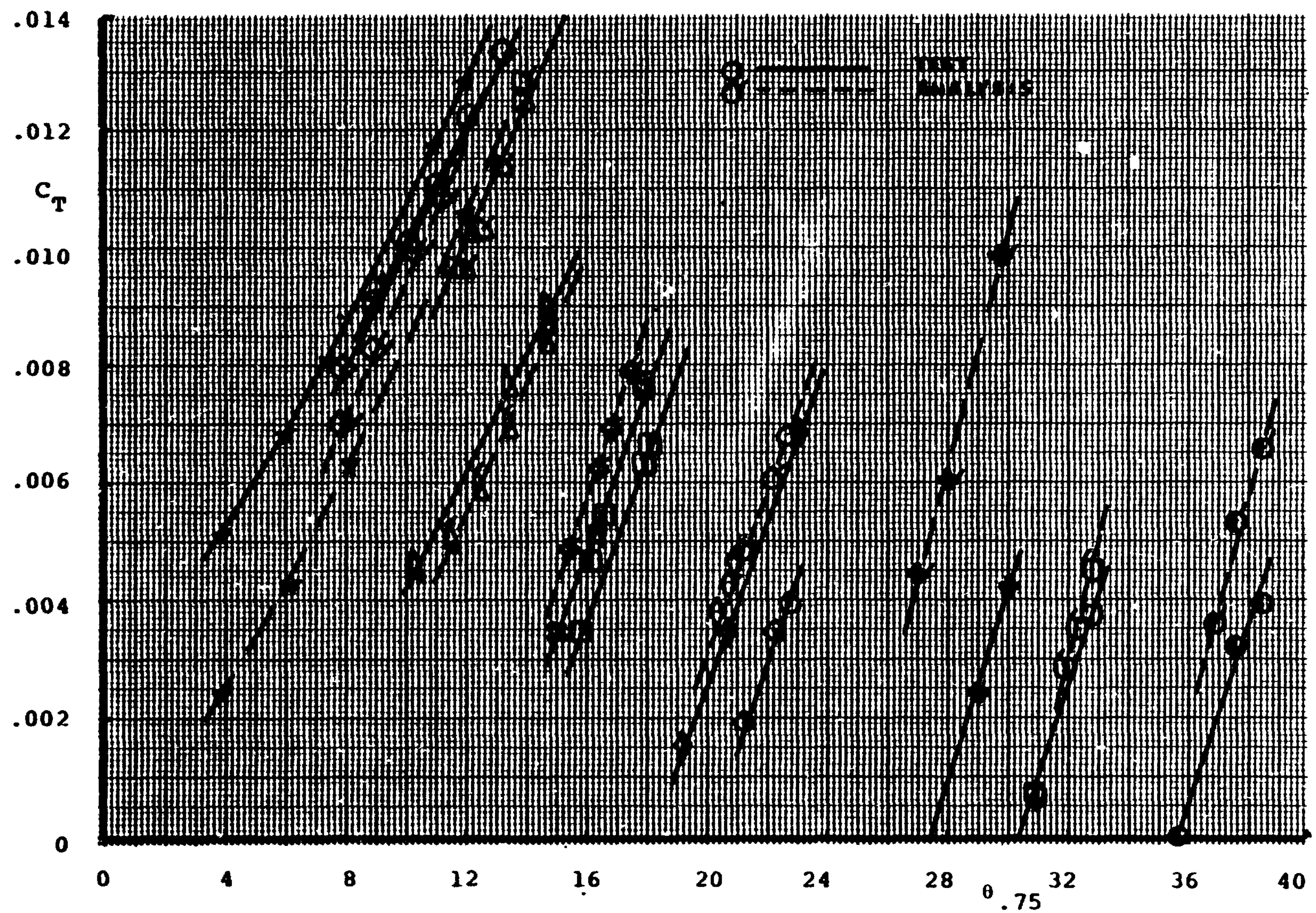

FIGURE B-2. Thrust Coefficient versus Collective Comparison

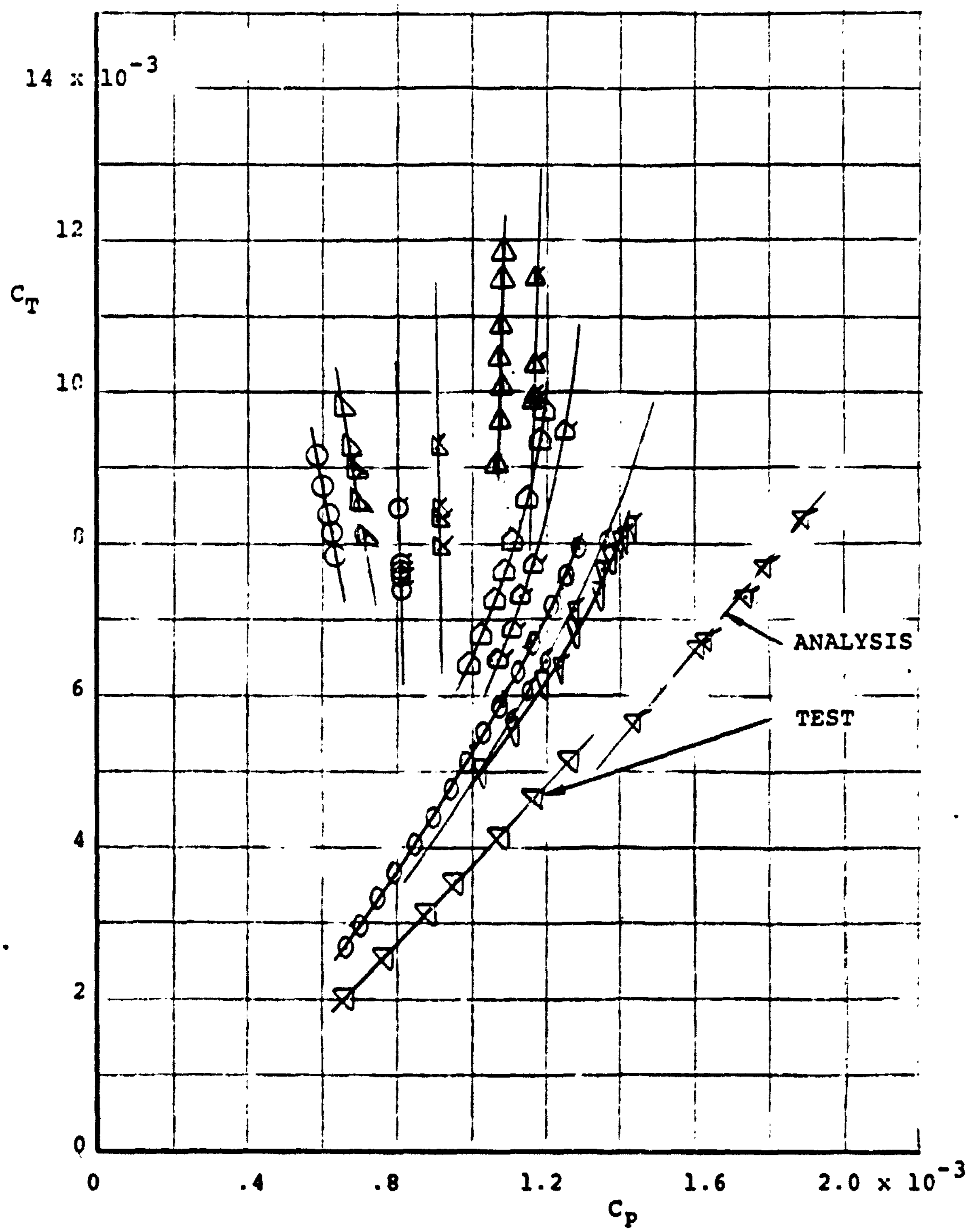

FIGURE B-3. Predicted and Measured Thrust Power Relationship during Shaft Angle Sweeps.

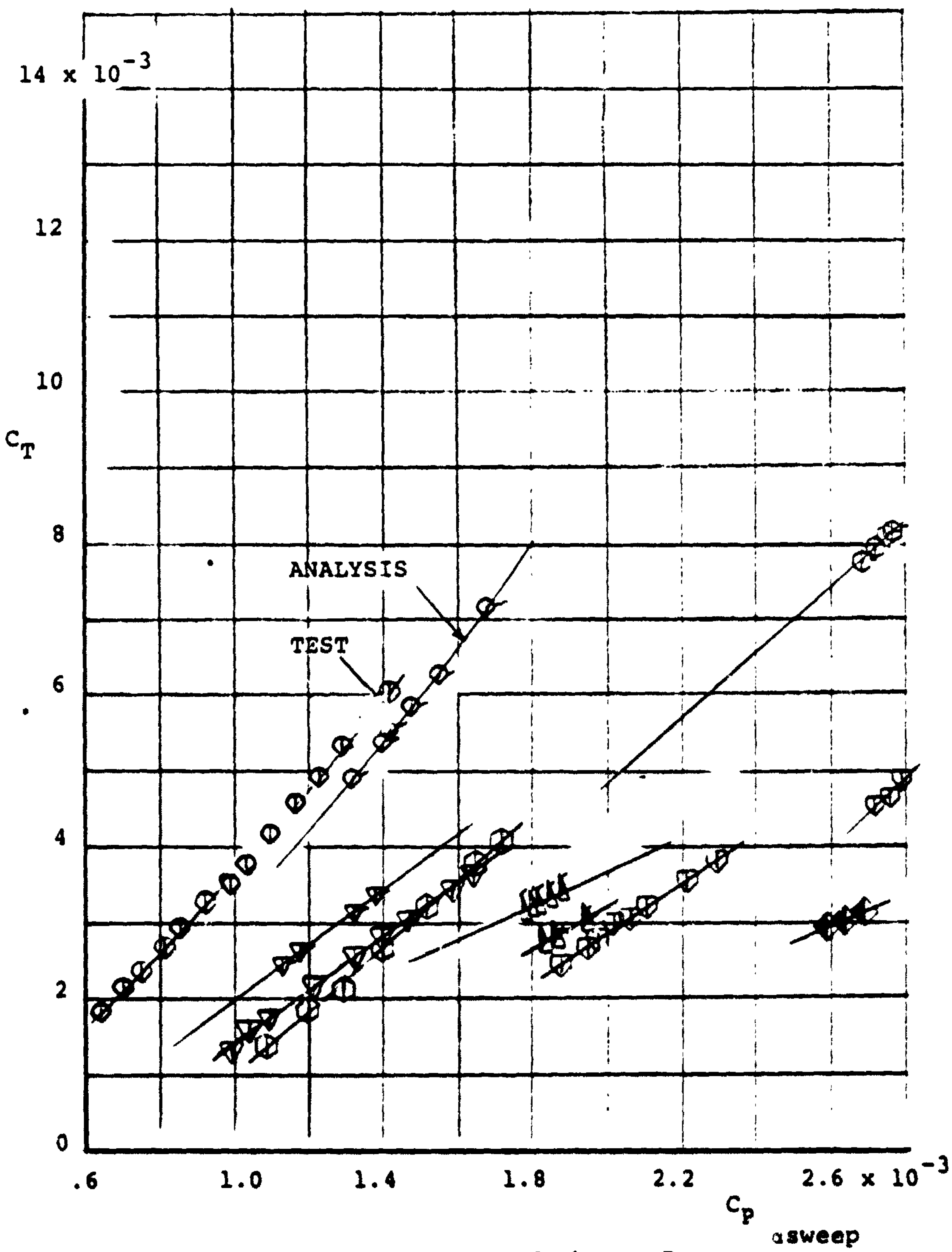

FIGURE B-3. Predicted and Measured Thrust Power Relationship during Shaft Angle Sweeps (Concluded)

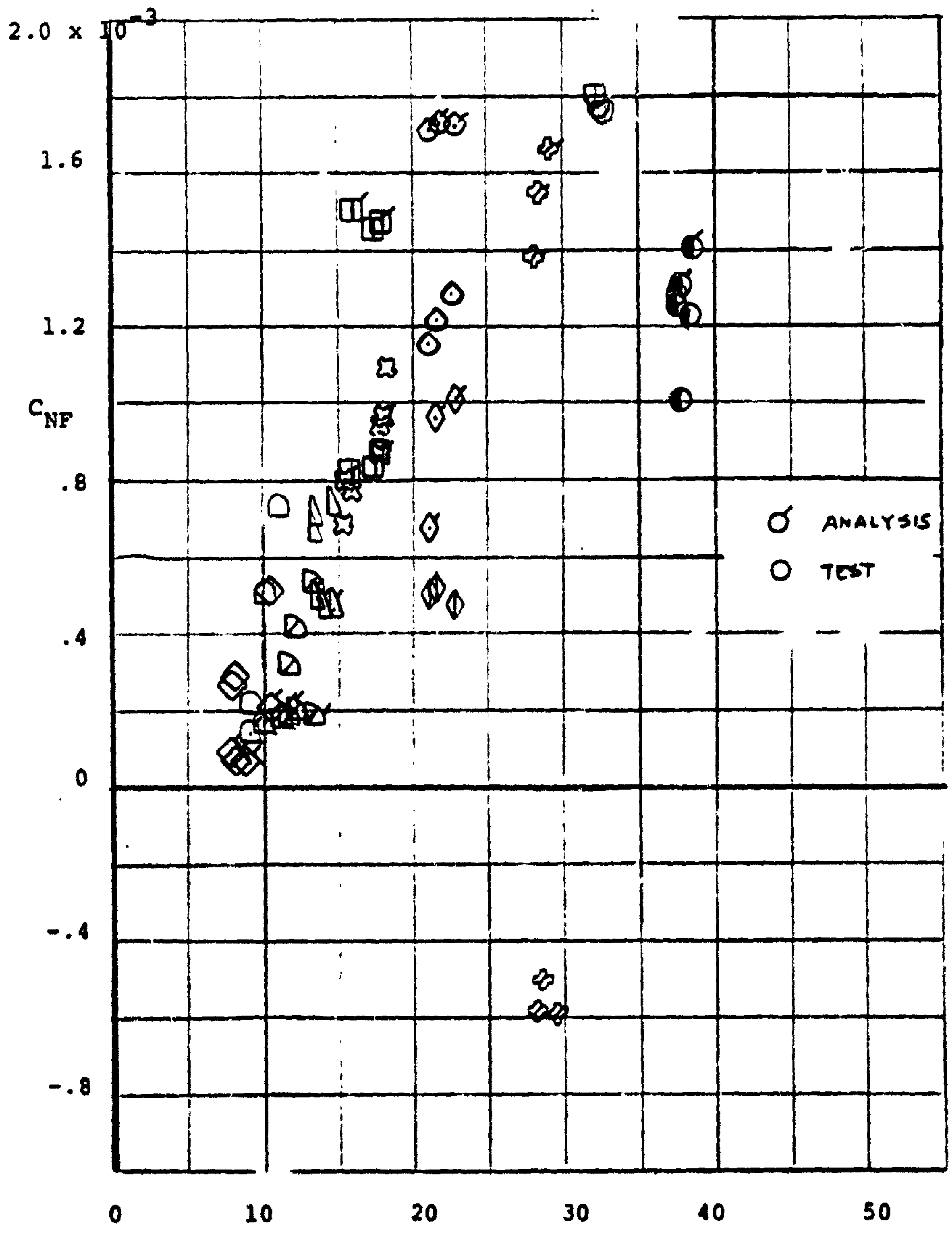

FIGURE B-4. Variation of Normal Force with Collective Pitch - Predicted vs. Test.

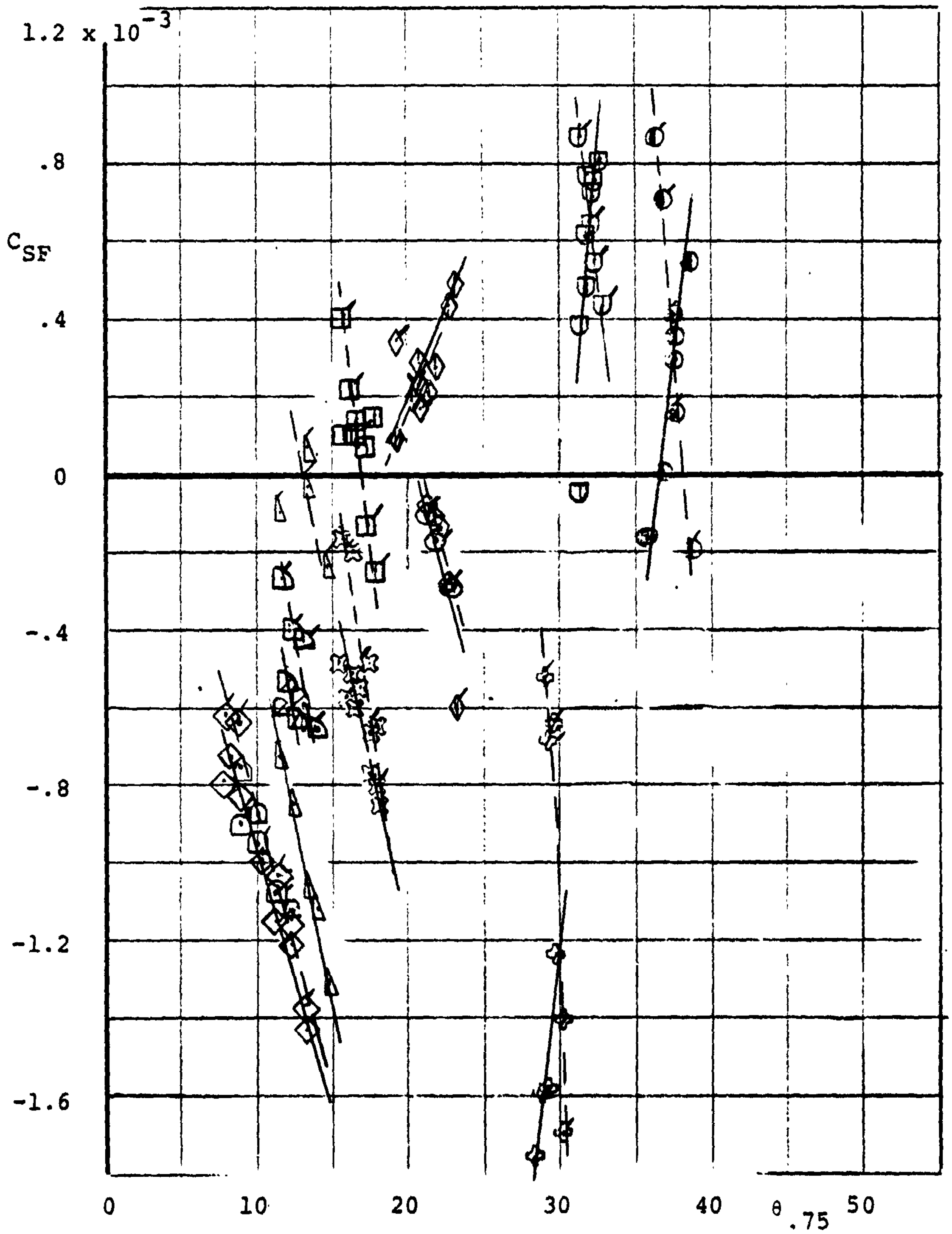

FIGURE B-5. Predicted and Measured Variations of Side-force with Collective Pitch.

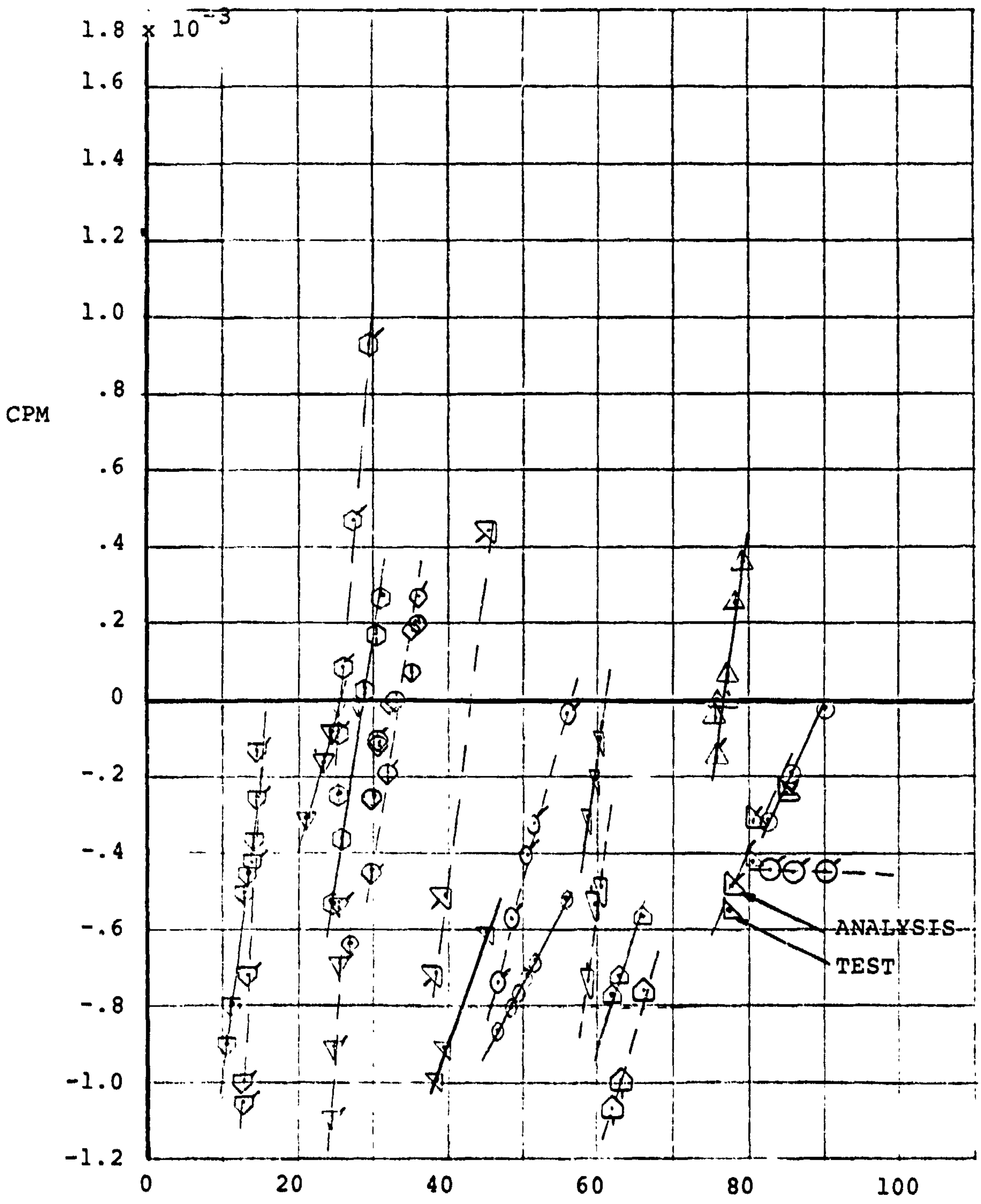

FIGURE B-6. Comparison of Predicted and Measured Pitching Moments during Shaft Angle Sweeps.

APPENDIX C. LISTING OF THE ROTOR MATH MODEL SUBROUTINE

```
      SUBROUTINE ROTOR(ALTSI,BITSI,COLL,ALFHR,BETAR,RPM,AMUP,CT,CF,
     1CMF,CSF,CFM)
      DIMENSION X(8,5,8)
C**** CALC ESTIMATED VALUES OF FORCES AND MOMENTS *************
      DO 333 I=1,8
      DO 333 J=1,5
      DO 333 K=1,8
333   X(I,J,K)=0.0
      X(1,1,1)=-.4606
      X(1,1,2)=-4.7883
      X(1,1,3)=-274.5381
      X(1,1,4)=1199.8266
      X(1,1,5)=-1752.2216
      X(1,1,6)=996.5716
      X(1,1,7)=-165.1875
      X(2,1,1)=-.0353
      X(2,1,2)=1.4955
      X(2,1,3)=-21.6829
      X(2,1,4)=20.5443
      X(3,1,1)=-1.3713
      X(3,1,2)=16.9001
      X(3,1,3)=-210.3956
      X(3,1,4)=517.6291
      X(3,1,5)=-503.7611
      X(3,1,6)=177.3255
      X(4,1,1)=.7213
      X(4,1,2)=10.8416
      X(4,1,3)=-176.0960
      X(4,1,4)=686.3241
      X(4,1,5)=-823.1688
      X(4,1,6)=320.6294
      X(5,1,1)=-.9261
      X(5,1,2)=-19.6913
      X(5,1,3)=116.0657
      X(5,1,4)=-150.7721
      X(5,1,5)=60.8424
      X(6,1,1)=3.0082
      X(6,1,2)=-.7260
      X(6,1,3)=66.1302
      X(6,1,4)=-199.5429
      X(6,1,5)=203.5398
      X(6,1,6)=-70.6067
```


ORIGINAL PAGE IS
OF POOR QUALITY

```
X(7,1,1)=21.6525                00000430
X(7,1,2)=80.9658                00000440
X(7,1,3)=-10.2575               00000450
X(7,1,4)=-377.4930              00000460
X(7,1,5)=234.4536               00000470
X(8,1,1)=6.7245                 00000480
X(8,1,2)=4.7956                 00000490
X(8,1,3)=-141.7667              00000500
X(8,1,4)=463.9147               00000510
X(8,1,5)=-327.1767              00000520
X(1,2,1)=-.1416                 00000530
X(1,2,2)=-57.3749               00000540
X(1,2,3)=247.9659               00000550
X(1,2,4)=-460.4381              00000560
X(1,2,5)=399.6938               00000570
X(1,2,6)=-131.9327              00000580
X(2,2,1)=.0267                  00000590
X(2,2,2)=-2.6925                00000600
X(2,2,3)=.8550                  00000610
X(2,2,4)=-14.8580               00000620
X(2,2,5)=17.1088                00000630
X(3,2,1)=-1.4225                00000640
X(3,2,2)=5.1466                 00000650
X(3,2,3)=-27.4211               00000660
X(4,2,1)=-1.2323                00000670
X(4,2,2)=1.7646                 00000680
X(4,2,3)=-48.9664               00000690
X(4,2,4)=63.0376                00000700
X(4,2,5)=-28.4635               00000710
X(5,2,1)=-3.2124                00000720
X(5,2,2)=-5.1175                00000730
X(5,2,3)=-11.7354               00000740
X(5,2,4)=43.8952                00000750
X(5,2,5)=-26.7432               00000760
X(6,2,1)=-.9117                 00000770
X(6,2,2)=-17.3490               00000780
X(6,2,3)=106.6433               00000790
X(6,2,4)=-122.5828              00000800
X(6,2,5)=40.0669                00000810
X(7,2,1)=22.9386                00000820
X(7,2,2)=43.8971                00000830
X(7,2,3)=267.0537               00000840
X(7,2,4)=-257.9979              00000850
X(8,2,1)=3.3847                 00000860
X(8,2,2)=104.3205               00000870
X(8,2,3)=-854.6753              00000880
X(8,2,4)=2363.6418              00000890
X(8,2,5)=-2457.6914             00000900
X(8,2,6)=907.4531               00000910
X(1,3,1)=-.0711                 00000920
X(1,3,2)=145.2747               00000930
X(1,3,3)=-1732.9126             00000940
```

```
X(1,3,4)=8800.0474
X(1,3,5)=-21977.7931
X(1,3,6)=28502.0645
X(1,3,7)=-16489.1633
X(1,3,8)=4752.5470
X(2,3,1)=.0110
X(2,3,2)=1.6510
X(2,3,3)=8.5067
X(2,3,4)=38.1397
X(2,3,5)=-220.2950
X(2,3,6)=287.7375
X(2,3,7)=-115.7626
X(3,3,1)=.2853
X(3,3,2)=-7.5021
X(3,3,3)=34.2657
X(4,3,1)=-.0117
X(4,3,2)=-5.5953
X(4,3,3)=78.4126
X(4,3,4)=-157.1991
X(4,3,5)=74.9577
X(5,3,1)=.3494
X(5,3,2)=4.5443
X(5,3,3)=-7.2098
X(6,3,1)=.0579
X(6,3,2)=6.2519
X(6,3,3)=-56.6109
X(6,3,4)=67.8128
X(6,3,5)=-25.6700
X(7,3,1)=2.1864
X(7,3,2)=40.1364
X(8,3,1)=1.2924
X(8,3,2)=39.4773
X(8,3,3)=-308.0650
X(8,3,4)=846.3157
X(8,3,5)=-978.8486
X(8,3,6)=446.9769
X(3,4,1)=.0208
X(3,4,2)=2.6330
X(3,4,3)=-28.2534
X(3,4,4)=49.6782
X(3,4,5)=-11.0460
X(4,4,1)=.1416
X(4,4,2)=-5.0626
X(4,4,3)=33.9888
X(4,4,4)=-10.3021
X(5,4,1)=.0525
X(5,4,2)=-2.9718
X(5,4,3)=29.7889
X(5,4,4)=-32.8614
X(5,4,5)=10.4779
X(6,4,1)=.1063
X(6,4,2)=5.3342
```

```
      X(6,4,3)=-12.0892
      X(6,4,4)=2.3666
      X(7,4,1)=.0360
      X(7,4,2)=48.3816
      X(7,4,3)=-93.3694
      X(7,4,4)=393.3716
      X(7,4,5)=-626.1853
      X(7,4,6)=293.2343
      X(8,4,1)=-.0301
      X(8,4,2)=6.6261
      X(8,4,3)=-23.8374
      X(8,4,4)=80.2836
      X(8,4,5)=-38.1702
      X(1,5,2)=.94
      X(2,5,1)=-.00097
      X(2,5,2)=-.00784
      X(2,5,3)=0.89403
      X(3,5,1)=.00016
      X(3,5,2)=.02342
      X(3,5,3)=-1.12935
      X(3,5,4)=1.71225
      X(3,5,5)=-.74232
      X(4,5,1)=.00055
      X(4,5,2)=-.01219
      X(4,5,3)=-5.26963
      X(4,5,4)=46.19188
      X(4,5,5)=-126.23074
      X(4,5,6)=141.12570
      X(4,5,7)=-55.68757
      X(5,5,1)=-.00010
      X(5,5,2)=-.09926
      X(5,5,3)=.12484
      X(5,5,4)=-.05549
      X(6,5,1)=.0005283
      X(6,5,2)=.1723509
      X(6,5,3)=-.7342283
      X(6,5,4)=1.6377934
      X(6,5,5)=-1.7332042
      X(6,5,6)=.6787662
C****** NOW FORM DERIVS WRT A1,B1,ALFA,PSI,ETC ******
67    Z=ABS(AMUP*COS(ALPHP))
      W=AMUP
      CTA1=GK(X,Z,1,1)
      CPA1=GK(X,Z,2,1)
      CNFA1=GK(X,Z,3,1)
      CSFA1=GK(X,Z,4,1)
      CPMA1=GK(X,Z,5,1)
      CYMA1=GK(X,Z,6,1)
      CBMA1=GK(X,Z,7,1)
      FHMA1=GK(X,Z,8,1)
      CTB1=GK(X,Z,1,2)
      CPB1=GK(X,Z,2,2)
```

```
      CNFB1=GK(X,Z,3,2)
      CSFB1=GK(X,Z,4,2)
      CPMB1=GK(X,Z,5,2)
      CYMB1=GK(X,Z,6,2)
      CRMB1=GK(X,Z,7,2)
      FBMB1=GK(X,Z,8,2)
      CTALF=GK(X,Z,1,3)
      CPALF=GK(X,Z,2,3)
      CNFALF=GK(X,Z,3,3)
      CNFALF=ABS(CNFALF)
      CSFALF=GK(X,Z,4,3)
      CPMALF=GK(X,Z,5,3)
      CYMALF=GK(X,Z,6,3)
      CRMALF=GK(X,Z,7,3)
      FBMALF=GK(X,Z,8,3)
      CTPSI=GK(X,Z,1,4)
      CPPSI=GK(X,Z,2,4)
      CNFPSI=GK(X,Z,3,4)
      CSFPSI=GK(X,Z,4,4)
      CPMPSI=GK(X,Z,5,4)
      CYMPSI=GK(X,Z,6,4)
      CRMPSI=GK(X,Z,7,4)
      FBMPSI=GK(X,Z,8,4)
      CTRPM=GK(X,Z,1,5)
      CPRPM=GK(X,Z,2,5)
      CNFRPM=GK(X,Z,3,5)
      CSFRPM=GK(X,Z,4,5)
      CPMRPM=GK(X,Z,5,5)
      CYMRPM=GK(X,Z,6,5)
      CRMRPM=GK(X,Z,7,5)
      FBMRPM=GK(X,Z,8,5)
C ******* NOW CALCULATE REFERENCE VALUES OF ALPHA *******
      ALFREF=89.7176+Z*(-322.8042+Z*(770.9108+Z*(-1446.3424+Z*
     1(1449.9018+Z*(-545.1154)))))
      SKLFAC=1.0
      RPM=RPM*SKLFAC
      EYENAC=0.
      RPMREF=1165.-(1165.-830.)*(1.-EYENAC/45.)
      IF(EYENAC.GT.45.) RPMREF=1165.
      DELRPM=RPM-RPMREF
      DELA1=A1TST-5.0
      DELB1=B1TST-5.0
      DELALF=ALPHR/DTR-ALFREF
      DELPSI=-BETAR/DTR
      ABS1=ABS(DELALF)
      ABS2=ABS(DELPSI)
      DELCT=(CTA1*DELA1+CTB1*DELB1+CTALF*DELALF+CTPSI*ABS2+CTRPM*
     1DELRPM)/10000.
      DELCP=(CPA1*DELA1+CPB1*DELB1+CPALF*DELALF+CPPSI*ABS2+CPRPM
     1*DELRPM)/10000.
      DELCNF=(CNFA1*DELA1+CNFB1*DFLB1+CNFALF*DELALF+CNFPSI*DELPSI
     1+CNFRPM*DELRPM)/10000.
```

```
      DELCSF=(CSFA1*DELA1+CSFB1*DELB1+CSFALF*DELALF+CSFPSI*DELPSI
     1+CSFRPM*DELRPM)/10000.
      DELCPM=(CPMA1*DELA1+CPMB1*DELB1+CPMALF*DELALF+CPMPSI*DELPSI
     1+CPMRPM*DELRPM)/10000.
      DELCYM=(CYMA1*DELA1+CYMB1*DELB1+CYMALF*DELALF+CYMPSI*DELPSI
     1+CYMRPM*DELRPM)/10000.
      DELCBM=CBMA1*DELA1+CBMB1*DELB1+CBMALF*ABS1+CBMPSI*ABS2
     1+CBMRPM*DELRPM
      DELFBY=FBMA1*DELA1+FBMB1*DELB1+FBMALF*ABS1+FBMPSI*ABS2
     1+FBMRPM*DELRPM
      IF(Z.LT.0.015) GO TO 30
      IF(Z.LT.0.055) GO TO 31
      IF(Z.LT.0.100) GO TO 32
      IF(Z.LT.0.147) GO TO 33
      IF(Z.LT.0.162) GO TO 34
      IF(Z.LT.0.210) GO TO 35
      IF(Z.LT.0.230) GO TO 36
      IF(Z.LT.0.234) GO TO 37
      IF(Z.LT.0.410) GO TO 38
      IF(Z.LT.0.457) GO TO 39
      GO TO 40
30    GRAD1=11.933
      CEPT1=.882
      GRAD2=106.667
      CEPT2=-1.5
      GRAD3=-.267
      CEPT3=.094
      GRAD4=-9.667
      CEPT4=.035
      GO TO 41
31    GRAD1=3.175
      CEPT1=1.013
      GRAD2=92.75
      CEPT2=-1.291
      GRAD3=.225
      CEPT3=.087
      GRAD4=5.5
      CEPT4=-.193
      GO TO 41
32    GRAD1=1.467
      CEPT1=1.107
      GRAD2=77.556
      CEPT2=-.456
      GRAD3=.578
      CEPT3=.067
      GRAD4=1.111
      CEPT4=.049
      GO TO 41
33    GRAD1=-.787
      CEPT1=1.333
      GRAD2=85.106
      CEPT2=-1.211
```

```
      GRAD3=.957
      CEPT3=.029
      GRAD4=1.702
      CEPT4=-.010
      GO TO 41
   34 GRAD1=10.4
      CEPT1=-.312
      GRAD2=193.333
      CEPT2=-17.12
      GRAD3=-.733
      CEPT3=.276
      GRAD4=-10.
      CEPT4=1.71
      GO TO 41
   35 GRAD1=-2.563
      CEPT1=1.768
      GRAD2=45.833
      CEPT2=6.775
      GRAD3=1.479
      CEPT3=-.081
      GRAD4=8.125
      CEPT4=-1.226
      GO TO 41
   36 GRAD1=1.150
      CEPT1=1.009
      GRAD2=-40.
      CEPT2=24.8
      GRAD3=1.
      CEPT3=.020
      GRAD4=6.
      CEPT4=-.780
      GO TO 41
   37 GRAD1=52.5
      CEPT1=-10.802
      GRAD2=1125.
      CEPT2=-243.15
      GRAD3=-10.
      CEPT3=2.55
      GRAD4=-103.75
      CEPT4=24.463
      GO TO 41
   38 GRAD1=1.
      CEPT1=1.249
      GRAD2=61.8182
      CEPT2=5.635
      GRAD3=1.364
      CEPT3=-.109
      GRAD4=.767
      CEPT4=.006
      GO TO 41
   39 GRAD1=3.0575
      CEPT1=.4054
```

```
      GRAD2=57.701
      CEFT2=7.3225
      GRAD3=.88
      CEFT3=.085
      GRAD4=.793
      CEFT4=-.005
      GO TO 41
40    GRAD1=1.6799
      CEFT1=1.0901
      GRAD2=51.155
      CEFT2=10.5759
      GRAD3=.88
      CEFT3=.085
      GRAD4=.793
      CEFT4=-.005
41    GRADCT=(GRAD1*Z+CEFT1)/1000.
      CEFTCT=GRAD2*Z+CEFT2
      GRADCP=GRAD3*Z+CEFT3
      CEFTCP=(GRAD4*Z+CEFT4)/1000.
      IF(W.GT.0.51) GO TO 21
      CEFCNF=-1.4499+W*(1.1164+W*(46.1585+W*(46.1533+W*(-4118.7472
     1+W*(27714.8692+W*(-74786.6559+W*(89304.8015+W*(-39318.3083
     1))))))))
      CEFCNF=CEFCNF/1000.
      GRDCNF=-.0017+W*(2.1220+W*(-10.9462+W*(-34.5193+W*(420.
     10141+W*(-1043.6843+W*(520.6263+W*(1029.2775+W*(-966.
     13633))))))))
      GO TO 22
21    CEFCNF=(.35-35.79*(W-.51))/1000.
      GRDCNF=.0304687-.26494*(W-.51)
      IF(W.GT.0.625) GRDCNF=0.
22    IF(W.GT.0.50) GO TO 23
      CEFCSF=-.3184+W*(31.8306+W*(-457.3674+W*(4745.5645+W*(-3
     16659.2177+W*(170991.2286+W*(-441355.4546+W*(580754
     1.9029+W*(-303701.0909))))))))
      GO TO 24
23    CEFCSF=-.51327+11.9*(W-.5)
24    CEFCSF=CEFCSF/1000.
      IF(W.GT.0.226) GO TO 25
      GRDCSF=-.0017+W*(-1.6734+W*(.0987+W*(70.5419+W*(-179.0345)))
     1)
      GO TO 27
25    IF(W.GT.0.55) GO TO 26
      GRDCSF=0.+W*(-12.8306+W*(213.4645+W*(-1172.8346+W*(1816.7802
     1+W*(4769.9642+W*(-20782.9608+W*(26637.2442+W*(-11791.4688
     1))))))))
      GO TO 27
26    GRDCSF=.211956-1.35*(W-.55)
      IF(W.GT.0.707) GRDCSF=0.
27    CEFCPM=-2.3861+W*(34.2316+W*(-266.8938+W*(250.2259+W*(3745.
     17836+W*(-12450.4146+W*(11267.8934))))))
      IF(W.GT.0.4) CEFCPM=-.8
```

```
      CEPCPM=CEPCPM/1000.
      GRDCPM=-0.0001+W*(1.4986+W*(-53.9096+W*(779.1001+W*(-4704.
     11758+W*(10912.7643+W*(-12167.8786+W*(3919.3933)))))))
      IF(W.GT.0.315) GRDCPM=0.
      IF(W.GT.0.35) GO TO 28
      GRDCYM=-.0069+W*(1.3799+W*(-13.6714+W*(-1.2748+W*(1274.55
     193+W*(-13035.8682+W*(59190.8797+W*(-127927.2065+W*(106845.
     17562))))))))
      GO TO 29
 28   GRDCYM=16.9481+W*(-131.5322+W*(368.4930+W*(-554.3724+W*
     1(365.7019+W*(-105.2687)))))
 29   CEPCYM=1.162+W*(14.8842+W*(-169.1834+W*(622.1258+W*(-3
     1053.1573+W*(7474.2981+W*(-10069.5247+W*(6758.6616+W*
     1(-1774.5129))))))))
      CEPCYM=CEPCYM/1000.
      CTBASE=GRADCT*(COLL-CEPTCT)
      CPBASE=GRADCP*CTBASE+CEPTCP
      CNFBAS=GRDCNF*CTBASE+CEPCNF
      CSFBAS=GRDCSF*CTBASE+CEPCSF
      CPMBAS=GRDCPM*CTBASE+CEPCPM
      CYMBAS=GRDCYM*CTBASE+CEPCYM
      CT=CTBASE+DELCT
      CP=CPBASE+DELCP
      CSF=CSFBAS+DELCSF
      CNF=CNFBAS+DELCNF
      CPM=CPMBAS+DELCPM
      CYM=CYMBAS+DELCYM
      RETURN
      END
      FUNCTION GK(G,DUM,I,J)
      DIMENSION G(8,5,8)
      GK=G(I,J,1)+DUM*(G(I,J,2)+DUM*(G(I,J,3)+DUM*(G(I,J,4)+DUM*
     1(G(I,J,5)+DUM*(G(I,J,6)+DUM*(G(I,J,7)+DUM*G(I,J,8)))))))
      RETURN
      END
```